The Role of Large-Scale Atmospheric Eddies in the Climate Equilibrium

by

Shuntai Zhou

S.B., S.M. in Meteorology
Nanjing Institute of Meteorology, China
(1982, 1984)

Submitted to
the Department of Earth, Atmospheric, and Planetary Sciences
in partial fulfillment of the requirements for the degree of

DOCTOR OF PHILOSOPHY
IN METEOROLOGY
at the
MASSACHUSETTS INSTITUTE OF TECHNOLOGY

September 1991

Signature of Author .....
Center for Meteorology and Physical Oceanography
Department of Earth, Atmospheric and Planetary Sciences
11 September 1991

Certified by .....
Peter H. Stone
Professor of Meteorology
Thesis Supervisor

Accepted by .....
Thomas H. Jordan
Chairman, Departmental Committee on Graduate Students

The Role of Large-Scale Atmospheric Eddies in the Climate Equilibrium

by

Shuntai Zhou

Submitted to the Department of Earth, Atmospheric and Planetary Sciences on September 11, 1991 in partial fulfillment of the requirements for the Degree of Doctor of Philosophy in Meteorology

Abstract

The forcing of climate states by eddy transports of heat and momentum, their interactions and feedbacks, and their responses to changes in the external parameters are studied by systematic numerical experiments. The model used is a low order model with intermediate complexity between simple climate models and sophisticated GCMs. It has two vertical levels and a reasonable horizontal resolution, typically, five zonal waves with fundamental planetary wavenumber 3 and five meridional modes on a hemisphere. Newtonian cooling, surface drag and interfacial friction are included. In addition, the static stability is variable. The eddy fluxes of heat and momentum are calculated explicitly.

In addition to meridional eddy transports of heat and momentum, we emphasize the interaction of the vertical eddy heat flux and the static stability, and the effect of spherical geometry. Whether the static stability is fixed or not, and whether the

model is on a β-plane or on a sphere, the models are similar in many features. For example, the meridional eddy heat flux plays the most important role in the eddy forcing of climate states. However, there are essential differences in the climate sensitivity between the models with fixed or variable static stability, and the models with or without spherical geometry. For instance, the meridional eddy heat flux is proportional to a power of ~ 15 of the midlatitude temperature gradient in the β-plane model with fixed static stability; the power is reduced to ~ 6 on a sphere, and is further reduced to $2 \sim 4$ when the static stability is variable. The baroclinic adjustment and the energy cascade mechanisms are more effective in the model with variable static stability. As a result, the isentropic slope is very insensitive to the change in the diabatic forcing, and the slope is much closer to observations.

Thesis supervisor: Peter H. Stone

Title: Professor of Meteorology

Acknowledgments

I wish to thank my advisor, Prof. Peter Stone, for his insightful and inspirational guidance throughout the course of this research. I also wish to thank Prof. Kerry Emanuel, Prof. Glenn Flierl and Prof. Ronald Prinn for their helpful suggestions and comments.

I would like to thank many of my fellow students for their friendship, encouragement and assistance. Among them, Nilton Renno, James Risbey, Kuanman Xu, Changsheng Chen, Zhengyu Liu, Dezheng Sun and Zhongxiang Wu deserve considerable thanks. I also wish to express my deep thanks to Jane McNabb at the CMPO headquarter, who made international students feel like home; to Diana Spiegel, who gave me a lot of assistance in the computer work; and to June Tankel at the English class of the US-China Friendship Association, who volunteered teaching Students from China (including me) for many years.

Most of all, I would like to thank my wife, Yingying, and my parents for their love, care and support. Without their unselfish commitment it would almost be impossible for me to finish this research.

Nanjing Institute of Meterology (NIM, China) gave me the precious opportunity to study in the Unite States. I am grateful to the support and encouragement from President Peichang Zhang and the Dept. of Meteorology of NIM.

This work was supported in part by the National Aeronautic and Space Administration (NASA) Goddard Space Flight Center under Grant NASA NGR 22-009-727 and in part by the National Science Foundation under Grant No. ATM-8803446.

Contents

Abstract 3

Acknowledgments 5

List of Figures 11

List of Tables 17

List of Symbols 19

1 Introduction 21

2 Background 27

3 Model description 37

3.1 Basic equations 37

3.2 Spectral representations 43

4 Hadley regime 47

4.1 Introduction 47

4.2 Equations in the Hadley regime 48

4.3 Numerical solutions 53

4.4 Instability analyses 55

5 Eddy regime – the Phillips system **65**

5.1 Introduction 65

5.2 Equations in the Phillips system 67

5.2.1 The numerics 67

5.2.2 The physics 69

5.3 The "standard" run 77

5.3.1 The equilibrium states 77

5.3.2 The momentum budgets 78

5.3.3 The heat budget 80

5.3.4 The energetics 81

5.3.5 Additional experiments 87

5.4 The "optimal" horizontal resolution 91

5.4.1 Introduction 91

5.4.2 Truncation levels 92

5.4.3 Fundamental wavenumbers 105

5.4.4 Dynamical constraints 115

5.5 Effects of changes in the external parameters 117

5.5.1 Introduction 117

5.5.2 Parameter experiments 118

5.5.3 The feedback factor 132

5.5.4 Summary 135

6 Eddy regime – the Lorenz system **141**

6.1 Introduction 141

6.2 Equations in the Lorenz system 142

6.3 The equilibrium static stability 145

6.4 The maintenance of the static stability 148

6.4.1 Comparison with the "standard" run 148

6.4.2 The budget of static stability 160

6.5 The parameter experiments 164

6.5.1 Diabatic forcing ΔT_E 164

6.5.2 Newtonian cooling time τ_h 168

6.5.3 Surface friction k 169

7 Adjustment of the temperature structure **179**

7.1 Introduction 179

7.2 Isentropic slope adjustment 181

7.2.1 Fixed static stability 181

7.2.2 Variable static stability 183

7.3 Temperature gradient and eddy heat flux 187

7.4 The main heat-transporting wave 191

8 Summary and Conclusions 199

References 207

List of Figures

4.1 Zonal winds and MMC stream functions in the Hadley regime for T = 20, 40, 80 days, where T is the dissipative time for the interfacial friction. The contour intervals are $5\,m/s$ for $[u]$ and $2\,mb.m/s$ for $[\chi]$. 58

4.2 As in Figure 4.1 but for T = 160, 320, 640 days and the contour interval for $[\chi]$ is $1\,mb.m/s$. 59

4.3 The upper layer wind fields for T = 20, 40, 80, 160, 320, 640 days. Also shown are the thermal wind, U_E, in the radiative equilibrium and the momentum conserving wind, $U_m (U_m = \frac{\Omega a \cos^2\theta}{\sin\theta})$. 60

4.4 Meridional momentum fluxes for various T. The theoretical curve is shown by the solid line. 60

4.5 As in Figure 4.4 but for meridional heat fluxes. 61

4.6 As in Figure 4.4 but for temperature adjustments, $[T_E(\phi) - T(\phi)]$. . . 61

4.7 Wave growth rate (ω_r) as a function of ΔT_E and zonal wavenumber (n). The e-folding time for wave growth is $(\omega_r \Omega)^{-1}$. 62

4.8 As in Figure 4.7 but for doubled static stability. 62

4.9 As in Figure 4.7 but the growth rate is a function of static stability (N^2) and n. 63

5.1 The profile of interfacial friction k' (solid line) and the distribution of the "hot tower" precipitation in the GISS model (cross signs). The model results are for January conditions in which the "heat equator" is at about $10°S$. 72

5.2 The vertical shears of zonal wind fields, the upper layer meridional winds, the eddy heat fluxes and the eddy momentum fluxes in the sensitivity experiments with varying k'_e, the maximal dissipative rate due to the vertical mixing process. 73

5.3 As in Figure 5.2 but for $(k'_e)^{-1} = 0.1\,day$. The solid line is for the case with k' profile of P_{20}^{20}, and the dashed line is for the case with k' profile of P_{38}^{38}. 74

5.4 The vertical shears of zonal wind fields, the upper layer meridional winds, the eddy heat fluxes and the eddy momentum fluxes in the experiments with varying h_e, the maximal Newtonian cooling rate due to the convective heat exchange. 75

5.5 The equilibrium states of [U], [V], [T] and [χ] fields in the "standard" run. T_E is the temperature in radiative equilibrium . The contour interval of [χ] is $10\,mb.m/s$. 84

5.6 The momentum budgets in the "standard" run. a) the upper layer; b) the lower layer; c) the vertical mean; d) the eddy momentum flux. Detailed explanations are given in the text. 85

5.7 a) The heat budget in the "standard" run. The solid line is the convergence of the eddy heat flux, the dotted line is the MMC heat transport and the dashed line is the diabatic heating; b) The heat fluxes by eddies (solid) and by the MMC (dotted). 86

5.8 The energy cycle diagram in the "standard" run. The unit in the boxes is $10^5\,J\,m^{-2}$; the unit beside the arrows is $W\,m^{-2}$. 87

5.9 Surface wind fields, temperature fields, eddy momentum fluxes and eddy heat fluxes obtained from the *linear* (solid lines) and *nonlinear* (dotted lines) balance models. 89

5.10 The zonal wind, the meridional wind , the mean momentum balance and the eddy momentum flux in the experiment similar to the "standard" run but with a fourth order horizontal diffusion ($A\nabla^4$, $A = 10^{17}\,m^4/s$). 90

5.11 The equilibrium zonal wind fields in the truncation experiments. The solid, dotted and dashed lines denote U_1, U_3 and U_4 respectively. . . . 97

5.12 The vertical mean momentum budgets in the truncation experiments. The meanings for the lines are the same as those of Figure 5.6(c). . . 98

5.13 The vertical mean eddy momentum fluxes in the truncation experiments. 99

5.14 The heat budgets in the truncation experiments. The meanings for the lines are the same as those of Figure 5.7 (a). 100

5.15 The heat fluxes by eddies and by the MMC in the truncation experiments. The meanings for the lines are the same as those in Figure 5.7 (b). 101

5.16 The MMC stream functions in the truncation experiments. The contour interval is $10\,mb.m/s$. 102

5.17 The energy cycle diagrams in the truncation experiments. 103

5.18 The eddy kinetic energy spectrum in the truncation experiments. The X-axis is the zonal wavenumber and the Y-axis is the amount of energy. The numbers 5, 6, 7 denote resolutions 5×5, 6×6, 7×7 respectively. 104

5.19 The equilibrium zonal wind fields in the fundamental wavenumber experiments. FN is the fundamental wavenumber. The meanings for the lines are the same as those of Figure 5.5 (a). 107

5.20 The vertical mean momentum budgets in the fundamental wavenumber experiments. The meanings for the lines are the same as those of Figure 5.6(c). 108

5.21 The vertical mean eddy momentum fluxes in the fundamental wavenumber experiments. 109

5.22 The heat budgets in the fundamental wavenumber experiments. The meanings for the lines are the same as those of Figure 5.7 (a). 110

5.23 The heat fluxes by eddies and by the MMC in the fundamental wavenumber experiments. The meanings for the lines are the same as those of Figure 5.7 (b). 111

5.24 The MMC stream functions in the fundamental wavenumber experiments. The contour interval is $10\,mb.m/s$. 112

5.25 The energy cycle diagrams in the fundamental wavenumber experiments. 113

5.26 The eddy kinetic energy spectrum in the fundamental wavenumber experiments. The X-axis is the zonal wavenumber and the Y-axis is the amount of energy. The numbers 1, 2, 3, 6 denote fundamental wavenumbers. 114

5.27 The surface winds, the upper layer meridional winds, the eddy momentum fluxes and the eddy heat fluxes in the ΔT_E experiments. . . 128

5.28 The surface winds, the upper layer meridional winds, the eddy momentum fluxes and the eddy heat fluxes in the τ_h experiments. 129

5.29 The surface winds, the upper layer meridional winds, the eddy momentum fluxes and the eddy heat fluxes in the Γ_0 experiments. 130

5.30 The surface winds, the upper layer meridional winds, the eddy momentum fluxes and the eddy heat fluxes in the τ_s experiments. 131

5.31 The feedback factors in the experiments without interfacial friction. The abscissa is R_S, the predicted value from the scaling method; the ordinate is R, the calculated value from the definition. 137

5.32 The feedback factors in the experiments without interfacial friction. The ordinate is R; the abscissa is R_{E-P}, the ratio of the horizontal to the vertical component of the E-P flux. 138

5.33 The schematic diagram for the dynamical processes and the effects of changes in the external parameters in the Phillips system. 139

6.1 The static stability $\hat{\Theta}_E$ ($\Gamma_E \propto \hat{\Theta}_E$) used in the model. Curve A is a radiative equilibrium; Curve B is a radiative-convective equilibrium. . 151

6.2 The equilibrium states of [u], [v], [T] and [χ] in experiment A(S). The contour interval of [χ] is $10\,mb.m/s$. 152

6.3 The momentum budgets in experiment A(S). The curves have the same meaning as those in Figure 5.6. 153

6.4 The heat budget in experiment A(S). The curves have the same meaning as those in Figure 5.7. 154

6.5 a) The static stability; b) the budget of static stability; c) the components of the ageostrophic temperature advection; and d) the vertical eddy heat flux in experiment A(S). Detailed explanations are given in the text. 155

6.6 As in Figure 6.2 but for experiment B(S). 156

6.7 As in Figure 6.3 but for experiment B(S). 157

6.8 As in Figure 6.4 but for experiment B(S). 158

6.9 As in Figure 6.5 but for experiment B(S). 159

6.10 The equilibrium states of zonal mean surface winds, upper layer meridional winds, eddy momentum fluxes, meridional eddy heat fluxes, vertical eddy heat fluxes and MMC heat fluxes in experiments A (ΔT_E).173

6.11 As in Figure 6.10 but for experiments B (ΔT_E). 174

6.12 The equilibrium states of zonal mean surface winds, upper layer meridional winds, eddy momentum fluxes, meridional eddy heat fluxes, vertical eddy heat fluxes and MMC heat fluxes in experiments A (τ_h). 175

6.13 As in Figure 6.12 but for experiments B (τ_h). 176

6.14 The equilibrium states of zonal mean surface winds, upper layer meridional winds, eddy momentum fluxes, meridional eddy heat fluxes, vertical eddy heat fluxes and MMC heat fluxes in experiments A (k). 177

6.15 As in Figure 6.14 but for experiments B (k). 178

7.1 The variation of the temperature gradient at 45° with ΔT_E. 185

7.2 The vertical shears at 45° as a function of static stability N^2. The cross signs are model results calculated with the Phillips system; the dashed line is $\hat{U} = 9.87 \times 10^4 N^2$; the dotted line is the criterion for baroclinic instability; the dot-dashed line is the shear in radiative equilibrium state. 186

7.3 As in Figure 7.2 but the model results are calculated in the Lorenz system (Γ_E is set to curve A, i.e., radiative equilibrium). The dashed line is $\hat{U} = 4.86 \times 10^4 N^2$. 186

7.4 As in Figure 7.2 but the model results are calculated in the Lorenz system (Γ_E is set to curve B, i.e., radiative-convective equilibrium). The dashed line is $\hat{U} = 4.40 \times 10^4 N^2$. 187

7.5 The eddy heat fluxes as a function of the temperature gradient in the mid latitudes. "A" and "B" are the model results with variable static stability (Γ_E is set to be curve A and B respectively); "C" is calculated with constant static stability. 190

7.6 The exponents in the power relationship between the eddy heat flux and the temperature gradient, as a function of ΔT_E. 190

7.7 The eddy heat fluxes by individual zonal wavenumbers for $\Delta T_E =$ 30, 48, 72, 144 K. The dashed line indicates the flux by wavenumber 3; the dotted line is by wavenumbers 3 and 6; ..., the solid line is the total flux. 194

7.8 The peak values of eddy heat flux by individual wavenumbers as a function of ΔT_E. The solid line is for the total wavenumbers, the dashed, dotted and dot-dashed lines are for wavenumber 3, 6, 9 respectively. 195

7.9 The peak values of eddy heat fluxes in the wavenumber domain. a) $5 \times 8(2)$, fixed static stability; b) $5 \times 8(2)$, variable static stability; c) $5 \times 15(1)$, fixed static stability; d) $5 \times 15(1)$, variable static stability. 196

7.10 The eddy kinetic energy in the wavenumber domain. a) $5 \times 8(2)$, fixed static stability; b) $5 \times 8(2)$, variable static stability; c) $5 \times 15(1)$, fixed static stability; d) $5 \times 15(1)$, variable static stability. 197

List of Tables

5.1 The spectrum of kinetic energy (unit: $10^5\ Jm^{-2}$). 83

5.2 Some characteristic quantities in the resolution experiments. 96

5.3 Some characteristic quantities in the ΔT_E experiments. 120

5.4 The energetics in the ΔT_E experiments. 120

5.5 The spectrum of eddy kinetic energy in the ΔT_E experiments. 121

5.6 Some characteristic quantities in the τ_h experiments. 122

5.7 The energetics in the τ_h experiments. 122

5.8 The spectrum of eddy kinetic energy in the τ_h experiments. 123

5.9 Some characteristic quantities in the Γ_0 experiments. 124

5.10 The energetics in the Γ_0 experiments. 125

5.11 The spectrum of eddy kinetic energy in the Γ_0 experiments. 125

5.12 Some characteristic quantities in the τ_s experiments. 127

5.13 The energetics in the τ_s experiments. 127

5.14 The spectrum of eddy kinetic energy in the τ_s experiments. 132

6.1 Some characteristic quantities in the resoltion experiments with the Lorenz system. 150

6.2 Dynamical time scales (days). 163

6.3 Some characteristic quantities in the experiments varying ΔT_E. . . . 167

6.4 Some characteristic quantities in the experiments varying τ_h. 170

6.5 Some characteristic quantities in the experiments varying τ_s. 172

List of Symbols

a	Radius of the earth
c_γ	Eigenvalue of spherical harmonic function
f	Coriolis parameter
g	Magnitude of gravity
h	Newtonian cooling rate
h_0	$\equiv \frac{f^2 u_z}{\beta N^2}$
k	Surface drag coefficient
k'	Interfacial friction coefficient
k_E	Ekman pumping coefficient
m	1) Meridional mode; 2) Fundamental wavenumber
n	1) Zonal wavenumber; 2) Exponent of the power relationship
p	Pressure
r	$\equiv \frac{\partial T/\partial \theta}{\partial T_E/\partial \theta}$
t	Time
t_M, t_e	Eddy time scale for momentum
t_T	Eddy time scale for heat
t_Γ	Eddy time scale for static stability
u	Zonal wind
v	Meridional wind
x, y, z	Eastward, northward and upward distance respectively
A	Horizontal diffusion coefficient
C	Energy conversion
D	Energy dissipation
$\mathcal{D}$	Friction
E	Eddy efficiency at heat transport
F	Eddy heat flux
$\vec{F}$	Eliassen-Pulm flux
G	Energy generation
H	Scale height
$I_{\alpha\beta\gamma}$	Interaction coefficient
J	Jacobian operator
K	Kinetic energy
$\mathcal{K}_{\alpha\beta\gamma}$	Interaction coefficient
L_γ	Interaction coefficient

M	1) Angular momentum; 2) Number of meridional modes
$\mathcal{M}_{\alpha\beta\gamma}$	Interaction coefficient
N	1) Brunt-Väisällä frequency; 2) Number of zonal waves
P	Potential energy
P_0	Surface pressure (1,000 mb)
P_γ	$\equiv P_{n_\gamma}^{l_\gamma}$, associated Legendre function
Q	Quasi-geostrophic potential vorticity
$\mathcal{Q}$	Diabatic heating
R	1) Gas constant for dry air; 2) Feedback factor
R_0	Rossby number
S_0	Solar constant
T	1) Temperature; 2) Frictional relaxation time
T_{ed}	Meridional eddy heat flux
T_{MMC}	MMC heat flux
$\hat{U}$	Vertical shear of zonal flow
Y_γ	Spherical harmonic function
α	Isentropic slope
β	$\equiv df/dy$
γ	$\equiv H/h_0$
δ	Divergence
ζ	Vorticity
θ	Colatitude
λ	Longitude
μ	$\equiv \cos\theta$
ρ	Air density
σ	Static stability parameter
τ_h	$\equiv 1/h$, Newtonian cooling time
τ_s	$\equiv 1/(2k)$, dissipative time by surface drag
τ_E	$\equiv 1/(2k_E)$, dissipative time by Ekman pumping
ϕ	Latitude
φ	Velocity potential
χ	MMC stream function
ψ	Geostrophic stream function
ω	$\equiv dp/dt$, vertical velocity in p-coordinates
ω_r	Wave growth rate
Γ	Static stability parameter
Θ	Potential temperature
Φ	Geopotential
Ω	Augular velocity of the earth

Chapter 1

Introduction

The capability of the atmosphere to adjust itself to external changes is very impressive. These adjustments occur on a large range of time scales: Buoyant oscillations take only a few minutes (Brunt, 1927); geostrophic adjustments may take several hours (Phillips, 1963); baroclinic adjustments have a time scale from days to seasons (Stone, 1978; Mole and James, 1990); climate fluctuations range from decades to centuries. Despite different physical mechanisms involved in these adjustments, the common feature is that the atmosphere tends to remain at some dynamical or statistical equilibrium state.

In this study we are mainly concerned about the long-term, large-scale atmospheric equilibrium which is referred to as climate equilibrium. The climate equilibrium is ultimately determined by such basic elements as the mass and composition of the atmosphere, the rotation rate and surface features of the earth, as well as the flux of solar radiation. From the dynamical point of view, although we do not rule out the importance of oceans and atmospheric axisymmetric circulation, it is recognized that large-scale atmospheric eddies play a very active and important role

in the general circulation and climate, especially in the troposphere of mid-high latitudes (Lorenz, 1967; Palmén and Newton, 1969; Oort and Rasmusson, 1971).

A climate state may be characterized by its temperature structure, which is determined by the diabatic heating and the dynamical transports. The observations show that a major portion of the atmosphere's meridional heat transport ($\sim 85\%$) is associated with eddies (Oort, 1971). The role of large-scale eddies has been investigated in terms of the meridional eddy heat transport ($[v^*\Theta^*]$). In general, the large-scale eddies transport heat poleward. As a result, the temperature gradient and the vertical wind shear are reduced from their radiative equilibrium states. Since transports are fundamentally a Lagrangian process (McIntyre, 1980) and potential temperature is a conservative quantity, heat transport would be better described in the Lagrangian framework. Unfortunately, the Langrangian method is almost intractable in practice. On the other hand, in the Eulerian framework, the heat transport is conventionally divided into two parts: the eddy flux and the MMC (mean meridional circulation) flux. Clearly, the eddy heat flux alone is not a proper measure of the eddy forcing on zonal mean states. Specifically, the heat flux by the MMC in the mid-latitudes is observed to be equatorward, due to the indirect Ferrel cell. This is opposite to the poleward heat flux by eddies. Thus, the net heat transport depends on the relative importance of the eddy flux and the MMC flux.

Alternatively, the role of eddies can be better understood by using the Eliassen-Palm theorem. In this framework, the quasi-geostrophic eddy forcing of mean states is represented by the divergence of the Eliassen-Palm flux (E-P flux), $\vec{F} = (-[u^*v^*], f[v^*\Theta^*]/\bar{\Theta}_p)$ (Edmon *et al.*, 1980). It combines the effects of both eddy heat transport and eddy momentum transport. In the midlatitudes, the contributions of these

transport processes are observed to be opposite in sign in the long-term mean state. The effect of the eddy heat flux outside the boundary layer is to increase the *convergence* of the E-P flux, but the effect of the eddy momentum flux is to increase the *divergence* of the E-P flux. This feature is very similar to the heat transport by eddies and by the MMC. In other words, the eddy momentum flux is a negative feedback to the eddy heat flux. Therefore, the eddy forcing of mean states is dependent on the relative importance of the eddy momentum flux and the eddy heat flux. For the earth's troposphere, the eddy heat flux is more important. However, for an adiabatic and inviscid atmosphere, $\nabla \cdot \vec{F} = 0$. This means that the eddy heat flux is exactly compensated by the eddy momentum flux. One must ask how much the effect of the eddy heat transport would be offset by the eddy momentum transport if the external forcing varies over a broad range. Essentially, this is equivalent to trying to understand how the eddies interact with the mean states to adjust the climate to the external forcing. This is the first goal of the present study.

The eddy forcing is also related to the static stability. As is seen in the vertical component of the E-P flux, the static stability ($\bar{\Theta}_p$) appears in the denominator. Strong static stability suppresses the role of the eddy heat flux. In quasi-geostrophy, the static stability is treated as a constant. But its temporal and spatial variations must undoubtably affect the eddy forcing. The interaction between the vertical eddy heat flux ($[\omega^* \Theta^*]$) and the static stability is an important physical mechanism. The eddies transport heat upward to increase the static stability, which in turn inhibits the eddy growth. Therefore, the effect of the vertical eddy heat flux is implicitly included even in the quasi-geostrophic form of the E-P flux if the static stability is not fixed. It is another negative feedback to the meridional eddy heat flux. The question is how important would this feedback be when the external forcing varies,

and to what extent is a constant static stability an appropriate approximation. This is the second goal of the present study.

The vertical eddy transport of momentum ($[u^*\omega^*]$) is omitted in the quasi-geostrophic theory. Unlike the vertical eddy transport of heat, $[u^*\omega^*]$ plays very little role in the general circulation, especially in the mid-high latitudes (Stone and Yao, 1987). Therefore, it can be neglected reasonably in studying the role of eddies.

It is clear from the Eulerian framework that the different components ($[v^*\Theta^*]$, $[u^*v^*]$, $[\omega^*\Theta^*]$) of the eddy transports interact in a very complicated way. The conservation principle is more or less obscured by the complex interactions. For some purposes, one may not need to know precisely the amount of these eddy transports in detail. Instead, one only needs to know the overall effect of eddies, which can be parameterized in terms of the mean states. This has been demonstrated in many simple climate models as discussed below.

There have been many attempts to parameterize heat transports by eddies. A simple parameterization is that the eddy heat flux is proportional to some power of the meridional temperature gradient, i.e., $F = A(\delta T)^n$, where F is the eddy heat flux, A is a proportionality constant, δT is the temperature gradient, and n an empirical exponent. For instance, in Budyko's and Sellers' energy balance models (Budyko, 1969; Sellers, 1969) $n = 1$. Thus, the empirical power relation is simply a diffusion law In Stone's radiative-dynamical model (Stone, 1972, 1973) $n = 2$, which is derived from the theory for baroclinic waves on an f-plane. Empirical relations from observations indicate that F is approximately proportional to the square of the gradient in the midlatitudes, but to the third or fourth power of the gradient near 30°N (Stone and Miller, 1980). Another simple form of parameterization is to

assume that the heat transport is carried by a hypothetical meridional circulation (Eliasen, 1982). This circulation is similar to the "residual meridional circulation" in the transformed Eulerian system (Andrews and McIntyre, 1976), although it is determined from the mean temperature field. The third type of parameterization is to assume a *baroclinic adjustment* (Stone, 1978), i.e., without explicit calculations of eddy heat transports. In this scheme, the mean temperature gradient in the mid-latitudes is always adjusted by eddies to the critical value for baroclinic instability in the sense of Phillips' two-level model (Phillips, 1954).

Although these parameterizations were, to some extent, successful in assessing the overall role of eddies in climate, they are based on empirical relationships that may not apply to more general conditions. We want to know to what extent the power relation and the baroclinic adjustment hypothesis are still valid when the external conditions, e.g., the diabatic forcing, vary. This is the third goal of the present study.

Our approach in this study is to use a reasonably simplified and relatively realistic model to calculate various characteristics of the statistical equilibrium states, such as the zonal mean flow and the temperature structure, the angular momentum and heat budgets, and the energetics, among others. Especially, we will calculate $[v^*T^*]$, $[u^*v^*]$, $[\omega^*T^*]$ explicitly and examine their interactions and feedbacks. We will also change the external parameters systematically to study the climatic sensitivity and the response of the eddy forcing.

Three steps will be taken to accomplish these goals. In the first, we will suppress all eddies artificially to find out the steady state, i.e., the solution of the Hadley regime. This will provide a background or reference frame for the eddy regime.

Then, we introduce large-scale eddies into a two-level system with constant static stability – the Phillips system (Phillips, 1954) or the P-model (Hollingsworth, 1975). Because the vertical eddy heat flux is neglected in the Phillips system, we will only focus on the meridional eddy fluxes of heat and momentum, and fix the static stability and treat it as an external parameter. Finally, we will relax this constraint by using another two-level system with variable static stability – the Lorenz system (Lorenz, 1960) or the L-model (Hollingsworth, 1975), so that the effect of vertical eddy heat flux can be included, along with meridional eddy fluxes of heat and momentum.

This paper is organized as follows. In chapter 2 a background review is given. Chapter 3 gives a description of the model equations, physics and numerics. The Hadley regime is discussed in chapter 4, where we show model results of experiments in the nearly inviscid limit. The experiments in the Phillips system are described in chapter 5, which include horizontal resolution experiments and external parameter experiments. In chapter 6 similar experiments in the Lorenz system are illustrated and compared with those in the Phillips system. In chapter 7 we examine the baroclinic adjustment hypothesis and the relationship between the meridional eddy heat flux and the temperature gradient in the mid latitudes, based on the model results. Then we summarize and conclude in chapter 8.

Chapter 2

Background

The importance of large-scale eddies has been recognized for a long time. It is highly visible on daily weather maps, in general circulation statistics and in various diagnostic studies. Previous studies about the role of eddies were usually associated with their dynamic transports of conventional quantities, such as momentum, heat and energy. In many aspects, the observed climate state is related to these transports. For instance, the maintenance of tropical easterlies and midlatitude westerlies is due to the eddy momentum transport (Starr, 1948); the adjustment of midlatitude temperature structure is attributed to the eddy heat transport (Stone, 1978; Stone and Carlson, 1979).

Quasi-geostrophic potential vorticity (QGPV) is a more useful property which has been increasingly used in theoretical and diagnostic studies of eddy transports. In the absence of diabaticity and dissipation, QGPV is conserved in the Eulerian framework (Charney and Stern, 1962). Similarly, the E-P flux (Eliassen and Palm, 1961) is also a powerful tool in studying the eddy forcing of zonal mean states. It combines both the meridional eddy momentum flux and the meridional eddy heat

flux. The divergence of the E-P flux is in fact proportional to the meridional flux of QGPV (Edmon *et al.*, 1980). Both QGPV and the E-P flux are superior to the conventional properties in diagnosing meridional eddy transports. However, quasi-geostrophy can not describe the effect of vertical eddy heat transports because it assumes a constant static stability.

In addition to the diagnostic studies, the role of eddies in climate has been studied by using a variety of models. Those models may be divided into three classes: 1) very sophisticated, 2) very simple, and 3) intermediate.

The first class of models is referred to as the *state-of-the-art* general circulation models (GCMs) which usually have multiple vertical layers, high horizontal resolutions and three-dimensional structure. They are based on the primitive equations and include sophisticated schemes for diabatic heating and dissipation. They calculate large-scale eddy transports explicitly instead of parameterizing them. Their advantage is to allow one to compare the three-dimensional structure of model results to the real atmosphere. But, the computation quantity is tremendous in those models, so that it is impractical to carry out numerical experiments that require very long time integrations or varying multiple parameters. Besides, the GCM results are very sensitive to the subgrid scale parameterizations. For instance, in the GISS (Goddard Institute for Space Studies) "Model I" GCM, the vertical eddy heat fluxes were very different when the moist adiabatic adjustment was used from those when the penetrative convection scheme was used to parameterize cumulus convection. In the latter, the small scale (subgrid) flux was 75% larger and the large scale (explicitly resolved) flux was 50% smaller (Stone and Risbey, 1990). In fact, the subgrid scale parameterizations are different from each other in current GCMs. All

of the GCMs are tuned to the current climate, explicitly or implicitly. In this sense, the GCMs are not much superior to simple climate models in simulating climate and climate changes.

The second class of models consists of the simple climate models (e.g. Budyko, 1969; Sellers, 1969; Stone, 1972; Saltzman, 1968; Eliasen, 1982). Those models have only one or two spatial dimensions. They are used in studying the climatic sensitivity, e.g., how the climate is sensitive to changes in the solar constant, in surface features, in radiative absorbing materials and in the planet's rotation rate. The effects of large-scale eddies are parameterized in these models. These parameterizations, by and large, are based on empirical relationships and differ from each other. Even though they are plausible and give reasonable results, none of them can be said to have a rigorous theoretical basis or wide acceptance.

The third class of models is of intermediate complexity, represented by the two-level, highly truncated models which are often referred to as low order models. They also explicitly calculate eddy transports, although, only for some leading components. They usually incorporate simple parameterizations of diabatic heating and friction. Like the second class of models, their main use is not to simulate the real climate. Instead, they belong to the "process-study models". Although the low order model results are not directly comparable to observations, they allow for easier interpretation of the dynamics involved, longer integrations, and more parameter experiments.

Depending on which eddy-mean flow interactions they have included, low order models can be further divided into three subclasses. The simplest one includes single zonal wave models with a single meridional mode, which has a constant static sta-

bility (e.g., Salmon, 1980; Thompson, 1987; and Vallis, 1987). The meridional eddy momentum flux and the vertical eddy heat flux are precluded. The effects of eddies in those models are entirely represented by the meridional eddy heat transport. Clearly, there are no wave-wave interactions in these models.

Another subclass includes models with more meridional modes but also with a constant static stability (e.g., Charney, 1959; Galin and Kirichkov, 1979a; Cehelsky and Tung, 1987; O'Brien and Branscome, 1989). Those models include meridional eddy fluxes of both heat and momentum. Some of them with more zonal waves also include wave-wave interactions. Therefore, the dynamics of eddy transports are better represented. But, they preclude interactions between the vertical eddy heat flux and the static stability.

The more complicated subclass is similar to the second one but the models have variable static stability (e.g., Bryan, 1959; Lorenz, 1963; Held and Suarez, 1978). Thus, they include the vertical eddy heat flux in addition to the meridional eddy fluxes of heat and momentum. They are the most reasonably simplified models to study the role of large-scale eddies. However, it should be pointed out that Held and Suarez's model has reached the edge of the GCM class in spite of its two vertical layers and two zonal waves. It is based on the primitive equations. It has a relatively high meridional resolution and complicated parameterizations of diabatic heating and dissipation. In order to carry out comprehensive parameter experiments, a simpler model is more desirable.

Compared to the sophisticated GCMs, low order models have much coarser resolutions in both horizontal and vertical directions. This seems not to be a serious problem in climate studies of large-scale processes. Diagnostic studies of atmo-

spheric energetics (e.g., Saltzman, 1971; Oort and Peixoto, 1974; Kung and Tanaka, 1983) have shown two important features:

1) Most of the eddy-mean flow interactions take place in a few large-scale waves;

2) Interactions between different zonal waves are weaker than the direct interactions of individual waves with the mean flow.

The first feature implies that the waves with short vertical wavelengths, which can not be well resolved by two-level models, are not important because they are associated with small horizontal scales. These small-scale and shallow waves are not efficient in transporting heat and momentum. They are usually confined to the lower part of the atmosphere and are prone to dissipation. The second feature implies that nonlinear wave-wave interactions play a relatively small role, therefore, low-order truncations of the zonal wavenumber spectrum are reasonable.

However, very low horizontal resolutions did cause problems in low order models. Even though the meridional eddy heat transport may be satisfactorily represented in very low order models, the eddy momentum transport and kinetic energy spectrum are often distorted due to insufficient resolution. Moreover, Cehelsky and Tung (1987) have shown that the multi-equilibrium phenomenon, which appears in very low order models but disappears in the relatively high order model ("full nonlinear model"), might be due to the very high truncations. O'Brien and Branscome (1989) found that, in a model with only two zonal waves and two meridional modes, most of the energy was built up in the shortest scale – a phenomenon termed "spectral blocking". As argued by Cehelsky and Tung (1989), the problems with very low order models are due to the fact that the energy and enstrophy undergo numer-

ous reflections in the limited spectral domain, and bounce around among the few retained modes.

Compared to sophisticated GCMs, most low order models have much simpler physics. Diabatic heating and friction are often incorporated in some simple formulations, such as Ekman pumping and Newtonian cooling. Topography and hydrology are often omitted. When topography is omitted, the models exhibit a single well-defined mean state. Although the transports by stationary eddies associated with the topography are precluded, they are relatively weak in annual mean states compared with the transports by transient eddies. This has been shown in observations and model results. For instance, in Cehelsky and Tung (1987)'s calculations, topography seems to have little effect on the *total* eddy heat transport, partly because of the dominance of transient eddies and partly because of the feedback mechanism in the model. When hydrology is omitted, the main differences are found in the low latitudes. For instance, in Held and Suarez (1978)'s experiments, the maintenance of static stability in low latitudes was markedly different in the dry and moist models. However, the differences between the dry and moist models, in either meridional or vertical eddy heat fluxes, were more likely quantitative rather than qualitative.

Low order models have been extensively used in climate studies. The numerical results with low order models can be used as a guidance for sophisticated climate modeling with the complex GCMs, because many parameter experiments and long time integrations can be done rapidly and inexpensively with low order models. They can also be used to validate empirical parameterizations used in simple climate models, because eddy transports can be calculated explicitly.

Although the role of eddies was embodied in the climate studies with various

models, only the overall effect of eddy transports was considered. The question of how different eddy transport processes interact with each other to affect the mean states has not yet been comprehensively studied. Simmons and Hoskins (1978, 1980) noted that the eddy momentum transport plays an important role in the barotropic stabilizing process of a life cycle of baroclinic waves. This role is the opposite of that played by the eddy heat transport. It restores the meridional temperature gradient which has been reduced by the poleward eddy heat flux. But, the time scale of the life cycle of waves is much shorter than that of climate variations. The role played by eddies on the time scale of climate variations is still not clear.

There is another question which has not been adequately addressed by the previous diagnostic and modeling studies, i.e., how the eddy transports are affected by the external parameters, such as diabaticity and dissipation. In particular, how do the meridional eddy momentum transports interact with the meridional eddy heat transports, and how do the vertical eddy heat transports influence the meridional heat transport, when those external parameters are changing? The significance of understanding these dynamical processes is to clarify the physical mechanisms behind climatic sensitivities and climate changes.

Recently, Stone and Branscome (1991) have investigated the role of eddies in the diabatically forced nearly inviscid eddy regime. The approach they used is a scaling analysis and numerical calculations with a low order model. The scaling analysis was performed in the quasi-geostrophic system. They defined a feedback factor which equals the ratio of the equatorward heat transport by the Ferrel cell to the poleward heat transport by eddies. If this factor equals unity then there is a complete feedback, i.e., there is no net eddy forcing of mean states. If the

factor equals zero then there is no feedback at all, i.e., the eddy heat transport is totally dominant. Stone and Branscome have shown that this factor is determined primarily by the strength of diabatic heating and other internal parameters.

The model they used is a β-plane model with constant static stability. It retained (typically) five zonal waves and five meridional modes. It was used to calculate numerically the feedback factor in a number of parameter experiments. The varying external parameters included the pole-to-equator temperature gradient in the radiative equilibrium, the Newtonian cooling time, the surface drag and the static stability. The model calculations supplemented and confirmed the scaling method. When the diabatic heating was enhanced, either by increasing the forcing temperature gradient or by decreasing the Newtonian cooling time, the feedback factor was reduced. In fact, this factor is very small for the midlatitude atmosphere. In other words, the poleword eddy heat transport is dominant in the forcing of zonal mean states.

The concept of feedback factor used by Stone and Branscome is identical to the E-P flux. The feedback by the Ferrel cell heat transport is equivalent to the feedback by the eddy momentum transport (Stone and Branscome, 1991). Although this concept is a useful tool in diagnosing interactions associated with meridional transports, it says nothing about vertical eddy heat transports if the static stability is fixed. Since the interaction between the vertical eddy heat transport and the static stabilty is an integral part of the eddy forcing of mean states, it is necessary to include this effect in the diagnostics and modeling studies. Perhaps because of the absence of this effect in Stone and Branscome's model, the meridional temperature gradient in the climate equilibrium is appreciably supercritical to that for baroclinic instablity,

in the sense of Phillips' two-level model; the eddy heat flux is extremely sensitive to the temperature gradient in that model, being proportional to the gradient to a power of about fifteen.

Clearly, more complete low order models, which allow the vertical eddy heat transport to interact with the static stability, are desirable to carry out numerical experiments similar to those performed by Stone and Branscome (1991). This mechanism can be included only in the vertically mean sense, because the vertical structure of static stability can not be resolved by two-level models. Nevertheless, the temporal and horizontal variations of static stability will bring out insights which were obscured by the models with fixed static stability. The concepts of feedback factor and the E-P flux are still useful in this kind of model, but the results will be modified by involving a variable static stability. More importantly, in this kind of model, static stability is an internal variable rather than an external parameter. It is determined by other "real" external parameters such as diabatic heating and friction. We will see if the model results would be significantly different from those calculated in the models with fixed static stability.

In the present study, we will use two kinds of low order models to extend Stone and Branscome's study: one is similar to their model except that it is on a sphere; the other is also on a sphere but with variable static stability. The purpose of including spherical geometry is not an attempt to simulate the general circulation in low latitudes. Instead, it is for better describing the meridional eddy momentum flux, which may be distorted in the β-plane models due to the rigid lateral walls. The first kind of model can be used to check the results obtained from the β-plane model of Stone and Branscome, and to understand the effect of spherical geometry.

Our main interest is in the second kind of model and in the effect of interactions associated with the vertical eddy heat flux. Similarly, we will carry out a series of parameter experiments to examine how eddies and zonal mean states are sensitive to external changes. The emphasis is put on the interaction between large-scale eddies and the midlatitude temperature structure.

Chapter 3

Model description

3.1 Basic equations

There has been a variety of two-level models in the literature, based on different simplifications of the basic equations, spatial domains, vertical coordinates, boundary conditions, horizontal resolutions, included physics, etc. The models used in this study are "filtered", in spherical-pressure coordinates, without vertical motion at the top, and without topography and hydrology. Nonlinear and linear balance equation approximations are used in two different dynamical regimes, i.e., the Hadley regime and the eddy regime, respectively. Ageostrophic temperature advection is omitted or included according to whether static stability is fixed or variable. Symmetry with respect to the equator is assumed. The spectral truncation is highly variable and will be discussed in detail in the relevant chapters.

Following conventional notations, the horizontal wind $\vec{V}$ can be written as

$$\vec{V} = \vec{V}_g + \vec{V}_a = \vec{k} \times \nabla\psi + \nabla\varphi, \tag{3.1}$$

where $\vec{V}_g$ is geostrophic wind, $\vec{V}_a$ is ageostrophic wind, ψ is stream function, φ is

velocity potential, and $\vec{k}$ is a vertical unit vector. The vorticity ζ and the divergence δ are expressed as

$$\zeta = \nabla^2\psi, \qquad \delta = \nabla^2\varphi. \tag{3.2}$$

Simplified vorticity and divergence equations, instead of momentum equations, are commonly used in "filtered" models. The order of approximation of a system is indicated by the simplification of the divergence equation. For instance, if the *nonlinear balance equation* approximation is used in the two-level model, the nondimensionalized divergence equation becomes:

$$\nabla^2\hat{\Phi} = 2\nabla\cdot(\mu\nabla\hat{\psi}) + \nabla\cdot[\nabla^2\bar{\psi}\nabla\hat{\psi} + \nabla^2\hat{\psi}\nabla\bar{\psi} - \nabla(\nabla\bar{\psi}\cdot\nabla\bar{\psi})], \tag{3.3}$$

where Φ is the geopotential; $\bar{(\,)} = \frac{1}{2}[(\,)_1 + (\,)_3]$, $\hat{(\,)} = \frac{1}{2}[(\,)_1 - (\,)_3]$. The subscripts 1 and 3 denote the upper level (i.e., 250 mb) and the lower level (i.e., 750 mb) respectively. The associated vorticity equations, also in nondimensionalized form, are

$$\begin{aligned}
\frac{\partial}{\partial t}\nabla^2\bar{\psi} = &- J(\bar{\psi},\nabla^2\bar{\psi}) - J(\hat{\psi},\nabla^2\hat{\psi}) - 2\frac{\partial\bar{\psi}}{\partial\lambda} - 2\nabla\cdot(\mu\nabla\bar{\varphi}) + \bar{\mathcal{D}} \\
&- \nabla\cdot[\nabla^2\hat{\psi}\nabla\hat{\varphi} + \nabla^2\bar{\psi}\nabla\bar{\varphi} + \nabla^2\hat{\varphi}\nabla\hat{\psi} + 2\nabla^2\bar{\varphi}\nabla\hat{\psi}], \qquad (3.4) \\
\frac{\partial}{\partial t}\nabla^2\hat{\psi} = &- J(\bar{\psi},\nabla^2\hat{\psi}) - J(\hat{\psi},\nabla^2\bar{\psi}) - 2\frac{\partial\hat{\psi}}{\partial\lambda} - 2\nabla\cdot(\mu\nabla\hat{\varphi}) + \hat{\mathcal{D}} \\
&- \nabla\cdot[\nabla^2\bar{\psi}\nabla\hat{\varphi} + \nabla^2\hat{\psi}\nabla\bar{\varphi} - \nabla^2\bar{\varphi}\nabla\hat{\psi}], \qquad (3.5)
\end{aligned}$$

where J is the Jacobian operator, i.e.,

$$J(A,B) = \frac{\partial A}{\partial\lambda}\frac{\partial B}{\partial\mu} - \frac{\partial B}{\partial\lambda}\frac{\partial A}{\partial\mu},$$

where $\mu = \cos\theta$, θ is colatitude and λ is longitude. Vertical velocity ω has been eliminated in Equations (3.4) and (3.5) through use of the continuity equation:

$$\nabla^2\varphi + \frac{\partial\omega}{\partial p} = 0. \tag{3.6}$$

The independent and dependent variables are all nondimensionalized in the spherical - pressure coordinates, in which Ω^{-1} is chosen as the characteristic time scale, a as the characteristic horizontal scale and P_0 as the characteristic vertical scale, where Ω is the angular velocity of the earth, a is the radius of the earth, and $P_0 = 1,000\,mb$. Then, t is divided by Ω^{-1}, ψ and φ by Ωa^2, Φ by $\Omega^2 a^2$, ω by ΩP_0.

The friction terms are represented by $\mathcal{D}$ in the vorticity equations. We assume a Rayleigh form of friction on the lower boundary, which is linearly damping the surface vorticity. It can be interpreted as a surface drag or Ekman pumping, depending on whether there are vertical motions on the lower boundary. We also include an interfacial stress which is proportional to the vertical shear. This is equivalent to incorporating vertical viscosity. We do not incorporate horizontal diffusion because it is relatively small. Therefore, the friction terms can be written as

$$\bar{\mathcal{D}} = k(2\nabla^2\hat{\psi} - \nabla^2\bar{\psi}), \tag{3.7}$$

$$\hat{\mathcal{D}} = -k(2\nabla^2\hat{\psi} - \nabla^2\bar{\psi}) - k'\nabla^2\hat{\psi}, \tag{3.8}$$

where k and k' are specified damping coefficients on the lower boundary and on the interface respectively, being nondimensionalized by Ω. The surface vorticity is linearly extrapolated from level 1 and 3.

If the *linear balance equation* approximation is used, then those terms in the square brackets of Equations (3.3), (3.4) and (3.5) are discarded, in order to conserve total energy (Lorenz, 1960). Further simplification can be made by setting the

Coriolis parameter f and its meridional derivative β to be constant. This simplification is often used in β-plane *quasi-geostrophic* models.

The thermodynamic equation has two different formulations in two-level models. In Phillips' (1954) model, the thermodynamic equation is written on the interface; the temperature advection by ageostrophic wind is omitted; the static stability is treated as a constant:

$$\frac{\partial \Theta_2}{\partial t} + \vec{V}_{g_2} \cdot \nabla \Theta_2 + \omega_2 \frac{\partial \bar{\Theta}}{\partial p} = \bar{Q}. \tag{3.9}$$

Through the hydrostatic relation

$$T = -\frac{p}{R}\frac{\partial \Phi}{\partial p} = \frac{2}{R}\hat{\Phi} \tag{3.10}$$

and the definition of potential temperature

$$\Theta = T\left(\frac{P_0}{p}\right)^{\kappa}, \tag{3.11}$$

where R is gas constant for dry air and $\kappa = R/C_p \simeq 2/7$, and using the boundary condition $\omega_0 = \omega_4 = 0$, Equation (3.9) can be written as

$$\frac{\partial \hat{\Phi}}{\partial t} = -J(\bar{\psi}, \hat{\Phi}) - \Gamma_0 \nabla^2 \hat{\varphi} + \bar{Q}, \tag{3.12}$$

where

$$\Gamma_0 \equiv \frac{N^2 H^2}{2\Omega^2 a^2} \sim \frac{L_r^2}{a^2},$$

N is the Brunt-Väisällä frequency, H is a scale height, and L_r is the Rossby deformation radius. Similar to Equations (3.4) and (3.5), Equation (3.12) is nondimensionalized.

In Lorenz's (1960) model, the thermodynamic equation is written on the two levels; the ageostrophic advection term is retained; the vertical mean potential temperature is represented by $\bar{\Theta} = \frac{1}{2}(\Theta_1 + \Theta_3)$, and the static stability is represented by $\hat{\Theta} = \frac{1}{2}(\Theta_1 - \Theta_3)$. The equations on the two levels are

$$\frac{\partial \Theta_1}{\partial t} + \vec{V}_1 \cdot \nabla \Theta_1 + \omega_1 \frac{\partial \Theta_1}{\partial p} = Q_1, \tag{3.13}$$

$$\frac{\partial \Theta_3}{\partial t} + \vec{V}_3 \cdot \nabla \Theta_3 + \omega_3 \frac{\partial \Theta_3}{\partial p} = Q_3, \tag{3.14}$$

where $\vec{V}_1$ and $\vec{V}_3$ are total horizontal velocity. The equation for $\bar{\Theta}$ is obtained by adding Equations (3.13) and (3.14). The equation for $\hat{\Theta}$ is obtained by subtracting Equation (3.14) from Equation (3.13). They are written as

$$\frac{\partial \bar{\Theta}}{\partial t} + \bar{\vec{V}} \cdot \nabla \bar{\Theta} + \hat{\vec{V}} \cdot \nabla \hat{\Theta} - \omega_2 \frac{\hat{\Theta}}{\Delta p} = \bar{Q}, \tag{3.15}$$

$$\frac{\partial \hat{\Theta}}{\partial t} + \bar{\vec{V}} \cdot \nabla \hat{\Theta} + \hat{\vec{V}} \cdot \nabla \bar{\Theta} = \hat{Q}, \tag{3.16}$$

where $\Delta p = p_3 - p_1$.

There is an essential difference between Lorenz's formulation and Phillips' formulation. For example, if we assume in Equation (3.15) $\hat{\Theta}$ is constant, $\vec{V}$ is replaced by $\vec{V}_g$, and $\frac{\hat{\Theta}}{\Delta p} = \frac{\Theta_1 - \Theta_3}{2\Delta p} \simeq -\frac{1}{2}\frac{\partial \bar{\Theta}}{\partial p}$, then the equation becomes

$$\frac{\partial \bar{\Theta}}{\partial t} + \bar{\vec{V}}_g \cdot \nabla \bar{\Theta} + \omega_2 (\frac{1}{2}\frac{\partial \bar{\Theta}}{\partial p}) = \bar{Q}. \tag{3.17}$$

Compared to Equation (3.9), the static stability is reduced by a half. This difference has been noticed by Hollingsworth (1975) and Arakawa and Moorthi (1988). The reason is that Equation (3.9) is just for the interface of the model, while Equation (3.17) is for the vertical mean of the model. Because of the higher vertical resolution for Θ, Lorenz's formulation is superior to Phillips' formulation in two aspects: 1) the static stability is variable; 2) the vertical mean potential temperature equation is more reasonable. When Phillips' formulation is used to study the

vertical mean heat budget, one must take caution in interpreting the value of static stability.

Likewise, we use nondimensional $\hat{\Phi}$ to represent $\bar{\Theta}$, and introduce a nondimensional parameter

$$\Gamma \equiv \frac{N^2 H^2}{4\Omega^2 a^2}$$

to represent $\hat{\Theta}$. Equations (3.15) and (3.16) can be written as

$$\frac{\partial \hat{\Phi}}{\partial t} = -J(\bar{\psi}, \hat{\Phi}) - J(\hat{\psi}, \Gamma) - \nabla \cdot (\Gamma \nabla \hat{\varphi}) - \nabla \cdot (\hat{\Phi} \nabla \bar{\varphi}) + \bar{\mathcal{Q}}, \tag{3.18}$$

$$\frac{\partial \Gamma}{\partial t} = -J(\bar{\psi}, \Gamma) - J(\hat{\psi}, \hat{\Phi}) - \nabla \cdot (\Gamma \nabla \bar{\varphi}) - \nabla \hat{\Phi} \cdot \nabla \hat{\varphi} + \hat{\mathcal{Q}}. \tag{3.19}$$

$\mathcal{Q}$ represents diabatic heating in the system. We use the Newtonian cooling form, i.e., $(T_E - T)/\tau_h$, as the differential heating. T_E is a specified equilibrium (or "target") temperature which may be regarded as the temperature in either *radiative equilibrium* or *radiative -convective equilibrium*, depending on which scheme is used to calculate T_E. We are mainly concerned about the pole-to-equator temperature gradient in the equilibrium state because it is the most important factor in the climate. Therefore, we represent T_E in terms of a second order Legendre function, which is the dominant component in either radiative equilibrium or radiative-convective equilibrium. τ_h is a thermal relaxation time, which is inversely proportional to the Newtonian cooling rate, h. In our notations, the diabatic heating terms can be written as

$$\bar{\mathcal{Q}} = h(\hat{\Phi}_E - \hat{\Phi}), \tag{3.20}$$

$$\hat{\mathcal{Q}} = h(\Gamma_E - \Gamma), \tag{3.21}$$

where h is nondimensionalized by Ω. $\hat{\Phi}_E$ and Γ_E are equivalent to the mean temperature and the static stability in the equilibrium.

We note that there are six variables $(\bar{\psi}, \hat{\psi}, \bar{\varphi}, \hat{\varphi}, \hat{\Phi}, \Gamma)$, but only five basic equations in the model with variable static stability. Lorenz (1960) assumed that there were no vertical motions on the top and bottom boundaries, so that $\bar{\varphi}$ vanished. These boundary conditions would yield vertically symmetric mean meridional circulations with centers at the middle level. Another way to close the equations is to assume a nonzero vertical velocity on the lower boundary introduced by an Ekman pumping. In this case, the mean meridional circulations are no longer vertically symmetric.

3.2 Spectral representations

We will solve the system in the spectral domain. The spectral form is convenient to represent eddies explicitly and easy to adjust horizontal resolutions of the model by adding or substracting wave modes. It also has many advantages in numerical computations, e.g., eliminating aliasing and conserving integral constraints such as energy and enstrophy.

We represent all variables in terms of spherical harmonics,

$$\tilde{\phi} = \sum_{\gamma} \tilde{\phi}_{\gamma}(t) Y_{\gamma}(\lambda, \mu),$$

where $\tilde{\phi} = (\bar{\psi},\ \hat{\psi},\ \bar{\varphi},\ \hat{\varphi},\ \hat{\Phi},\ \Gamma)$, $\gamma = n_{\gamma} + \mathrm{i} l_{\gamma}$ represents a wave vector index in terms of rank and degree of the solid harmonic,

$$Y_{\gamma}(\lambda, \mu) = P_{\gamma}(\mu) e^{i l_{\gamma} \lambda}, \tag{3.22}$$

which is the eigenfunction on a sphere and satisfies the equation

$$\nabla^2 Y_{\gamma} = -n_{\gamma}(n_{\gamma} + 1) Y_{\gamma}. \tag{3.23}$$

For $l_\gamma = 0$, the spectral coefficient is real, and it represents a meridional mode of the zonal mean state. For $l_\gamma \neq 0$, the spectral coefficient is complex, and it represents a wave component with zonal wavenumber l_γ.

In our model, the stream function is assumed to be antisymmetric to the equator and represented by odd spherical harmonics (n_γ is odd). The geopotential and the velocity potential are assumed to be symmetric to the equator and have even parity of harmonics (n_γ is even). These spectral representations are self-consistent in the equations. They describe approximately the distributive characteristics of the annual mean atmosphere.

We use a rhomboidal truncation with M zonal wavenumbers and N meridional modes. The fundamental zonal wavenumber is denoted by m, i.e., all of the zonal wavenumbers are multiples of m. The truncation level is then indicated by $M \times N(m)$. Here we will not specify M, N and m *a priori*. The appropriate truncation level and fundamental wavenumber will be investigated in the resolution experiments.

The procedure of spectral transformation is essentially the Galerkin method, which has been described by Siberman (1954), Platzman (1962), and others. In the equations, all linear terms transform to be a constant times the spectral coefficient, while the nonlinear terms transform into a sum of the product of two spectral coefficients modified by a constant which is referred to as the " interaction coefficient". Basically, only two types of interaction coefficient are generated. They are integrals of trigonometric polynomial representations of associated Legendre functions, i.e.,

$$\mathcal{K}_{\alpha\beta\gamma} = \int_{-1}^{1} P_\gamma (l_\beta P_\beta \frac{dP_\alpha}{d\mu} - l_\alpha P_\alpha \frac{dP_\beta}{d\mu}) d\mu, \tag{3.24}$$

$$\mathcal{M}_{\alpha\beta\gamma} = \int_{-1}^{1} P_\alpha P_\beta P_\gamma d\mu. \tag{3.25}$$

The procedure for calculating the first type of integrals ($\mathcal{K}$) has been discussed by Baer and Platzman (1961). The second type ($\mathcal{M}$) can be calculated in a similar way.

Chapter 4

Hadley regime

4.1 Introduction

Although the main focus of this study is the eddy regime rather than the axisymmetric or Hadley regime, it is interesting to know the basic flow which is driven by a simple diabatic forcing, while large-scale baroclinic and barotropic instabilities are absent. Since large-scale eddies arise from these instabilities of the basic flow, it is important to know the structure of the basic flow in the Hadley regime. This basic flow will be used in linear analyses of instability, and in the initialization of the nonlinear eddy regime in time integrations.

There have been many theoretical and numerical works on the axisymmetric regime. Among them, Held and Hou (1980) proposed an approximate theory, in which the fluid is nearly inviscid and the poleward flow of the Hadley cell is nearly angular momentum conserving. They used a simple Newtonian cooling form of radiative forcing, and assumed conservation of potential temperature, Θ, as well as continuity of Θ at the polar boundary of the Hadley cell. They also assumed that

the static stability is unaffected by the circulation, and that the vertical profiles of zonal wind, u, and Θ are self-similar. Their theory predicted such features of the tropospheric circulation as the width of Hadley cell, the position of the subtropical jet, the distribution of the surface wind and the meridional heat and momentum fluxes. They also used a primitive equation model with a fine resolution mesh to calculate the numerical solutions in the inviscid limit. Their theoretical predictions are in good agreement with the numerical results.

It is not our intention to explore the theory of axisymmetric circulation in this study. However we did repeat Held and Hou's numerical experiments with our two-level model, to see whether it can reproduce their results. This is an indirect test of the adequacy of our model's vertical resolution and the balance equation.

4.2 Equations in the Hadley regime

We use the *nonlinear balance equation* system to calculate the numerical solutions of the axisymmetric circulation. The basic equations are simplified by omitting all terms related to zonal eddies. Consistent with the theory and numerical calculations of Held and Hou (1980), we assume that the Newtonian cooling rate, the interfacial friction coefficient and the static stability parameter are all constants. We also assume a similar structure of radiative equilibrium temperature (the second order Legendre polynomial) but with a more realistic pole-to-equator temperature difference. The simplified equations are:

$$\frac{\partial}{\partial t}\nabla^2\bar{\psi} = -\nabla\cdot[\nabla^2\hat{\psi}\nabla\hat{\varphi} + \nabla^2\bar{\psi}\nabla\bar{\varphi} + \nabla^2\hat{\varphi}\nabla\hat{\psi} + 2\nabla^2\bar{\varphi}\nabla\hat{\psi}]$$

$$-\nabla\cdot(2\mu\nabla\bar{\varphi}) - k(\nabla^2\bar{\psi} - 2\nabla^2\hat{\psi}), \tag{4.1}$$

$$\frac{\partial}{\partial t}\nabla^2\hat{\psi} = -\nabla\cdot[\nabla^2\bar{\psi}\nabla\hat{\varphi} + \nabla^2\hat{\psi}\nabla\bar{\varphi} - \nabla^2\bar{\varphi}\nabla\hat{\psi}] - \nabla\cdot(2\mu\nabla\hat{\varphi}) + k(\nabla^2\bar{\psi} - 2\nabla^2\hat{\psi}) - k'\nabla^2\hat{\psi}, \tag{4.2}$$

$$\frac{\partial}{\partial t}\hat{\Phi} = -\Gamma_0\nabla^2(\bar{\varphi} + \hat{\varphi}) + h(\hat{\Phi}_E - \hat{\Phi}), \tag{4.3}$$

$$\nabla^2\hat{\Phi} = \nabla\cdot(2\mu\nabla\hat{\psi}) + \nabla\cdot[\nabla^2\bar{\psi}\nabla\hat{\psi} + \nabla^2\hat{\psi}\nabla\bar{\psi} - \nabla(\nabla\bar{\psi}\cdot\nabla\bar{\psi})], \tag{4.4}$$

$$\nabla^2\bar{\varphi} = \frac{k_E}{2\mu}(\nabla^2\bar{\psi} - 2\nabla^2\hat{\psi}). \tag{4.5}$$

Zonal averaging has been performed on the equations. Therefore the Jacobian terms and the zonal derivative terms have disappeared. The gradient, the divergence and the Laplacian operators have actually become only meridional derivatives. The continuity equation has been used, particularly,

$$\omega_2 = -\frac{1}{2}\nabla^2(\hat{\varphi} + \bar{\varphi}), \tag{4.6}$$

$$\omega_4 = -\nabla^2\bar{\varphi}. \tag{4.7}$$

where ω_4 is the vertical velocity on the lower boundary, introduced by an Ekman pumping formulation and proportional to the surface vorticity.

The reason for using the Ekman friction, instead of assuming $\bar{\varphi} = 0$, to close the equations is to simulate more realistic mean meridional circulations which are not necessarily vertically symmetric. In addition, in two-level models with quasi-geostrophic or linear balance equation approximations, the formulation for the Ekman friction is identical to that for the surface drag. For instance, in Equations (4.1) and (4.2), the terms associated with vertical velocities are $-2\mu\nabla^2\bar{\varphi}$ and $-2\mu\nabla^2\hat{\varphi}$. By using Equations (4.5), (4.6) and (4.7), we can show

$$-2\mu\nabla^2\bar{\varphi} = -k_E(\nabla^2\bar{\psi} - 2\nabla^2\hat{\psi}), \tag{4.8}$$

$$-2\mu\nabla^2\hat{\varphi} = -2\mu\nabla^2(\hat{\varphi} + \bar{\varphi}) + k_E(\nabla^2\bar{\psi} - 2\nabla^2\hat{\psi}). \tag{4.9}$$

The Ekman friction appearing in the vorticity equations has the same formulation as the surface drag. Therefore, we will omit the surface drag by setting $k = 0$. However, the different lower boundary conditions do lead to different vertical structures of mean meridional circulations.

The Ekman damping rate is represented by $\frac{k_E}{2\mu}$, where k_E is a specified constant. In the conventional formula for the Ekman pumping, the Coriolis parameter is assumed to be constant. This is equivalent to replacing μ by a constant μ_0 in our formulation. Thus, the Ekman damping rate is independent of latitude. However, because φ (and ω) is symmetric to the equator and ψ is antisymmetric to the equator, μ has to be an odd function of latitude in order to satisfy Equation (4.5). This requires the Coriolis parameter f, which enters the Ekman damping coefficient, to be a function of latitude. Similar treatment has been used by Baer and Alyea (1971) to represent a heating function. Although $\mu = 0$ at the equator, it is not a singular point in our model because the vorticity also vanishes at the equator.

The external parameters are chosen as the realistic values for the earth's atmosphere, i.e.,

$$\tau_h = 20\,days,\ \tau_E = 5\,days,\ N^2 = 10^{-4}\,s^{-2},\ \Delta T_E = 48\,K,$$

where τ_E is the relaxation time for the Ekman damping ($\tau_E = \frac{1}{2k_E}$), and ΔT_E is the pole-to-equator temperature difference in the radiative equilibrium. In our inviscid limit experiments, the relaxation time for interfacial friction is chosen to vary from 20 to 640 days, which is equivalent to a vertical viscosity coefficient varying from 32 to $1\,m^2/s$. The system of equations is truncated by keeping 20 meridional modes on a hemisphere. Higher resolution is required when the viscosity is weaker. Therefore, we represent the stream function and the velocity potential as:

$$\bar{\psi} = \bar{\psi}_1 P_1 + \bar{\psi}_3 P_3 + \cdots + \bar{\psi}_{39} P_{39}, \tag{4.10}$$

$$\hat{\psi} = \hat{\psi}_1 P_1 + \hat{\psi}_3 P_3 + \cdots + \hat{\psi}_{39} P_{39}, \tag{4.11}$$

$$\bar{\varphi} = \bar{\varphi}_2 P_2 + \bar{\varphi}_4 P_4 + \cdots + \bar{\varphi}_{40} P_{40}, \tag{4.12}$$

$$\hat{\varphi} = \hat{\varphi}_2 P_2 + \hat{\varphi}_4 P_4 + \cdots + \hat{\varphi}_{40} P_{40}. \tag{4.13}$$

The spectral forms of Equations (4.1)-(4.5) in the steady state are:

$$\begin{aligned}
\sum_{\beta}\sum_{\gamma}[\mathcal{H}^{(2)}_{\alpha\beta\gamma}\hat{\psi}_\beta\hat{\varphi}_\gamma &+ \mathcal{H}^{(1)}_{\alpha\beta\gamma}(\bar{\psi}_\beta\bar{\varphi}_\gamma + 2\bar{\varphi}_\beta\hat{\psi}_\gamma)] \\
&+ c_\alpha^{-1}(L_{\alpha+1}\bar{\varphi}_{\alpha+1} + L_\alpha\bar{\varphi}_{\alpha-1}) = 0, \qquad (4.14)\\
\sum_{\beta}\sum_{\gamma}[\mathcal{H}^{(1)}_{\alpha\beta\gamma}\bar{\psi}_\beta\hat{\varphi}_\gamma &+ \mathcal{H}^{(3)}_{\alpha\beta\gamma}\hat{\psi}_\beta\bar{\varphi}_\gamma] - k'\hat{\psi}_\alpha \\
&+ c_\alpha^{-1}(L_{\alpha+1}\hat{\varphi}_{\alpha+1} + L_\alpha\hat{\varphi}_{\alpha-1}) = 0, \qquad (4.15)\\
\sum_{\beta}\sum_{\gamma}[\mathcal{H}^{(4)}_{\alpha+1\beta\gamma}\bar{\psi}_\beta\hat{\psi}_\gamma] &+ \frac{\Gamma_0}{h}c_{\alpha+1}(\bar{\varphi}_{\alpha+1} + \hat{\varphi}_{\alpha+1}) + \hat{\Phi}_{E_{\alpha+1}} \\
&+ c_{\alpha+1}^{-1}(L_{\alpha+1}\hat{\psi}_\alpha + L_{\alpha+2}\hat{\psi}_{\alpha+2}) = 0, \qquad (4.16)\\
\mathcal{H}^{(5)}_{\alpha,\alpha+1}\bar{\varphi}_{\alpha+1} &+ \mathcal{H}^{(5)}_{\alpha,\alpha-1}\bar{\varphi}_{\alpha-1} - k_E(\bar{\psi}_\alpha - 2\hat{\psi}_\alpha) = 0, \qquad (4.17)\\
\alpha &= 1, 3, \cdots, 39,
\end{aligned}$$

where $\hat{\Phi}$ has been eliminated through the nonlinear balance equation. The coefficients are defined as follows:

$$\mathcal{H}^{(1)}_{\alpha\beta\gamma} = \frac{c_\beta}{2c_\alpha}(c_\alpha + c_\gamma - c_\beta)\mathcal{M}_{\alpha\beta\gamma}, \tag{4.18}$$

$$\mathcal{H}^{(2)}_{\alpha\beta\gamma} = \mathcal{H}^{(1)}_{\alpha\beta\gamma} + \mathcal{H}^{(1)}_{\alpha\gamma\beta}, \tag{4.19}$$

$$\mathcal{H}^{(3)}_{\alpha\beta\gamma} = \mathcal{H}^{(1)}_{\alpha\beta\gamma} - \mathcal{H}^{(1)}_{\alpha\gamma\beta}, \tag{4.20}$$

$$\mathcal{H}^{(4)}_{\alpha\beta\gamma} = \frac{2c_\beta c_\gamma}{c_\alpha}\mathcal{M}_{\alpha\beta\gamma}, \tag{4.21}$$

$$\mathcal{H}^{(5)}_{\alpha,\beta} = \frac{2c_\beta}{c_\alpha}\int_{-1}^{1} P_\alpha P_\beta \mu \, d\mu, \tag{4.22}$$

$$c_\alpha = n_\alpha(n_\alpha+1), \tag{4.23}$$

$$L_\alpha = 2\int_{-1}^{1} P_\alpha[(1-\mu^2)\frac{dP_{\alpha-1}}{d\mu} - c_{\alpha-1}\mu P_{\alpha-1}]\, d\mu. \tag{4.24}$$

All together we have 80 quadratic equations. The summation terms in these equations include all retained meridional modes of ψ and φ.

The zonal mean flow, $[u]$, $[v]$, temperature, $[T]$, and vertical velocity , $[\omega]$, can be readily constructed from the spectral coefficients of ψ, φ and $\hat{\Phi}$. By definition,

$$[\bar{u}] = \frac{1}{a}\frac{\partial[\bar{\psi}]}{\partial\theta} = \frac{1}{a}\sum_\alpha \bar{\psi}_\alpha \frac{\partial P_\alpha}{\partial\theta}, \tag{4.25}$$

$$[\hat{u}] = \frac{1}{a}\frac{\partial[\hat{\psi}]}{\partial\theta} = \frac{1}{a}\sum_\alpha \hat{\psi}_\alpha \frac{\partial P_\alpha}{\partial\theta}, \tag{4.26}$$

$$[\bar{v}] = -\frac{1}{a}\frac{\partial[\bar{\varphi}]}{\partial\theta} = -\frac{1}{a}\sum_\alpha \bar{\varphi}_{\alpha+1} \frac{\partial P_{\alpha+1}}{\partial\theta}, \tag{4.27}$$

$$[\hat{v}] = -\frac{1}{a}\frac{\partial[\hat{\varphi}]}{\partial\theta} = -\frac{1}{a}\sum_\alpha \hat{\varphi}_{\alpha+1} \frac{\partial P_{\alpha+1}}{\partial\theta}, \tag{4.28}$$

$$[\bar{\omega}] = -\frac{1}{2}[\nabla^2(\hat{\varphi}+\bar{\varphi})] = \frac{1}{2}\sum_\alpha c_{\alpha+1}(\hat{\varphi}_{\alpha+1}+\bar{\varphi}_{\alpha+1})P_{\alpha+1}, \tag{4.29}$$

$$[\bar{T}] = \frac{2}{R}[\hat{\Phi}] = \frac{2}{R}\sum_\alpha \hat{\Phi}_{\alpha+1}P_{\alpha+1}. \tag{4.30}$$

Through the continuity equation we can define a stream function, χ, for the mean meridional circulation.

$$\frac{\partial[\chi]}{\partial\theta} = -[\omega]a\sin\theta, \tag{4.31}$$

$$\frac{\partial[\chi]}{\partial p} = -[v]\sin\theta. \tag{4.32}$$

4.3 Numerical solutions

There are two kinds of numerical methods to solve Equations (4.14)-(4.17). One is by integrating the time-dependent version of these equations until a steady state is achieved. The other is by using the Newton-Raphson iterative method (Press *et al.*, 1986) to solve the steady equations. Because of its fast convergence rate, the Newton-Raphson method is more efficient for this particular set of equations. The iteration converges very rapidly if the initial guess is close to the solution. Different initial values have been tested, but the values always converged to a unique solution. Therefore, we use the Newton-Raphson method for the following experiments.

The experiments are similar to the inviscid limit experiments by Held and Hou (1980). We decrease the interfacial friction gradually to see how the numerical solutions approach the theoretical solutions. The zonal wind, $[u]$, and the MMC stream function, $[\chi]$, are shown in Figures 4.1 and 4.2. Here $[\chi]$ has been calculated by vertical integrations of Equation (4.32). To represent a complete vertical structure of $[v]$, we need to know the values of $[v_0]$ and $[v_4]$ at the boundaries in addition to $[v_1]$ and $[v_3]$. They can be estimated from the steady zonal mean momentum equations:

$$-[v_i]\frac{\partial[u_i]}{a\partial\theta}+[\omega_i]\frac{\partial[u_i]}{\partial p}-f[v_i]=-k_i[u_i], \qquad i=0,\,4. \tag{4.33}$$

At the upper boundary $\omega_0 = 0$, $k_0 = 0$, thus, $[v_0] = 0$. At the lower boundary, the advection terms are relatively small, thus,

$$f[v_4] \simeq k_4[u_4], \qquad k_4 = 2k_E. \tag{4.34}$$

In general, there are broad westerlies occupying most of the area, except in the lower equatoral latitudes where easterlies are prevailing. There are deep, vertical

asymmetric Hadley cells in the low latitudes. When the interfacial friction is decreased, the subtropical jet becomes stronger and steeper, the Hadley cell becomes weaker and more narrow, and a shallow Ferrel cell on the polar side of the Hadley cell gets stronger. Although the peak of the jet and the core of the Hadley cell shift somewhat toward the equator, they seem to approach a limiting latitude, never violating Hide's theorem (Hide, 1969). This feature is more clearly seen in Figure 4.3. The profile of zonal wind in the nearly inviscid case is confined by the wind required for the conservation of angular momentum, U_m, on the equatoral side, and by the thermal wind in radiative equilibrium, U_E, on the polar side.

Figure 4.4 shows the momentum fluxes in the upper layer, and Figure 4.5 shows the vertically integrated heat fluxes. The solid curves are the theoretical results calculated according to Held and Hou (1980), i.e.,

$$\frac{1}{H}\int_0^H v\Theta\, dz = \frac{5}{18}\left(\frac{5}{3}\right)^{\frac{1}{2}} \frac{\Theta_0 a \Delta_H}{\tau_h} R^{\frac{3}{2}} \left[\frac{\phi}{\phi_H} - 2\left(\frac{\phi}{\phi_H}\right)^3 + \left(\frac{\phi}{\phi_H}\right)^5\right], \quad (4.35)$$

$$\frac{1}{H}\int_0^H uv\, dz \simeq \frac{\Omega a \phi^2}{\Delta_v \Theta_0}\frac{1}{H}\int_0^H v\Theta\, dz, \quad (4.36)$$

where Θ_0 is the mean potential temperature, ϕ is latitude, Δ_H and Δ_v are, respectively, the fractional change in the potential temperature from equator to pole and from the top to the bottom boundaries in the radiative equilibrium. $R = (gH\Delta_H)/(\Omega^2 a^2)$; $\phi_H = (5R/3)^{\frac{1}{2}}$, is the width of Hadley cell. They can be readily calculated from the given set of parameters in our experiments. Particularly, here $\phi_H \simeq 20°$, beyond which there is neither momentum fluxes nor heat fluxes. The numerical solution for a nearly inviscid flow is very close to the theoretical prediction. When the interfacial friction is decreased, the magnitudes and

positions of these fluxes gradually approach the theoretical values. The temperature adjustment $[T_E(\phi) - T(\phi)]$ is shown in Figure 4.6. The numerical solutions show that the adjustment occurs in the low latitudes, supporting qualitatively the "equal-area" hypothesis by Held and Hou (1980). In the mid-high latitudes, except for some wiggles which are apparently caused by the spectral truncation, the temperature is basically in radiative equilibrium.

The features of our numerical solutions are very similar to those calculated by Held and Hou, although their model is more sophisticated and its vertical resolution is much higher. The agreement implies that the two-level model can resolve the Hadley regime very well. The vertical resolution in our model does not seem to be a serious problem, since axisymmetric circulations have large vertical scales. However, a rather high meridional resolution is needed, particularly when the interfacial friction is weak, because in this case, the subtropical jet becomes very narrow. We also note that the *nonlinear balance equation* approximation, if not the *primitive equations*, must be used to obtain reasonable solutions in the Hadley regime, due to the importance of ageostrophic motions.

4.4 Instability analyses

Traditionally, linear analyses of baroclinic instability are performed on a meridionally uniform flow. Considering the sharpness of the subtropical jet in the Hadley regime, we wish to include both baroclinic and barotropic mechanisms in our analyses. In order to include the barotropic mechanism in a truncated spectral model, there must be at least two meridional modes for the zonal flow and for the eddy flow (O'Brien and Branscome, 1989). Therefore, we include meridional modes $m = 3$ and

$m = 5$ which have the largest components of eddy kinetic energy in the atmosphere (Eliasen and Machenhauer, 1965). We also noted that the instability analyses are not sensitive to the choice of meridional modes, probably due to the fact that the baroclinic mechanism is generally dominant.

The procedure for the linear analyses of instability is straightforward. At first, we linearize the basic equations in chapter 3 with respect to the steady state of the Hadley regime, and obtain a set of ordinary differential equations for the spectral components of a specified zonal wavenumber. The coefficients of the equations are functions of external parameters and the zonal wavenumber, which are all specified; therefore, they are constants in each case. Then we find eigenvalues of the equations, which correspond to wave growth rate (and phase speed). There are several pairs of eigenvalues, which are usually complex. Unless all of them have negative real parts the perturbation will grow with time and the basic flow is unstable. In the parameter space, those eigenvalues with real parts ≤ 0 form a boundary separating stable and unstable regions. Because there are many external parameters, e.g., ΔT_E, $\Gamma_0, \cdots$, the parameter space is indeed multi-dimensional. For convenience, we only consider its projections on individual parameter surfaces, so that the neutral boundary becomes a curve on those surfaces.

The wave growth rate in one of the parameter surfaces, i.e., wavenumber vs. diabatic forcing, ΔT_E, is shown in Figure 4.7. Other parameters are fixed at the realistic values for the earth's midlatitude atmosphere, i.e.,

$$\tau_h = 20\,days,\ \tau_s = 5\,days,\ N^2 = 10^{-4}s^{-2},\ k' = 0,$$

where $\tau_s = \frac{1}{2k}$ is the dissipative time for the surface drag (there is very little difference when using the Ekman friction in the analysis). Figure 4.7 looks like traditional

diagrams of baroclinic instability. There is a criterion for radiative equilibrium temperature gradient ($\Delta T_{Ec} \simeq 23\,K$) and a short wave cut-off. The growth rate increases with increasing diabatic forcing. The most unstable wave is $n = 5$, where n is the zonal wavenumber. However, the characteristics of instability are subject to changes of other parameters. For instance, if the static stabilty parameter is doubled, then the critical temperature gradient increases ($\Delta T_{Ec} \simeq 40\,K$) and the most unstable wave becomes $n = 3$ (see Figure 4.8).

A similar figure, i.e., wavenumber vs. static stability is shown in Figure 4.9. There is also a criterion for static stability. Supercritical static stabilities stabilize the basic flow and suppress wave growth. In less statically stable situations, the short wave growth rate increases dramatically. This feature is approximately similar to the analysis based on the inviscid β-plane model (Reinhold, 1986).

The Hadley regime and its instability in this chapter are preliminary studies for the role of eddies in the climate. They provide a background for eddy regimes which will be studied in the following chapters. They also show the capability of our model to study large-scale processes. The numerical results from our two-level model is surprisingly similar to those from Held and Hou's complicated model. This indicates that a properly "filtered" and "truncated" model is as useful as complicated models.

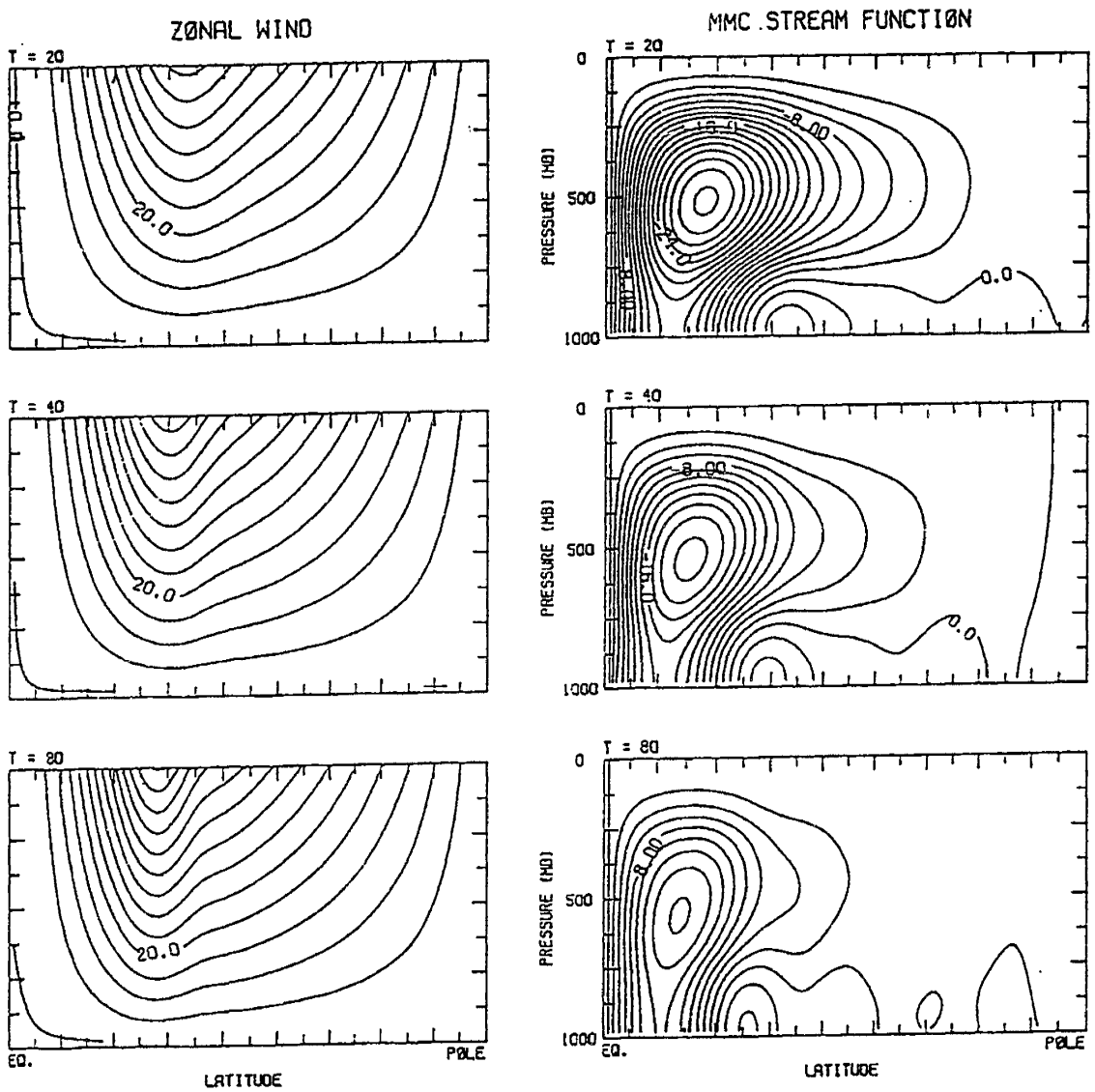

Figure 4.1: Zonal winds and MMC stream functions in the Hadley regime for T = 20, 40, 80 days, where T is the dissipative time for the interfacial friction. The contour intervals are $5\,m/s$ for $[u]$ and $2\,mb.m/s$ for $[\chi]$.

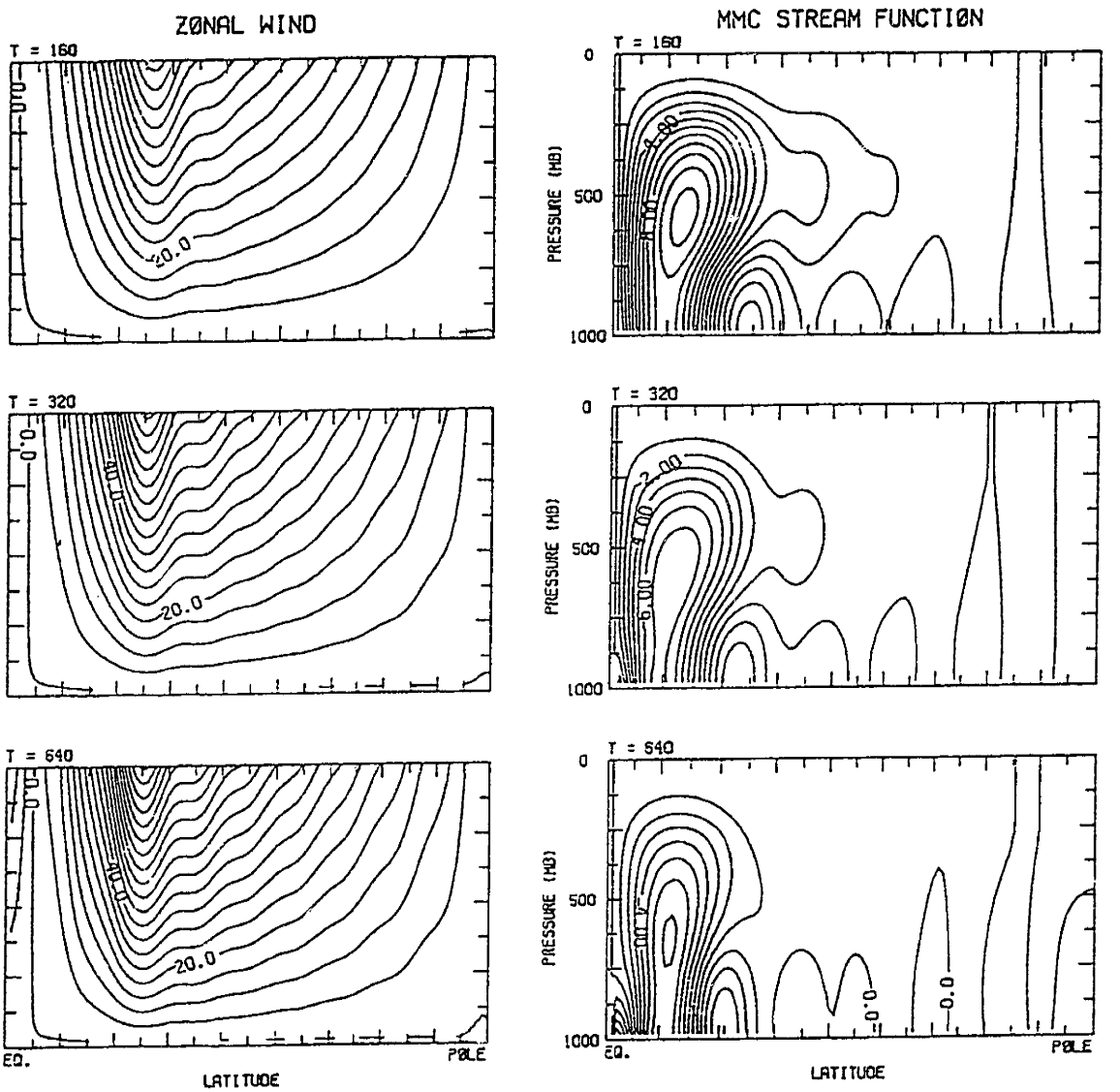

Figure 4.2: As in Figure 4.1 but for T = 160, 320, 640 days and the contour interval for $[\chi]$ is $1\,mb.m/s$.

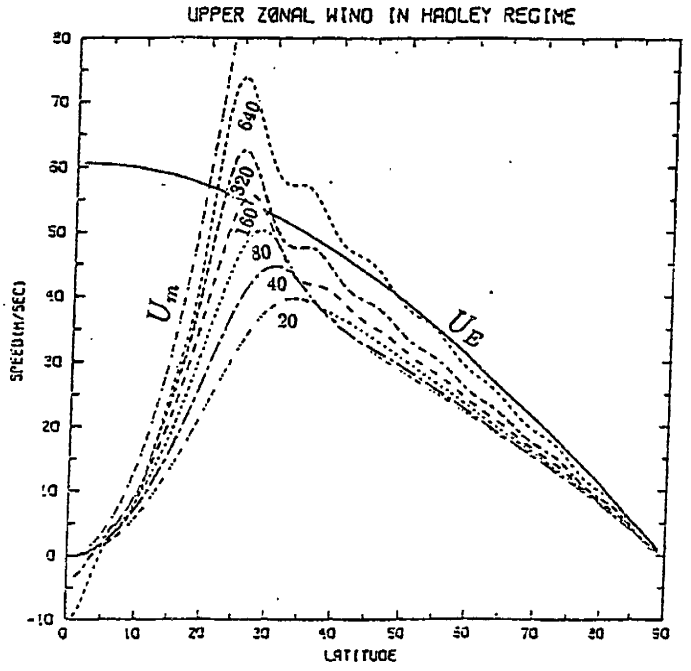

Figure 4.3: The upper layer wind fields for T = 20, 40, 80, 160, 320, 640 days. Also shown are the thermal wind, U_E, in the radiative equilibrium and the momentum conserving wind, $U_m (U_m = \frac{\Omega a \cos^2 \theta}{\sin \theta})$.

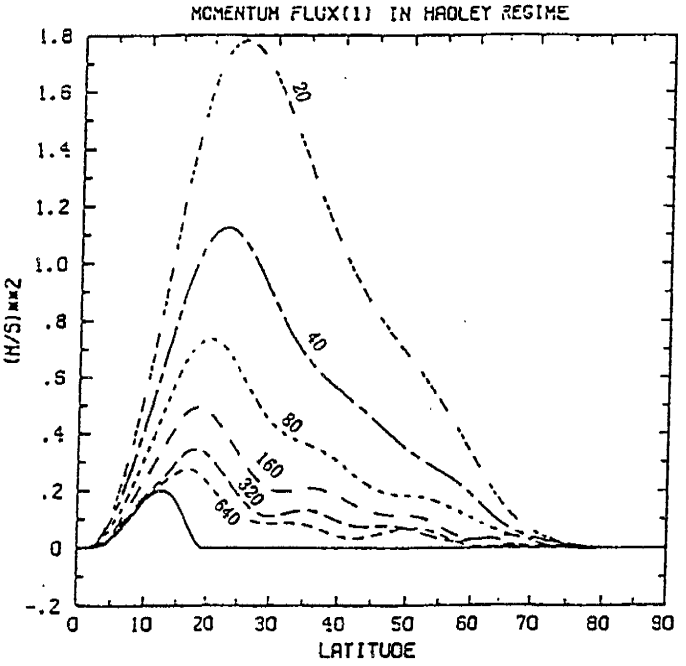

Figure 4.4: Meridional momentum fluxes for various T. The theoretical curve is shown by the solid line.

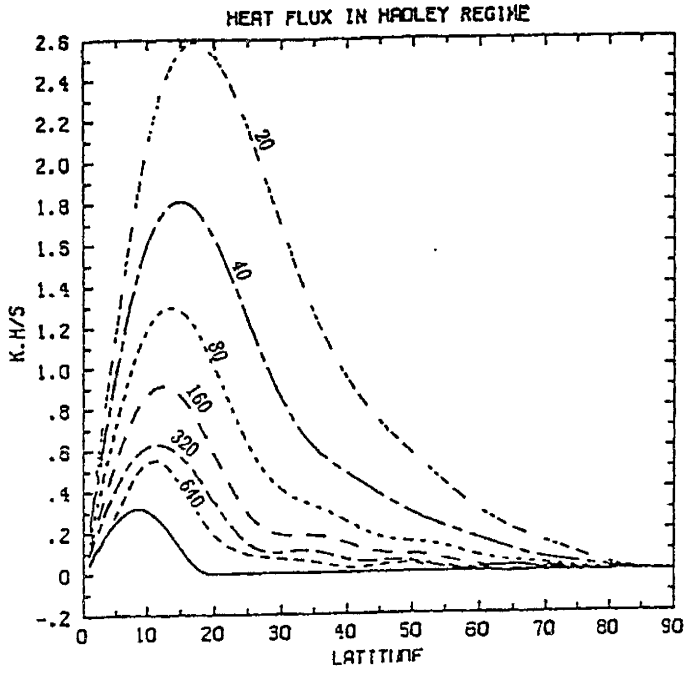

Figure 4.5: As in Figure 4.4 but for meridional heat fluxes.

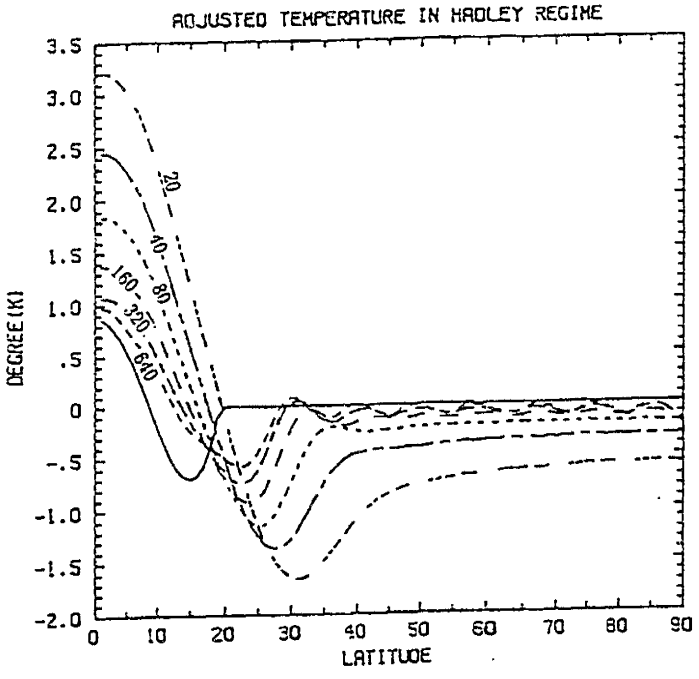

Figure 4.6: As in Figure 4.4 but for temperature adjustments, $[T_E(\phi) - T(\phi)]$.

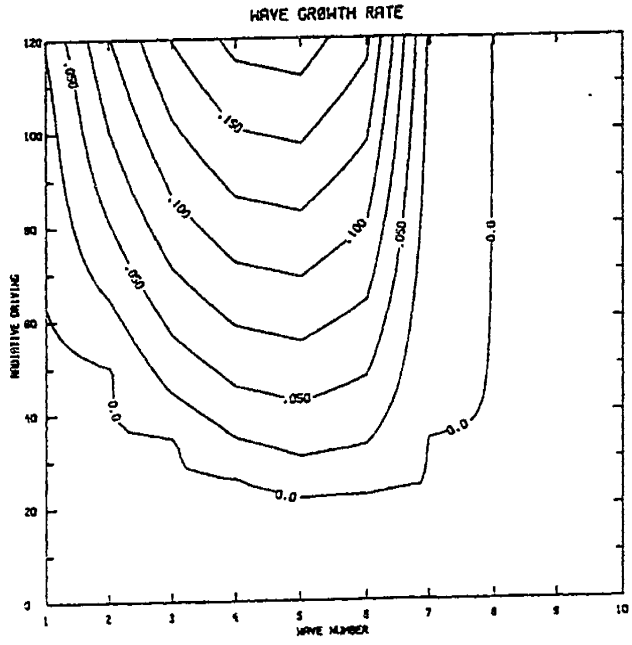

Figure 4.7: Wave growth rate (ω_r) as a function of ΔT_E and zonal wavenumber (n). The e-folding time for wave growth is $(\omega_r \Omega)^{-1}$.

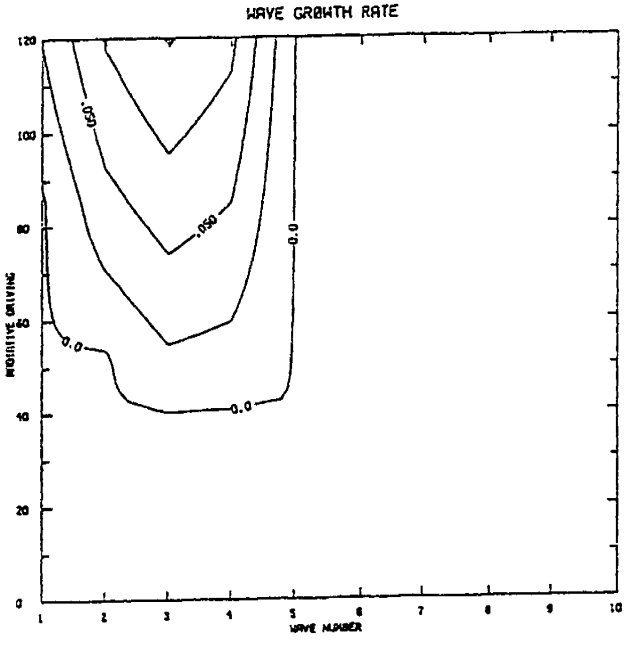

Figure 4.8: As in Figure 4.7 but for doubled static stability.

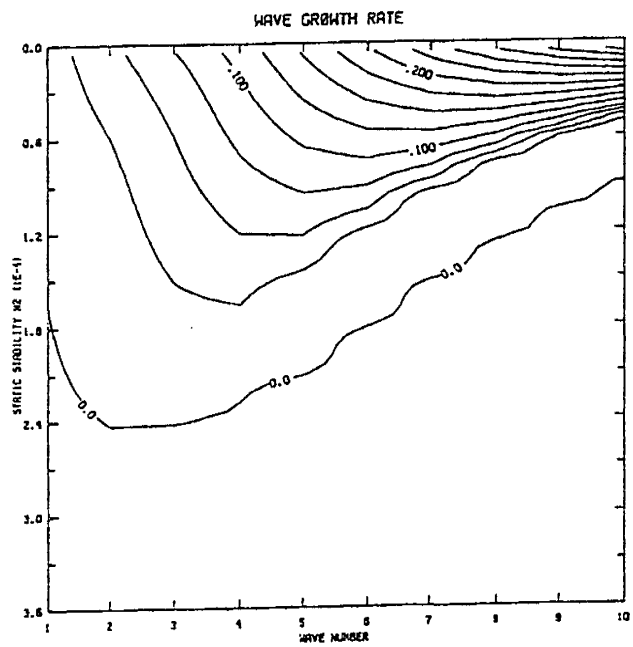

Figure 4.9: As in Figure 4.7 but the growth rate is a function of static stability (N^2) and n.

Chapter 5

Eddy regime – the Phillips system

5.1 Introduction

In this chapter, we will study an eddy regime in which large-scale eddies arise from baroclinic or barotropic instabilities of the Hadley regime. In this regime we only consider meridional transports of heat and momentum. The effect of vertical eddy heat transport is neglected by assuming a constant static stability, and vertical eddy momentum transport is also omitted. This simplification, which is based on the quasi-geostrophic theory, has been commonly adopted in theoretical and numerical studies.

Such an eddy regime can be described by Phillips' two-level model (Phillips, 1954). However on a sphere one necessary modification is that the Coriolis parameter f should be a function of latitude. In addition, the quasi-geostrophic approximation should be modified by the balance equation approximation. Unlike in the Hadley regime, we use the *linear* instead of the *nonlinear balance equation* approximation for

the eddy regime. Although the omitted terms in the vorticity equation associated with nonlinear ageostrophic motions are important in the Hadley regime, they are negligible in the eddy regime, because their magnitudes are at least one order smaller than the remaining terms (Holton, 1979). Furthermore, the eddy regime is in mid latitudes, where most of the eddy energy and maximal eddy transports are observed (Peixoto and Oort, 1974); while the Hadley regime is in low latitudes. Since the dynamics in the two regimes are very different, it is reasonable to use different "filtered" models. This will be demonstrated later by comparisons of numerical solutions of the *linear* and *nonlinear* balanced models.

We will use this simplified model to carry out a series of numerical experiments, which include long-term time integrations to achieve statistical equilibrium states, calculations of the model's general circulations and dynamical transports, and examinations of the effects of changing external parameters on the model's climate and climatic sensitivity. In particular, this chapter comprises three major parts: 1) the "standard" experiment; 2) horizontal resolution experiments; and 3) external parameter experiments. The goals are to clarify how the eddy transports of heat and momentum interact with each other in the climatic processes, how the numerical results depend on the horizontal resolution of the model, and how the transports of heat and momentum by eddies and by the MMC are affected by changes in the external parameters, such as diabatic heating, surface friction, etc.

5.2 Equations in the Phillips system

5.2.1 The numerics

From chapter 3, the equations in this eddy regime are written as follows:

$$\frac{\partial}{\partial t}\nabla^2\bar{\psi} = -J(\bar{\psi},\nabla^2\bar{\psi}) - J(\hat{\psi},\nabla^2\hat{\psi}) - 2\frac{\partial\bar{\psi}}{\partial\lambda} + \bar{\mathcal{D}}, \tag{5.1}$$

$$\frac{\partial}{\partial t}\nabla^2\hat{\psi} = -J(\bar{\psi},\nabla^2\hat{\psi}) - J(\hat{\psi},\nabla^2\bar{\psi}) - 2\frac{\partial\hat{\psi}}{\partial\lambda} - 2\nabla\cdot(\mu\nabla\hat{\varphi}) + \hat{\mathcal{D}}, \tag{5.2}$$

$$\frac{\partial\hat{\Phi}}{\partial t} = -J(\bar{\psi},\hat{\Phi}) - \Gamma_0\nabla^2\hat{\varphi} + \bar{\mathcal{Q}}, \tag{5.3}$$

$$\nabla^2\hat{\Phi} = 2\nabla\cdot(\mu\nabla\hat{\psi}). \tag{5.4}$$

The corresponding spectral forms of Equations (5.1) - (5.4) are:

$$\frac{d}{dt}\bar{\psi}_\gamma = \mathrm{i}\Big[\sum_\alpha\sum_\beta I_{\gamma\alpha\beta}(\bar{\psi}_\alpha\bar{\psi}_\beta + \hat{\psi}_\alpha\hat{\psi}_\beta) + 2c_\gamma^{-1}l_\gamma\bar{\psi}_\gamma\Big] + \bar{\mathcal{D}}_\gamma, \tag{5.5}$$

$$\begin{aligned}\frac{d}{dt}\hat{\psi}_\gamma = {}& \mathrm{i}\Big[\sum_\alpha\sum_\beta I_{\gamma\alpha\beta}(\bar{\psi}_\alpha\hat{\psi}_\beta + \hat{\psi}_\alpha\bar{\psi}_\beta) + 2c_\gamma^{-1}l_\gamma\hat{\psi}_\gamma\Big] \\ & + c_\gamma^{-1}(L_{\gamma+1}\hat{\varphi}_{\gamma+1} + L_\gamma\hat{\varphi}_{\gamma-1}) + \hat{\mathcal{D}}_\gamma,\end{aligned} \tag{5.6}$$

$$\frac{d}{dt}\hat{\Phi}_{\gamma+1} = \mathrm{i}\Big[\sum_\alpha\sum_\beta \mathcal{K}_{\gamma+1,\alpha,\beta+1}\bar{\psi}_\alpha\hat{\Phi}_{\beta+1}\Big] + \Gamma_0 c_{\gamma+1}\hat{\varphi}_{\gamma+1} + \bar{\mathcal{Q}}_{\gamma+1}, \tag{5.7}$$

$$\hat{\Phi}_{\gamma+1} = -c_{\gamma+1}^{-1}(L_{\gamma+1}\hat{\psi}_\gamma + L_{\gamma+2}\hat{\psi}_{\gamma+2}), \tag{5.8}$$

where

$$\gamma = n_\gamma + \mathrm{i}l_\gamma,\ [\gamma + j = (n_\gamma + j) + \mathrm{i}l_\gamma],$$

$$n_\gamma = 1, 3, 5, \cdots, 2M-1,$$

$$
\begin{aligned}
l_\gamma &= m(0, \pm 1, \pm 2, \cdots, \pm N), \\
\mathrm{i} &= \sqrt{-1}, \\
I_{\gamma\alpha\beta} &= c_\gamma^{-1}(c_\alpha - c_\beta)\mathcal{K}_{\gamma\alpha\beta}.
\end{aligned}
$$

The definitions for c_γ and L_γ have been given in Equations (4.23) and (4.24). In general, l_γ is a multiple of the fundamental wavenumber, m. Particularly, when $l_\gamma = 0$, it represents zonal mean equations. In the summation terms, the subscripts α and β denote those spectral components which satisfy the requirement $l_\gamma = l_\alpha + l_\beta$. Through a little algebra we can eliminate $\hat{\Phi}$ and $\hat{\varphi}$ and obtain a set of equations only for the stream functions $\bar{\psi}$ and $\hat{\psi}$. Altogether there are $2M + 4MN$ spectral equations for a resolution $M \times N$. They form an initial value problem of ordinary differential equations.

We initialize the system with a basic flow, which is obtained from the Hadley regime, plus a random perturbation. Then, we integrate the model equations for an adequately long time, until a statistical equilibrium is achieved. The time integration scheme adopted here is that developed by Shampine and Gordon (1975), which is based on the "predictor-corrector" method, and is able to adjust time steps internally according to the desired accuracy, so that computational instabilities are prevented. Cehelsky and Tung (1987) compared this scheme with others and demonstrated its advantage in the β-plane model. We also tested this scheme in our spherical model and found it to be very stable. In our integrations double precision was used. The accumulated computational error was negligible.

5.2.2 The physics

i) Surface drag

For convenience, we assume that there are no vertical motions at the top and the bottom boundaries so that $\bar{\varphi} = 0$. The surface friction is assumed to have a drag form, which has the same formulation in the two-level model as the Ekman pumping (both are proportional to the surface vorticity). This assumption simplifies the analysis of the dynamical heat transport, because the meridional heat transport by the MMC is identically represented by the adiabatic term if $\omega_4 = 0$, i.e.,

$$\nabla \cdot (\overline{[v][\Theta]}) = \overline{[\omega]} \frac{\partial \Theta}{\partial p},$$

where $\overline{(\,)}$ denotes vertical average; otherwise it needs to be modified by a surface flux $(-[\omega_4][\Theta_4]/P_0)$.

ii) Interfacial friction

In order to parameterize the effects of small-scale vertical mixing of horizontal momentum, we have included an interfacial friction in our model, except for special cases. In the tropical atmosphere, because the frictional effect of convective mixing is very strong, the dissipative time scale is much shorter than that in the mid-high latitudes. Although it may be neglected in the quasi-geostrophic system with a midlatitude domain, this mixing term has the same order as other large-scale processes in the tropical region (Houze, 1973). Therefore, it must be incorporated in a spherical model to simulate realistic tropical circulations.

Stone *et al.* (1974) have investigated the role of vertical mixing with the GISS GCM (Somerville *et al.*, 1974). They used a vertical diffusion law to parameterize

this mixing process. When the viscosity was absent or small, the vertical shear in the tropics became unrealistically strong and the Hadley cell became very weak. When a large, meridionally uniform viscosity was included, the vertical shear was reduced and the Hadley cell became stronger, but meanwhile the eddy activity in mid latitudes was also suppressed. Therefore, Stone *et al.* suggested that the viscosity coefficient should be very large ($\sim 100\, ms^{-2}$) in the tropics but very small ($\sim 1\, ms^{-2}$) in the mid-high latitudes, in order to simulate realistic global circulations. Helfand (1979) extended Stone *et al.*'s investigation, also with the GISS model (now known as the GLAS model), but using a sophisticated cumulus convection scheme instead of a diffusion law. He found that not every type of convective cloud could contribute to the process of the vertical mixing. Only " hot towers" were responsible for the dramatic changes due to cumulus friction. Schneider and Lindzen (1976, 1977) also recognized the importance of cumulus friction in simulating tropical circulations. They derived a parameterized form of vertical momentum exchange by cumulus friction and used it in the study of axially symmetric circulations. They found that inclusion of cumulus friction produced more realistic structure of tropical circulations.

In our model, the interfacial friction plays the same role as the vertical viscosity in the GISS model. We assume its coefficient, k', to be a function of latitude. Unfortunately, there is a large uncertainty in the distribution and magnitude of k'. For instance, the diagnostic and modeling studies (Holton and Colton, 1972; Colton, 1973) have suggested that the dissipative time scale varies from less than one day to several days. In this study we specify a profile similar to the "hot tower" precipitation in Helfand (1979)'s experiments, represented by a single associated Legendre function, $P_{20}^{20}(\mu)$, as shown in Figure 5.1. This distribution is also similar

to that of the zonal mean cumulus precipitation assumed by Schneider and Lindzen (1977). We specify $(k_e')^{-1} = 1$ day, *a priori*, in our model, where k_e' is the maximal dissipation rate at the equator.

We have carried out several sensitivity experiments to examine the effect of the "uncertain" interfacial friction. Fortunately, this effect on the mid-high latitudes is very small when the magnitude and the distribution vary on a reasonable range. Figure 5.2 shows the vertical shear, the meridional wind, the eddy heat flux and the eddy momentum flux for different k_e'. The solid curves represent the case without any interfacial friction, and the other curves represent the cases with $(k_e')^{-1} = 0.5$, 1 and 2 days respectively. With interfacial friction the vertical shear in low latitudes is appreciably reduced; the strength of the Hadley cell is greatly increased; the eddy heat flux in the mid latitudes is enhanced; and the eddy momentum flux is reduced in the low latitudes but increased in the mid-high latitudes. Clearly, the characteristics of the mid-high latitudes are not sensitive to k_e' when $(k_e')^{-1}$ is doubled or halved from 1 day. Specifically, the vertical shear and the meridional circulation (the Ferrel cell) in mid latitudes show little difference; the eddy fluxes of heat and momentum have almost not changed. The differences are significant only in the low latitudes.

However, if the interfacial friction is too strong, its effect on the mid latitudes can not be neglected. For example, we have run two cases with $(k_e')^{-1} = 0.1 day$. The model results are shown in Figure 5.3. In one case we used the profile of P_{20}^{20}; in the other we used the profile of P_{38}^{38} which declines poleward more sharply. In both cases, the eddy momentum fluxes were greatly suppressed.

iii) Diabatic forcing

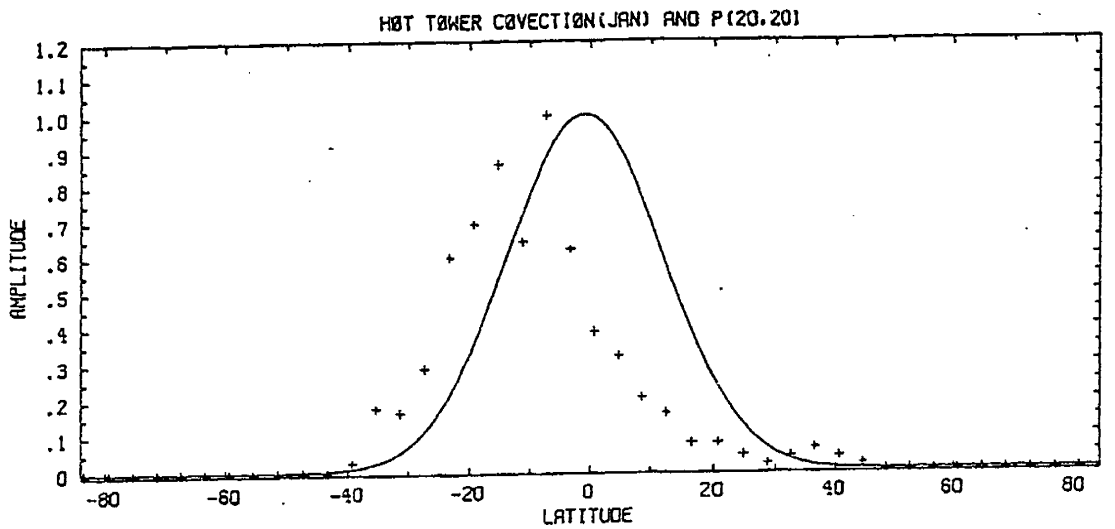

Figure 5.1: The profile of interfacial friction k' (solid line) and the distribution of the "hot tower" precipitation in the GISS model (cross signs). The model results are for January conditions in which the "heat equator" is at about $10°S$.

The diabatic heating in the eddy regime has an identical form to that used in the Hadley regime, i.e., Newtonian cooling with a specified, axisymmetric equilibrium temperature gradient. We have assumed the Newtonian cooling time τ_h to be constant. More realistically, τ_h should be a function of latitude. In mid-high latitudes, τ_h can be interpreted as the time scale for radiative cooling. In low latitudes, however, the small-scale convective process plays a very important role. It is responsible not only for the vertical mixing of momentum, but also for the vertical exchange of heat. In order to include this effect we need a different time scale for τ_h in low latitudes, which should be much smaller than that in mid-high latitudes.

To examine the effect of the meridional variation of τ_h on the model's results, we have also carried out a few experiments. The meridional distribution of h ($h = 1/\tau_h$) in these experiments is the same as that of k'. Different time scales for τ_h have been used, i.e, h has a maximum $h_e = (1,\ 2,\ 4\,days)^{-1}$, respectively, at the equator, and

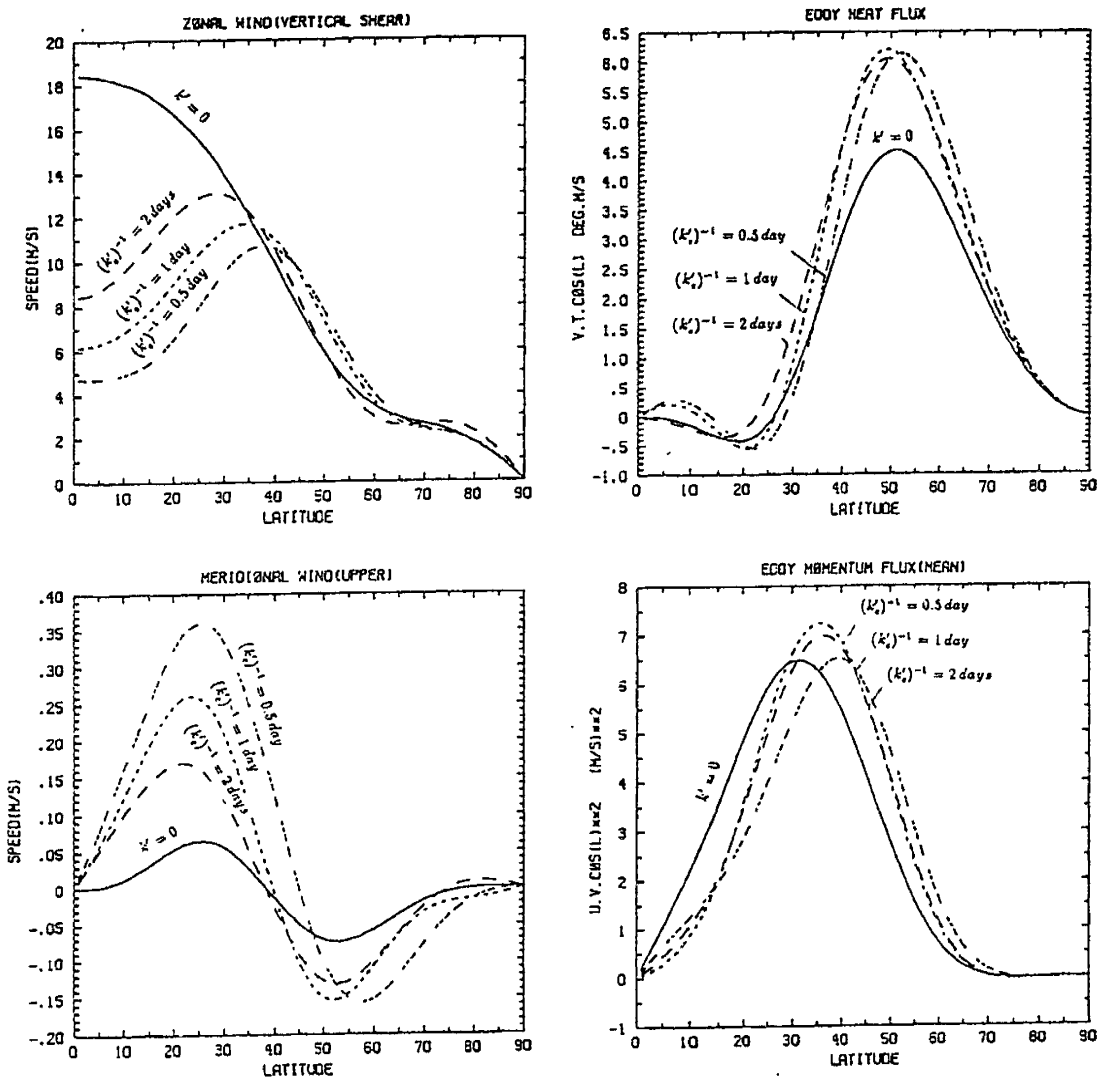

Figure 5.2: The vertical shears of zonal wind fields, the upper layer meridional winds, the eddy heat fluxes and the eddy momentum fluxes in the sensitivity experiments with varying k'_e, the maximal dissipative rate due to the vertical mixing process.

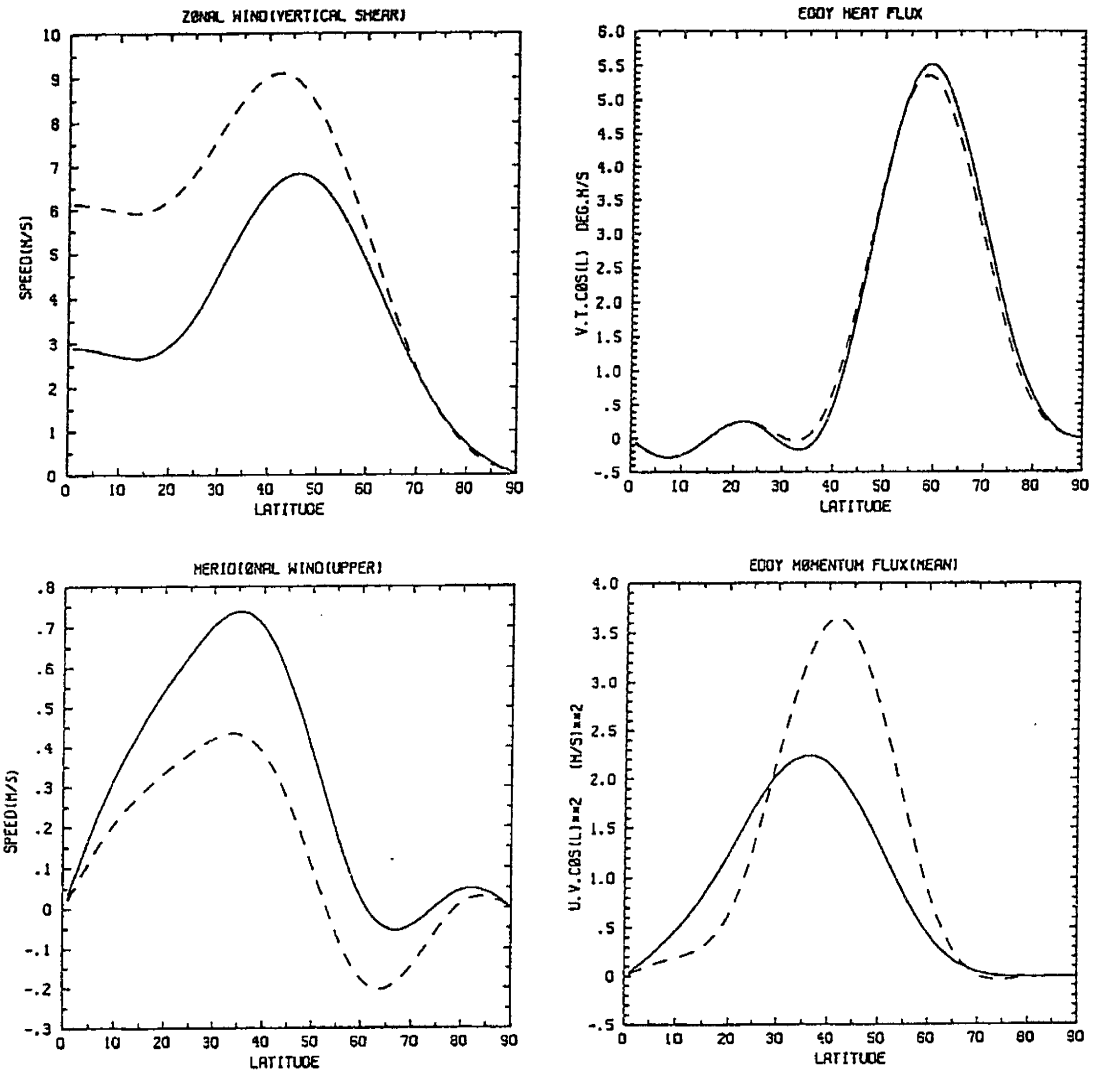

Figure 5.3: As in Figure 5.2 but for $(k'_e)^{-1} = 0.1\,day$. The solid line is for the case with k' profile of P_{20}^{20}, and the dashed line is for the case with k' profile of P_{38}^{38}.

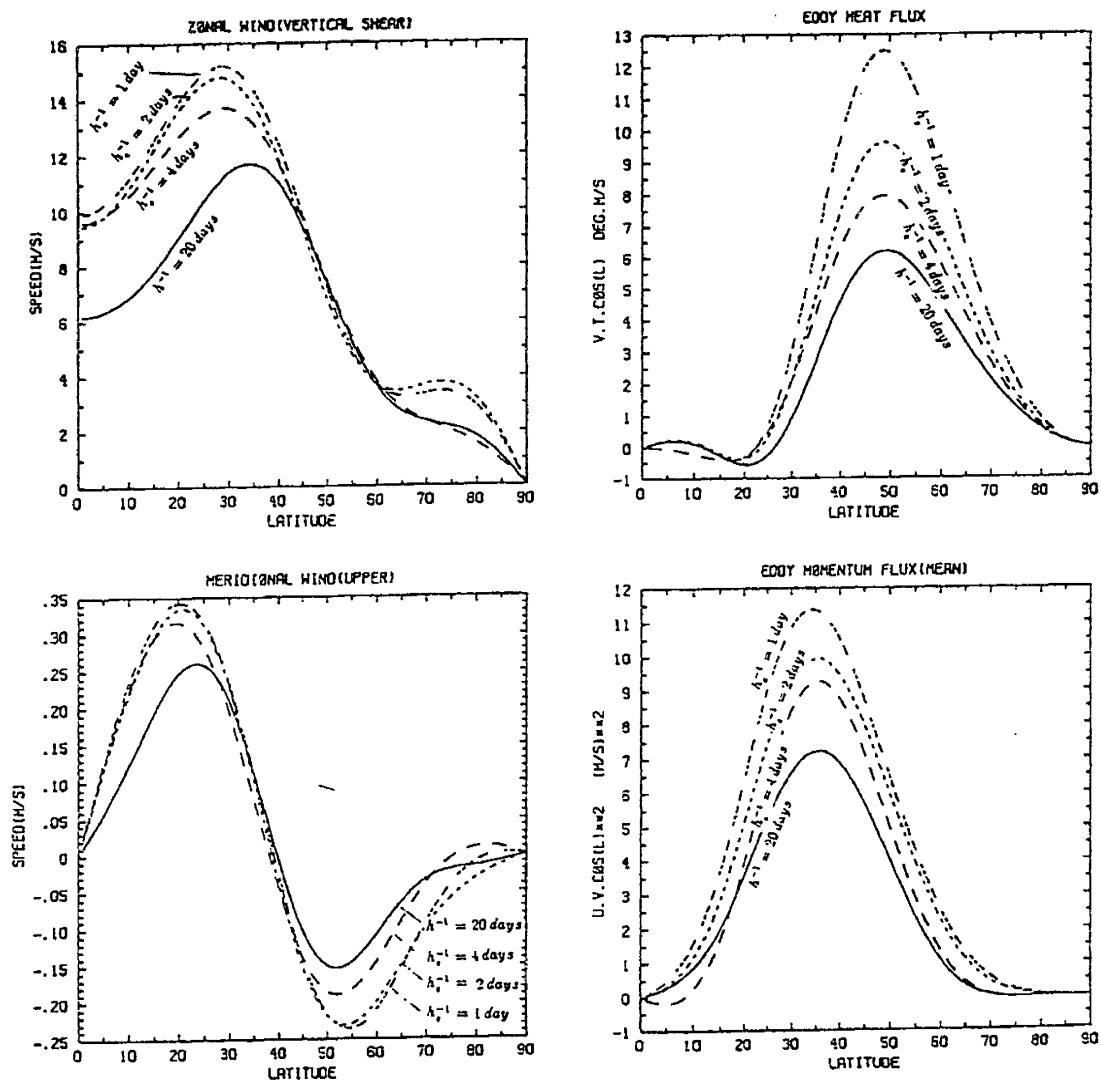

Figure 5.4: The vertical shears of zonal wind fields, the upper layer meridional winds, the eddy heat fluxes and the eddy momentum fluxes in the experiments with varying h_e, the maximal Newtonian cooling rate due to the convective heat exchange.

approaches gradually the value of $(20\,days)^{-1}$ in the mid-high latitudes. Figure 5.4 shows the vertical shear, the upper layer meridional wind, the eddy heat flux and the eddy momentum flux, similar to Figure 5.2. Compared with the results with a constant $\tau_h = 20$ days (solid curve), the most remarkable difference is that the eddy fluxes of heat and momentum in the mid latitudes increase appreciably when h_e increases. This feature is due to the fact that the gradient of differential diabatic heating ($\Delta\bar{Q}$) is increased by enhancing the tropical heat exchange rate, despite the fact that ΔT_E has not changed. It is $\Delta\bar{Q}$ rather than ΔT_E that determines the intensity of eddy transports. Therefore, the effect of increasing h_e is similar to that of increasing ΔT_E or increasing the value of a meridionally uniform h (which will be shown in section 5.5). Even though the time scale of Newtonian cooling is highly latitude-dependent, the meridional structures of equilibrium states and dynamical transports are very similar to those with meridionally uniform h. This implies that the overall effect of the heat exchange by small-scale convection can be approximately incorporated by using a proper and constant τ_h (τ_h should take a value between radiative time scale and convective time scale).

5.3 The "standard" run

5.3.1 The equilibrium states

To illustrate the characteristics of general circulations in the eddy regime, we have run an experiment with this model in which the external parameters are set to realistic values for the "standard" atmosphere. Particularly,

$$\Delta T_E = 48\,K,\ \tau_h = 20\,days,\ \tau_s = 5\,days,\ N^2 = 10^{-4}\,s^{-2}.$$

The statistical equilibrium states of this "standard" run can be directly compared with those obtained in the Hadley regime, to highlight the effect of eddies. They can also be compared with observations as well as the results from GCMs, to check the model's performance, although we do not attempt to simulate the real climate with this simplified model. In addition, the "standard" experiment will serve as a "control" run in the parameter experiments.

The model equations are truncated by keeping 5 meridional modes and 5 zonal waves with fundamental wavenumber 3, i.e., the horizontal resolution is denoted by $5 \times 5(3)$. In two-level β-plane models, this resolution is sufficient to allow energy and enstrophy to cascade among different scales of eddies (Cehelsky and Tung, 1987; O'Brien and Branscome, 1989). However, it might not be adequate in the spherical model. This resolution will be justified later.

The equilibrium states of $[u]$, $[v]$, $[T]$ and $[\chi]$ fields (the square brackets denote zonal mean) are shown in Figure 5.5. Generally, their characteristics resemble the observed atmospheric states very well. Due to the existence of eddies, the narrow subtropical jet in the Hadley regime is broadened, the pole-to-equator tempera-

ture contrast is weakened. The Hadley and the Ferrel cells have relatively realistic strength and positions, associated with easterly surface wind in the tropics and westerly surface wind in mid latitudes.

The main difference between the model's circulations and observations is the westerlies instead of easterlies appearing in the upper and lower layers of the tropics. This is due to the *linear balance equation* approximation and insufficient meridional resolution, which are not appropriate to describe tropical circulations. Nevertheless, this is not a serious problem since the eddy regime is in mid latitudes. Moreover, the coupling between low and mid latitudes in our model is obviously superior to that in the β-plane model where a rigid wall is assumed.

5.3.2 The momentum budgets

The relative angular momentum (u-momentum) is defined as

$$M = ua\sin\theta$$

The dimensional momentum budget equations in the upper layer and in the lower layer can be written as:

$$\frac{1}{a\sin\theta}\frac{\partial}{\partial\theta}[M_1^* v_1^*]\sin\theta \quad + \quad fa\sin\theta[v_1] - k'[\hat{M}] = 0, \tag{5.9}$$

$$\frac{1}{a\sin\theta}\frac{\partial}{\partial\theta}[M_3^* v_3^*]\sin\theta \quad + \quad fa\sin\theta[v_3] + k'[\hat{M}] - 2\,k[M_4] = 0. \tag{5.10}$$

In these equations, the first term is the meridional convergence of eddy flux of u-momentum ("$*$" denotes zonal deviation). The second term represents the convergence of Ω-momentum ($\Omega a^2\sin^2\theta$) flux by the mean circulation (Galin and

Kirichkov, 1979b), i.e.,

$$fa\sin\theta[v] = \frac{1}{a\sin\theta}\frac{\partial}{\partial\theta}[v]\Omega a^2\sin^3\theta - \frac{\partial}{\partial p}[\omega]\Omega a^2\sin^2\theta. \tag{5.11}$$

The other terms involving k and k' stand for the frictional dissipation of u-momentum.

The characteristics of these terms are shown in Figure 5.6 (a), (b). In the upper layer, the convergence of eddy u-momentum flux (solid line) is approximately balanced by the MMC transport of Ω-momentum (dotted line) in the mid latitudes, because the interfacial friction (dashed line) is very small. This implies that the strength of the Ferrel cell can be estimated from the eddy momentum transport in the upper layer. In the lower layer, the MMC transport of Ω-momentum (dotted line), which is exactly opposite to its upper layer counterpart, is approximately balanced by the surface friction (dot-dashed line) in mid latitudes, while the convergence of eddy u-momentum flux (solid line) and the interfacial friction (dashed line) are relatively small. Therefore, the strength of the Ferrel cell can also be estimated from the surface drag.

The vertical mean momentum budget becomes very simple in the two-level system:

$$\frac{1}{a\sin\theta}\frac{\partial}{\partial\theta}\overline{[M^*v^*]}\sin\theta - k[M_4] = 0, \tag{5.12}$$

where

$$\overline{[M^*v^*]} = [M_1^*v_1^* + M_3^*v_3^*]/2.$$

The vertical mean eddy momentum transport is exactly balanced by the surface friction, because the MMC transport and the interfacial friction terms have vanished.

This feature is shown in Figure 5.6 (c). The meridional eddy momentum flux can be calculated by integrating the first term of equation (5.12). It is poleward in all latitudes and peaks at $\sim 35°$ of latitude, as shown in Figure 5.6 (d).

5.3.3 The heat budget

The dimensional heat budget equation is written as

$$\frac{1}{a\sin\theta}\frac{\partial}{\partial\theta}[\bar{v}^*\bar{T}^*]\sin\theta + \sigma[\bar{\omega}] + h\,[\bar{T}_E - \bar{T}] = 0, \tag{5.13}$$

where σ ($\sigma = 4\Omega^2 a^2 \Gamma_0 / RP_0$) is a static stability parameter which is proportional to Γ_0. The first term is the meridional convergence of the eddy heat flux, the second term represents the heat transport by the MMC, and the last term is the diabatic heating. These terms are depicted in Figure 5.7 (a). In the low latitudes, the eddy heat transport is relatively small. Therefore, the diabatic heating is mostly balanced by the MMC heat transport, which is the adiabatic cooling caused by the rising branch of the Hadley cell. In the mid-high latitudes, the balance is approximately between the eddy heat transport and the diabatic cooling. However, the MMC heat transport (by the Ferrel cell) also cools the atmosphere, giving a negative feedback to the eddy heat transport. This negative feedback is demonstrated more clearly in terms of the heat fluxes by eddies and by the MMC, as shown in Figure 5.7 (b).

In the mid-high latitudes, the feedback of the MMC heat transports can be viewed as a result of the eddy momentum transports. We have seen, from the momentum budgets, that the strength of the Ferrel cell is closely related to the convergence of eddy momentum flux in the upper layer. The dynamical scenario

can be described as follows: In the upper layer the convergence of eddy momentum flux accelerates the zonal wind. The meridional wind speed increases due to the Coriolis effect. Consequently, the vertical motions of the Ferrel cell are strengthened through the continuity of mass. Thus, there is more adiabatic cooling on the polar side of the Ferrel cell, and more adiabatic heating on the equatorial side of the Ferrel cell. The meridional temperature gradient, which has been reduced by the poleward eddy heat transport, is then restored to some extent.

In another point of view, the lower layer zonal wind does not change much compared to the upper layer zonal wind, because the eddy momentum transport is very weak in the lower layer. Therefore, the vertical shear (or the meridional temperature gradient, from the thermal wind relation) increases. This is consistent with the up-gradient heat transport by the Ferrel cell.

5.3.4 The energetics

We define zonal kinetic energy K_Z, eddy kinetic energy K_E, zonal potential energy P_Z and eddy potential energy P_E as follows:

$$K_Z = \frac{1}{2}\sum_{\alpha} c_\alpha(\bar{\psi}_\alpha^2 + \hat{\psi}_\alpha^2), \tag{5.14}$$

$$K_E = \sum_{\gamma} c_\gamma(|\bar{\psi}_\gamma|^2 + |\hat{\psi}_\gamma|^2), \tag{5.15}$$

$$P_Z = \frac{1}{2\Gamma_0}\sum_{\alpha} \hat{\Phi}_{\alpha+1}^2, \tag{5.16}$$

$$P_E = \frac{1}{\Gamma_0}\sum_{\gamma} |\hat{\Phi}_{\gamma+1}|^2, \tag{5.17}$$

where the subscripts α and γ denote spectral components for the zonal mean and for eddies respectively. The energy equations in the spectral domain are:

$$\frac{dK_Z}{dt} = C(P_Z,K_Z) + C(K_E,K_Z) + D(K_Z), \tag{5.18}$$

$$\frac{dK_E}{dt} = C(P_E,K_E) - C(K_E,K_Z) + D(K_E), \tag{5.19}$$

$$\frac{dP_Z}{dt} = -C(P_Z,P_E) - C(P_Z,K_Z) + G(P_Z), \tag{5.20}$$

$$\frac{dP_E}{dt} = C(P_Z,P_E) - C(P_E,K_E) + G(P_E), \tag{5.21}$$

where the energy conversion (C), dissipation (D) and generation (G) terms are defined as:

$$\begin{aligned} C(K_E,K_Z) &= \sum_\alpha \sum_\beta \sum_\gamma 2c_\alpha I_{\alpha\beta\gamma}[\bar{\psi}_\alpha \cdot Im(\bar{\psi}^*_\beta \bar{\psi}_\gamma + \hat{\psi}^*_\beta \hat{\psi}_\gamma) \\ &\quad + \hat{\psi}_\alpha \cdot Im(\hat{\psi}^*_\beta \bar{\psi}_\gamma + \bar{\psi}^*_\beta \hat{\psi}_\gamma)], \end{aligned} \tag{5.22}$$

$$C(P_Z,P_E) = -\frac{2}{\Gamma_0} \sum_\alpha \sum_\beta \sum_\gamma \mathcal{K}_{\beta,\gamma+1,\alpha+1} \hat{\Phi}_{\alpha+1} \cdot Im(\bar{\psi}^*_\beta \hat{\Phi}_{\gamma+1}), \tag{5.23}$$

$$C(P_Z,K_Z) = -\sum_\alpha c_{\alpha+1} \hat{\Phi}_{\alpha+1} \hat{\varphi}_{\alpha+1}\,, \tag{5.24}$$

$$C(P_E,K_E) = -\sum_\gamma 2c_{\gamma+1} Re(\hat{\Phi}_{\gamma+1} \hat{\varphi}^*_{\gamma+1})\,, \tag{5.25}$$

$$G(P_Z) = \frac{1}{\Gamma_0} \sum_\alpha \hat{\Phi}_{\alpha+1} \bar{\mathcal{Q}}_{\alpha+1}\,, \tag{5.26}$$

$$G(P_E) = \frac{2}{\Gamma_0} \sum_\gamma Re(\hat{\Phi}_{\gamma+1} \bar{\mathcal{Q}}^*_{\gamma+1})\,, \tag{5.27}$$

$$D(K_Z) = \sum_\alpha c_\alpha (\bar{\psi}_\alpha \bar{\mathcal{D}}_\alpha + \hat{\psi}_\alpha \hat{\mathcal{D}}_\alpha)\,, \tag{5.28}$$

$$D(K_E) = \sum_\gamma 2c_\gamma Re(\bar{\psi}_\gamma \bar{\mathcal{D}}^*_\gamma + \hat{\psi}_\gamma \hat{\mathcal{D}}^*_\gamma)\,, \tag{5.29}$$

where "$*$" denotes a complex conjugate, "Re" and "Im" denote real and imaginary parts of a complex quantity respectively.

The energy diagram is shown in Figure 5.8. The main energy conversion pro-

Table 5.1: The spectrum of kinetic energy (unit: $10^5\ Jm^{-2}$).

m\ n	0	3	6	9	12	15	sum
1	15.75	.30	.48	.15	.07	.03	1.03
3	2.60	.77	.66	.19	.08	.05	1.75
5	.72	.64	.39	.17	.09	.06	1.35
7	.55	.50	.24	.14	.08	.05	1.01
9	.21	.27	.17	.10	.07	.05	.66
sum	19.83	2.48	1.94	.75	.39	.24	5.80

cesses are very similar to those computed from observations (Oort and Rasmusson, 1971), i.e., the zonal potential energy is converted to the eddy potential energy through baroclinic processes, which in turn is converted to the eddy kinetic energy. The eddy kinetic energy is partly dissipated and partly converted to zonal kinetic energy through barotropic processes. The baroclinic conversion is much larger than the barotropic conversion, consistent with the fact that the eddy heat transport is more important than the eddy momentum transport in the earth's atmosphere. Some differences from the observations, such as the very small P_E and the negative G_E, are due to the zonally symmetric diabatic forcing.

The spectrum of kinetic energy is given in Table 5.1. Most of the eddy energy is in zonal wavenumber 3, implying that there is a nonlinear upscale cascade in our model. In agreement with the observations (Eliasen and Manchenhauer, 1965), the meridional mode $m = 1$ has the largest part of the zonal kinetic energy, while the meridional modes $m = 3$ and $m = 5$ have largest part of the eddy kinetic energy.

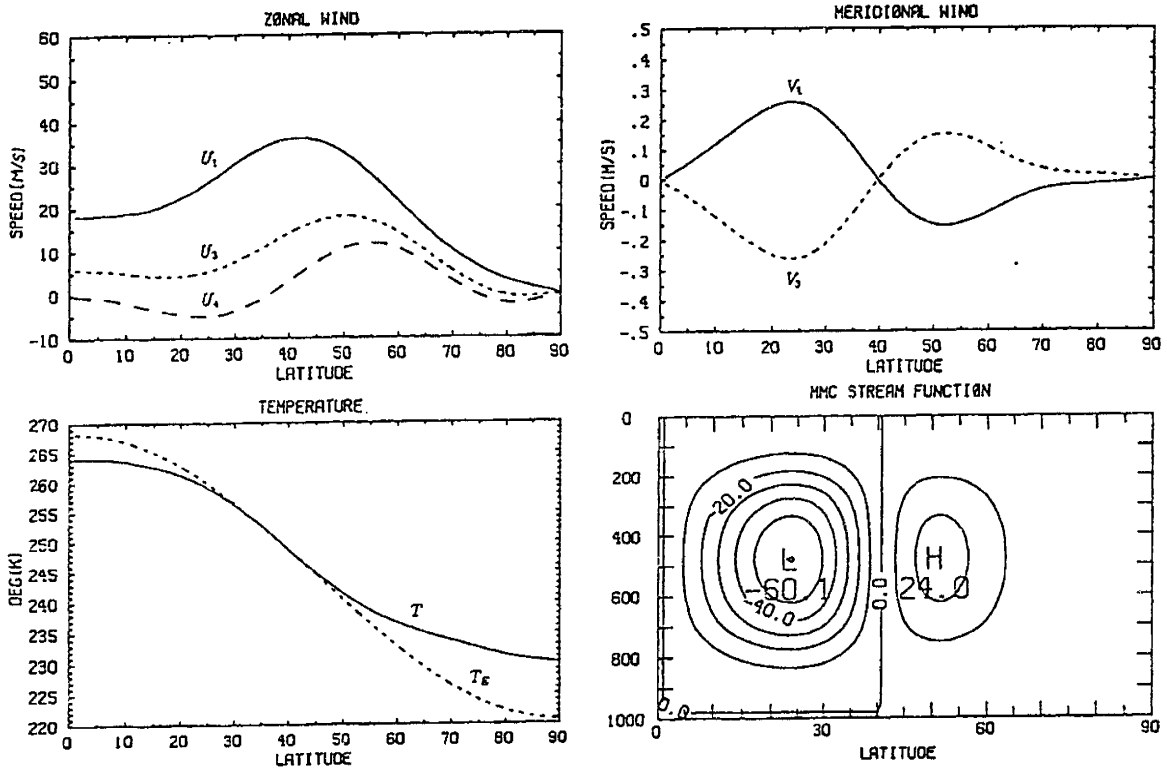

Figure 5.5: The equilibrium states of [U], [V], [T] and [χ] fields in the "standard" run. T_E is the temperature in radiative equilibrium . The contour interval of [χ] is $10\,mb.m/s$.

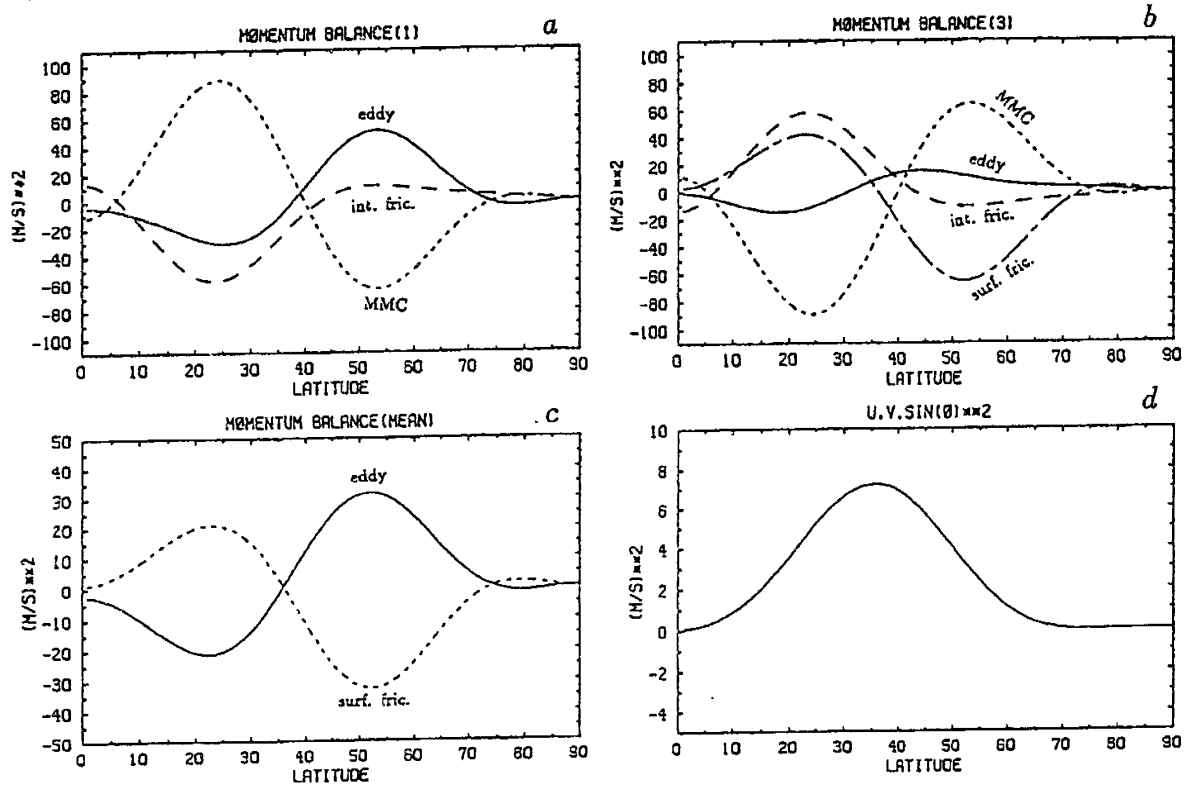

Figure 5.6: The momentum budgets in the "standard" run. a) the upper layer; b) the lower layer; c) the vertical mean; d) the eddy momentum flux. Detailed explanations are given in the text.

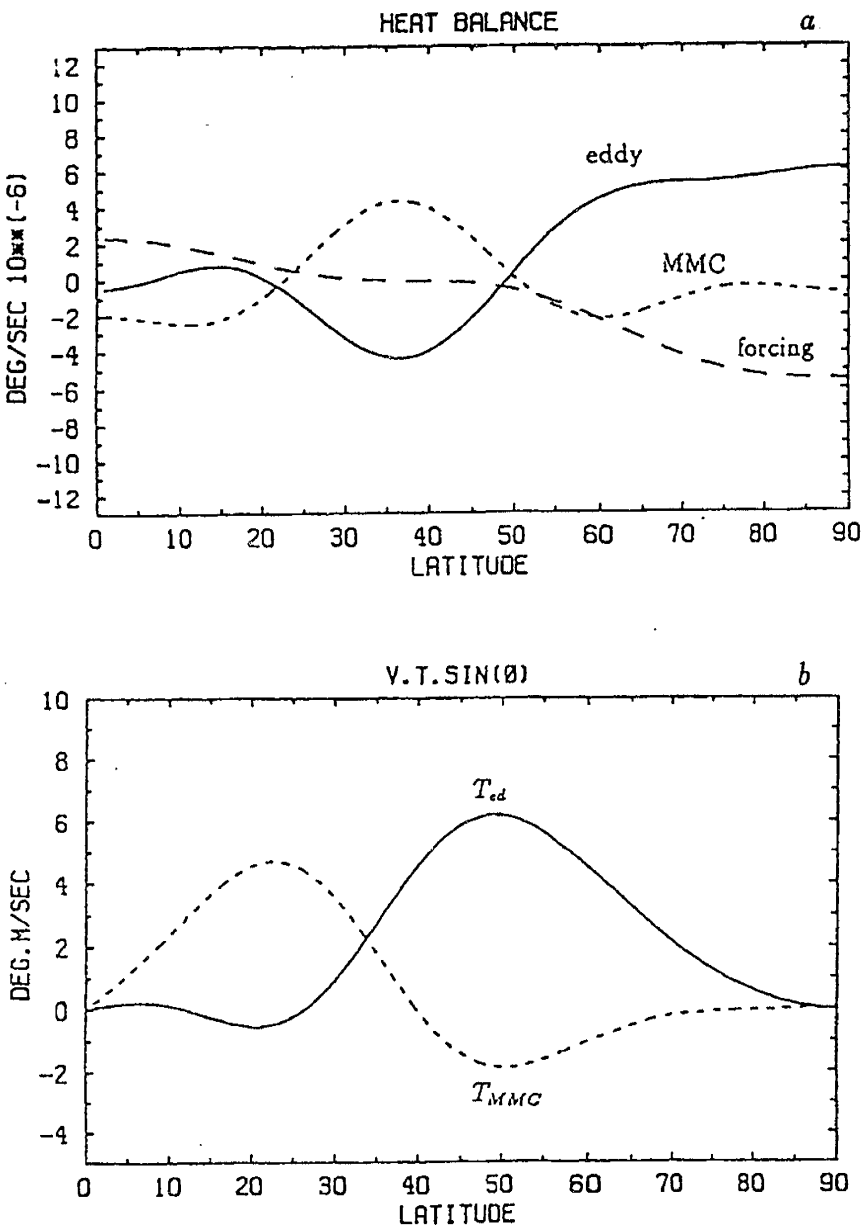

Figure 5.7: a) The heat budget in the "standard" run. The solid line is the convergence of the eddy heat flux, the dotted line is the MMC heat transport and the dashed line is the diabatic heating; b) The heat fluxes by eddies (solid) and by the MMC (dotted).

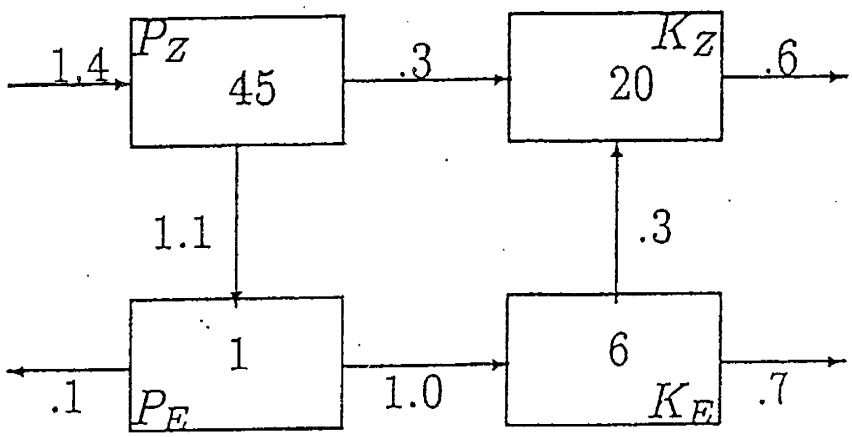

Figure 5.8: The energy cycle diagram in the "standard" run. The unit in the boxes is $10^5\, J\, m^{-2}$; the unit beside the arrows is $W\, m^{-2}$.

5.3.5 Additional experiments

i) The nonlinear balance model's results

In the introduction of this chapter we discussed briefly why we use the *linear* instead of the *nonlinear* balance model in the eddy regime. To further justify the simplification we have carried out an experiment similar to the "standard" run, but with the *nonlinear* balance model. The features of the general circulation from the *nonlinear* balance model are very similar to those from the *linear* balance model. In Figure 5.9 we compare surface winds, temperature fields, eddy momentum fluxes and eddy heat fluxes obtained from the two models. The quantitative differences are generally within 10 % in the mid latitudes for each of these quantities. The differences are even smaller in the low latitudes, although the nonlinear terms as-

sociated with ageostrophic motions are more important in low latitudes than in mid-high latitudes. This is probably due to the fact that we have incorporated a strong interfacial friction in the low latitudes, which plays a dominant role in the low latitude momentum balance.

ii) The effect of horizontal diffusion

We have not included any horizontal diffusion in the "standard" run. However, high order selective horizontal diffusions are often used in other models to prevent "spectral blocking" and to accelerate the convergence of model results (Baer and Alyea, 1971; Cehelsky and Tung, 1987; Eliasen and Laursen, 1990; Held and Phillipps, 1991). In order to examine the effect of horizontal diffusion on our model's results, we add a ∇^4 diffusion with a coefficient $10^{17}\, m^4/s$ in our model to modify the "standard" run. Since we are mainly interested in the effect on the momentum balance, we only show $[u]$, $[v]$, $[u^*v^*]\sin^2\theta$ and the mean momentum budget in Figure 5.10. In general the effect is small. Compared with the "standard" run (see Figure 5.5 and 5.6), the jet position shifts somewhat poleward; easterlies and a direct meridional cell appear in high latitudes. The eddy mometum flux is not poleward everywhere, rather, it becomes equatorward on the polar side of the jet, although the amplitude is very small. The horizontal diffusion is in phase with the surface drag, but its role in the momentum balance is much weaker.

These additional experiments indicate that the *linear balance* model is adequate and the horizontal diffusion is negligible. Therefore we will use the same kind of model as that used in the "standard" run in the parameter experiments. In other words, the model's simplification and physics will not change. However, the model's horizontal resolution needs to be tested.

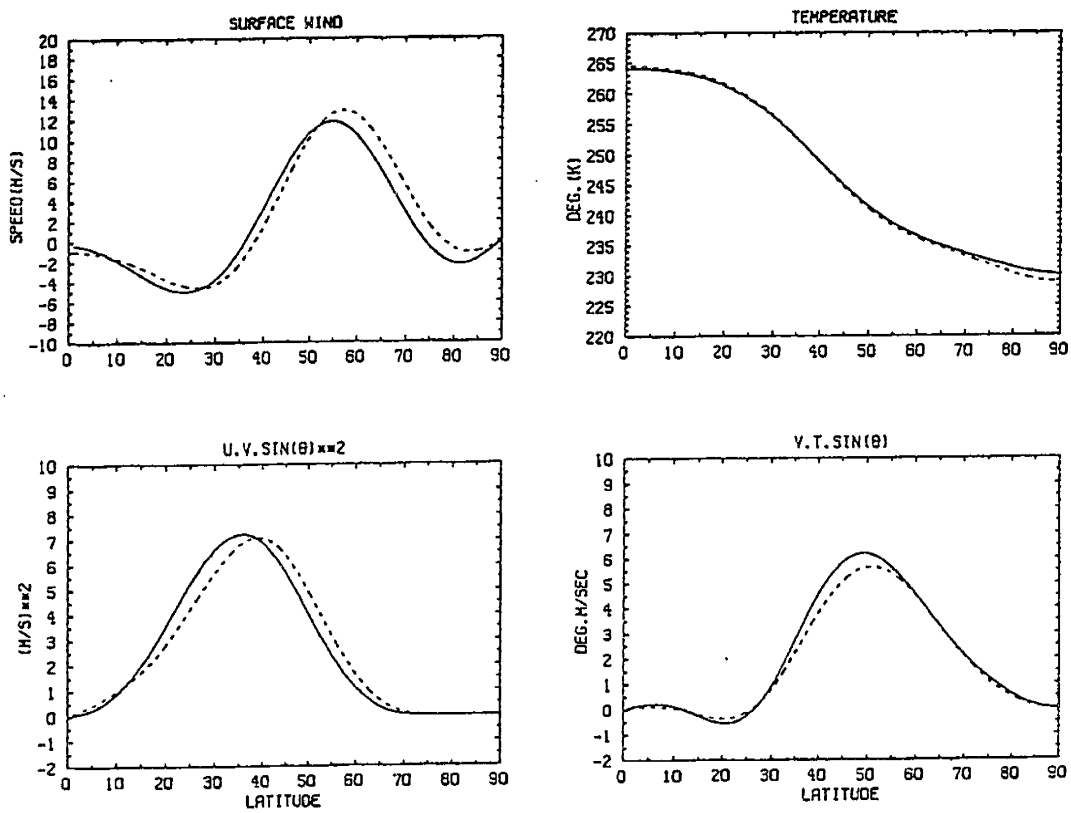

Figure 5.9: Surface wind fields, temperature fields, eddy momentum fluxes and eddy heat fluxes obtained from the *linear* (solid lines) and *nonlinear* (dotted lines) balance models.

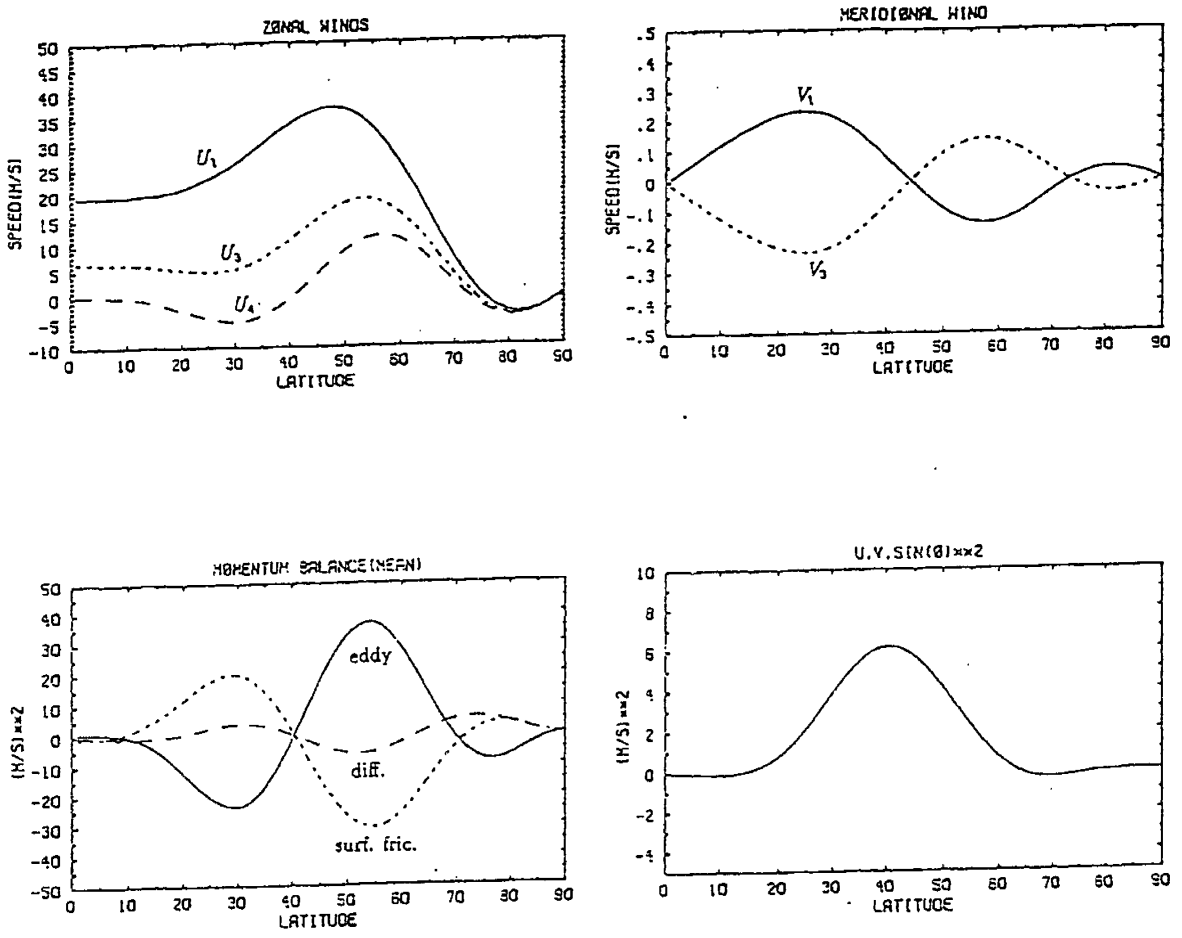

Figure 5.10: The zonal wind, the meridional wind , the mean momentum balance and the eddy momentum flux in the experiment similar to the "standard" run but with a fourth order horizontal diffusion ($A\nabla^4$, $A = 10^{17}\, m^4/s$).

5.4 The "optimal" horizontal resolution

5.4.1 Introduction

A proper horizontal resolution is the key to success in numerical experiments with two-level low order models. Special caution must be taken with highly truncated models. Explicitly, wave-wave interactions are excluded in a single zonal wave model; eddy momentum transports are inhibited if only one meridional mode is kept. Implicitly, more than a few wave modes are needed to provide a path for energy and enstrophy cascades, otherwise it may lead to a spurious chaotic behavior (Cehelsky and Tung, 1987) and eddy kinetic energy build-up on the smallest scale (O'Brien and Branscome, 1989).

In the Hadley regime we have truncated the spectrum by keeping 20 meridional modes on a hemisphere, in order to resolve the structure of the narrow subtropical jet. It should not be necessary to use as much meridional resolution in the eddy regime as that in the Hadley regime, because eddies can diffuse the subtropical jet, as shown in the "standard" run. In addition, since most of the atmospheric energy falls into the spectrum of long waves, it may not be necessary to have very much zonal resolution either.

Although there might be a critical truncation level or a minimal resolution in a specific model, there is no universal criterion for the choice of an adequate resolution. A necessary and sufficient resolution depends not only on the model's physics and geometry, but also on the nature of the problem to be studied. A proper resolution for a midlatitude channel model may differ from that for a spherical model. A time mean solution may require different resolution from a time-dependent solution.

For example, in the two-level spherical model of Baer and Alyea (1971, 1974), the general circulation could be predicted with 12 zonal waves and 8 meridional modes (8×12), whereas detailed prediction for shorter periods (15-20 days) required at least a resolution of 10×16. In simulations of the general circulation with a semi-spectral primitive equation model, Held and Suarez (1978) included only two zonal waves (wavenumber 3 and 6) and a rather high meridional resolution. When a third zonal wave (wavenumber 9) was added, the total amount of eddy kinetic energy and eddy heat transport did not change much; although the portion for each wave was quite different from that in the two-wave experiment. Recently, O'Brien and Branscome (1989) have done a series of resolution experiments in the quasi-geostrophic β-plane model. They concluded that a minimal resolution of 3×3 is necessary for modeling the zonal mean and time mean states of the general circulation (their fundamental wavenumber is approximately 3). Therefore, in order to determine a proper resolution in a specific problem, one needs to do experiments by progressively modifying the resolution and comparing the model's results. If the results "converge" at some resolution, then this resolution should be appropriate.

5.4.2 Truncation levels

We first fix the fundamental wavenumber, *a priori*, $m = 3$, and modify the zonal and meridional truncation levels. A series of experiments has been carried out, in which the external parameters are set to the same values as in the "standard" run. The model's results in which we are interested include the equilibrium states of zonal mean flow and MMC, the dynamical transports and budgets of heat and momentum, the energy cycle and the kinetic energy spectrum, among others. They are shown in Figures 5.11 - 5.17 for nine different resolutions: 2×2, 3×3, 4×4, 5×5, $6 \times$

6, 7×7, 7×5, 9×5 and 11×5. Obviously, the lowest resolution, 2×2, exhibits very different features from higher resolutions. The main qualitative difference of the 3×3 from the higher resolutions is on the momentum budget in the tropics. The qualitative characteristics of the model's climatology are very similar when the resolution is beyond 4×4.

The spectral distribution of eddy kinetic energy is shown in Figure 5.18 for resolutions 5×5, 6×6 and 7×7. If a model correctly simulates nonlinear wave-wave interactions, the eddy kinetic energy cascades toward long waves and its distribution in an inertial subrange follows an inverse cube law (Wiin-Nelson, 1967; Julian *et al.*, 1970). In our experiments, these features are satisfactorily simulated for resolutions beyond 4×4. Higher resolutions hardly change either the total eddy kinetic energy or the characteristics of energy distribution in the spectral domain.

Some characteristic quantities, which will be considered in later analyses, are listed in Table 5.2. They generally "converge" very well beyond the resolution 4×4. In some other models, e.g., those primitive equation models with sophisticated physics, the numerical results do not "converge" until very high horizontal resolution (Eliasen and Laursen, 1990; Held and Phillipps, 1991). The momentum budget and the zonal wind field in those models are very sensitive to the horizontal resolution, especially the meridional resolution. For instance, the eddy momentum flux was increased by a factor of 2 by increasing the resolution from M36 to M72 in Eliasen and Laursen's two-level model (M36 stands for a triangular truncation with 36 zonal wavenumbers). A similar feature was found in Held and Phillipps' multi-level model when the resolution was increased from R15 to R30 (R15 stands for a rhomboidal truncation with 15 zonal wavenumbers). In our model, the eddy momentum flux is

not so sensitive to the horizontal resolution as in those models. For example, it is increased only by 10 % from the resolution 7×5 to 11×5.

Detailed examination of Eliasen and Laursen's model results (their Figures 5, 6, 7) indicates that the Ferrel cell in their model is extremely sensitive to the horizontal resolution and the high order selective horizontal diffusion. The Ferrel cell is hardly seen, if any, in the M36 model without the diffusion, but is strong enough in the M72 model without the diffusion, or in the M36 model with the diffusion. The results of Held and Phillipps' model are also similar. However, the Ferrel cell in our model is insensitive to the horizontal resolution beyond 4×4. If a high order horizontal diffusion is included in our model, as shown in Figure 5.10, the Ferrel cell as well as the eddy momentum flux are slightly weakened rather than strengthened.

It is difficult to explain the differences between the results from our model and the aforementioned models, because the simplifications, physics and numerics in our model and those models are different. In particular, the nonlinear terms in our model are calculated through direct evaluations in the spectral space, as stated in chapter 3. However, in the aforementioned models, the nonlinear terms were calculated through spectral grid transforms, i.e., the nonlinear products were evaluated on a grid-point mesh and then transformed back to the spectral space (Orszag, 1970; Bourke, 1974). The transform method is economical but may not be as accurate as the direct evaluation, especially for long time integrations. For instance, in the momentum budget of Eliasen and Laursen' model (their Figure 7), the horizontal diffusion (which was not explicitly shown but can be easily estimated from the balance) seems to *accelerate* the zonal flow in the mid latitudes, contrary to common sense. In our model, the horizontal diffusion *decelerates* the zonal fow (Figure 5.10).

In our model, it seems that at least a resolution of 4×4 is required. Compared the resolution 5×5 with higher resolutions such as 7×7 and 11×5, most features are similar except that the jet position is more poleward for higher resolutions, and that the heat budget is different in high latitudes, where the direct polar cell disappears for the resolution 5×5. However, we are more concerned about some features such as vertical shear (or δT), heat and momentum transports in the mid latitudes. They are not very different for the resolution of 5×5 and higher resolutions. For example, there is little difference in δT and $[v^* M^*]_y$; the differences in other quantities are generally within $10 \sim 20\%$. These differences are much smaller than those in the parameter experiments, which will be described in next section. Therefore we have used the resolution of 5×5 in the "standard" run. The insight of climatic sensitivity will not be obscured by using the resolution of 5×5, although 7×5 would be better. When the truncation is further relaxed, the features of the model's general circulation do not change much, even the magnitudes of dynamical transports and energetics "converge" very well.

Table 5.2: Some characteristic quantities in the resolution experiments.

	2×2	3×3	4×4	5×5	6×6	7×7	7×5	9×5	11×5
ΔT	31.5	32.1	33.3	34.0	36.4	37.8	36.3	36.6	38.0
δT	10.8	12.7	12.9	14.1	13.3	14.0	13.7	14.7	14.0
M	.73	.97	1.04	1.19	1.03	1.07	1.04	1.14	1.07
$[v^*M^*]_y$	7.6	16.3	21.4	24.5	18.0	19.6	21.7	25.7	24.3
t_M	110.0	68.8	56.2	56.0	66.4	63.0	55.5	51.3	50.7
$[u]_s$	3.0	5.8	8.2	11.8	14.2	15.4	14.3	13.2	15.7
(lat.)	(59)	(55)	(52)	(55)	(59)	(63)	(61)	(58)	(61)
$[v]_1$	.09	.38	.21	.26	.25	.24	.24	.25	.25
(lat.)	(24)	(17)	(24)	(23)	(24)	(26)	(26)	(25)	(25)
$[u^*v^*]$	2.9	6.2	5.7	7.2	7.9	8.4	8.3	7.7	8.9
(lat.)	(27)	(26)	(36)	(36)	(40)	(39)	(40)	(39)	(39)
T_{ed}	8.44	8.17	6.49	6.20	5.69	5.00	5.37	4.74	4.82
T_{MMC}	-.53	-2.74	-2.06	-1.88	-1.95	-1.84	-1.89	-1.58	-1.76
R	.06	.34	.32	.30	.34	.37	.35	.33	.37

ΔT : the pole-to-equator temperature difference (K)
δT : $T_{35°} - T_{55°}(K)$
M : the vertical mean angular momentum at $45°(10^8\, m^2/s)$
$[v^*M^*]_y$: the convergence of eddy momentum flux at $45°(m^2/s^2)$
t_M : $M/[v^*M^*]_y$ (days)
$[u]_s$: the peak value of the zonal surface wind (m/s)
$[v]_1$: the peak value of the meridional wind (m/s)
$[u^*v^*]$: the peak value of $\overline{[u^*v^*]} \sin^2\theta (m^2/s^2)$
(lat.): the latitude of the peak value
T_{ed} : the peak value of $[v^*T^*] \sin\theta (K.m/s)$
T_{MMC} : the peak value of the MMC heat flux
R : $-T_{MMC}/T_{ed}$

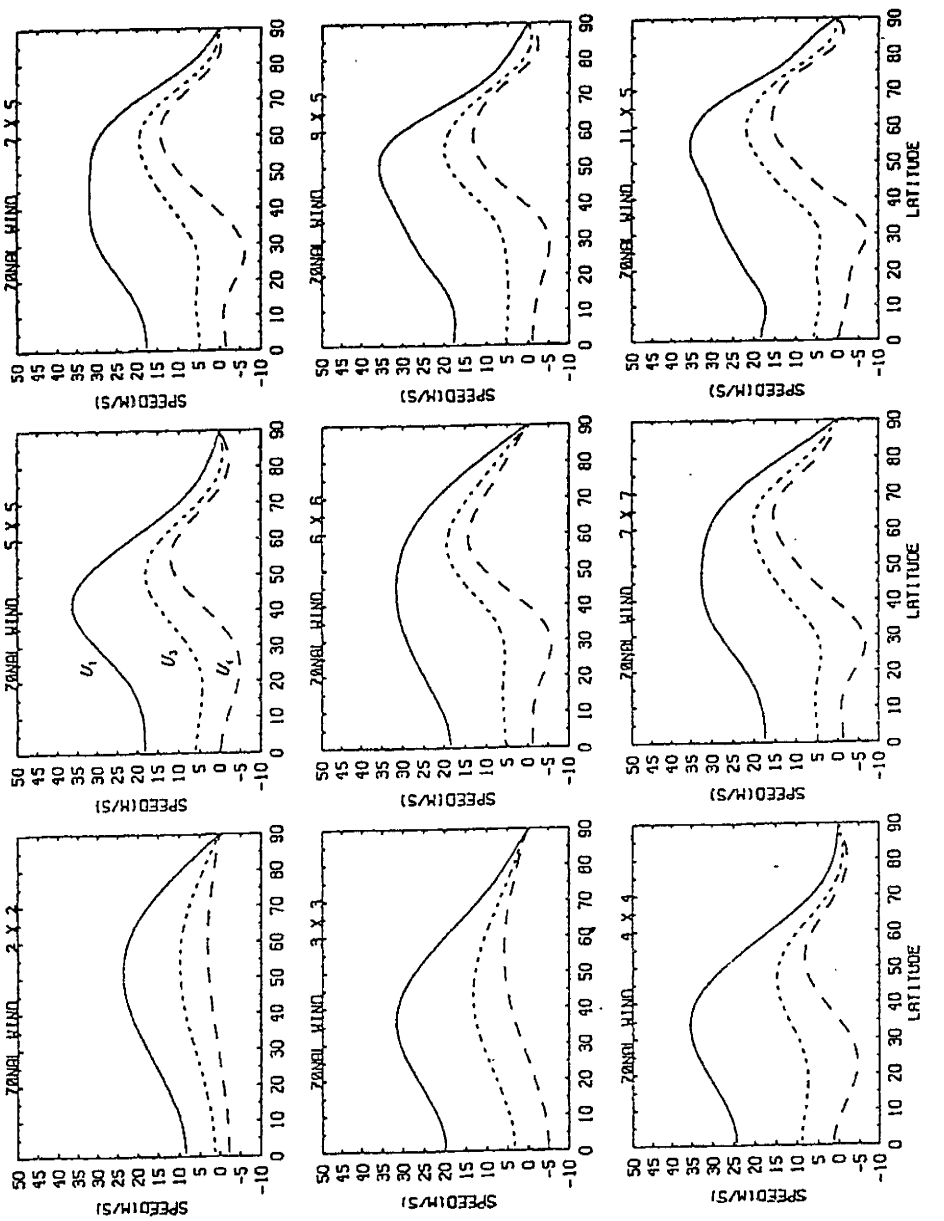

Figure 5.11: The equilibrium zonal wind fields in the truncation experiments. The solid, dotted and dashed lines denote U_1, U_3 and U_4 respectively.

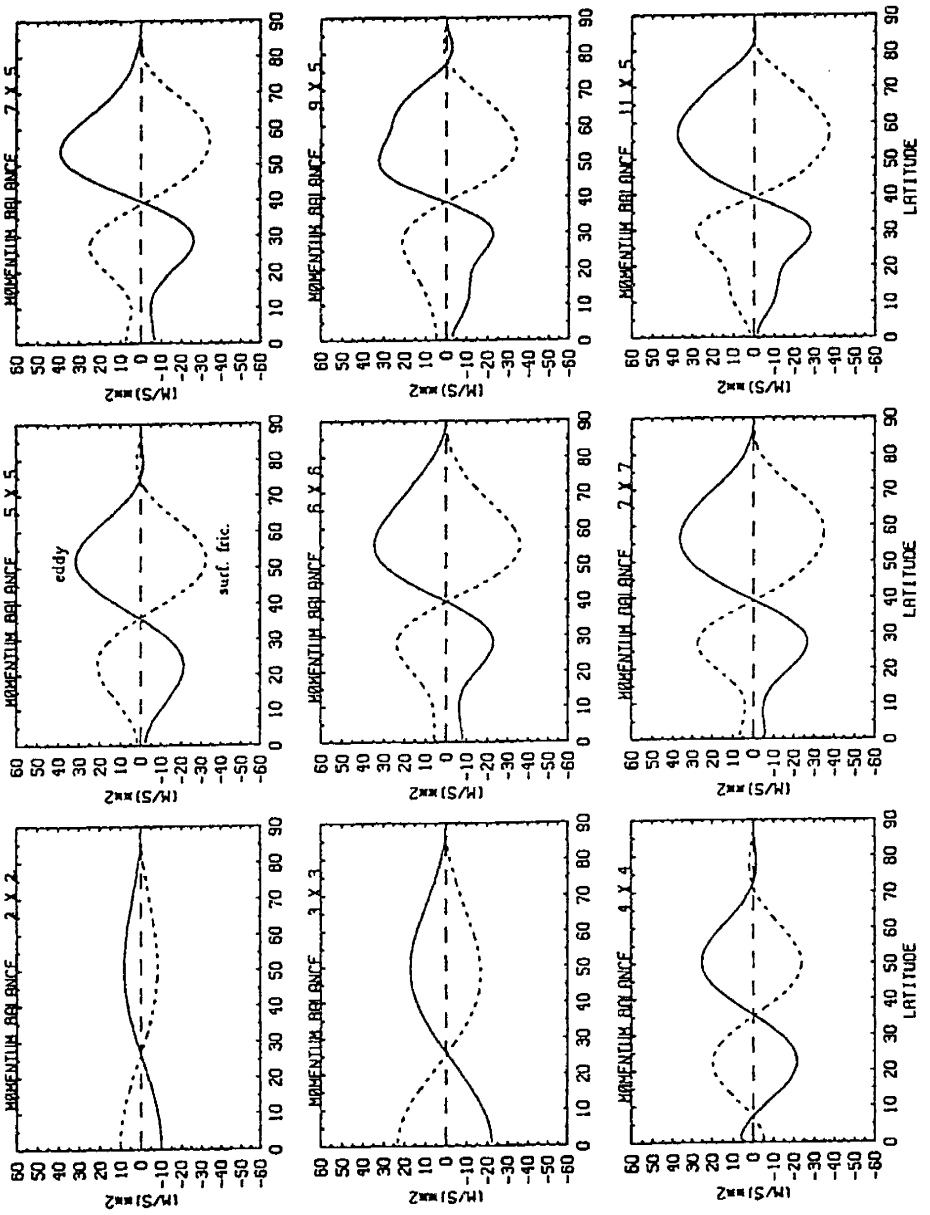

Figure 5.12: The vertical mean momentum budgets in the truncation experiments. The meanings for the lines are the same as those of Figure 5.6(c).

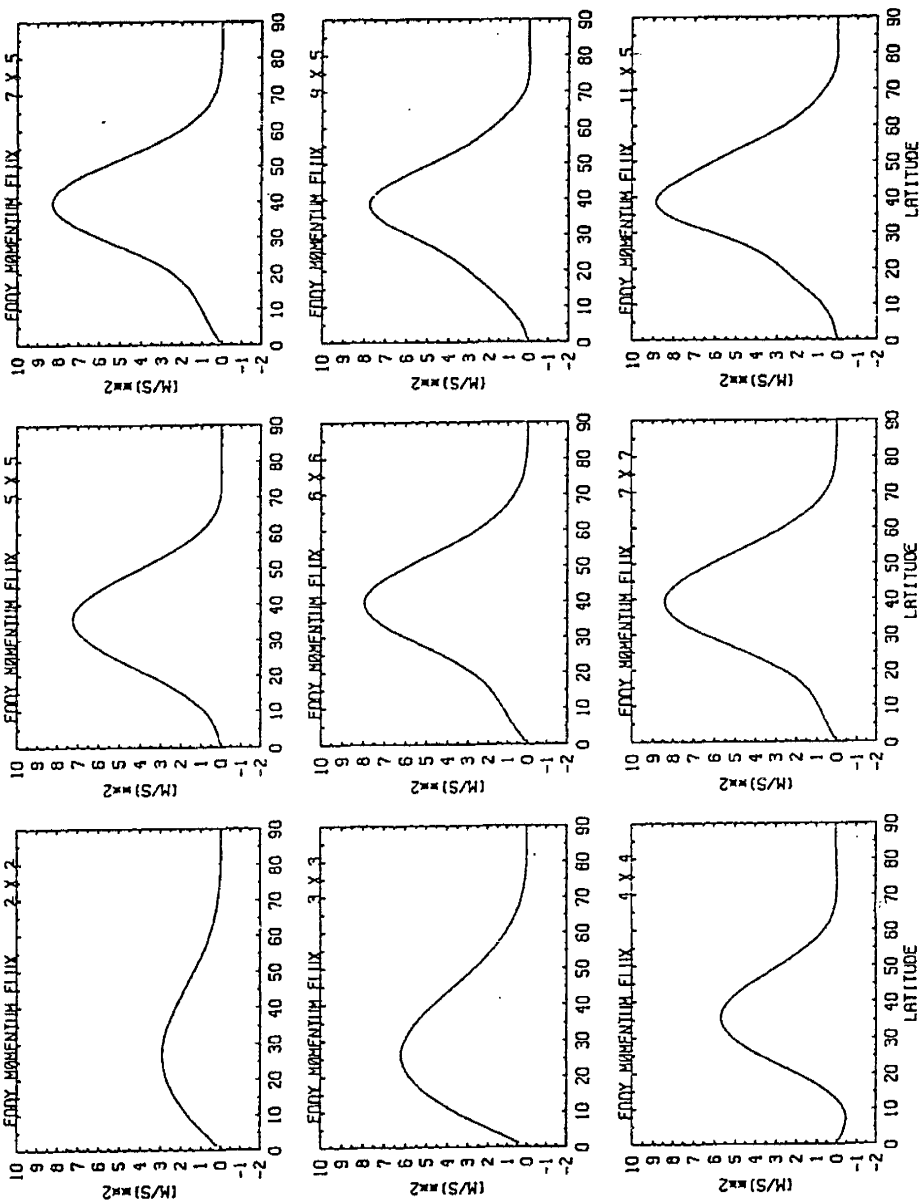

Figure 5.13: The vertical mean eddy momentum fluxes in the truncation experiments.

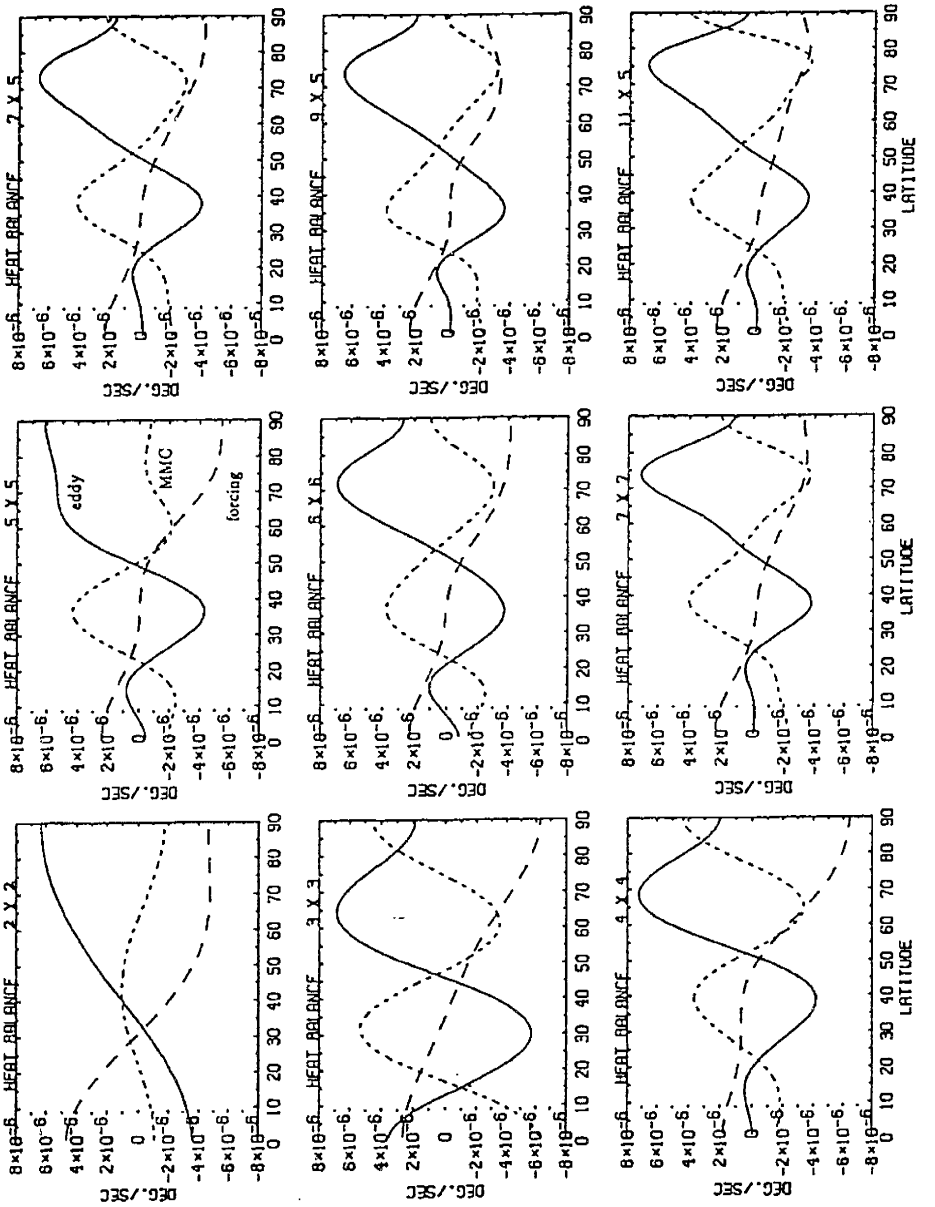

Figure 5.14: The heat budgets in the truncation experiments. The meanings for the lines are same as those of Figure 5.7 (a).

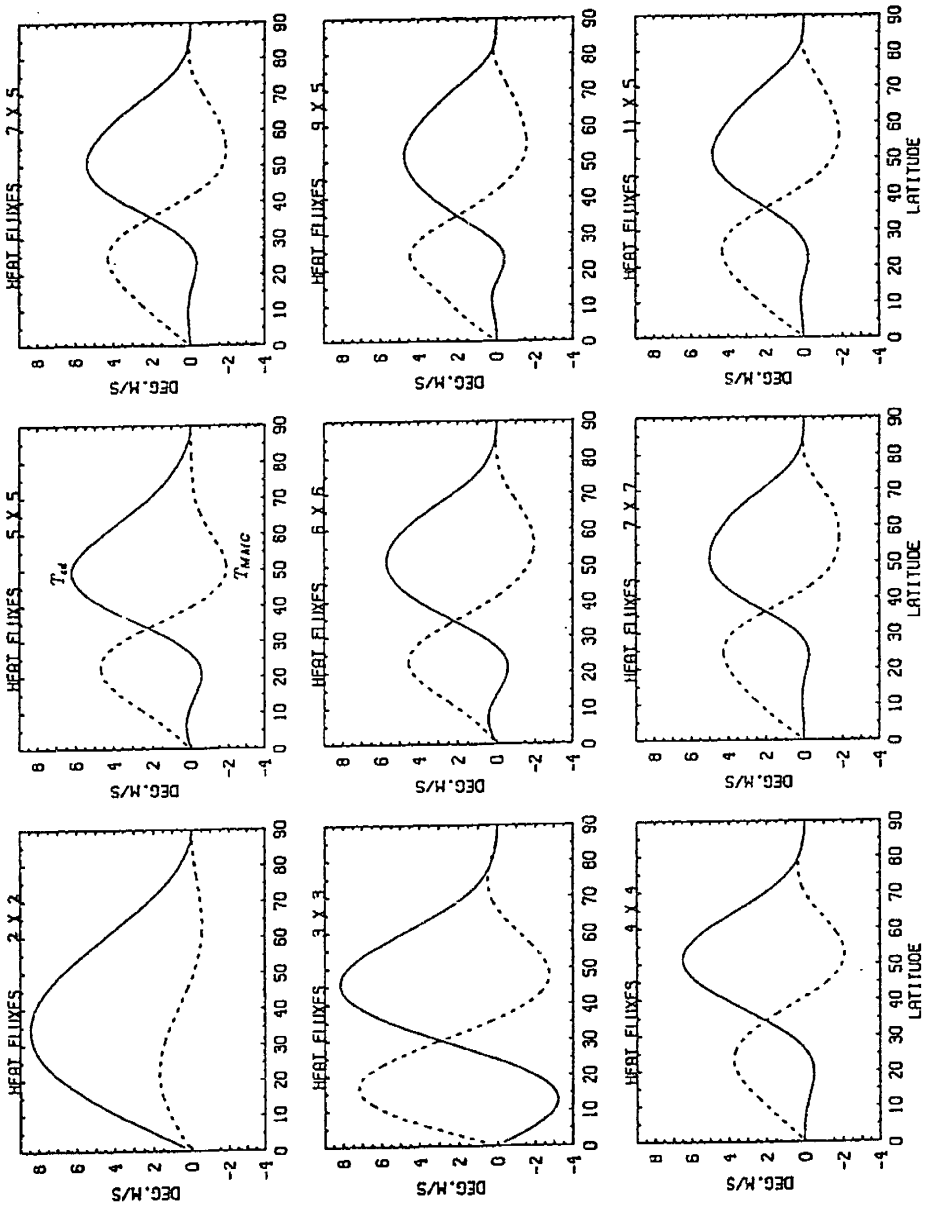

Figure 5.15: The heat fluxes by eddies and by the MMC in the truncation experiments. The meanings for the lines are same as those in Figure 5.7 (b).

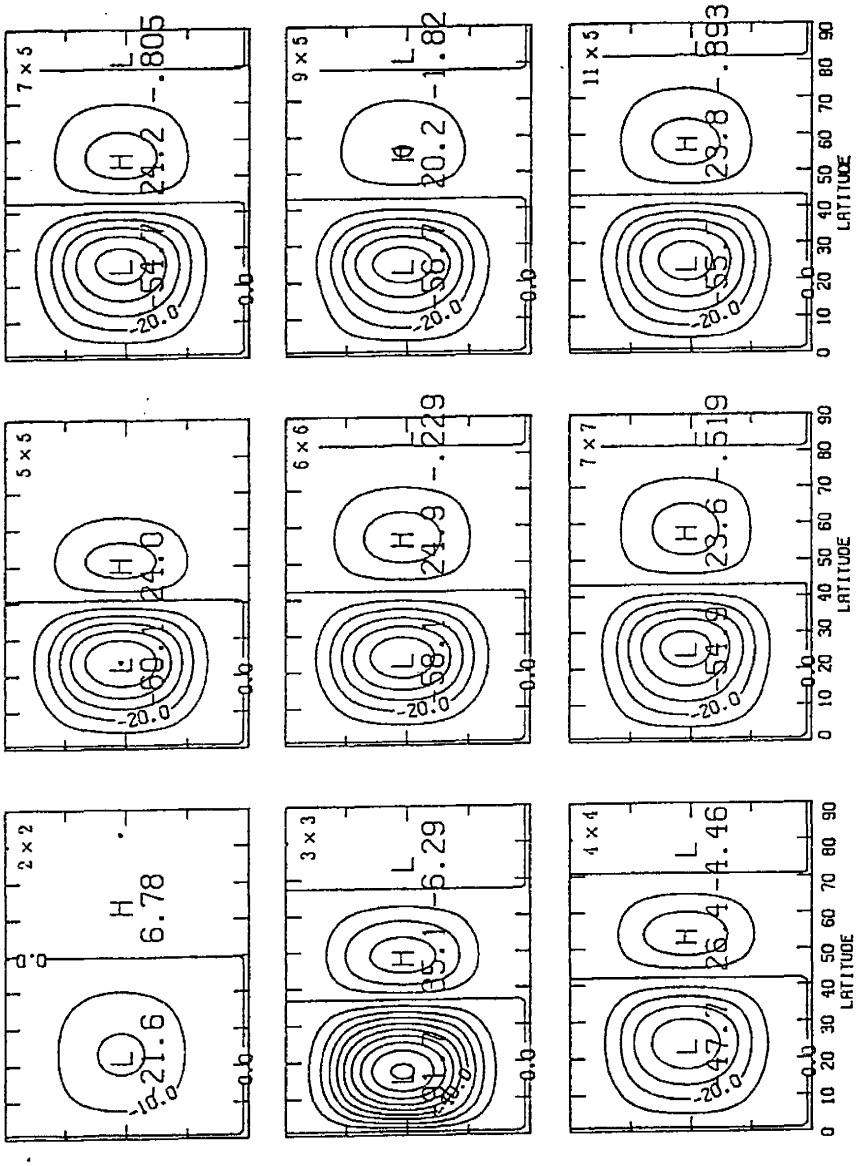

Figure 5.16: The MMC stream functions in the truncation experiments. The contour interval is $10\,mb.m/s$.

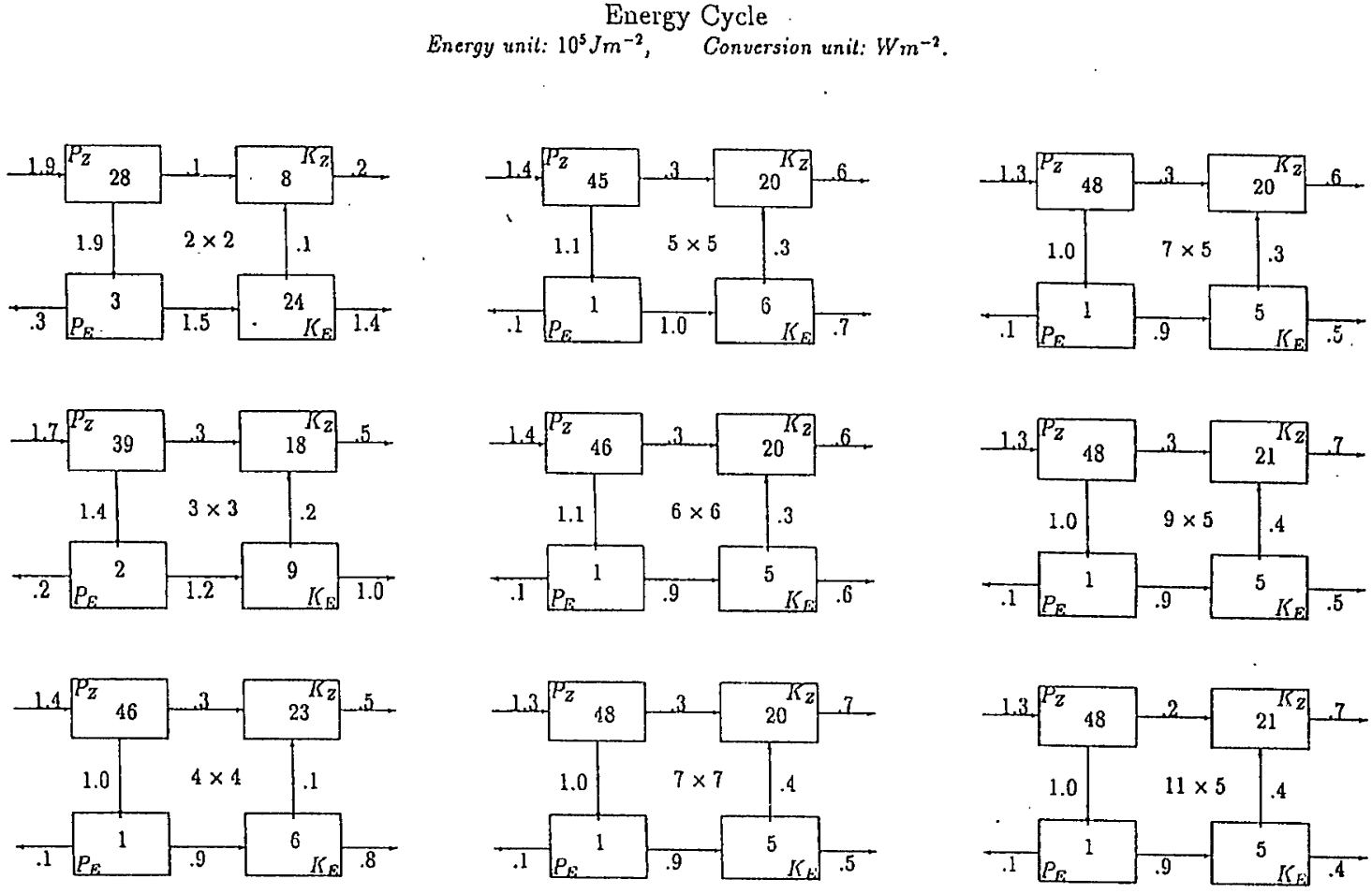

Figure 5.17: The energy cycle diagrams in the truncation experiments.

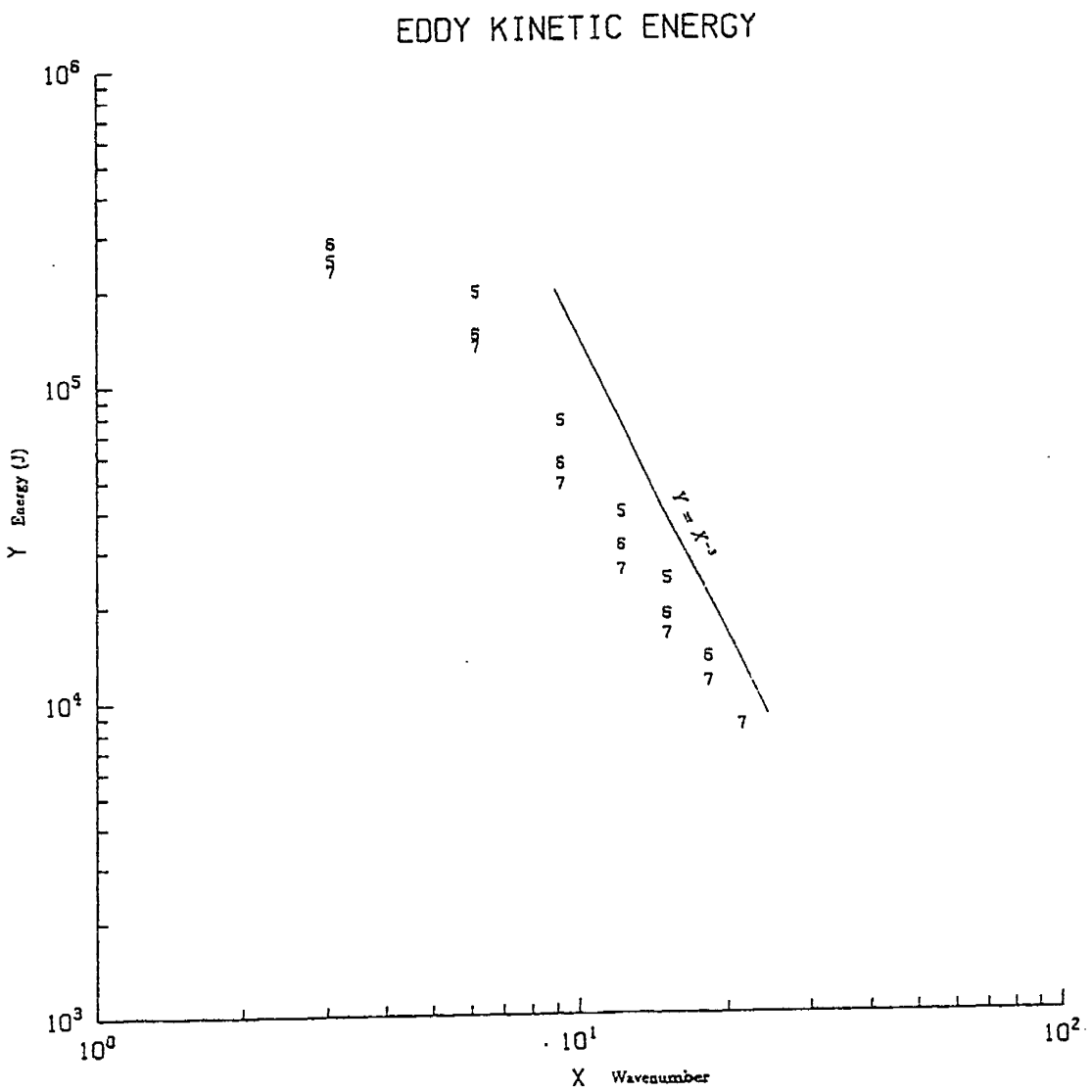

Figure 5.18: The eddy kinetic energy spectrum in the truncation experiments. The X-axis is the zonal wavenumber and the Y-axis is the amount of energy. The numbers 5, 6, 7 denote resolutions 5×5, 6×6, 7×7 respectively.

5.4.3 Fundamental wavenumbers

Although many studies have been done on truncation levels, there has been little attention to the choice of fundamental wavenumbers. Here we examine the impact of variations of the fundamental wavenumber. First, we choose a reference resolution, e.g., $5 \times 5(3)$, which has the fundamental wavenumber 3 and is truncated at zonal wavenumber 15. Then, we fix the meridional resolution at the same level (i.e., 5 meridional modes) and vary the fundamental zonal wavenumber. Three more experiments, $5 \times 15(1)$, $5 \times 8(2)$ and $5 \times 5(6)$, have been done with the fundamental wavenumber $m = 1, 2, 6$ respectively. The $5 \times 15(1)$ is also truncated at zonal wavenumber 15, while the $5 \times 8(2)$ is truncated at zonal wavenumber 16, and the $5 \times 5(6)$ is truncated at zonal wavenumber 30.

The model's results of these experiments are shown in Figures 5.19 - 5.25. There is very little difference for $m = 1, 2, 3$. However, for $m = 6$, the upper layer zonal wind seems to have a double-jet structure. This feature is similar to that found in the wavenumber experiments by Held and Suarez (1978). Furthermore, for $m = 6$ the dynamical transports and energy conversion processes are slightly weaker than those for $m = 1, 2, 3$. This behavior is probably due to the short wave cut-off in the two-level model. Held and Suarez suggested that because of the convergence of meridians $m = 6$ is too small to be strongly baroclinically unstable poleward of $\sim 70°$ of latitude, thus, heat is transported into high latitudes very inefficiently. From the point of view of wave-wave interaction. In the case of $m = 6$, zonal wavenumber 6 is the longest wave [illegible] possibly the only unstable wave. Unlike the cases of $m = 1, 2, 3$ which contain at least two unstable waves, the zonal wavenumber 6 can not interact actively with other higher wavenumbers because they are all stable. As

a result, the eddy transports are less efficient in the case of $m = 6$.

Furthermore, the total amount of eddy kinetic energy is about same for $m = 1, 2, 3$ but smaller for $m = 6$. For all these cases, the eddy kinetic energy is allocated to each zonal wavenumber following approximately the inverse cube law in the inertial range of wave spectrum (Figure 5.26). Clearly, fundamental wavenumber 3 is a better choice to calculate the climatic equilibrium accurately and economically. Thus, most of the numerical experiments are carried out by using models with $m = 3$ in this study.

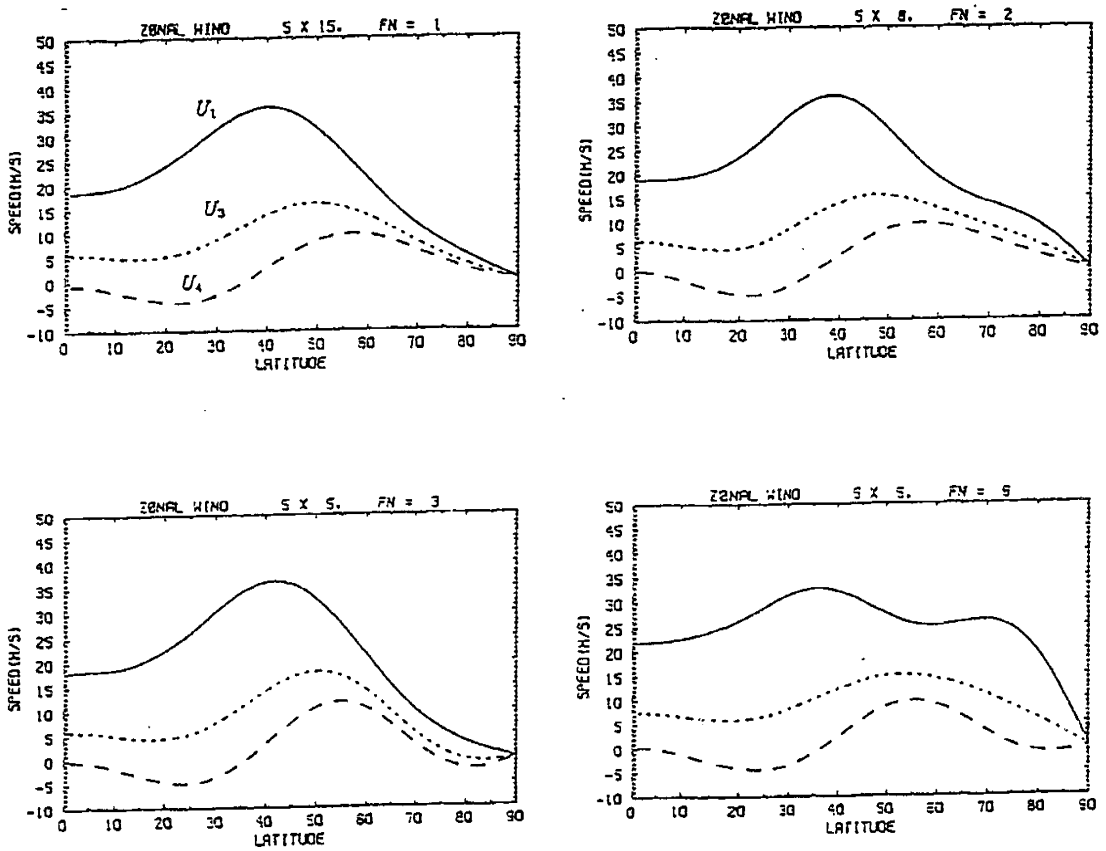

Figure 5.19: The equilibrium zonal wind fields in the fundamental wavenumber experiments. FN is the fundamental wavenumber. The meanings for the lines are same as those of Figure 5.5 (a).

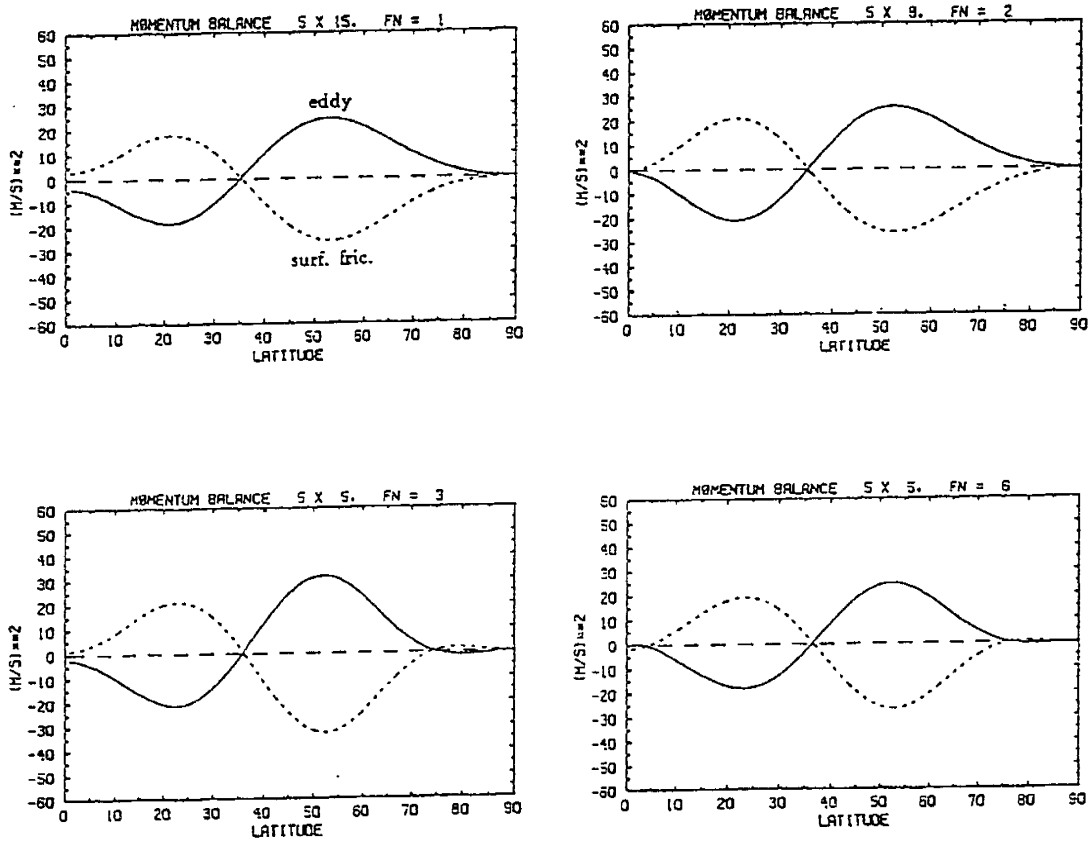

Figure 5.20: The vertical mean momentum budgets in the fundamental wavenumber experiments. The meanings for the lines are same as those of Figure 5.6(c).

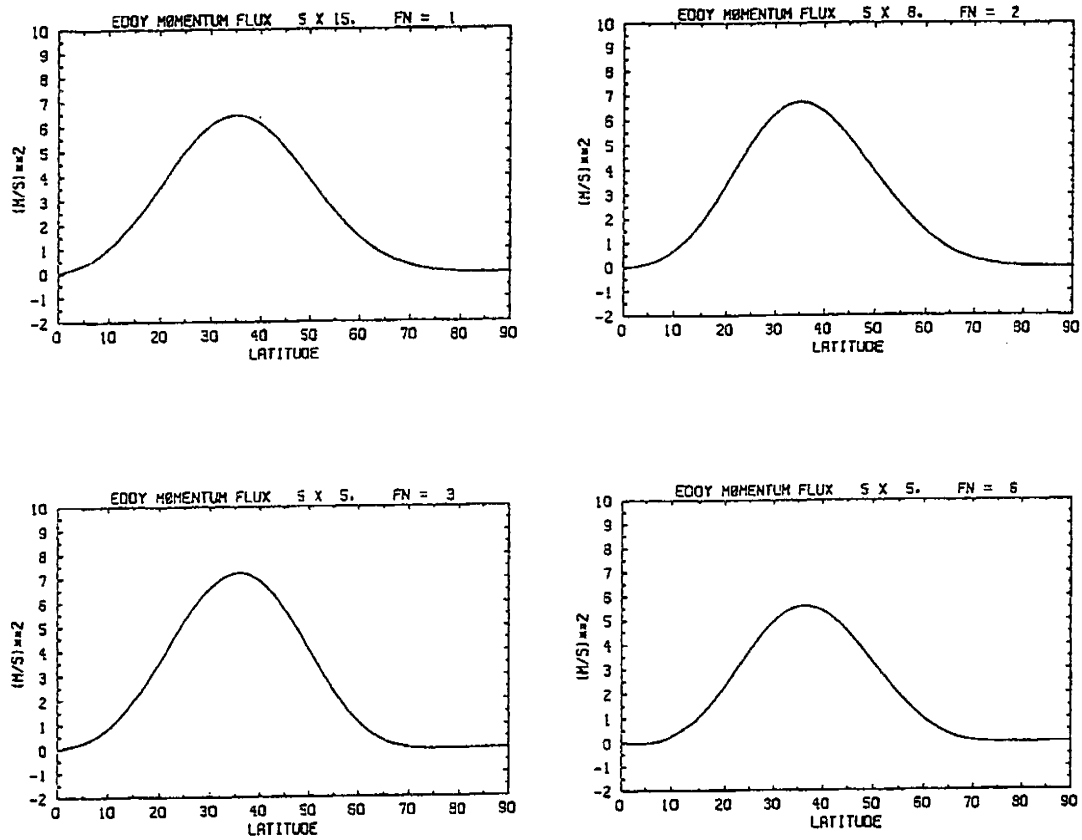

Figure 5.21: The vertical mean eddy momentum fluxes in the fundamental wavenumber experiments.

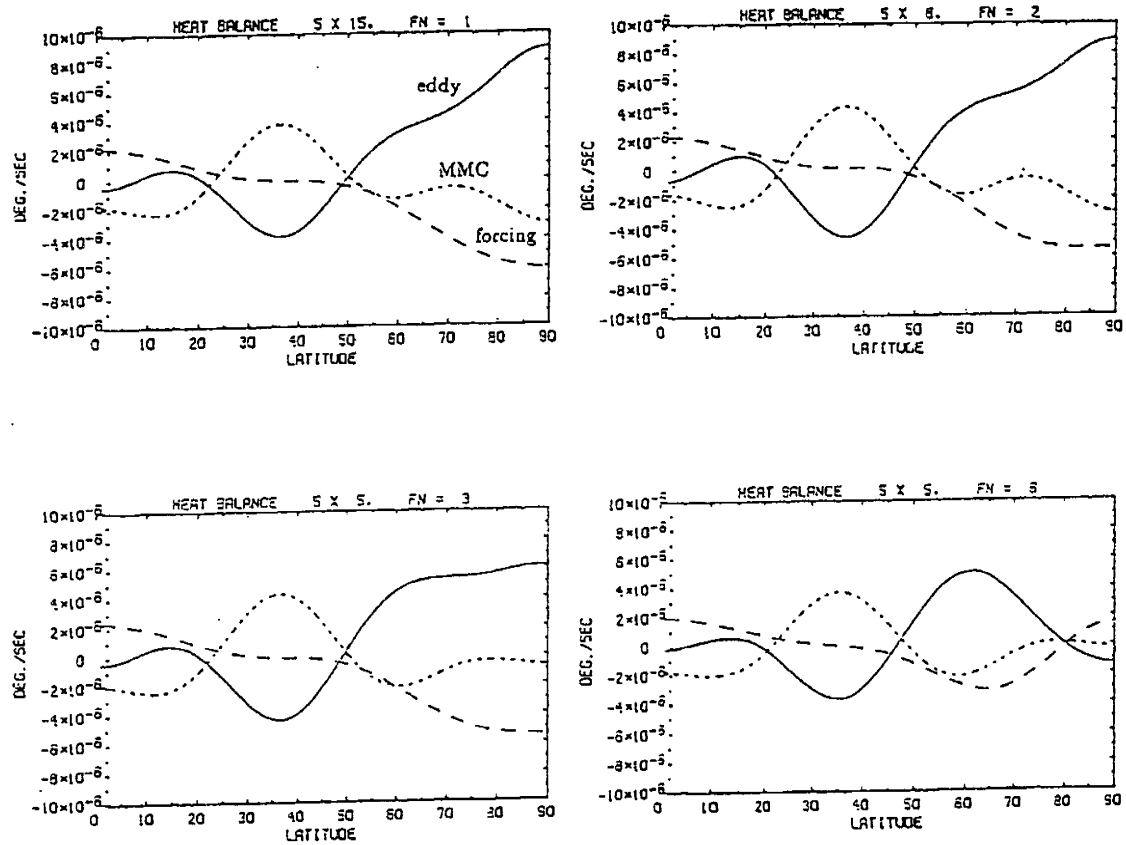

Figure 5.22: The heat budgets in the fundamental wavenumber experiments. The meanings for the lines are same as those of Figure 5.7 (a).

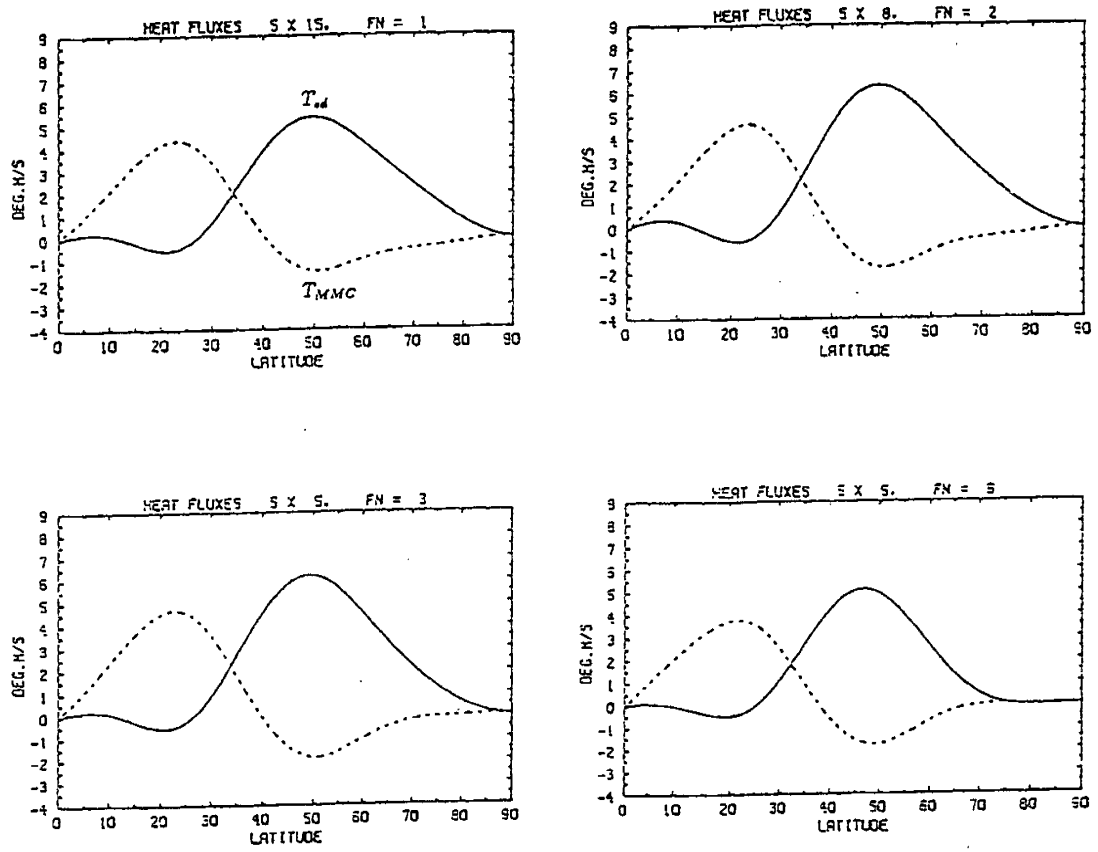

Figure 5.23: The heat fluxes by eddies and by the MMC in the fundamental wavenumber experiments. The meanings for the lines are same as those of Figure 5.7 (b).

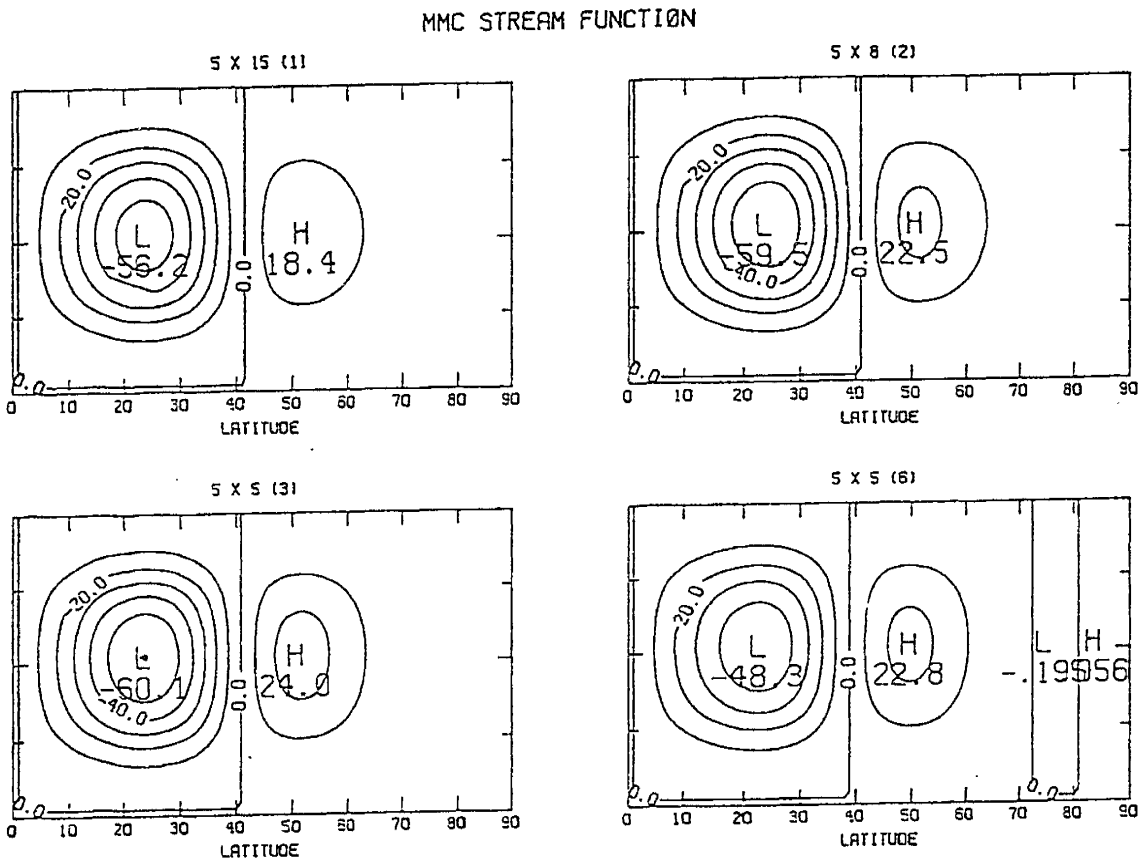

Figure 5.24: The MMC stream functions in the fundamental wavenumber experiments. The contour interval is $10\,mb.m/s$.

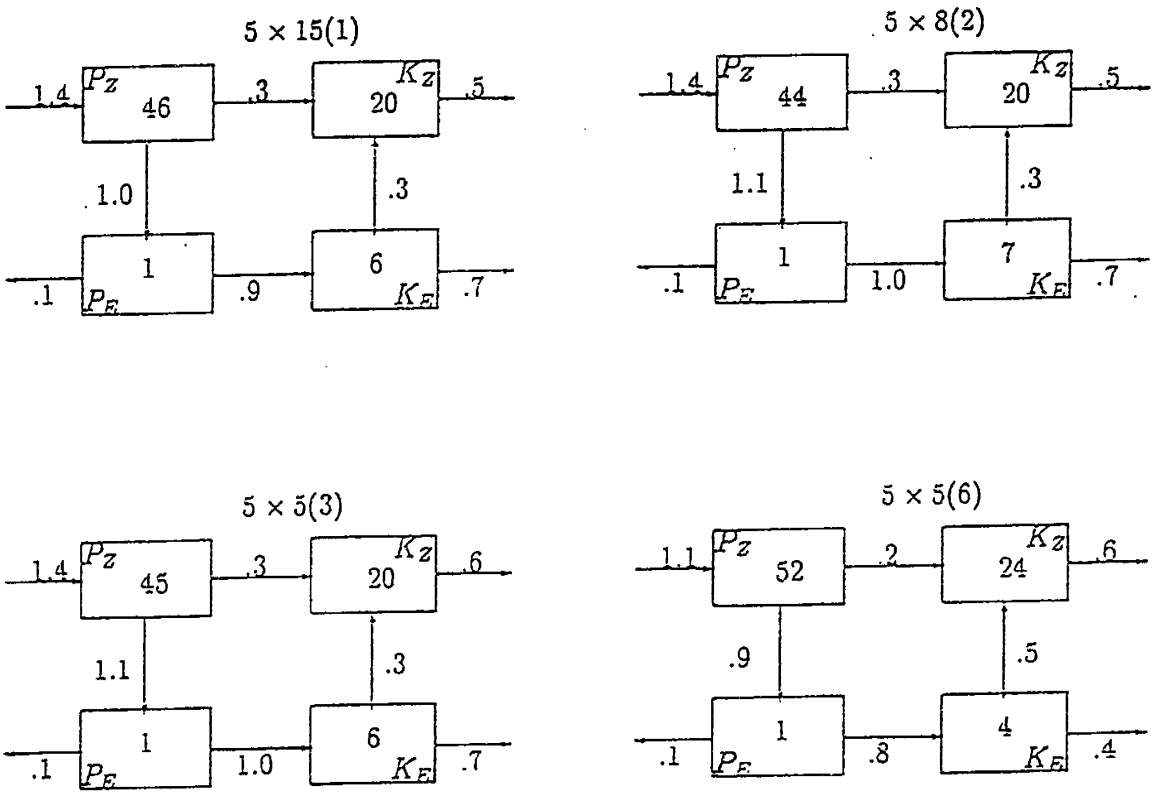

Figure 5.25: The energy cycle diagrams in the fundamental wavenumber experiments.

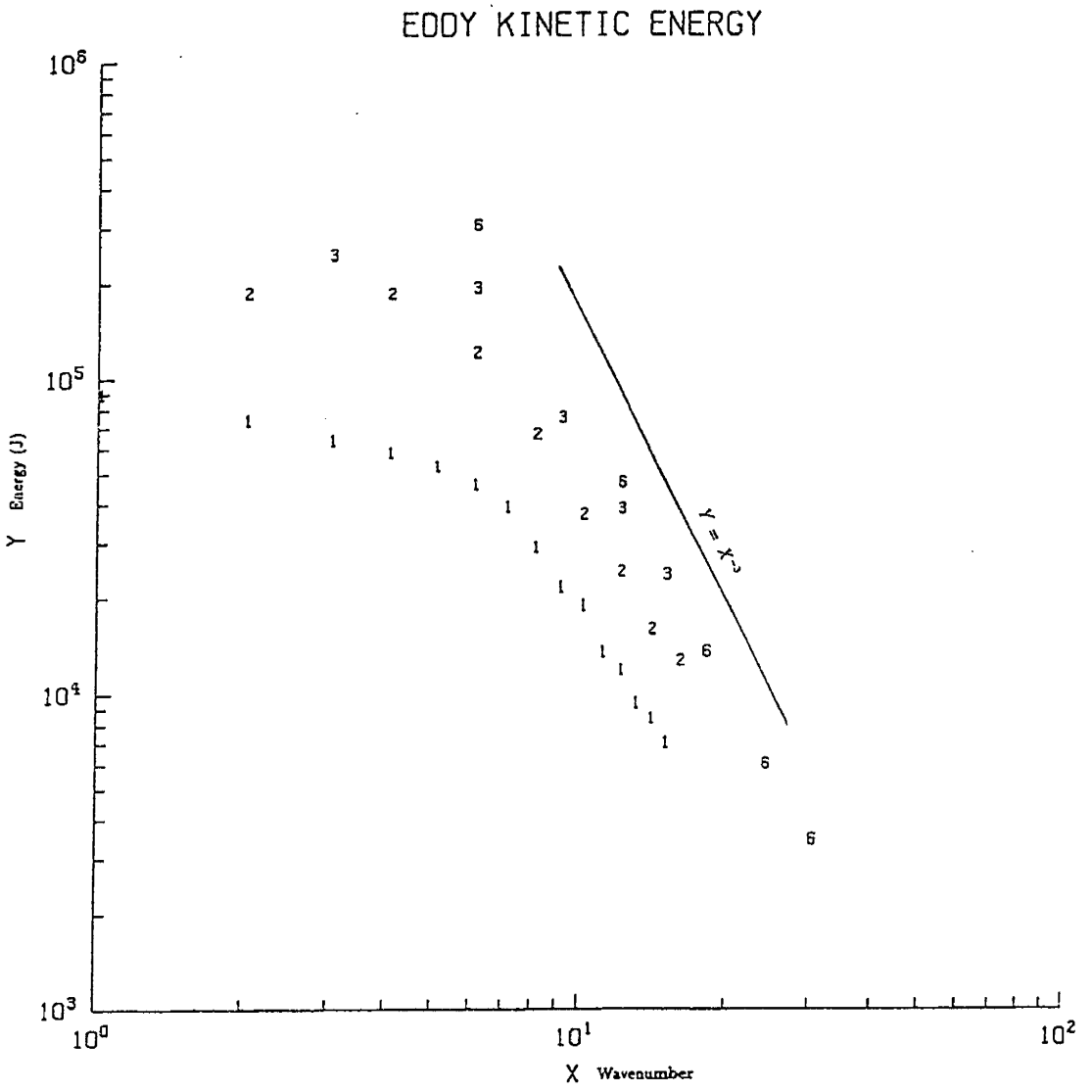

Figure 5.26: The eddy kinetic energy spectrum in the fundamental wavenumber experiments. The X-axis is the zonal wavenumber and the Y-axis is the amount of energy. The numbers 1, 2, 3, 6 denote fundamental wavenumbers.

5.4.4 Dynamical constraints

From the resolution experiments we might conclude that $5 \times 5(3)$ is the "optimal" horizontal resolution for our model. But these experiments are carried out with the "standard" values for the external parameters. If the parameters are allowed to vary, like in the climatic sensitivity studies, we still do not know whether or not this resolution is adequate. Instead of repeating those resolution experiments for each set of parameters, we will check to what extent of parameter changes the "optimal" horizontal resolution meets the condition for the simplification of the basic equations, and is consistent with the vertical resolution.

We have used the *linear balance equation* as the basis of the "filtered" model. This assumes that the Rossby number, R_0 ($R_0 = \frac{U}{fL}$), is of the order 10^{-1} or less. Obviously, the balance equation breaks down near the equator. In spectral models with fixed zonal wavenumber, the wavelength shrinks near the poles due to the convergence of meridians. In very high latitudes the Rossby number can be very large and the balance equation can also break down.

In the "standard" run, R_0 can be estimated from the model results. If we consider the latitude range from 20° to 70° (encompassing the mid latitudes and subtropics), the smallest horizontal wavelength $L = 2\pi a \sin\theta/n$, where $n = 15$ is the largest zonal wavenumber, and the mean zonal wind $U \simeq 20\,m/s$, then

$$R_0 = \frac{U}{fL} \leq 0.16\,.$$

The balance equation is a reasonable simplification for the "standard" run. But, if the external parameters change, for instance, ΔT_E increases or k decreases, U will increase due to stronger forcing or weaker dissipation. R_0 increases with U, so that

to some limit the *linear balance equation* approximation will break down. In fact, for any given resolution the parameter changes are confined by the balance equation approximation.

In order to calculate the dynamical processes accurately, the model must be able to resolve the vertical scale, h_0, of the most unstable baroclinic wave (Held, 1978), i.e.,

$$\gamma \equiv \frac{H}{h_0} \leq 1, \tag{5.30}$$

where H is a scale height, $h_0 = \frac{f^2 U_z}{\beta N^2}$, $U_z = \frac{\partial U}{\partial z}$. If N^2 is very large (or U_z is very small), then h_0 becomes too small to be resolved by the model. Since U_z is determined by the external parameters, such as the diabatic forcing, when we specify the values of those parameters we need to consider this constraint.

Besides, in a model the horizontal resolution should match the vertical resolution, in order to calculate the physical processes accurately. This is because the horizontal scale of a baroclinic wave is related to its vertical scale. For instance, in a modified Charney model with a normal Ekman friction, the most unstable wavelength is about three times the Rossby deformation radius (Lin and Pierrehumbert, 1988). However, the Rossby deformation radius is not a constant. In continuous or multi-level models each vertical mode is associated with a deformation radius (Gill, 1982). Even though in two-level models there is only one vertical scale $\Delta Z \approx H$, therefore, only one deformation radius, the radius is still a function of latitude and static stability. Its variation must be taken into account as these parameters change.

We denote the highest zonal wave number in the model as k_c ($k_c = 2\pi/L_c$, where L_c is the shortest wavelength which can be resolved by the model's horizontal

resolution). The consistent horizontal and vertical resolutions require

$$\frac{1}{k_c} \leq \frac{NH}{f}. \tag{5.31}$$

This implies that the static stability parameter, N (or Γ_0), can not take very small values; otherwise the horizontal resolution must increase. For example, in the resolution of $5 \times 5(3)$, we calculated the lower limit of Γ_0, which is ~ 0.0022.

According to above discussions, for a horizontal resolution to meet the requirement of small Rossby number, all external parameters which affect the strength of mean flow are confined to certain ranges; to be consistent with the vertical resolution, the static stability can not be very small. In any case, $\gamma \leq 1$ must be satisfied. This implies that all parameters which affect the baroclinity (both U_z and N^2) are confined in the model. One can not choose a value of each parameter arbitrarily without considering these constraints. We will keep this in mind in the following parameter experiments.

5.5 Effects of changes in the external parameters

5.5.1 Introduction

We have carried out a series of numerical experiments to examine the effects of changes in the external parameters, i.e., ΔT_E, τ_h, Γ_0, and τ_s, on the climatic equilibrium and eddy transports. The parameters were changed separately, with other remaining parameters fixed at the "standard" values. The ranges of the parameters were chosen carefully, such that the horizontal resolutions remain appropriate and the dynamical constraints are not violated. Most of the experiments were carried

out with the resolution of $5 \times 5(3)$. A few required higher resolutions, e.g., $7 \times 7(3)$, for very small static stability.

In general, these experiments are very similar to those carried out by Stone and Branscome (1991), except that their model is on a β-plane and without interfacial friction, whereas our model is on a sphere and has a specified interfacial friction. We have calculated the statistical equilibrium states for each set of parameters. The integration time to arrive at statistical equilibrium is different for each experiment. Some of the experiments have been integrated from 500 to 1,000 days, while others have been integrated even longer, e.g., for very large τ_h the integration time exceeds 5,000 days. The results are described in the next subsection (5.5.2).

In order to compare our results directly with those obtained by Stone and Branscome (1991), particularly, to compare the variations of the feedback factor (R), we carried out several parameter experiments *without* any interfacial friction. These experiments are used to check the effect of spherical geometry. The results are presented in subsection 5.5.3. A schematic summary is given in subsection 5.5.4.

5.5.2 Parameter experiments

i) Diabatic forcing ΔT_E

We have varied ΔT_E from $24\,K$ to $144\,K$. For values of ΔT_E smaller than $24\,K$ the system is stable and in radiative equilibrium , therefore, eddies can not grow. For very large values of ΔT_E the zonal wind is so strong that R_0 becomes too large to justify the "filtered" model. The surface zonal wind, the meridional flow, the eddy momentum flux and the eddy heat flux are shown in Figure 5.27

for ΔT_E = 30, 48, 72, 144 K. The strength of all these quantities increases with ΔT_E. The surface winds are linearly extrapolated from the upper layer and lower layer winds. In fact, the vertical shear is much less sensitive than the vertical mean wind to ΔT_E, implying that baroclinic adjustment takes place. This feature will be examined in detail in chapter 7.

Some characteristic quantities are shown in Table 5.3 for various values of ΔT_E. The meanings and units of symbols in this table are the same as in Table 5.2. We note that the feedback factor, R, decreases with ΔT_E. The energetics are given in Table 5.4. The units are conventional, i.e., $10^5 J/m^2$ for energy storage terms and W/m^2 for other terms. When ΔT_E increases, all forms of energy storage increase; the energy generation, dissipation and conversion terms also increase monotonically. The distribution of eddy kinetic energy in the wavenumber domain is given in Table 5.5. Most of the energy is concentrated at wavenumber 3 and 6. When ΔT_E increases, the energy of the longest wave in the model – wavenumber 3 becomes more and more dominant (as will be discussed in chapter 7, the proportion in the eddy heat transport by wavenumber 3 also becomes more and more dominant). This feature is consistent with that found by Cehelsky and Tung in their β-plane model (Cehelsky and Tung, 1991). They calculated the heat transport by each wave component, and found that when the diabatic forcing is strong most of the heat is transported by the longest wave.

Table 5.3: Some characteristic quantities in the ΔT_E experiments.

$\Delta T_E(K)$	30	48	72	144
ΔT	25.2	34.0	44.3	59.5
δT	10.9	14.1	16.2	20.4
M	.58	1.19	1.46	2.26
$[v^*M^*]_y$	10.9	24.5	32.8	70.8
t_M	61.4	56.0	51.7	36.9
$[u]_s$	4.7	11.8	21.1	39.0
(lat.)	(61)	(55)	(58)	(58)
$[v]_1$	.13	.26	.72	2.08
(lat.)	(25)	(23)	(25)	(24)
$[u^*v^*]$	2.4	7.2	12.9	26.8
(lat.)	(41)	(36)	(37)	(34)
T_{ed}	1.75	6.20	15.1	42.0
T_{MMC}	-.60	-1.88	-3.99	-7.84
R	.34	.30	.26	.19

Table 5.4: The energetics in the ΔT_E experiments.

$\Delta T_E(K)$	30	48	72	144
P_Z	23.	45.	62.	104.
P_E	.2	1.2	2.4	5.4
K_E	2.	6.	11.	26.
K_Z	8.	20.	30.	66.
$C(P_Z, P_E)$	.2	1.1	3.3	12.8
$C(P_E, K_E)$	.2	1.0	3.0	12.0
$C(K_E, K_Z)$	.1	.3	.9	3.6
$C(P_Z, K_Z)$	.1	.3	1.3	5.8
G_Z	.3	1.4	4.6	18.5
G_E	-.04	-.1	-.3	-.6
D_E	-.1	-.7	-2.1	-8.5
D_Z	-.2	-.6	-2.2	-9.3

Table 5.5: The spectrum of eddy kinetic energy in the ΔT_E experiments.

$n \backslash \Delta T_E(K)$	30	48	72	144
3	.68	2.48	5.66	16.39
6	.52	1.94	2.83	5.53
9	.22	.75	1.12	2.01
12	.09	.39	.56	1.04
15	.05	.24	.35	.62

ii) Newtonian cooling time τ_h

We have varied the Newtonian cooling time τ_h from 5 to 5120 days. The lower value is more phisically plausible, while the higher value was chosen to test the nearly adiabatic case. Some of the equilibrium states and eddy transports, i.e., the surface zonal wind, the meridional flow, the eddy momentum flux and the eddy heat flux, are shown in Figure 5.28 for $\tau_h = 5$, 20, 80, 320 days. They all increase when τ_h decreases. These features are very similar to those found in the experiments with increasing ΔT_E, probably due to the overall effect of diabatic heating. This happens because $\bar{Q}$ can be strengthened either by increasing ΔT_E or by decreasing τ_h, in the Newtonian cooling form.

The characteristic quantities are listed in Table 5.6 for different τ_h. The feedback factor, R, increases with τ_h. The energetics and the spectrum of eddy kinetic energy are given in Tables 5.7 and 5.8 respectively. Again, they are similar to those in the ΔT_E experiments.

Table 5.6: Some characteristic quantities in the τ_h experiments.

$\tau_h(days)$	5	20	80	320
ΔT	42.0	34.0	26.5	24.9
δT	15.6	14.1	11.8	10.0
M	1.34	1.19	.73	.52
$[v^*M^*]_y$	30.9	24.5	12.5	6.2
t_M	50.0	56.0	67.5	96.4
$[u]_s$	16.0	11.8	5.2	2.9
(lat.)	(57)	(55)	(57)	(59)
$[v]_1$	.32	.26	.16	.05
(lat.)	(20)	(23)	(27)	(26)
$[u^*v^*]$	10.3	7.2	2.8	1.5
(lat.)	(37)	(36)	(39)	(41)
T_{ed}	9.70	6.20	2.32	.86
T_{MMC}	-2.32	-1.88	-.79	-.37
R	.24	.30	.34	.43

Table 5.7: The energetics in the τ_h experiments.

$\tau_h(days)$	5	20	80	320
P_Z	62.	45.	25.	16.
P_E	1.4	1.2	.5	.3
K_E	7.	6.	3.	1.5
K_Z	29.	20.	9.	5.
$C(P_Z, P_E)$	2.1	1.1	.3	.1
$C(P_E, K_E)$	1.4	1.0	.3	.1
$C(K_E, K_Z)$	.6	.3	.1	.02
$C(P_Z, K_Z)$	.4	.3	.2	.1
G_Z	2.5	1.4	.5	.1
G_E	-.7	-.1	-.02	-.00
D_E	-.9	-.7	-.2	-.01
D_Z	-1.0	-.6	-.3	-.1

Table 5.8: The spectrum of eddy kinetic energy in the τ_h experiments.

$n \backslash \tau_h(days)$	5	20	80	320
3	3.44	2.48	.70	.24
6	2.14	1.94	.76	.28
9	.68	.75	.10	.02
12	.35	.39	.04	.01
15	.22	.24	.01	.00

iii) Static stability parameter Γ_0

The static stability parameter Γ_0 has been varied from .003 to .026 (equivalent to N^2 varying from $.25 \times 10^{-4}\, s^{-2}$ to $2.0 \times 10^{-4}\, s^{-2}$). If Γ_0 is too large, the instability will be inhibited and eddies can not grow. On the other hand, if Γ_0 is too small, it requires very high horizontal resolution to meet the dynamical constraint (as discussed in subsection 5.4.4). The computation time will increase drastically. For instance, we have used a resolution of $7 \times 7(3)$ to carry out experiments with $\Gamma_0 \leq .010$. The computation time increased about a factor of 8 from $5 \times 5(3)$.

The model's results for $\Gamma_0 = .010,\ .013,\ .016,\ .023$ are shown in Figure 5.29. When Γ_0 decreases, the eddy fluxes of momentum and heat increase appreciably. This is consistent with the linear analysis of instability, which shows that smaller static stabilities favor greater wave growth rate. Although the strength of the MMC increases when Γ_0 decreases, the intensity of the MMC heat flux, T_{MMC}, does not change much. This is because T_{MMC} is represented by $\Gamma_0\bar{\omega}$ and a larger Γ_0 is always associated with a smaller $\bar{\omega}$.

Similarly, Table 5.9 shows variations of the characteristic quantities with Γ_0.

Table 5.9: Some characteristic quantities in the Γ_0 experiments.

Γ_0	.010	.013	.016	.023
ΔT	33.6	34.0	36.9	41.0
δT	12.3	14.1	15.9	16.6
M	1.16	1.19	1.07	.96
$[v^*M^*]_y$	38.3	24.5	18.9	12.9
t_M	35.1	56.0	65.4	86.0
$[u]_s$	17.0	11.8	10.1	7.5
(lat.)	(60)	(55)	(60)	(65)
$[v]_1$	.32	.26	.20	.14
(lat.)	(22)	(23)	(26)	(30)
$[u^*v^*]$	11.8	7.2	5.2	2.8
(lat.)	(35)	(36)	(42)	(46)
T_{ed}	6.59	6.20	4.03	2.47
T_{MMC}	-1.73	-1.88	-1.53	-1.31
R	.26	.30	.38	.53

R increases when the static stability increases. Table 5.10 shows the energetics in these experiments. All forms of the energy and the main energy processes, such as $C(P_Z, P_E)$ and $C(P_E, K_E)$, increase when Γ_0 decreases. In this respect, decreasing the static stability has the same effect as increasing the diabatic heating. However, their effects on the eddy kinetic energy cascade are different. As is seen in Table 5.11, the proportion of eddy kinetic energy in the longest wave seems insensitive to the change in static stability.

Table 5.10: The energetics in the Γ_0 experiments.

Γ_0	.010	.013	.016	.023
P_Z	55.	45.	40.	31.
P_E	1.7	1.2	.7	.3
K_E	8.	6.	3.	1.
K_Z	22.	20.	18.	16.
$C(P_Z, P_E)$	1.6	1.1	.6	.2
$C(P_E, K_E)$	1.5	1.0	.5	.2
$C(K_E, K_Z)$	.53	.29	.21	.12
$C(P_Z, K_Z)$	.3	.3	.3	.3
G_Z	2.1	1.4	1.0	.5
G_E	-.20	-.14	-.08	-.03
D_E	-.9	-.7	-.3	-.1
D_Z	-.8	-.6	-.5	-.4

Table 5.11: The spectrum of eddy kinetic energy in the Γ_0 experiments.

$n\backslash\Gamma_0$	.010	.013	.016	.023
3	3.53	2.48	1.63	.81
6	2.16	1.94	1.11	.29
9	.80	.75	.37	.09
12	.43	.39	.19	.06
15	.25	.24	.11	.03

iv) Surface drag k

We have varied the dissipative time scale associated with the surface drag, τ_s, from 1.25 to 40 days (equivalent to varying k from .0025 to .08). For very large values of τ_s the zonal wind becoms very strong, therefore, R_0 becomes too large to justify the simplified equations. In Figure 5.30 we only show the results for τ_s = 2.5, 5, 10, 20 days. When τ_s increases, i.e., the surface drag weakens, the surface wind increases appreciably. In fact, the increase of surface wind is due to the increase of the vertical mean wind . The vertical shear is insensitive to the change in τ_s. The eddy heat flux and the the meridional flow are also insensitive to the change in τ_s.

The characteristic quantities in the τ_s experiments are shown in Table 5.12. We note that R decreases slightly and the eddy time scale, t_M, increases drastically when τ_s increases. The energetics are given in Table 5.13. Most of the energy forms and the main energy conversion processes are insensitive to the change in τ_s. However, when τ_s increases, K_Z and $C(K_E, K_Z)$ increase correspondingly. Though the dissipation terms vary slightly, D_Z and D_E vary in opposite direction. When τ_s increases, the zonal mean surface wind becomes stronger, therefore D_Z increases. The decrease in D_E is associated with the increase in $C(K_E, K_Z)$. The spectrum of eddy kinetic energy is given in Table 5.14. When τ_s decreases, the proportion of eddy kinetic energy in wavenumber 3 also decreases but the proportion in wavenumber 6 increases. In other words, strong surface drag (small τ_s) prevents upscale cascades of eddy kinetic energy (Rhines, 1975; Williams, 1978).

Table 5.12: Some characteristic quantities in the τ_s experiments.

$\tau_s(days)$	2.5	5	10	20
ΔT	35.3	34.0	36.0	36.6
δT	13.8	14.1	13.5	13.3
M	1.01	1.19	1.23	1.56
$[v^*M^*]_y$	26.0	24.5	16.7	14.2
t_M	44.8	56.0	85.1	127.
$[u]_s$	7.1	11.8	20.1	27.8
(lat.)	(55)	(55)	(60)	(58)
$[v]_1$	.27	.26	.23	.22
(lat.)	(24)	(23)	(23)	(23)
$[u^*v^*]$	7.9	7.2	6.0	4.9
(lat.)	(37)	(36)	(35)	(34)
T_{ed}	6.51	6.20	5.66	5.64
T_{MMC}	-2.19	-1.88	-1.69	-1.66
R	.34	.30	.30	.29

Table 5.13: The energetics in the τ_s experiments.

τ_s	2.5	5.	10.	20.
P_Z	45.	45.	46.	47.
P_E	1.2	1.2	1.3	1.3
K_E	5.	6.	6.	6.
K_Z	19.	20.	23.	31.
$C(P_Z, P_E)$	1.1	1.1	1.1	1.1
$C(P_E, K_E)$	1.0	1.0	1.0	.9
$C(K_E, K_Z)$	.2	.3	.3	.4
$C(P_Z, K_Z)$	.3	.3	.3	.3
G_Z	1.4	1.4	1.4	1.4
G_E	-.13	-.14	-.15	-.15
D_E	-.8	-.7	-.6	-.5
D_Z	-.5	-.6	-.6	-.7

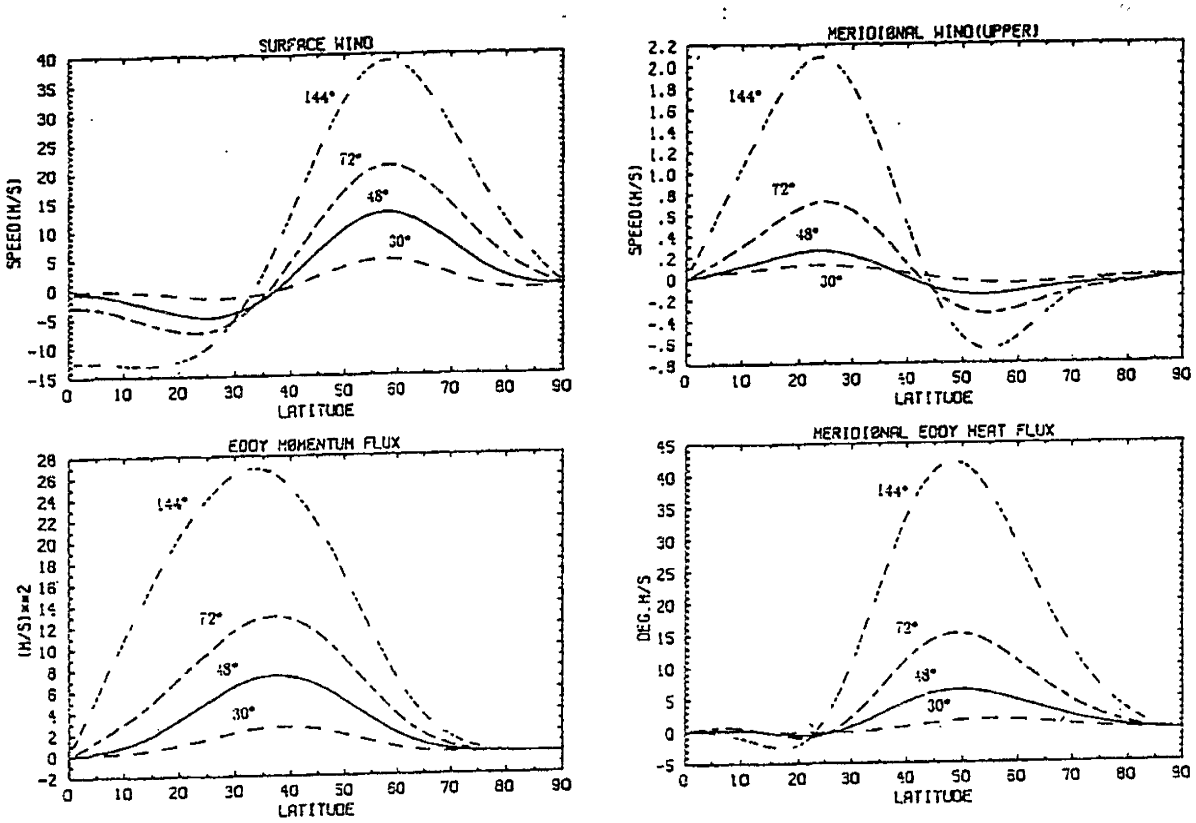

Figure 5.27: The surface winds, the upper layer meridional winds, the eddy momentum fluxes and the eddy heat fluxes in the ΔT_E experiments.

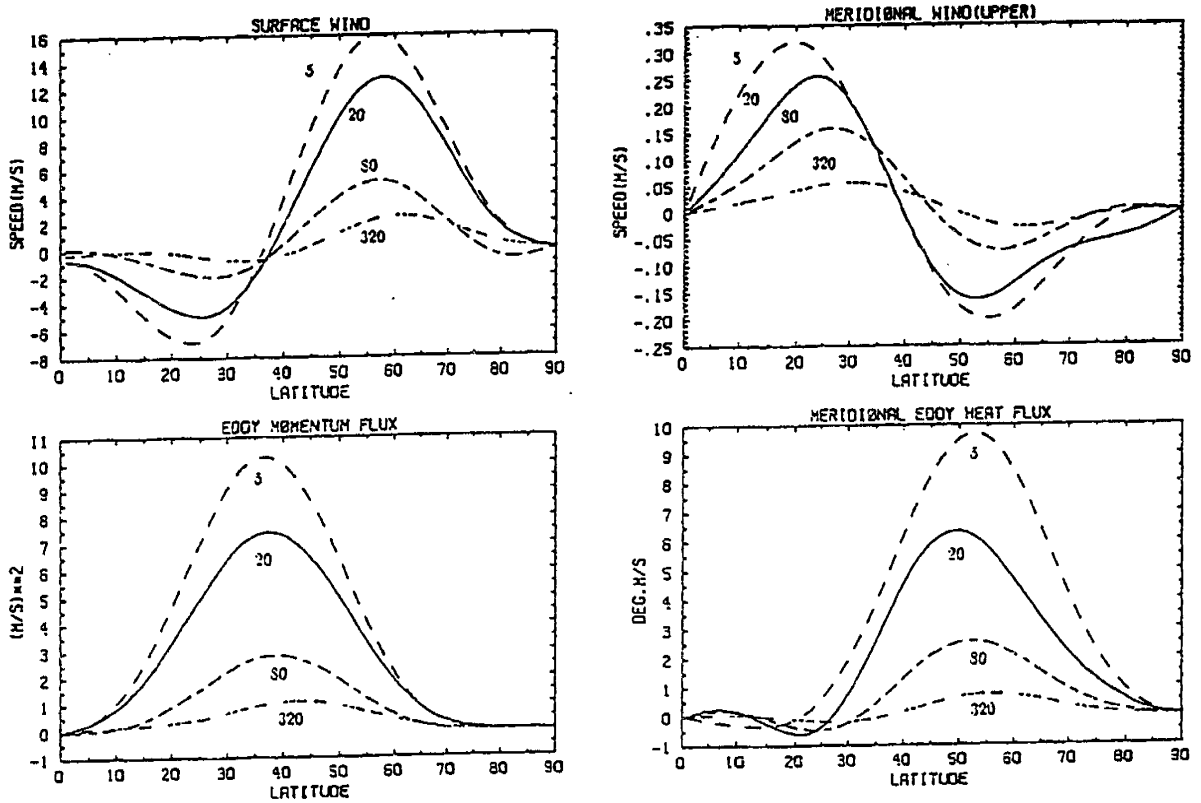

Figure 5.28: The surface winds, the upper layer meridional winds, the eddy momentum fluxes and the eddy heat fluxes in the τ_h experiments.

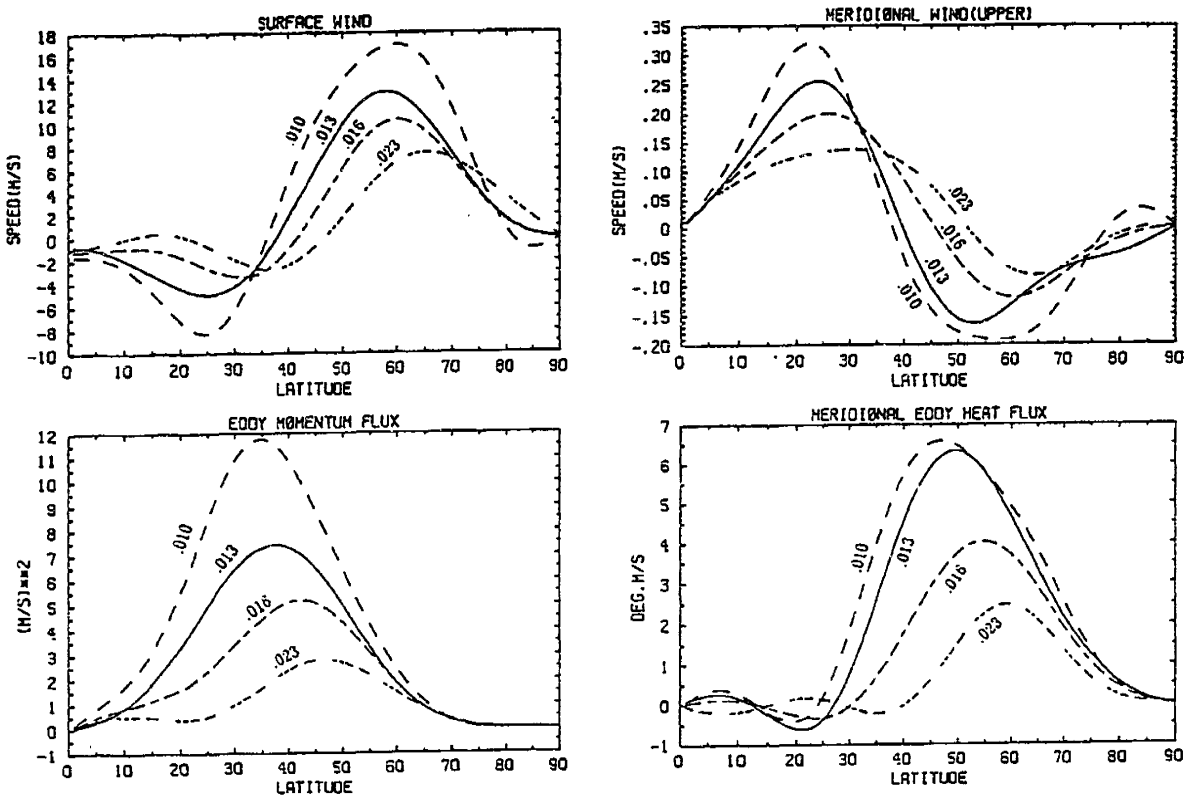

Figure 5.29: The surface winds, the upper layer meridional winds, the eddy momentum fluxes and the eddy heat fluxes in the Γ_0 experiments.

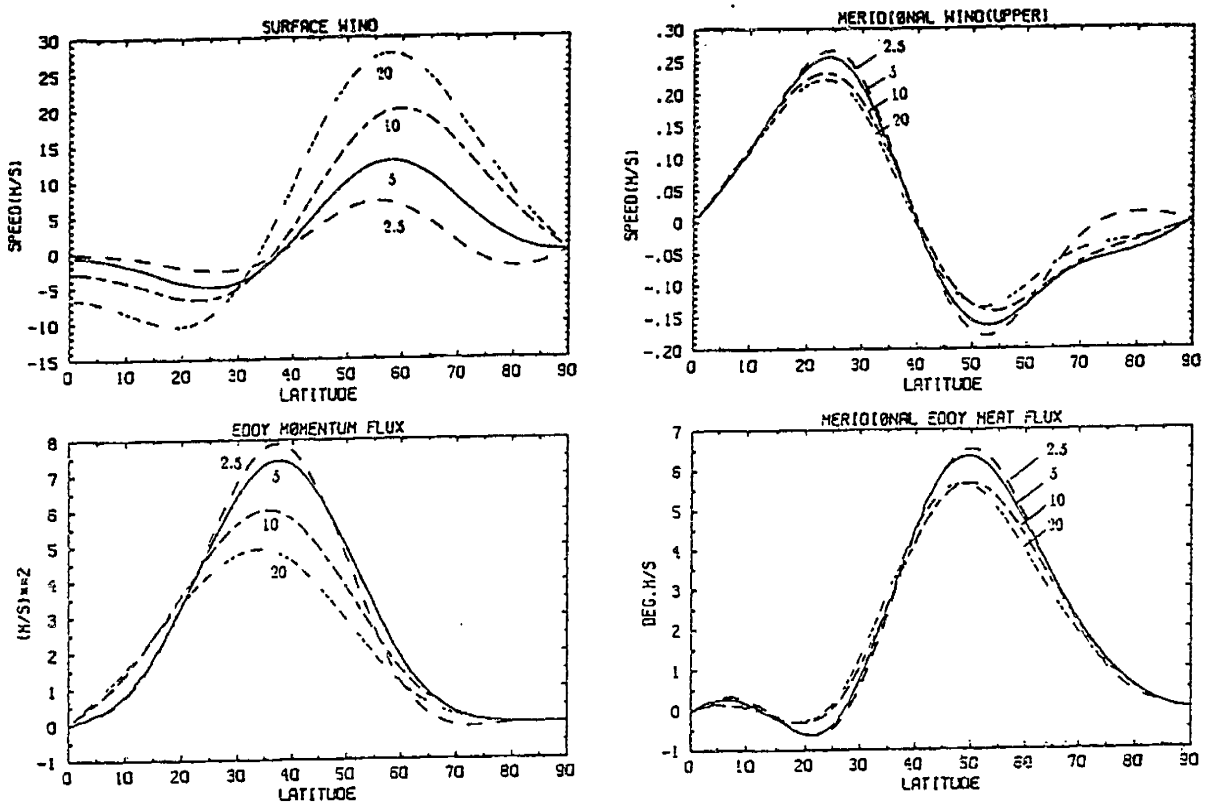

Figure 5.30: The surface winds, the upper layer meridional winds, the eddy momentum fluxes and the eddy heat fluxes in the τ_s experiments.

Table 5.14: The spectrum of eddy kinetic energy in the τ_s experiments.

$n \backslash \tau_s$	2.5	5.	10.	20.
3	2.31	2.48	2.76	3.13
6	1.91	1.94	1.76	1.65
9	.63	.75	.80	.76
12	.32	.39	.42	.47
15	.17	.24	.28	.32

5.5.3 The feedback factor

In order to describe quantitatively how much the MMC heat flux offsets the eddy heat flux in the mid-high latitudes, Stone and Branscome (1991) have defined a feedback factor:

$$R = -\frac{T_{MMC}}{T_{ed}}, \tag{5.32}$$

where T_{MMC} and T_{ed} denote characteristic heat fluxes (e.g., the maximal magnitudes) by the MMC and by eddies respectively. By using a quasi-geostrophic scaling analysis, Stone and Branscome have shown that R can be estimated by

$$R \sim R_S = \frac{\delta r}{1 - r(1-\delta)}, \tag{5.33}$$

where

$$\delta = \frac{4L_r^2}{a^2}\frac{\tau_h}{t_e}, \tag{5.34}$$

$$t_e = \frac{[\bar{U}]}{\frac{1}{a\sin^2\theta}\frac{\partial}{\partial\theta}[\overline{u^*v^*}]\sin^2\theta}, \tag{5.35}$$

$$r = \frac{\partial T/\partial\theta}{\partial T_E/\partial\theta}. \tag{5.36}$$

R_S is the predicted feedback factor from the scaling method; t_e is the *eddy time scale* associated with the forcing of the zonal mean flow by the zonal mean eddy fluxes of momentum.

From the numerical solutions of a two-level β-plane model, Stone and Branscome calculated the values of R and R_S. In their calculations, T_{MMC}, T_{ed}, $[\bar{U}]$ and $\frac{1}{a\sin^2\theta}\frac{\partial}{\partial\theta}[\overline{u^*v^*}]\sin^2\theta$ are evaluated at the center of the channel. The relationship between R and R_S is well defined in broad parameter ranges, except that R is systematically larger than R_S (about 2.5 times).

In order to compare with Stone and Branscome's calculations, which neglected interfacial friction, we have carried out several numerical experiments *without any interfacial friction.* In our calculations of R and R_S, we calculated T_{MMC} and T_{ed} at the latitudes where they peak. Although those latitudes are somewhat different for each experiment, usually they are around 45°. To estimate $\frac{\partial T}{\partial\theta}$ and $\frac{\partial T_E}{\partial\theta}$ we chose $\theta = 45°$ as the reference colatitude, i.e., $\frac{\partial T}{\partial\theta} \sim T_{55°} - T_{35°}$, $\frac{\partial T_E}{\partial\theta} \sim T_{E_{55°}} - T_{E_{35°}}$, because the maximal gradient of T_E is at 45°. Since the profiles of $[\bar{U}]$ and $\frac{1}{a\sin^2\theta}\frac{\partial}{\partial\theta}[\overline{u^*v^*}]\sin^2\theta$ are irregular in the spherical model, we also calculate their characteristic values at 45°.

The calculated R and R_S are shown in Figure 5.31, in which the abscissa is R_S, and the ordinate is R; each letter represents the results from one of the experiments, specially, "H", "T" and "F" refer to experiments varying τ_h, ΔT_E and τ_s respectively. The straight line shows what the results would have been if the values of R and R_S had been identical.

First, we note that all the letters are very close to the straight line, implying that R and R_S are in good agreement with each other. Unlike the results in the β-plane model, the values of calculated R are not significantly larger than the values of predicted R_S. The difference between the spherical and the β-plane models is probably due to the calculations of eddy momentum fluxes, which are closely related

to the strength of the Ferrel cell. In the β-plane model, because of the absence of the earth's curvature and the unrealistic lateral boundary conditions, the eddy momentum transport is distorted.

Next, we note that, like the results with the β-plane model, R increases and approaches unity when τ_h increases or ΔT_E decreases. In the limit of the diabatic heating vanishing, a complete MMC feedback would occur, and there would be no net eddy forcing on the zonal mean flow in the mid-high latitudes. On the other hand, R decreases and approaches zero when the diabatic heating increases or the surface friction decreases.

Finally, we should mention that the dependence of R on the external parameters is similar when an interfacial friction is included. This has been demonstrated in the parameter experiments described in the previous subsection. However, the calculated values of R can not be directly compared with the predicted values of R_S, because they are modified when the interfacial friction is included.

In their scaling analyses, Stone and Branscome (1991) have shown that the magnitude of R is equivalent to the ratio of the horizontal component to the vertical component of the divergence of the E-P flux. Therefore R is a measure of how accurately the E-P theorem is satisfied. We have calculated this ratio, R_{E-P}, and compared it with R. Their relationship is shown in Figure 5.32, which is similar to Figure 5.31 except that the abscissa is R_{E-P} and the ordinate is R. Clearly, the model's results are consistent with the scaling analyses.

5.5.4 Summary

Figure 5.33 summarizes schematically the processes of temperature adjustment and the effects of changes in the external parameters. The thick arrows denote the basic dynamical processes: The diabatic heating (Q) drives the temperature gradient (ΔT) away from its climatic equilibrium state, meanwhile it energizes large-scale eddies through baroclinic instability. The eddies develop and transport heat and momentum poleward. The eddy heat transport adjusts the temperature gradient directly, while the eddy momentum transport regulates the strength of the MMC (the Ferrel cell), and influences the temperature field indirectly through the equatorward MMC heat transport. For the earth's atmosphere, the eddy heat transport dominates, and the net effect of heat transport is to bring the temperature gradient back to its climatic equilibrium state.

The thin arrows in Figure 5.33 indicate the effects of changes in the external parameters on the eddy efficiency in transporting heat, E, where E is defined as the ratio of the net heat flux to the eddy heat flux, i.e.,

$$E \equiv \frac{T_{ed} + T_{MMC}}{T_{ed}} = 1 - R. \tag{5.37}$$

A small feedback factor means a large eddy efficiency. The inward arrows to a parameter denote positive effects, e.g., increasing ΔT_E or h enhances the eddy efficiency. The outward arrows to a parameter denote negative effects, e.g., increasing k or Γ_0 reduces the eddy efficiency. Compared with changes in the diabatic heating, the change in the surface drag has only secondary effects.

Furthermore, the thin arrows also indicate the climatic sensitivity to the external parameters. Particularly, ΔT increases with ΔT_E; eddy amplitudes get larger when

h or k gets larger; the strength of the MMC increases when k increases or Γ_0 decreases. Because static stability is fixed in the Phillips system, the interaction between ΔT and Γ_0 remains unclear. It will be examined in next chapter.

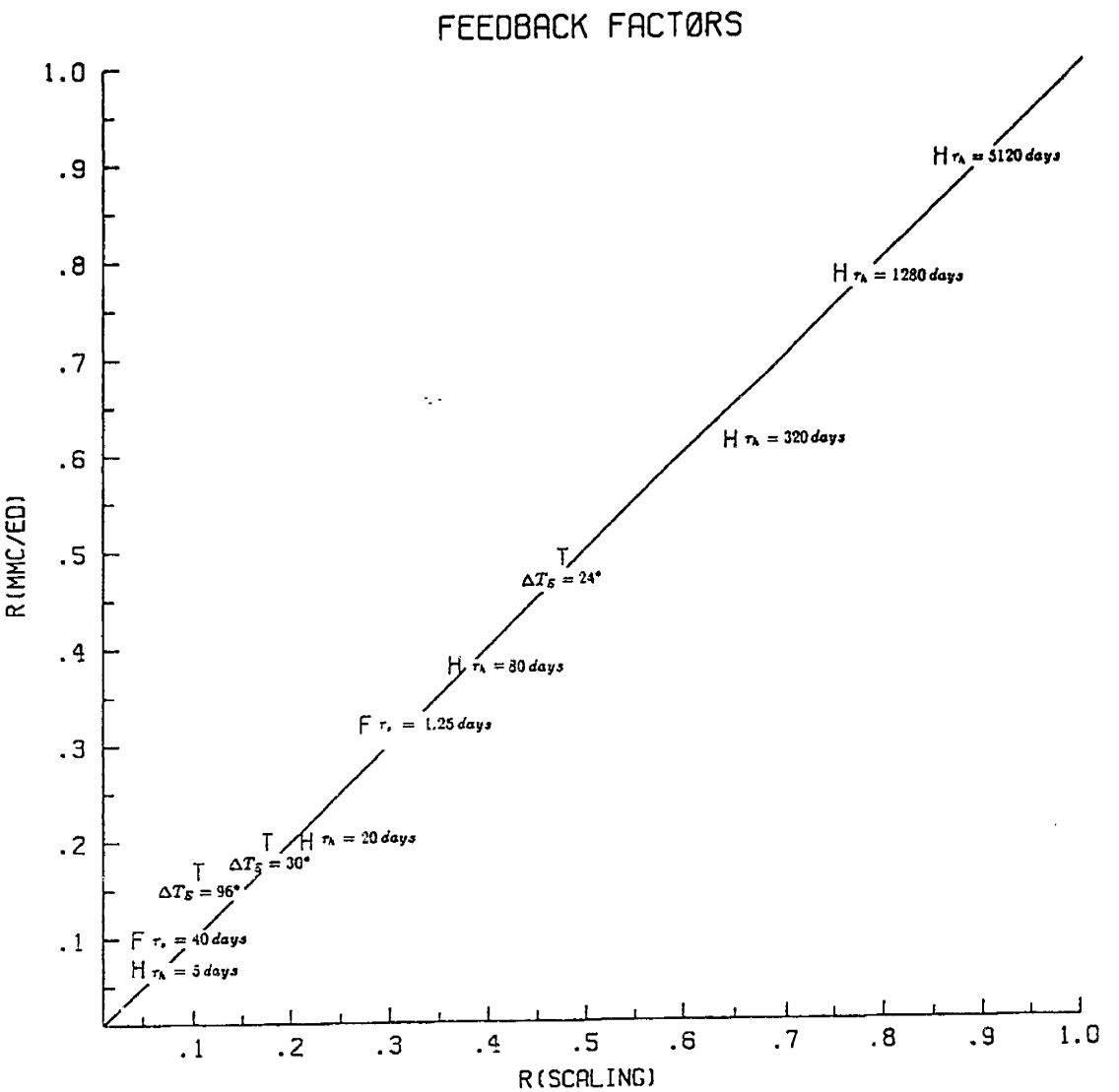

Figure 5.31: The feedback factors in the experiments without interfacial friction. The abscissa is R_S, the predicted value from the scaling method; the ordinate is R, the calculated value from the definition.

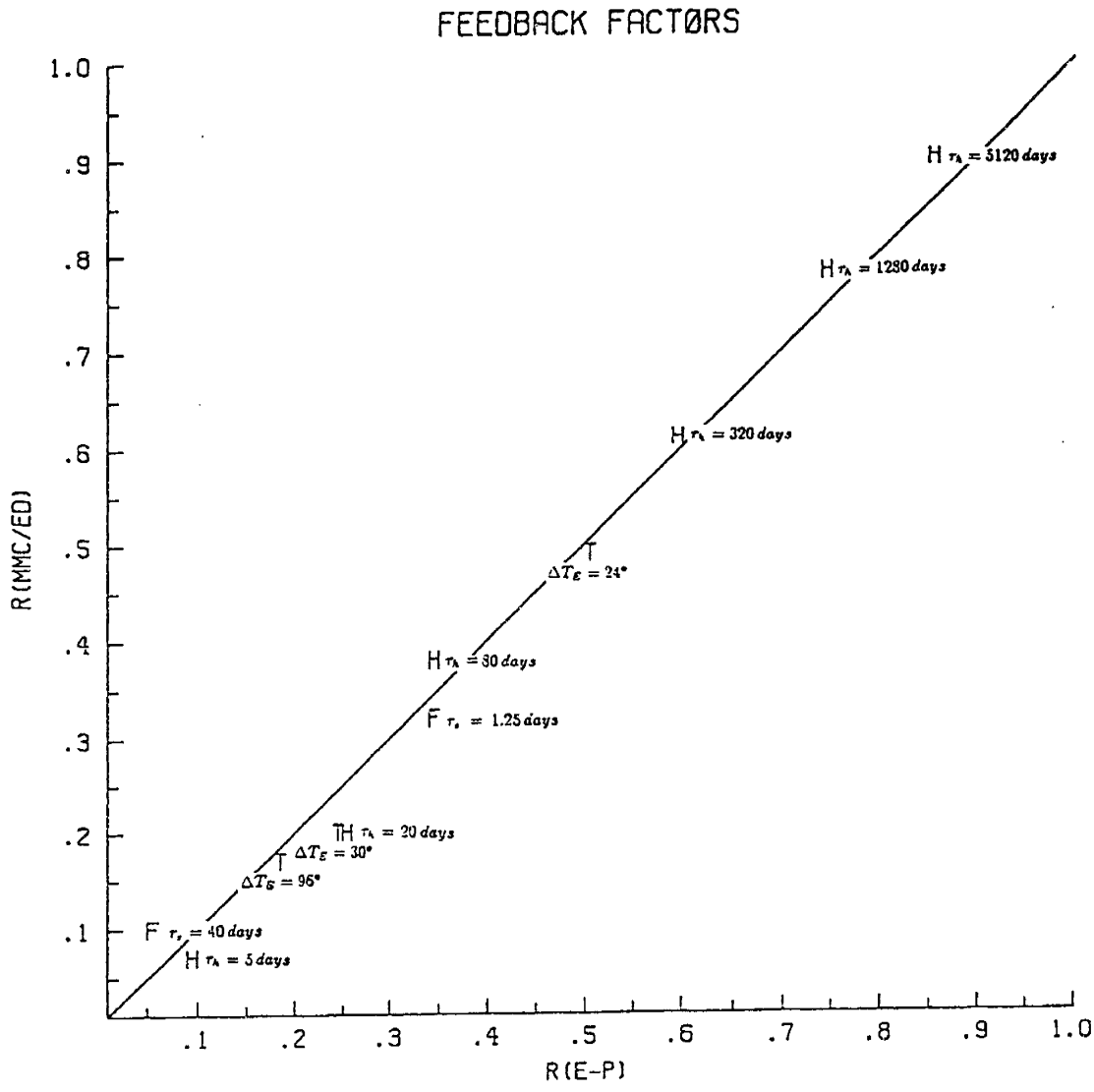

Figure 5.32: The feedback factors in the experiments without interfacial friction. The ordinate is R; the abscissa is R_{E-P}, the ratio of the horizontal to the vertical component of the E-P flux.

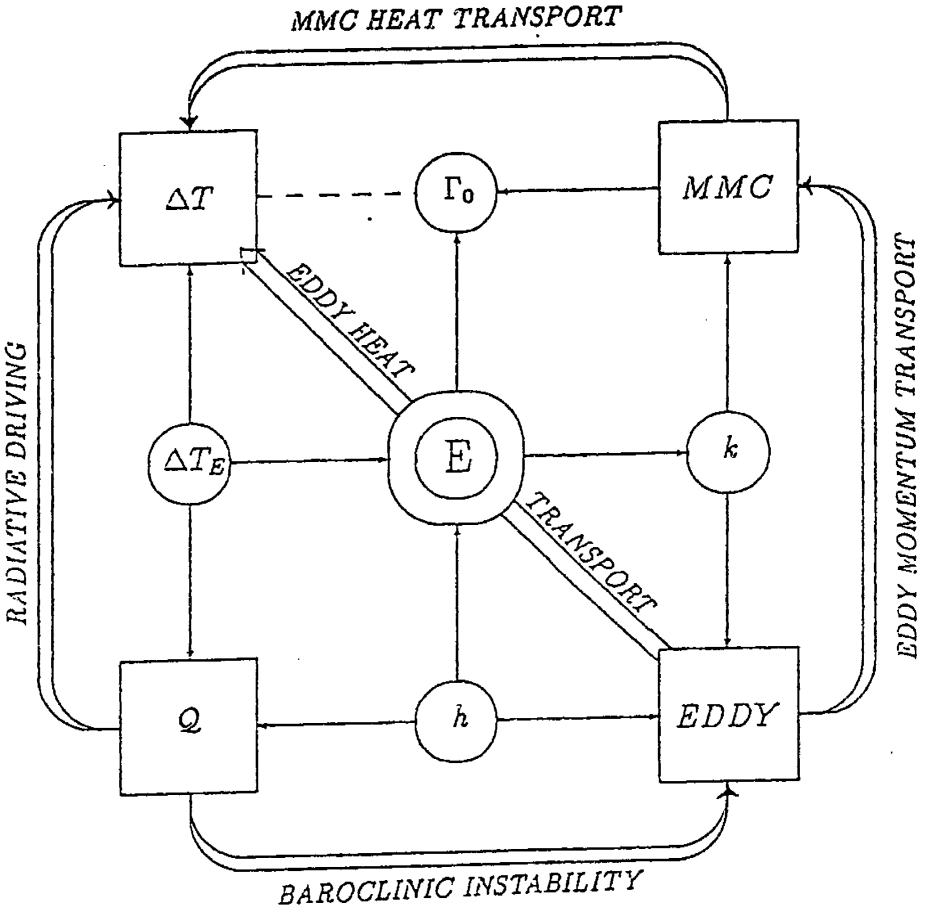

Figure 5.33: The schematic diagram for the dynamical processes and the effects of changes in the external parameters in the Phillips system.

Chapter 6

Eddy regime – the Lorenz system

6.1 Introduction

Although the static stability is treated as a constant in many simple climate models, there is no doubt that the interaction between vertical eddy heat fluxes and the static stability is one of the important mechanisms in climate equilibrium. Models that omit this mechanism may be missing an important part of the atmospheric physics. Based upon a highly simplified model and the Charney-Stern theorem, Gutowski (1985b) has shown that the observed midlatitude temperature structure could be understood in terms of such a mechanism. Held and Suarez (1978) calculated explicitly the vertical eddy heat flux and the static stability using a two-level primitive equation model. They found that the static stability in the mid latitudes was maintained mainly by the vertical eddy heat transport and diabatic heating processes. In a continued study with the same model, Held (1978b) found that the static stability played an important role in the climate sensitivity to changes in the solar constant.

In this chapter, we relax the constraint of constant static stability, by allowing the vertical eddy heat flux to interact with the static stability. The model we use is Lorenz's two-level system (Lorenz, 1960). This model differs from the Phillips system only in the formulation of the thermodynamic equation. In the Lorenz system, the static stability can vary temporally and horizontally, but can not vary vertically due to the two-level constraint. Therefore, the temperature difference between the two levels only represents the "bulk" static stability. The role of the "bulk" static stability (or the vertical temperature gradient) is parallel to the pole-to-equator temperature contrast (or the meridional temperature gradient), although the vertical structure of static stability may also be an important feature (Gutowski, 1985a).

We have carried out a series of parameter experiments in the Lorenz system. In addition to those features we have studied in the Phillips system, these experiments provide us with the information on the equilibrium state of static stability and vertical eddy heat transports. We compare the relative importance of the dynamical processes in the vertical direction with those in the meridional direction, and examine their connections in order to get a two-dimensional picture of the role of large-scale eddies in regulating the climate state.

6.2 Equations in the Lorenz system

Although the formulation of the thermodynamic equation in the Lorenz system is different from that in the Phillips system, the status of static stability does not affect the formulation of vorticity and balance equations. Similarly, the *linear balance equation* approximation is adopted in the Lorenz system. As shown in chapter

3, the equations in this system are written as:

$$\frac{\partial}{\partial t}\nabla^2\bar{\psi} = -J(\bar{\psi},\nabla^2\bar{\psi}) - J(\hat{\psi},\nabla^2\hat{\psi}) - 2\frac{\partial\bar{\psi}}{\partial\lambda} + \bar{\mathcal{D}}, \tag{6.1}$$

$$\frac{\partial}{\partial t}\nabla^2\hat{\psi} = -J(\bar{\psi},\nabla^2\hat{\psi}) - J(\hat{\psi},\nabla^2\bar{\psi}) - 2\frac{\partial\hat{\psi}}{\partial\lambda} - 2\nabla\cdot(\mu\nabla\hat{\varphi}) + \hat{\mathcal{D}}, \tag{6.2}$$

$$\frac{\partial\hat{\Phi}}{\partial t} = -J(\bar{\psi},\hat{\Phi}) - J(\hat{\psi},\Gamma) - \nabla\cdot(\Gamma\nabla\hat{\varphi}) + \bar{\mathcal{Q}}, \tag{6.3}$$

$$\frac{\partial\Gamma}{\partial t} = -J(\bar{\psi},\Gamma) - J(\hat{\psi},\hat{\Phi}) - \nabla\hat{\Phi}\cdot\nabla\hat{\varphi} + \hat{\mathcal{Q}}, \tag{6.4}$$

$$\nabla^2\hat{\Phi} = 2\nabla\cdot(\mu\nabla\hat{\psi}). \tag{6.5}$$

The corresponding spectral equations are:

$$\frac{d}{dt}\bar{\psi}_\gamma = \mathrm{i}\Big[\sum_\alpha\sum_\beta I_{\gamma\alpha\beta}(\bar{\psi}_\alpha\bar{\psi}_\beta + \hat{\psi}_\alpha\hat{\psi}_\beta) + 2c_\gamma^{-1}l_\gamma\bar{\psi}_\gamma\Big] + \bar{\mathcal{D}}_\gamma, \tag{6.6}$$

$$\begin{aligned}\frac{d}{dt}\hat{\psi}_\gamma = {}& \mathrm{i}\Big[\sum_\alpha\sum_\beta I_{\gamma\alpha\beta}(\bar{\psi}_\alpha\hat{\psi}_\beta + \hat{\psi}_\alpha\bar{\psi}_\beta) + 2c_\gamma^{-1}l_\gamma\hat{\psi}_\gamma\Big] \\ & + c_\gamma^{-1}(L_{\gamma+1}\hat{\varphi}_{\gamma+1} + L_\gamma\hat{\varphi}_{\gamma-1}) + \hat{\mathcal{D}}_\gamma,\end{aligned} \tag{6.7}$$

$$\begin{aligned}\frac{d}{dt}\hat{\Phi}_{\gamma+1} = {}& \mathrm{i}\Big[\sum_\alpha\sum_\beta \mathcal{K}_{\gamma+1,\alpha,\beta+1}(\bar{\psi}_\alpha\hat{\Phi}_{\beta+1} + \hat{\psi}_\alpha\Gamma_{\beta+1})\Big] + c_{\gamma+1}\Gamma_0\hat{\varphi}_{\gamma+1} \\ & + \sum_\alpha\sum_\beta \mathcal{M}^{(+)}_{\gamma+1,\alpha+1,\beta+1}\Gamma_{\beta+1}\hat{\varphi}_{\alpha+1} + \bar{\mathcal{Q}}_{\gamma+1},\end{aligned} \tag{6.8}$$

$$\begin{aligned}\frac{d}{dt}\Gamma_{\gamma+1} = {}& \mathrm{i}\Big[\sum_\alpha\sum_\beta \mathcal{K}_{\gamma+1,\alpha,\beta+1}(\bar{\psi}_\alpha\Gamma_{\beta+1} + \hat{\psi}_\alpha\hat{\Phi}_{\beta+1})\Big] \\ & + \sum_\alpha\sum_\beta \mathcal{M}^{(-)}_{\gamma+1,\alpha+1,\beta+1}\hat{\Phi}_{\beta+1}\hat{\varphi}_{\alpha+1} + \hat{\mathcal{Q}}_{\gamma+1},\end{aligned} \tag{6.9}$$

$$\hat{\Phi}_{\gamma+1} = -c_{\gamma+1}^{-1}(L_{\gamma+1}\hat{\psi}_\gamma + L_{\gamma+2}\hat{\psi}_{\gamma+2}), \tag{6.10}$$

where

$$\mathcal{M}^{(+)}_{\gamma+1,\alpha+1,\beta+1} = \frac{1}{2}(c_{\gamma+1} + c_{\alpha+1} - c_{\beta+1})\mathcal{M}_{\gamma+1,\alpha+1,\beta+1},$$

$$\mathcal{M}^{(-)}_{\gamma+1,\alpha+1,\beta+1} = \frac{1}{2}(c_{\gamma+1} - c_{\alpha+1} - c_{\beta+1})\mathcal{M}_{\gamma+1,\alpha+1,\beta+1}.$$

$\mathcal{M}^{(+)}$ and $\mathcal{M}^{(-)}$ are spectral coefficients associated with operators $\nabla \cdot (A\nabla B)$ and $\nabla A \cdot \nabla B$ respectively, where A and B are any scale quantities. The subscripts α, β and γ are wave vector indicies, and n_α, n_β and n_γ are all odd numbers, which are consistent with the symmetry of $\hat{\Phi}$, $\hat{\varphi}$, Γ and the antisymmetry of $\bar{\psi}$, $\hat{\psi}$. Except for Equation (6.9), $n_\gamma = 1, 3, 5, \cdots, 2M-1$. In Equation (6.9) $\gamma = -1$ $(d\Gamma_0/dt)$ should be included, which represents the equation for global mean static stability.

Because there is neither zonal variation of the thermal forcing nor topography in our model, further simplication can be made by assuming that the static stability is zonally symmetric, i.e.,

$$\Gamma = \Gamma(t,\mu) = \Gamma_0(t) + \sum_\alpha \Gamma_{\alpha+1}(t) P_{\alpha+1}(\mu), \tag{6.11}$$

where $\Gamma_0(t)$ is the global mean static stability, and $\Gamma_{\alpha+1}(t)$ is a meridional component. Unlike the global mean temperature, T_0, which does not interact with eddies and remains constant, $\Gamma_0(t)$ interacts with the vertical eddy heat flux and plays an important role in the dynamics. For the real atmosphere, the meridional variation of the static stability is also larger than its longitudinal variation according to the thermal wind relation and observations (Oort and Rasmusson, 1971). If we use $\frac{\partial \bar{\Theta}}{\partial z}$ to represent the static stability, where $\bar{\Theta}$ is the mean potential temperature, then

$$|\frac{\partial}{\partial y}(\frac{\partial \bar{\Theta}}{\partial z})| = |-\frac{f\bar{\Theta}}{g}\frac{\partial^2 \bar{u}}{\partial z^2}| \sim \frac{f_0 \Theta_0 U}{gH^2} \simeq 6 \times 10^{-10},$$

$$|\frac{\partial}{\partial x}(\frac{\partial \bar{\Theta}}{\partial z})| = |-\frac{f\bar{\Theta}}{g}\frac{\partial^2 \bar{v}}{\partial z^2}| \sim \frac{f_0 \Theta_0 V}{gH^2} \simeq 6 \times 10^{-11},$$

where we have assumed annual mean and zonal mean conditions for the midlatitude atmosphere, typically, $f_0 = 10^{-4} s^{-1}$, $\Theta_0 = 300\,K$, $H = 7\,km$, $U = 10\,m/s$, $V = 1\,m/s$. Therefore, the longitudional variation of Γ can be neglected. The simplified

static stability equation becomes

$$\frac{\partial[\Gamma]}{\partial t} = -[J(\hat{\psi}, \hat{\Phi})] - [\nabla\hat{\Phi} \cdot \nabla\hat{\varphi}] + [\hat{Q}]. \tag{6.12}$$

This simplification greatly reduces the computation time while having little effect on the budget of static stability.

The spectral form of the energetics in the Lorenz system is similar to that in the Phillips system, except that P_Z, G_Z and $C(P_E, P_Z)$ are modified as shown below in order to conserve the total energy.

$$P_Z = \frac{1}{2\Gamma_0}\sum_{\alpha}(\hat{\Phi}^2_{\alpha+1} + \Gamma^2_{\alpha+1}), \tag{6.13}$$

$$G_Z = \frac{1}{\Gamma_0}\sum_{\alpha}(\hat{\Phi}_{\alpha+1}\bar{Q}_{\alpha+1} + \Gamma_{\alpha+1}\hat{Q}_{\alpha+1}), \tag{6.14}$$

$$\begin{aligned} C(P_E, P_Z) = \frac{2}{\Gamma_0}\sum_{\alpha}\sum_{\beta}\sum_{\gamma}\{&\mathcal{K}_{\beta,\gamma+1,\alpha} \times \\ &[\hat{\Phi}_{\alpha+1} Im(\bar{\psi}^*_{\beta}\hat{\Phi}_{\gamma+1}) + \Gamma_{\alpha+1} Im(\hat{\psi}^*_{\beta}\hat{\Phi}_{\gamma+1})] \\ &- \mathcal{M}^{(-)}_{\alpha+1,\beta+1,\gamma+1}\Gamma_{\alpha+1} Re(\hat{\varphi}_{\beta+1}\hat{\Phi}^*_{\gamma+1})\}. \end{aligned} \tag{6.15}$$

6.3 The equilibrium static stability

In the Lorenz system, we need to specify the external forcing of the static stability, Γ_E. Similar to ΔT_E, Γ_E can be regarded as the static stability in the radiative equilibrium state or in the radiative-convective equilibrium state. For instance, Bryan (1959) simply assumed that $\Gamma_E = 0$, which means that the equilibrium atmosphere always remains at a dry neutral state. In other cases, Γ_E was calculated from various models, simple or sophisticated. For instance, the temperature structures in radiative-convective equilibrium have been calculated by integrating in time the thermodynamic equations with an explicit forcing, such as radiative fluxes,

boundary fluxes and convective adjustment, until a steady state was achieved (Held and Suarez, 1978; Eliasen, 1982). Because the explicit forcing was parameterized in different formulations, the obtained equilibrium states were also different. None of them can be said to be robust except for their basic characteristics. Nevertheless, common features are shown by these calculations, and they seem to be physically meaningful, e.g., the atmosphere is more stable in the high latitudes than in the low latitudes; the radiative-convective equilibrium state is more stable than the pure radiative equilibrium state, etc.

Without loss of generality, we specify two types of Γ_E in our model, which are shown in Figure 6.1 by the curves A and B respectively. Curve A represents a pure radiative equilibrium state. We used a simple earth-atmosphere coupled model (Saltzman, 1968; Wiin-Nielson, 1969) to calculate it. This model includes two radiative balance equations, one for the atmosphere and the other for the earth's surface. The solar radiation forcing (Q_{rad}) is given by its annual mean distribution, which can be approximately expressed as

$$Q_{rad}(\mu) \simeq \frac{S_0}{4}[1 - 0.3017P_2(\mu)],$$

where S_0 is the solar constant, and $P_2(\mu) = \sqrt{\frac{5}{2}} \cdot \frac{1}{2}(3\mu^2 - 1)$ is the normalized second order Legendre function (Coakley, 1979). Other parameters, such as albedos of the atmosphere and the earth's surface, the opacity and the long-wave absoptivity of the atmosphere, etc., are given empirical values similar to those used by Saltzman (1968). From the model we can calculate the mean atmospheric temperature $\bar{T}_E$ and the surface temperature T_{S_E} in the radiative equilibrium state as a function of latitude. In fact, the equilibrium temperature gradient ($\Delta T_E = 48K$) used in the "standard" run presented in chapter 5 is obtained from the same model. Thus this equilibrium gradient represents the gradient in the absence of any meridional

transports by the atmosphere or oceans.

We assume that $T_{E_{500\,mb}} \simeq \bar{T}_E$ and $T_{E_{1000\,mb}} \simeq T_{S_E}$. In general, the surface temperature is not equal to the air temperature above the surface, but the difference is small. The equilibrium static stability in the lower layer of the model is calculated from $T_{E_{500\,mb}}$ and $T_{E_{1000\,mb}}$. We further assume that the vertical mean static stability equals the lower layer static stability. This assumption somewhat overestimates the magnitude of the equilibrium lapse rate (or underestimates the static stability), because the radiative equilibrium atmosphere is more stable in the upper troposphere than in the lower troposphere (Goody, 1964). Therefore it gives a sharp contrast to the second type of Γ_E – Curve B.

Curve B represents a radiative-convective equilibrium state. It was obtained from a numerical experiment with the GISS zonal mean statistical- dynamical model (Stone and Yao, 1990). In that experiment, the lower boundary condition was specified by the observed ocean surface temperature; the equilibrium state was calculated for January conditions by incorporating all dynamical processes (e.g., the mean circulation heat fluxes, the moist convection, etc.) except for the large-scale vertical eddy transports (Stone, 1990). The annual mean lapse rate was calculated by averaging Northern and Southern hemispheric values. The equilibrium static stability has a relatively uniform meridional structure. The atmosphere is more stable than that in the pure radiative equilibrium (curve A), especially in the low latitudes. The standard value of ΔT_E used when Γ_E was given by curve B was again chosen to be $48K$. Although this value of ΔT_E is calculated from the radiative equilibrium model, we used it for easier comparison with the "standard" run in the Phillips system. The value of ΔT_E in the radiative-convective equilibrium is somewhat dif-

ferent. However, because our model is a "process-study" model, and because we will run a series of experiments varying ΔT_E over a broad range, it is not necessary to use a consistent value of ΔT_E with Γ_E in the radiative-convective equilibrium.

6.4 The maintenance of the static stability

6.4.1 Comparison with the "standard" run

In order to compare the model results in the Lorenz system with those in the Phillips system, we have carried out two experiments in which Γ_E was specified as the state in radiative equilibrium (curve A) and in radiative-convective equilibrium (curve B) respectively. All other external parameters have been set to the same values as those used in the "standard" run with constant static stability. In particular, $\Delta T_E = 48K$. In addition, the horizontal resolution for these experiments is again $5 \times 5(3)$. We hereafter refer to these two experiments as A(S) and B(S).

First, we look at the model results of A(S). The calculated statistical equilibrium states of the zonal flow, the meridional wind, the temperature and the MMC stream function are shown in Figure 6.2. The general characteristics are similar to those in the "standard" run with constant static stability (see Figure 5.5), although the Hadley cell is stronger than that in the "standard" run (It might be due to the very weak Γ_E in the low latitudes). The momentum budgets and the heat budget are shown in Figures 6.3 and 6.4. Their qualitative features are also similar to those in the "standard" run (see Figures 5.6 and 5.7).

The equilibrium static stability in the eddy regime is shown in Figure 6.5 (a).

Compared with that in the radiative equilibrium state (dotted line), the global mean static stability in the eddy regime (solid line) has increased appreciably; whereas the meridional structure of the static stabilty has only slightly changed. This feature is similar to that found by Held and Suarez (1978) in their "dry model" experiment.

Next, we look at the model results of B(S) which are shown in Figures 6.6 – 6.9. Likewise, the characteristics of the equilibrium states and the budgets of momentum and heat are very similar to those obtained in the "standard" run. Furthermore, in many aspects, e.g., the strength of the Hadley cell, B(S) is even closer than A(S) to the "standard" run. This is because the static stability in B(S) has little meridional variation, and its mean value is very close to the constant static stability used in the "standard" run.

Owing to the similarities between the results in the Lorenz system and in the Phillips system, especially in the mid-high latitudes, it may not be necessary to repeat all resolution experiments which have been done in the Phillips system. Therefore, we have only tested a few of higher resolutions, such as $7 \times 7(3)$, $5 \times 8(2)$ and $5 \times 15(1)$, with Γ_E in radiative equilibrium (curve A). The results are very similar to those calculated with the resolution $5 \times 5(3)$, implying that $5 \times 5(3)$ is also appropriate in the Lorenz system. We will use this resolution in most of the parameter experiments which will be described in the next section.

Table 6.1: Some characteristic quantities in the resoltion experiments with the Lorenz system.

	$5 \times 5(3)$	$7 \times 7(3)$	$5 \times 8(2)$	$5 \times 15(1)$
ΔT	61.6	59.8	54.8	57.4
δT	18.9	19.9	19.0	21.2
M	2.04	2.08	1.83	2.12
$[v^*M^*]_y$	68.8	84.4	52.3	65.8
t_M	34.3	28.4	40.4	37.3
$[u]_s$	27.8	35.3	23.2	28.5
(lat.)	(55)	(63)	(56)	(58)
$[v]_1$	.67	.67	.60	.63
(lat.)	(20)	(20)	(20)	(18)
$[u^*v^*]$	23.6	25.3	18.8	22.1
(lat.)	(34)	(35)	(32)	(33)
T_{ed}	22.9	19.2	22.0	20.1
T_{MMC}	-7.8	-5.7	-6.4	-5.9
R	.34	.30	.29	.29
$\hat{\Theta}_0$	24.4	24.2	23.6	24.3

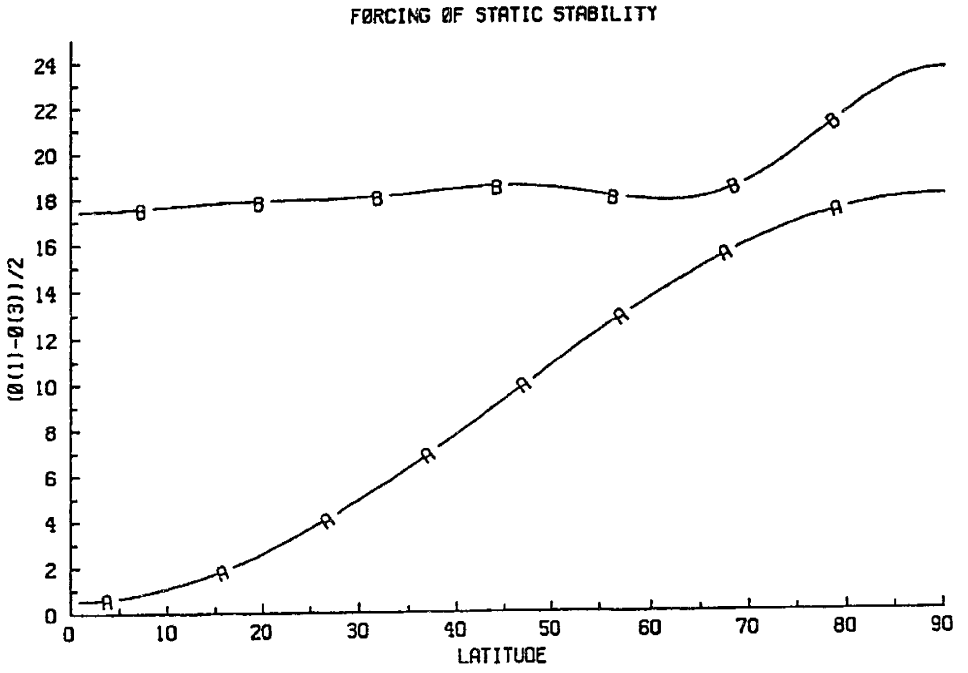

Figure 6.1: The static stability $\hat{\Theta}_E$ ($\Gamma_E \propto \hat{\Theta}_E$) used in the model. Curve A is a radiative equilibrium; Curve B is a radiative-convective equilibrium.

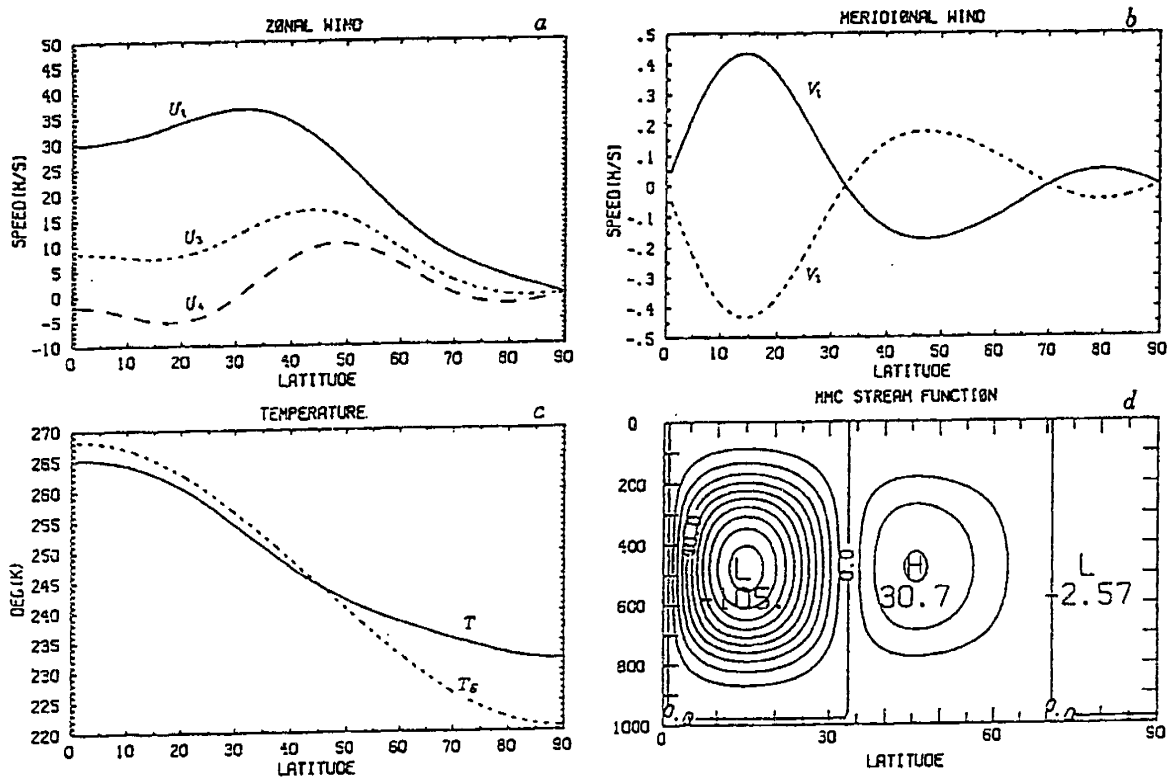

Figure 6.2: The equilibrium states of [u], [v], [T] and [χ] in experiment A(S). The contour interval of [χ] is $10\,mb.m/s$.

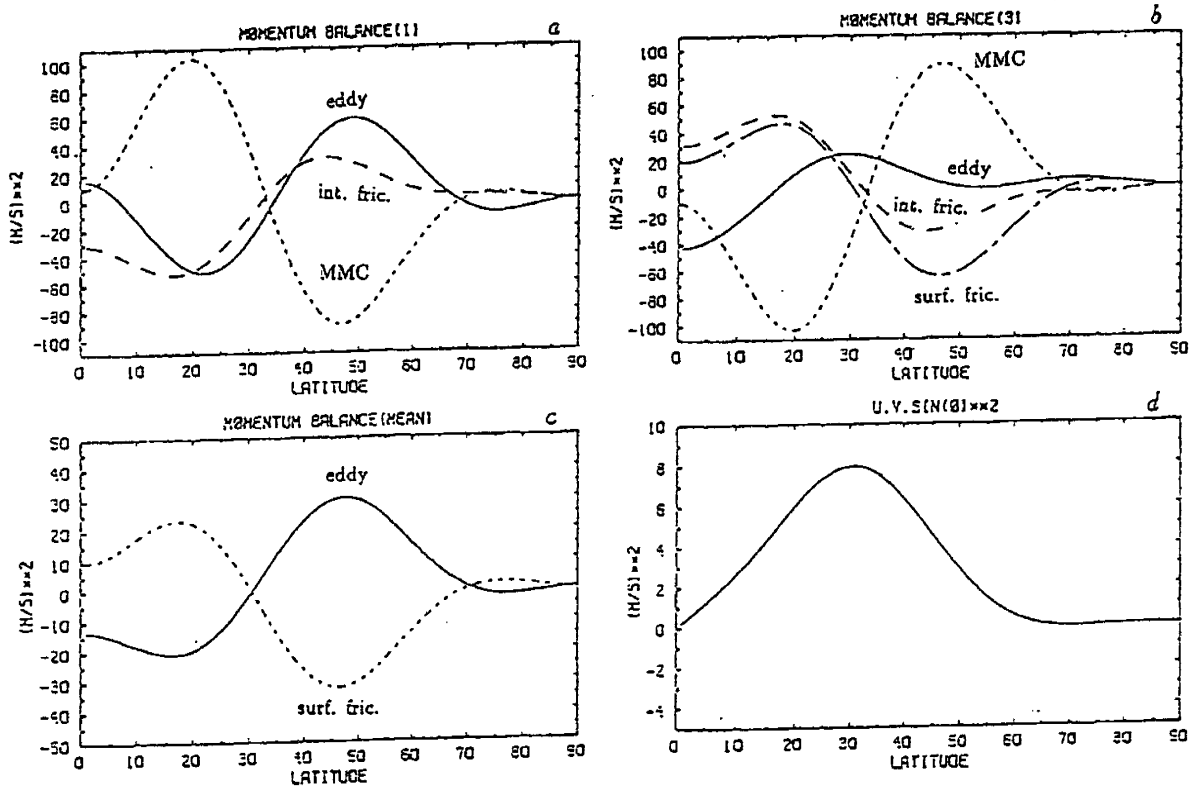

Figure 6.3: The momentum budgets in experiment A(S). The curves have the same meaning as those in Figure 5.6.

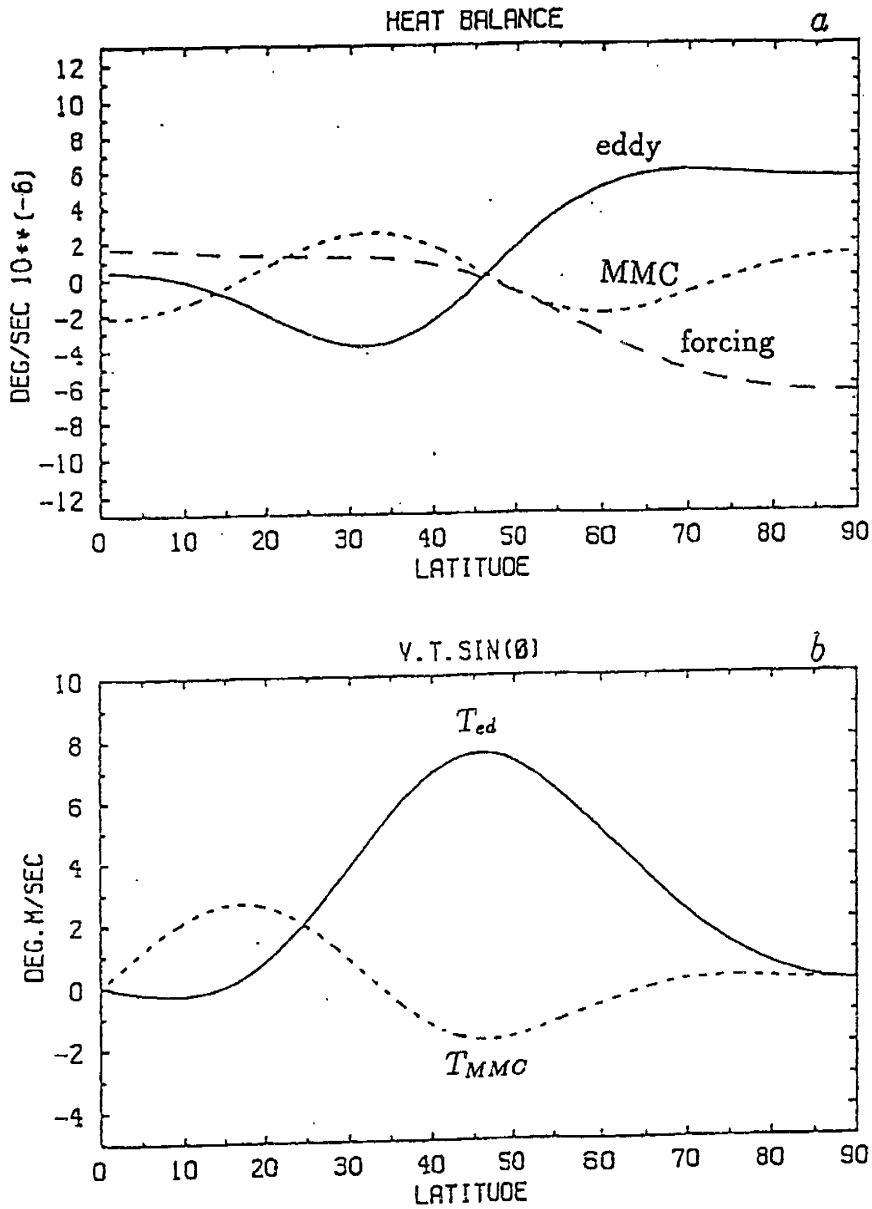

Figure 6.4: The heat budget in experiment A(S). The curves have the same meaning as those in Figure 5.7.

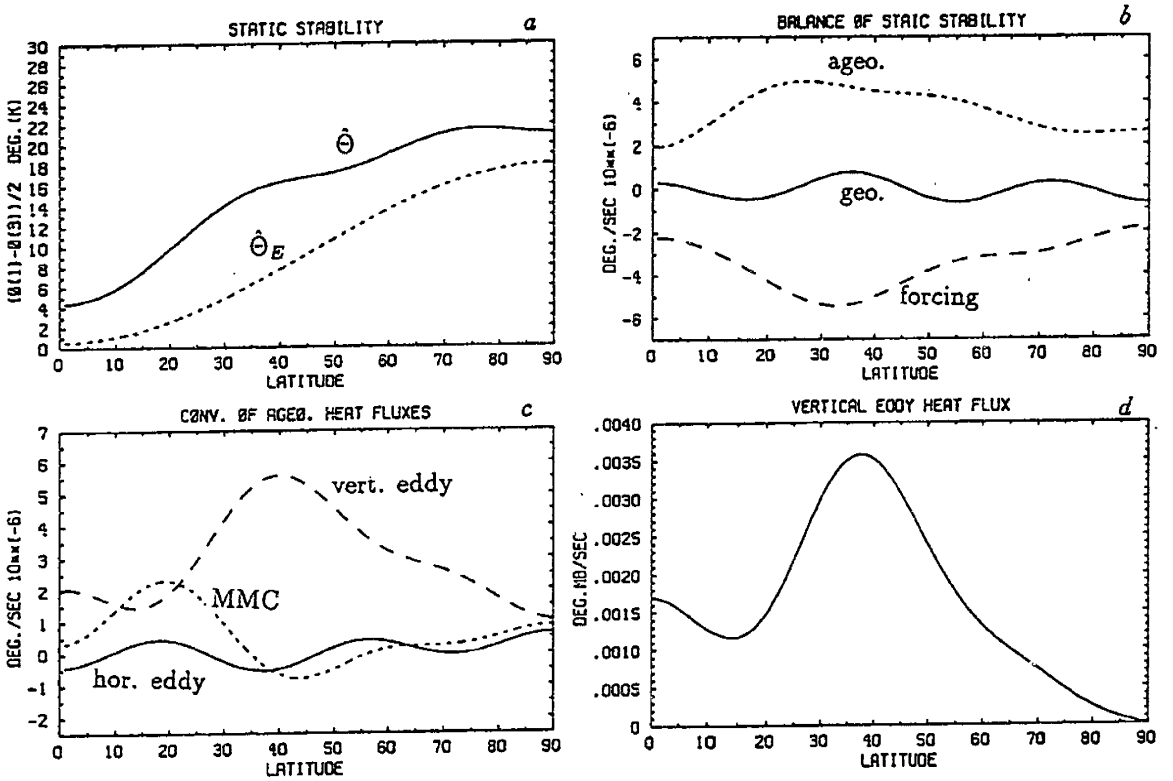

Figure 6.5: a) The static stability; b) the budget of static stability; c) the components of the ageostrophic temperature advection; and d) the vertical eddy heat flux in experiment A(S). Detailed explanations are given in the text.

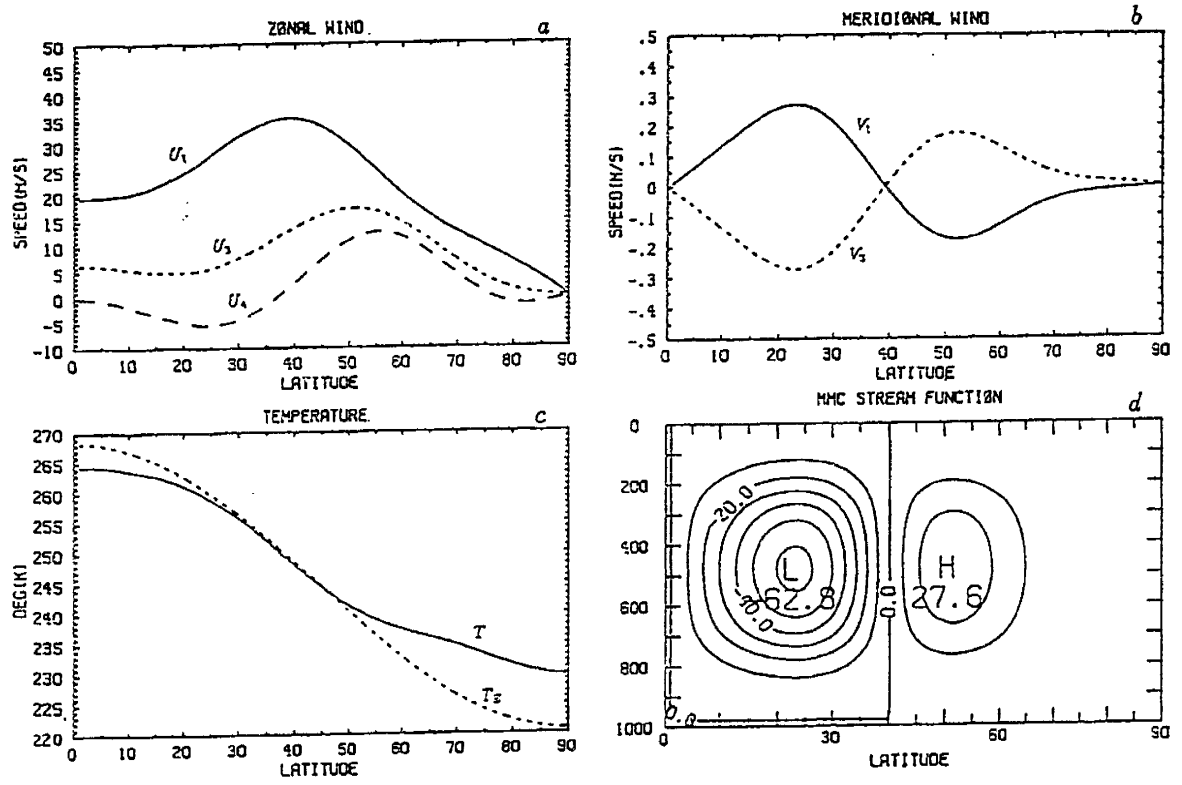

Figure 6.6: As in Figure 6.2 but for experiment B(S).

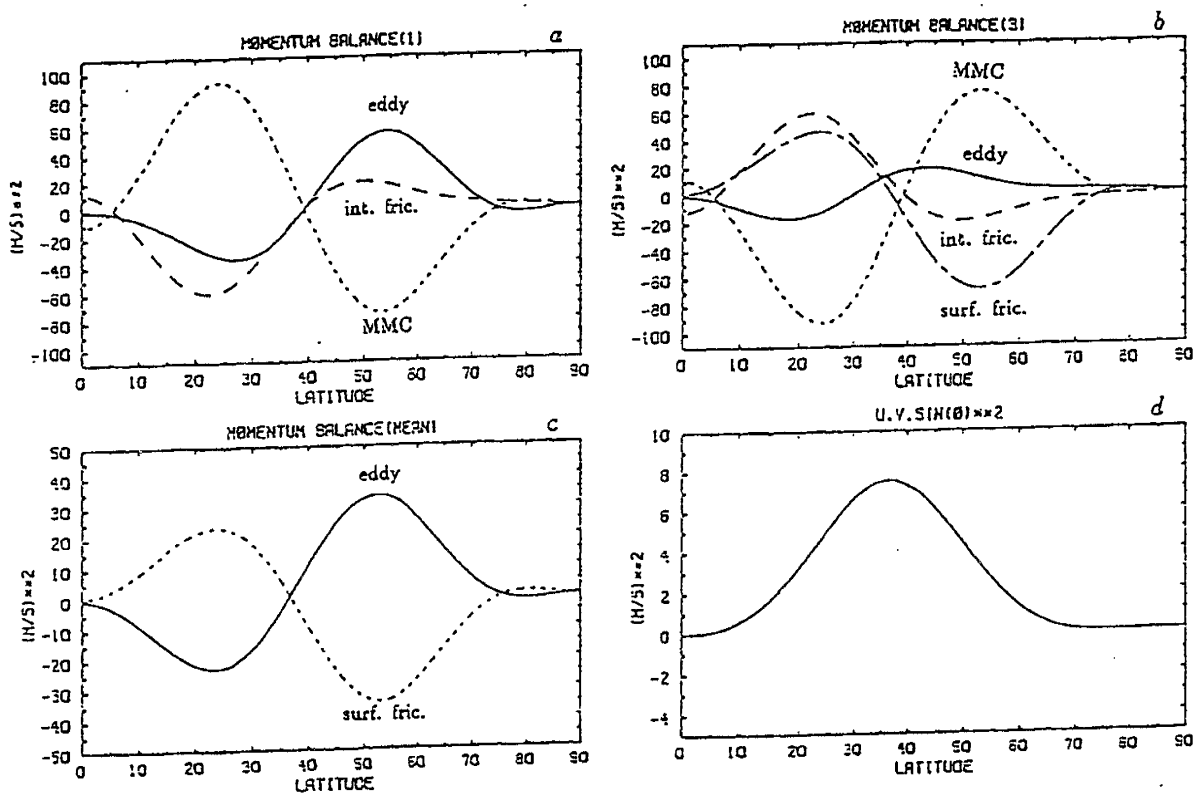

Figure 6.7: As in Figure 6.3 but for experiment B(S).

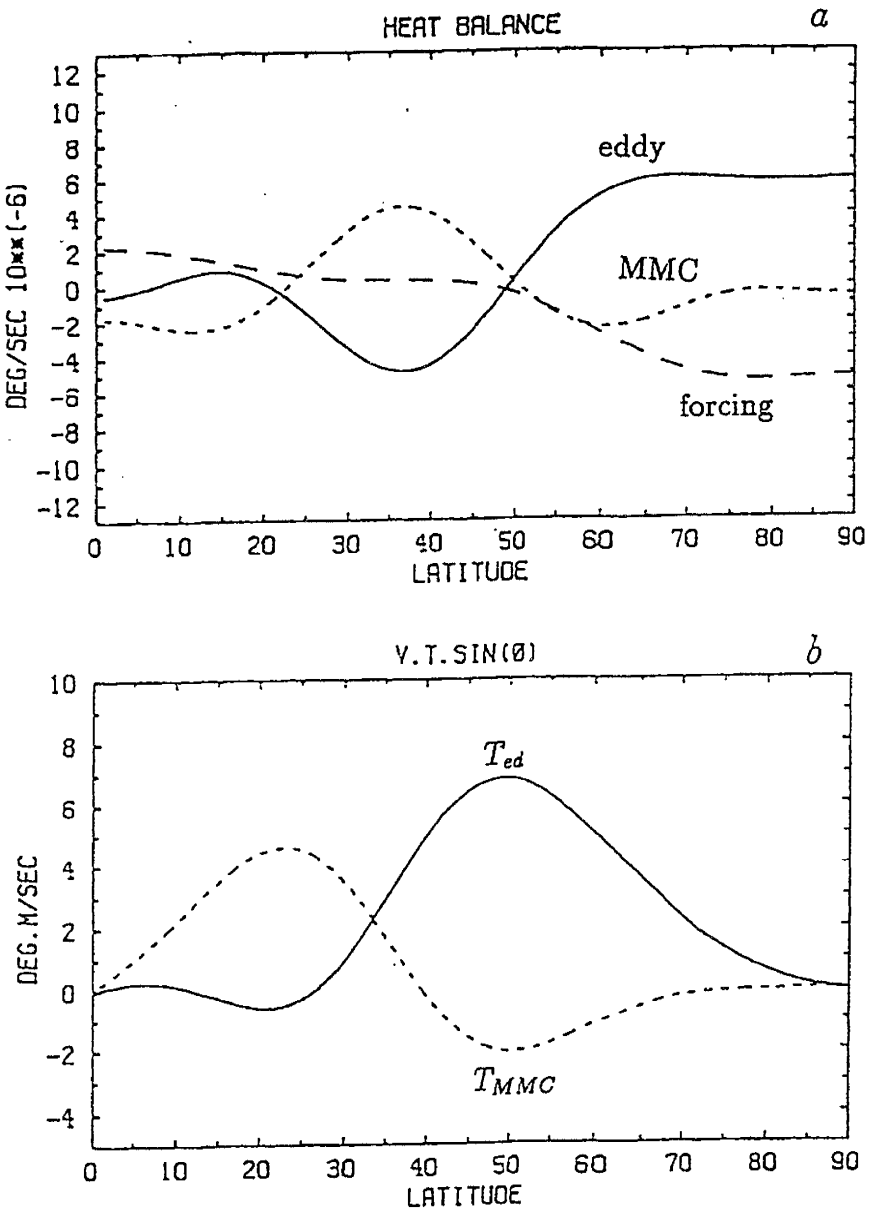

Figure 6.8: As in Figure 6.4 but for experiment B(S).

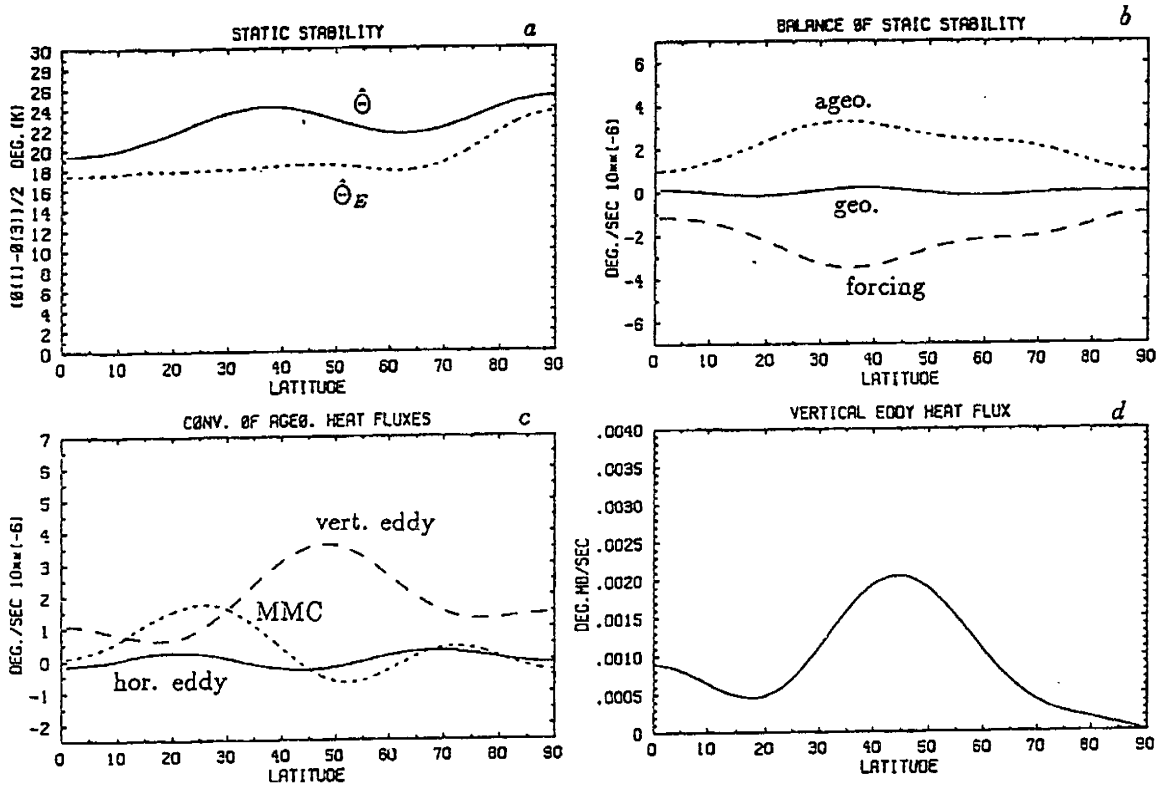

Figure 6.9: As in Figure 6.5 but for experiment B(S).

6.4.2 The budget of static stability

The balance of steady static stability, $[\Gamma]$, is maintained by three different physical processes, i.e.,

$$[J(\hat{\psi}, \hat{\Phi})] + [\nabla\hat{\Phi} \cdot \nabla\hat{\varphi}] - [\hat{\mathcal{Q}}] = 0. \tag{6.16}$$

The first term represents the *geostrophic* temperature advection by the thermal wind (eddies); the second term is the temperature advection by all *ageostrophic* motions; the last term denotes the diabatic forcing of static stability. It should be pointed out that the first term would vanish if the quasi-geostrophic approximation were used. As shown in Figures 6.5 (b) and 6.9 (b), whether in A(S) or in B(S), the geostrophic term (solid line) is relatively small compared to the other terms. Therefore, the balance of static stability is primarily between the ageostrophic term (dotted line) and the diabatic term (dashed line). The ageostrophic heat transport tends to increase the static stability in all latitudes, with peaks in the subtropics rather than in the mid latitudes. The diabatic heating term tends to decrease the static stability.

The ageostrophic heat transport can be decomposed into three parts, i.e.,

$$[\nabla\hat{\Phi} \cdot \nabla\hat{\varphi}] = \nabla[\hat{\Phi}] \cdot \nabla[\hat{\varphi}] + [\nabla \cdot (\hat{\Phi}^*\nabla\hat{\varphi}^*)] - [\hat{\Phi}^*\nabla^2\hat{\varphi}^*]. \tag{6.17}$$

The first term on the right hand side of Equation (6.17) represents the heat transport by the MMC; the second term represents the meridional heat transport by ageostrophic eddies; the third term represents the vertical heat transport by ageostrophic eddies.

Alternatively, if we use $[\hat{\Theta}]$ as the static stability parameter, then the dimensional

budget equation for static stability can be written as:

$$\frac{\partial[\hat{v}_g^*\bar{\Theta}^*]\sin\theta}{a\sin\theta\partial\theta}+[\hat{v}_a]\frac{\partial[\bar{\Theta}]\sin\theta}{a\sin\theta\partial\theta}+\frac{\partial[\hat{v}_a^*\bar{\Theta}^*]\sin\theta}{a\sin\theta\partial\theta}-\frac{[\omega^*\Theta^*]}{\Delta p}+[\hat{Q}]=0. \qquad (6.18)$$

The characteristics of the ageostrophic terms are shown in Figures 6.5 (c) and 6.9 (c). The common features found in A(S) and B(S) include:

1) The vertical eddy heat transport (dashed line) dominates in the mid-high latitudes;

2) The MMC heat transport (dotted line) is always out of phase with the vertical eddy heat transport. The direct Hadley cell tends to increase the static stability in the low latitudes, while the indirect Ferrel cell tends to decrease the static stability in the mid latitudes. The role of the MMC in the maintenance of static stability is similar to its role in the maintenance of the meridional temperature gradient. In other words, the MMC heat transports are always negative feedbacks to the eddy heat transports;

3) The meridional heat transports by ageostrophic eddies (solid line) are small and out of phase with the transports by geostrophic eddies [solid line in Figures 6.5 (b) and 6.9 (b)]. Thus, the total meridional heat transports by eddies are negligible in the balance of the static stability.

The vertical eddy heat flux, $[\omega^*T^*\sin\theta]$, is shown in Figures 6.5 (d) and 6.9 (d). The magnitudes of vertical eddy heat fluxes are at least two orders smaller than that of the meridional eddy heat flux. However, the change rate of Γ due to the differential convergence of the vertical eddy heat flux ($\partial^2[\omega^*T^*]/\partial p^2$]) has the same order of magnitude as the change rate of $\bar{T}$ due to the convergence of the meridional

eddy heat flux ($\frac{\partial[v^*T^*\sin\theta]}{a\sin\theta\partial\theta}$). For example, in A(S) the maximal change rate of $[\hat{\Theta}]$ by the vertical eddy heat transport is $5.6\times10^{-6}\ K/sec.$ [see Figure 6.5 (c)], and the maximal change rate of $\bar{T}$ by the meridional eddy heat transport is $6.0\times10^{-6}\ K/sec.$ [see Figure 6.4 (a)].

In order to compare the relative importance of vertical and meridional eddy heat transports, we define

$$t_\Gamma \equiv |\frac{\hat{\Theta}}{[\omega^*\Theta^*]/(\Delta p)}| = |\frac{\Gamma}{\Omega[\hat{\Phi}^*\nabla^2\hat{\varphi}^*]}|, \tag{6.19}$$

$$t_T \equiv |\frac{\Delta T}{\Delta(\frac{\partial[v^*T^*]\sin\theta}{a\sin\theta\partial\theta})}|, \tag{6.20}$$

where t_Γ is the e-folding time for the static stability change due to the vertical eddy heat transport, and t_T is a measure of the time scale for the temperature gradient change due to the meridional eddy heat transport. Similarly, we have defined in chapter 5 an eddy time scale

$$t_M \equiv |\frac{M}{\frac{\partial[v^*M^*]\sin\theta}{a\sin\theta\partial\theta}}|, \tag{6.21}$$

which is the time scale for the meridional eddy momentum transport to adjust the angular momentum [t_M is equivalent to t_e in Stone and Branscome (1991)].

These time scales are calculated from the model results of A(S) and B(S) and are shown in Table 6.2. The values of Γ, ΔT, M and eddy transports at $\theta = 45°$ are used.

In both A(S) and B(S) t_T is much shorter than t_Γ. This implies that the meridional eddy heat transport is more important than the vertical eddy heat transport. This may not necessarily be true if the external parameters change. Since we have used "standard" values of the external parameters for the earth's atmosphere, it

Table 6.2: Dynamical time scales (days).

RUN	t_T	t_Γ	t_M
A(S)	17	37	42
B(S)	19	77	53

seems that, for the earth's atmosphere, the meridional eddy heat transport is dominant among other dynamical transporting processes. The meridional eddy momentum transport and the vertical eddy heat transport, though giving some negative feedback, are of secondary importance. Therefore, in spite of requiring a constant static stability, the quasi-geostrophic theory has been successfully used in diagnostic and modeling studies for the earth's midlatitude atmosphere. However, it is not suitable for climatic sensitivity studies, as will be discussed in chapter 7.

We also note that the meridional eddy transports of heat and momentum are not sensitive to the forcing of static stability, Γ_E. But the vertical eddy heat transport is very sensitive to Γ_E. The Γ_E used in A(S) is less stable than that used in B(S). The model results have shown that the vertical eddy heat flux in A(S) is much stronger than that in B(S). The dynamical time scale t_Γ in A(S) is much shorter than that in B(S) (less than a half). As a result, the static stability has increased more drastically for the smaller Γ_E. The global mean static stability in A(S) has increased more than 100% from that of the radiative equilibrium. In B(S) the increase of Γ from Γ_E is only about 20%.

6.5 The parameter experiments

6.5.1 Diabatic forcing ΔT_E

Using parameter experiments like those we have carried out with the Phillips system, we will examine the effects of changes in the external parameters on climate states and eddy transports, while not fixing the static stability. The first parameter we look at is ΔT_E. Two groups of experiments, in which ΔT_E is varied, have been done in the Lorenz system. One group is denoted by A (ΔT_E) in which Γ_E is specified as the radiative equilibrium state (curve A). The other group is denoted by B (ΔT_E) in which Γ_E is specified as the radiative-convective equilibrium state (curve B). The other parameters are all fixed at the "standard" values.

The model results are shown in Figures 6.10 and 6.11 for A (ΔT_E) and B (ΔT_E) respectively. Those results include the zonal mean surface wind, the upper layer meridional wind, the meridional eddy fluxes of momentum and heat, the vertical eddy heat flux and the MMC heat flux. Except for the vertical eddy heat flux and the MMC heat flux, other quantities can be directly compared with the ΔT_E experiments in the Phillips system (see Figure 5.27). In fact, the midlatitude features are very similar to those obtained from the Phillips system. When ΔT_E is very small, the mean flow is stable and eddies can not develop. When ΔT_E increases, the zonal mean surface wind and the meridional wind increase in strength; the eddy transports, $[u^*v^*]$, $[v^*T^*]$ and $[\omega^*T^*]$, all increase.

However, the effect of changes in ΔT_E on the Hadley cell and its heat transport are very different between the Lorenz system and the Phillips system. In the Lorenz system, changes in ΔT_E does not change much the strength of the Hadley cell. For

instance, when ΔT_E increases from $48\,K$ to $144\,K$, the peak meridional wind in low latitudes only increases by a factor of 2.5 in B (ΔT_E). But in the Phillips system the change in the strength of the Hadley cell is more dramatic. For the same increase in ΔT_E, the peak meridional wind increases by about 8 times. This difference is due to a negative feedback between the static stability and the strength of the Hadley cell, which is omitted in the Phillips system. In low latitudes, the heat balance is primarily maintained by the Hadley cell heat transport and the diabatic heating, whereas the eddy heat transport is relatively small. It is approximately given by

$$-2\,\Gamma[\bar{\omega}] \simeq \bar{Q}. \tag{6.22}$$

If Γ is fixed, then the magnitude of $[\bar{\omega}]$ (which measures the strength of Hadley cell) increases with $\bar{Q}$ proportionally. However, if Γ is variable, both Γ and $[\bar{\omega}]$ increase with $\bar{Q}$ when ΔT_E increases. Thus, $[\bar{\omega}]$ does not need to increase as much as is required in the case with fixed static stability.

In Table 6.3 we list some characteristic quantities for various values of ΔT_E. The notations for these quantities are the same as those in Table 5.2, except that we add a parameter for the global mean static stability, $\hat{\Theta}_0$. Both ΔT and $\hat{\Theta}_0$ increase with ΔT_E. It implies that the temperature structure varies in a subtle way by which the ratio of ΔT and $\hat{\Theta}_0$, a proper measure of baroclinity, is not sensitive to the change in ΔT_E. We will further examine this feature in next chapter. Compared to the results with constant static stability (see Table 5.3), most of the quantities vary with ΔT_E in a similar way. However, the feedback factor, R, increases with ΔT_E, contrary to its variation when the static stability is fixed. This behavior can be explained by two reasons: first, as ΔT_E increases the meridional eddy heat flux, T_{ed}, increases less when Γ is variable than it does when Γ is fixed, because the vertical eddy heat flux can cooperate in adjusting the temperature structure; second, as ΔT_E increases

the MMC heat flux, T_{MMC}, increases more when Γ is variable than it does when Γ is fixed, because T_{MMC} is proportional to the magnitude of Γ which also increases with ΔT_E in the Lorenz system. This is a significant difference between the Phillips system and the Lorenz system.

Table 6.3: Some characteristic quantities in the experiments varying ΔT_E.

RUN	$\Delta T_E(K)$	24	30	48	72	144
A (ΔT_E)	ΔT	21.6	24.2	33.4	46.8	92.6
	δT	7.4	8.4	10.9	14.4	27.5
	M	.35	.76	1.06	1.52	2.94
	$[v^*M^*]_y$	5.1	20.1	29.6	59.1	116.
	t_M	77.8	44.0	41.5	29.8	29.2
	$[u]_s$	3.3	6.0	10.2	17.6	38.6
	(lat.)	(43)	(45)	(48)	(51)	(57)
	$[v]_1$	.25	.33	.43	.56	.76
	(lat.)	(13)	(13)	(14)	(19)	(20)
	$[u^*v^*]$	2.8	5.8	8.0	16.4	31.0
	(lat.)	(27)	(29)	(31)	(33)	(34)
	T_{ed}	1.35	2.87	7.51	15.6	34.1
	T_{MMC}	-.26	-.69	-1.82	-4.96	-12.8
	R	.19	.24	.24	.32	.37
	$\tilde{\Theta}_0$	7.5	9.5	12.6	17.9	35.2
B (ΔT_E)	ΔT	21.4	26.6	34.7	49.0	89.4
	δT	8.6	10.0	13.1	16.5	28.3
	M	.60	.75	1.12	1.52	2.73
	$[v^*M^*]_y$	5.4	10.5	24.7	40.6	75.6
	t_M	128.	83.0	52.6	43.3	41.8
	$[u]_s$	3.3	4.9	12.6	19.4	36.8
	(lat.)	(57)	(56)	(56)	(56)	(56)
	$[v]_1$	.11	.16	.27	.42	.68
	(lat.)	(23)	(23)	(23)	(23)	(24)
	$[u^*v^*]$	1.9	3.3	7.5	13.7	26.4
	(lat.)	(38)	(36)	(36)	(36)	(37)
	T_{ed}	1.36	2.45	6.85	14.3	35.8
	T_{MMC}	-.41	-.74	-2.07	-4.66	-13.2
	R	.30	.30	.30	.33	.37
	$\tilde{\Theta}_0$	18.4	18.9	21.6	26.4	42.6

6.5.2 Newtonian cooling time τ_h

Likewise, the experiments varying τ_h are denoted by A (τ_h) and B (τ_h), according to which type of Γ_E is used. The model results are shown in Figures 6.12 and 6.13. The zonal mean surface wind, the meridional wind and the eddy fluxes of momentum and heat simply increase when τ_h decreases. In this aspect, the effects of decreasing τ_h and increasing ΔT_E are very similar. The effects of the change in τ_h on the climate equilibrium are qualitatively consistent with those found in the Phillips system (see Figure 5.28).

Table 6.4 exhibits the variations of some important quantities with τ_h, same as those in Table 6.3. There is no qualitative difference from the results with fixed static stability (see Table 5.6). In particular, the feedback factor, R, increases with τ_h whether the static stability is fixed or variable. When τ_h increases, the static stability increases and the temperature gradient decreases. The dynamical meaning is clear: slowing down the diabatic heating tends to enhance baroclinic stability. Meanwhile all eddy transports are reduced. On the other hand, when τ_h decreases, $\Gamma \rightarrow \Gamma_E$, $\Delta T \rightarrow \Delta T_E$. The climate equilibrium in the eddy regime approaches the specified state of radiative or radiative-convective equilibrium. Meanwhile, the eddy transports are enhanced due to the strong forcing. In this aspect, the effects of decreasing τ_h and increasing ΔT_E are totally different.

6.5.3 Surface friction k

The experiments in which the surface drag coefficient k is varied are denoted by A (k) and B (k) respectively, for the two types of Γ_E. The results are shown in Figures 6.14 - 6.15 and Table 6.5. They are very similar to those obtained from the experiments in the Phillips system (see Figure 5.30 and Table 5.12). The zonal mean surface wind increases appreciably when k decreases (or τ_s increases). Although the eddy momentum flux changes slightly with k, the eddy time scale t_M increases considerably as k decreases, due to the strenghthened zonal mean wind. The meridional and vertical eddy heat fluxes, the strength of the MMC and the MMC heat flux are all insensitive to the change in k. Consequently, the temperature structure, which is represented by the meridional temperature gradient and the static stability, has not significantly changed by the change in k. The feedback factor R is slightly reduced when the surface drag gets weaker.

The external parameters are reduced by one in the Lorenz system because the static stability is no longer an external parameter. The effect of the interaction between the vertical eddy heat flux and the static stability has been discussed in the previous text. In short, the variable static stability plays a significant role in regulating the strength of the MMC and the feedback of meridional heat transport. It also plays a role in adjusting the baroclinic instability, which controls the intensity of eddy fluxes of heat and momentum. The baroclinity in the climate equilibrium will be studied in next chapter.

Table 6.4: Some characteristic quantities in the experiments varying τ_h.

RUN	$\tau_h(days)$	(Equil.)	5	20	80	320
A (τ_h)	ΔT	(48.0)	39.9	33.4	27.7	20.6
	δT	(16.4)	12.5	10.9	11.1	8.8
	M		1.55	1.06	.91	.52
	$[v^*M^*]_y$		70.8	29.6	16.2	7.8
	t_M		25.4	41.5	64.9	77.1
	$[u]_s$		21.2	10.2	5.8	3.3
	(lat.)		(53)	(48)	(50)	(59)
	$[v]_1$		1.42	.43	.22	.08
	(lat.)		(14)	(14)	(20)	(24)
	$[u^*v^*]$		21.7	8.0	4.0	1.4
	(lat.)		(29)	(31)	(33)	(43)
	T_{ed}		19.0	7.51	2.95	.86
	T_{MMC}		-3.90	-1.82	-1.06	-.39
	R		.21	.24	.36	.45
	$\hat{\Theta}_0$	(6.4)	11.2	12.6	14.2	15.1
B (τ_h)	ΔT	(48.0)	42.0	34.7	26.2	16.5
	δT	(16.4)	14.4	13.1	11.9	7.2
	M		1.34	1.12	.78	.40
	$[v^*M^*]_y$		36.5	24.7	14.6	4.2
	t_M		42.6	52.6	61.8	111.
	$[u]_s$		18.9	12.6	6.6	1.6
	(lat.)		(58)	(56)	(58)	(59)
	$[v]_1$		.53	.27	.16	.06
	(lat.)		(21)	(23)	(27)	(35)
	$[u^*v^*]$		12.6	7.5	3.3	.7
	(lat.)		(35)	(36)	(41)	(44)
	T_{ed}		13.5	6.85	2.69	.71
	T_{MMC}		-3.24	-2.07	-.94	-.22
	R		.24	.30	.35	.31
	$\hat{\Theta}_0$	(18.1)	19.8	21.6	23.2	23.6

Table 6.5: Some characteristic quantities in the experiments varying τ_s.

RUN	$\tau_s(days)$	1.25	2.5	5	10	20
A (k)	ΔT	35.6	35.7	33.4	32.2	32.8
	δT	12.6	10.8	10.9	11.3	11.6
	M	.91	.83	1.06	1.39	1.91
	$[v^*M^*]_y$	44.2	35.2	29.6	29.0	25.5
	t_M	23.8	27.3	41.5	55.7	86.7
	$[u]_s$	3.8	5.5	10.2	17.4	30.6
	(lat.)	(50)	(51)	(48)	(48)	(51)
	$[v]_1$	.55	.41	.43	.46	.48
	(lat.)	(18)	(15)	(14)	(14)	(14)
	$[u^*v^*]$	11.6	9.6	8.0	8.0	8.0
	(lat.)	(33)	(33)	(31)	(32)	(28)
	T_{ed}	7.63	7.13	7.51	7.31	7.00
	T_{MMC}	-2.62	-1.85	-1.82	-1.68	-1.67
	R	.34	.26	.24	.23	.24
	$\hat{\Theta}_0$	12.6	12.3	12.6	12.6	12.8
B (k)	ΔT	37.0	36.2	34.7	37.1	35.8
	δT	13.4	13.4	13.1	12.5	13.0
	M	.65	.95	1.12	1.21	1.60
	$[v^*M^*]_y$	30.1	25.5	24.7	19.4	14.8
	t_M	25.1	43.3	52.6	72.0	125.
	$[u]_s$	2.9	8.0	12.6	19.5	28.6
	(lat.)	(55)	(57)	(56)	(58)	(57)
	$[v]_1$	.27	.28	.27	.24	.24
	(lat.)	(24)	(24)	(23)	(23)	(22)
	$[u^*v^*]$	6.5	8.9	7.5	6.6	5.2
	(lat.)	(38)	(39)	(36)	(35)	(33)
	T_{ed}	6.49	6.60	6.85	6.39	6.19
	T_{MMC}	-2.00	-2.18	-2.07	-1.89	-1.75
	R	.31	.33	.30	.30	.28
	$\hat{\Theta}_0$	21.4	21.5	21.6	21.5	21.5

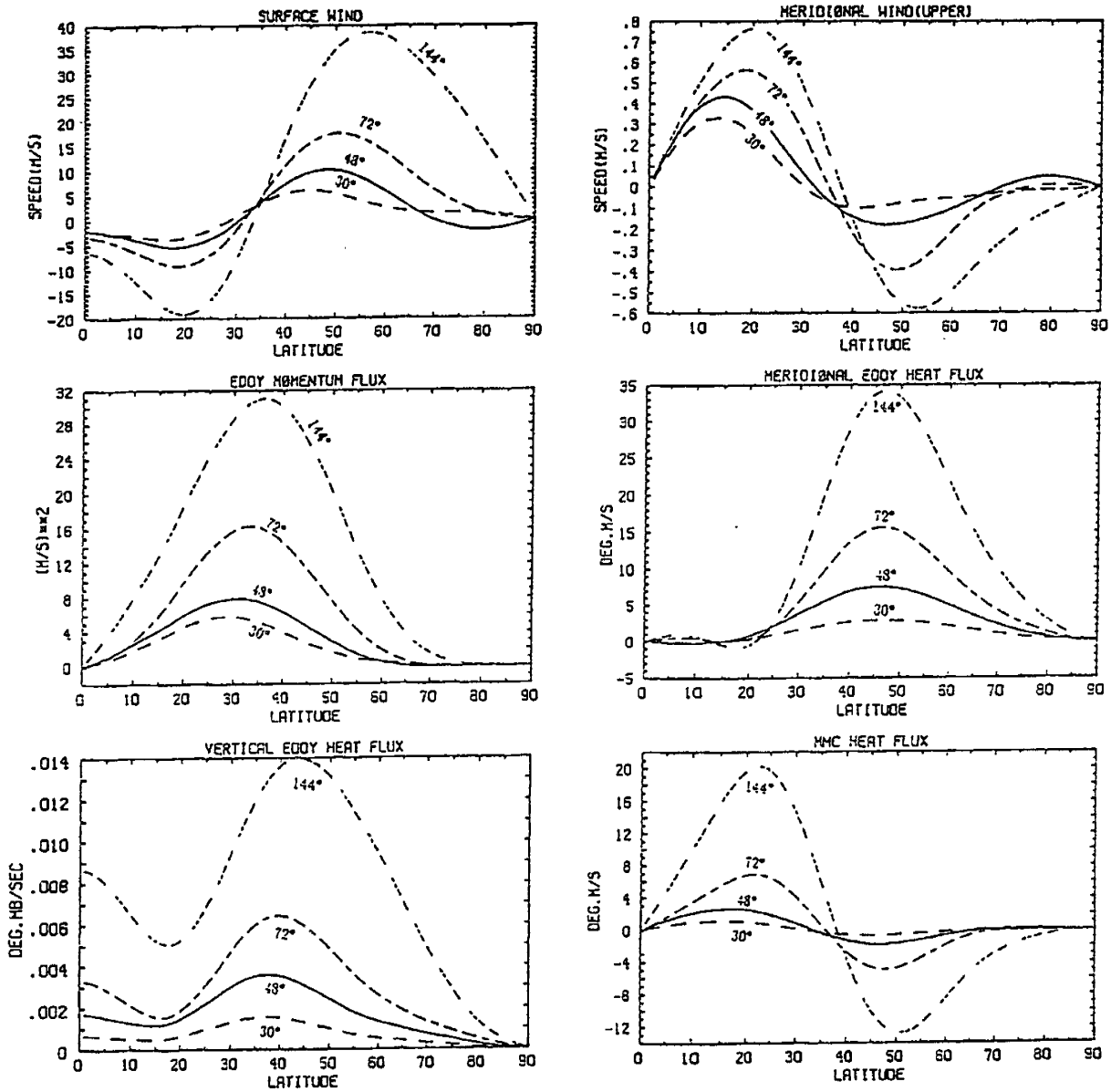

Figure 6.10: The equilibrium states of zonal mean surface winds, upper layer meridional winds, eddy momentum fluxes, meridional eddy heat fluxes, vertical eddy heat fluxes and MMC heat fluxes in experiments A(ΔT_E).

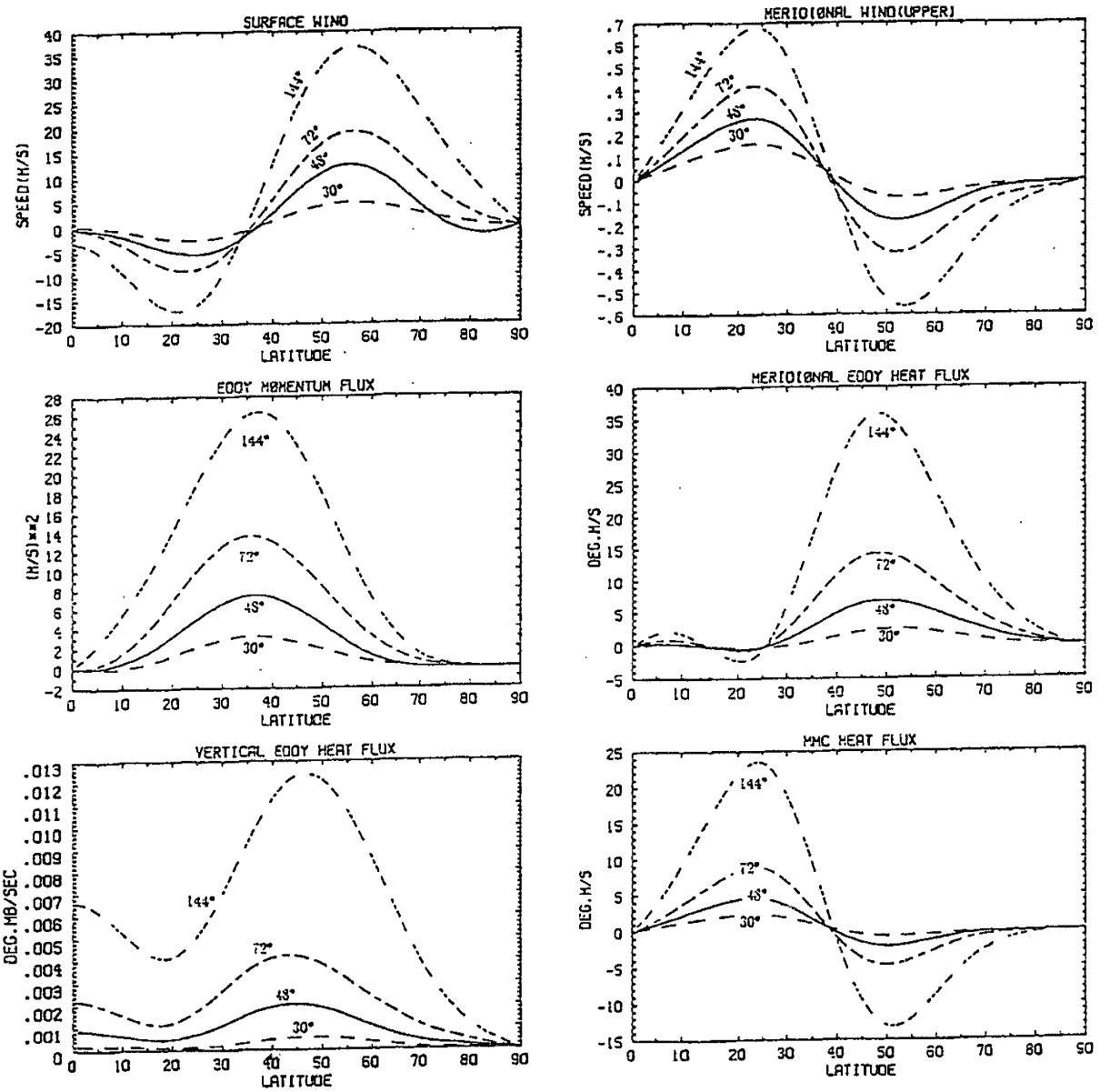

Figure 6.11: As in Figure 6.10 but for experiments B (ΔT_E).

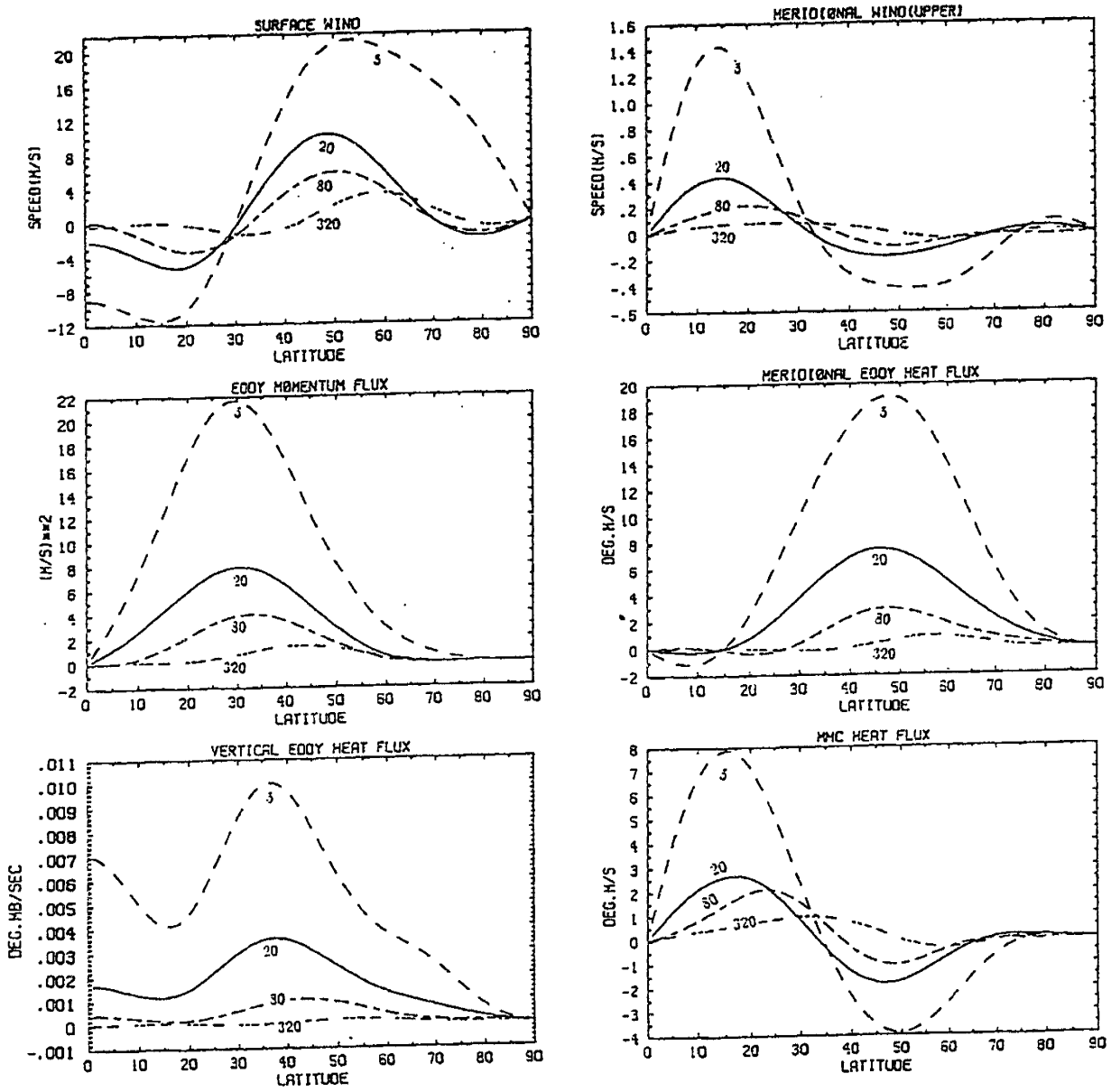

Figure 6.12: The equilibrium states of zonal mean surface winds, upper layer meridional winds, eddy momentum fluxes, meridional eddy heat fluxes, vertical eddy heat fluxes and MMC heat fluxes in experiments A(τ_h).

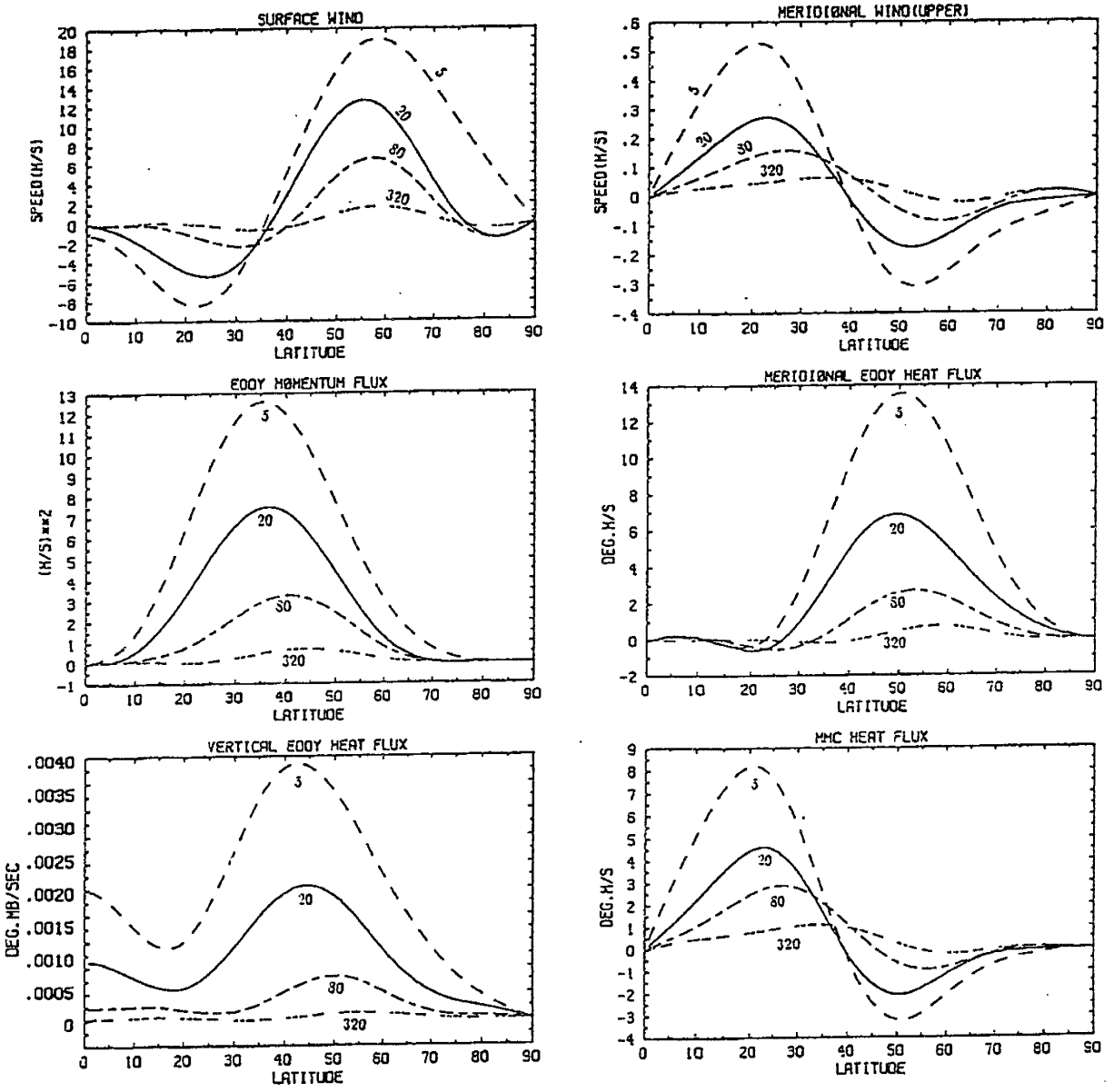

Figure 6.13: As in Figure 6.12 but for experiments B (τ_h).

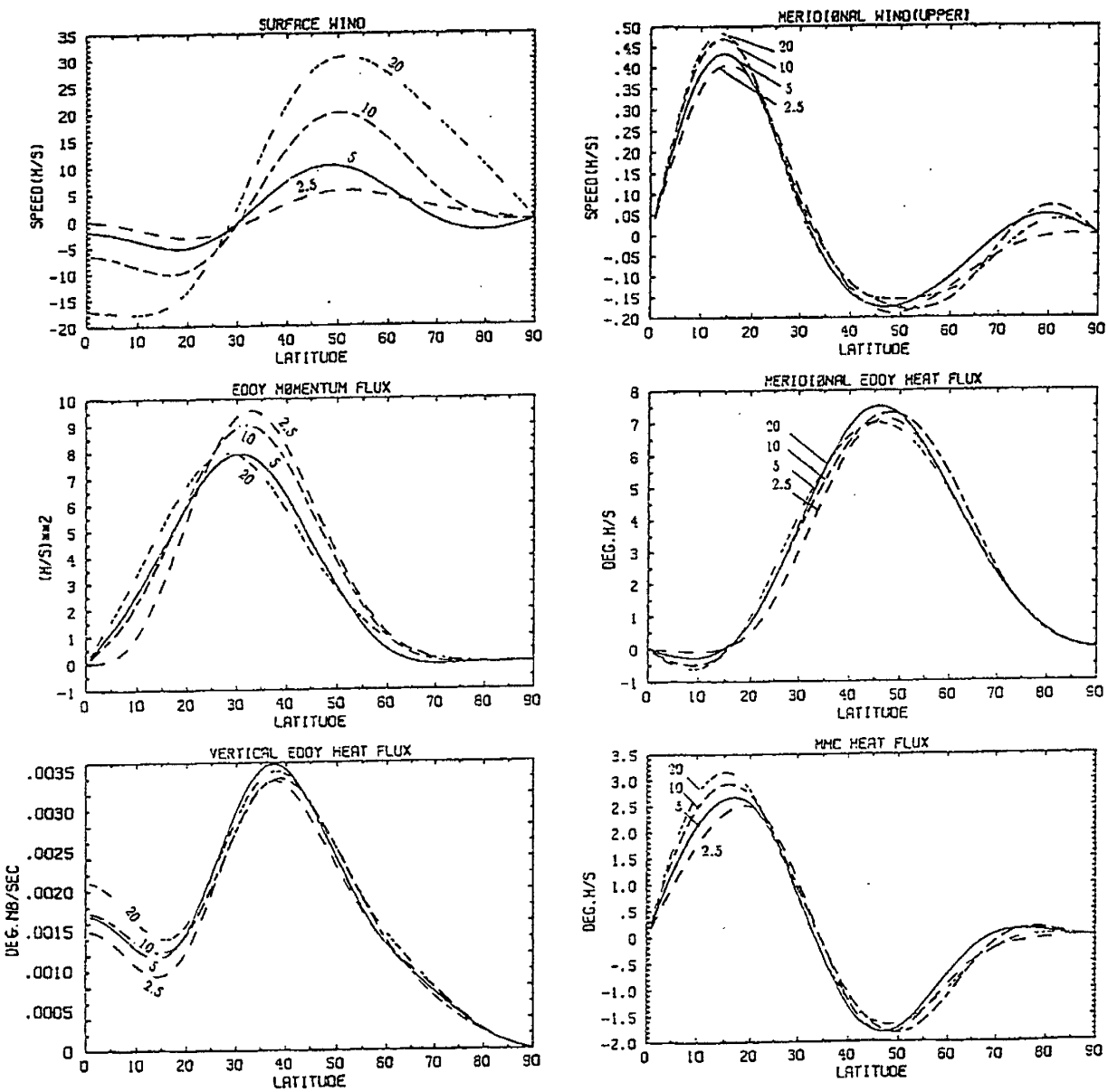

Figure 6.14: The equilibrium states of zonal mean surface winds, upper layer meridional winds, eddy momentum fluxes, meridional eddy heat fluxes, vertical eddy heat fluxes and MMC heat fluxes in experiments A(k).

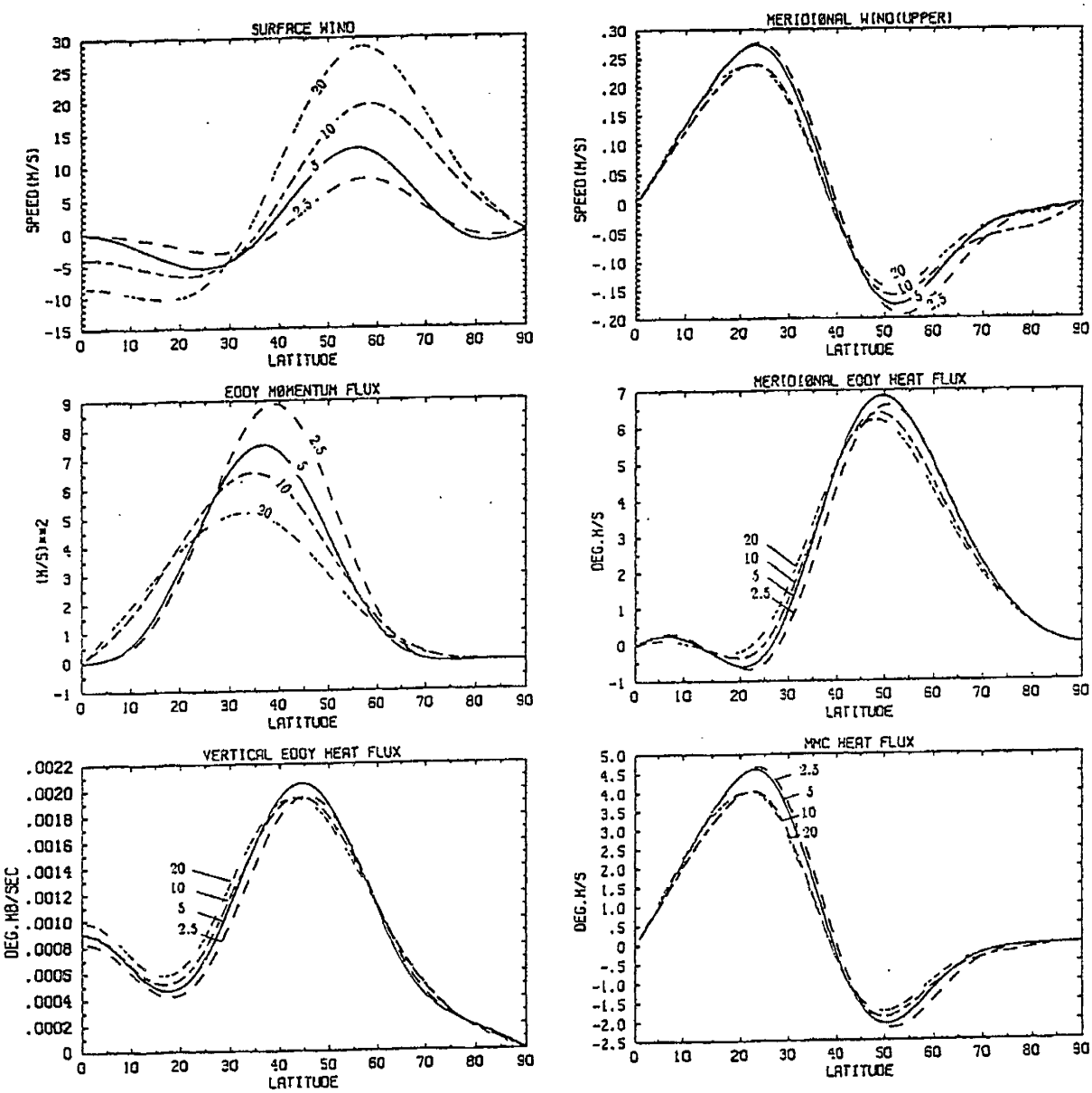

Figure 6.15: As in Figure 6.14 but for experiments B (k).

Chapter 7

Adjustment of the temperature structure

7.1 Introduction

According to diagnostic studies (Stone, 1978; Mole and James, 1990) the zonal mean midlatitude temperature gradient, δT, tends to equilibrate at the critical value, δT_c, for baroclinic instability in the sense of two-level models, despite strong seasonal changes in the radiative forcing. Stone has pointed out that this critical gradient corresponds to a transition from conditions where the dominant baroclinic instabilities are inefficient in transporting heat to conditions where they are efficient. By examining the correlation between the eddy flux of sensible heat and the excess of the mean shear over the critical shear, Stone hypothesized that the heat transport by long and deep baroclinic waves is responsible for the process of baroclinic adjustment.

There have been many attempts to explore the mechanism of baroclinic adjustment. For instance, Lindzen and Farrell (1980) and Gutowski (1985b) assumed that

the effect of baroclinic eddies is to reduce the meridional gradient of quasi-geostrophic potential vorticity (Q), so that the gradient of $[Q]$ vanishes in the adjustment layer, i.e.,

$$[Q_y] = \beta - \frac{f^2[u_z]}{\rho}\frac{d}{dz}(\frac{\rho}{N^2}) = 0,$$

where ρ is the air density, y and z are meridional and vertical coordinates. In their calculations, Lindzen and Farrell fixed N^2 to compute $[u_z]$, whereas Gutowski fixed $[u_z]$ to compute N^2. Even if the assumption of vanishing $[Q_y]$ is valid, neither of their calculations can be said to be appropriate since the adjustments of $[u_z]$ and N^2 should take place simultaneously.

Another attempt to explore the mechanism of baroclinic adjustment was made by the use of two-level models to calculate the temperature gradient and the eddy heat transport (Cehelsky and Tung, 1991; Stone and Branscome, 1991). Cehelsky and Tung found that the calculated δT was indeed supercritical to the most unstable wave. They postulated that a nonlinear baroclinic adjustment mechanism may exist, by which the temperature gradient equilibrates at a critical value for which the longest wave is neutral and the most unstable wave is saturated. They attributed this mechanism to nonlinear upscale energy cascades. Stone and Branscome (1991) also found that the calculated δT is supercritical. They suggested a modified baroclinic adjustment, i.e., $\delta T \propto \delta T_c$ instead of $\delta T \simeq \delta T_c$. Of course, this modification is more general and appropriate, if we consider that δT_c is dependent on the arbitrary depth of a two-level model. Nevertheless, the observed δT is not appreciably supercritical. The discrepancy of the observations and the model results may be related to errors in the estimates of δT_c, which is proportional to the static stability. The static stability in the diagnostic studies is calculated from observed data and is not a constant, but in the models it is fixed as a constant.

In this chapter, we use our model results to investigate the interactions between large-scale eddies and the midlatitude temperature structure. The zonal mean temperature structure can be better represented by the slope of isentropic surfaces, which combines the meridional temperature gradient and the vertical lapse rate. We first examine how baroclinic adjustments occur in the Phillips system and in the Lorenz system. Then we check the empirical relationship between the eddy heat flux and the temperature gradient. Finally, we study the eddy heat transports in the wavenumber domain, to identify the main heat-transporting waves.

7.2 Isentropic slope adjustment

7.2.1 Fixed static stability

The isentropic slope, α, is defined as

$$\alpha = \left(\frac{\partial z}{\partial y}\right)_{\Theta} = -\frac{(\partial\Theta/\partial y)}{(\partial\Theta/\partial z)} \sim \frac{\delta T}{N^2} \sim \frac{\hat{U}}{N^2}. \tag{7.1}$$

Since in the Phillips system N^2 is fixed α is proportional to δT. First, we show the model results for experiments in which N^2 is set to the realistic value ($10^{-4}\,s^{-2}$) and ΔT_E is varied. The adjustment of δT is shown in Figure 7.1 for experiments in which ΔT_E is varied. The abscissa represents ΔT_E, the pole-to-equator temperature contrast in the radiative equilibrium. The dashed line represents δT_E at 45° of latitude in radiative equilibrium. The solid line represents the calculated δT at 45° of latitude, which is the midlatitude temperature gradient in the model's climate equilibrium. When $\Delta T_E < 23\,K$, there are no eddies, so δT is identical to δT_E. This is a Hadley regime in which the mid latitudes are in radiative equilibrium. When ΔT_E increases, δT deviates gradually from δT_E but it also increases slightly.

This feature is very similar to that found in β-plane models (e.g., Cehelsky and Tung, 1991). The relative insensitivity of δT is obviously attributed to the active meridional eddy heat flux.

Next, we present the model results for experiments in which ΔT_E is fixed at the realistic value ($48\,K$) and the static stability is varied. For convenience we use N^2 instead of Γ_0 as the static stability parameter in the following illustrations. N^2 is set to be constant in each of the experiments. Correspondingly, for each experiment there is a critical shear $\hat{U}_c$ (or δT_c):

$$\hat{U}_c \simeq \left(\frac{H^2 \sin\theta}{4\Omega a \cos^2\theta} \right) N^2 \tag{7.2}$$

(Phillips, 1954). The calculated shears, $\hat{U}$, at $\theta \doteq 45°$ are shown in Figure 7.2 as a function of N^2. Each cross sign represents one experiment. The dotted line stands for the critical shear, $\hat{U}_c$, at $\theta = 45°$, i.e., $\hat{U}_c = 4.17 \times 10^4 N^2$. Its slope is proportional to the critical isentropic slope α_c. The horizontal dot-dashed line represents the vertical shear in the radiative equilibrium, $\hat{U}_E$, which has been fixed for all of the experiments. The dashed line through the origin is a best fit to the calculated points, which corresponds to $\hat{U} = 9.87 \times 10^4 N^2$.

The figure exhibits two different regimes: one for $N^2 > 1.3 \times 10^{-4}\,s^{-2}$, in which case the calculated shear is similar to the shear associated with the radiative equilibrium state; the other for $N^2 < 1.3 \times 10^{-4}\,s^{-2}$, in which case the calculated shear varies linearly with N^2. These results imply that the isentropic slope is insensitive to the change in static stability, but the slope is appreciably supercritical to the critical slope for baroclinic instability.

The transition value of N^2 from the Hadley regime to the eddy regime seems to

be somewhat small compared with the values observed in the real atmosphere. This is due to the formulation of thermodynamic equation in the Phillips system (see chapter 3). The effective static stability in the Phillips system should be amplified by a factor of 2.

7.2.2 Variable static stability

In the Lorenz system, when the forcing ΔT_E varies, $\hat{U}$ and N^2 vary simultaneously. The variations of isentropic slope are shown in Figures 7.3 and 7.4, for the two types of equilibrium static stability (curve A and B) used in chapter 6. Here we have included several experiments with very small values of ΔT_E (e.g., $\Delta T_E = 16,\ 20\,K$). This was done because baroclinic instability is possible when the static stability is very small. For each experiment with a specified ΔT_E, we calculate the values of $\hat{U}$ and N^2 at 45° correspondingly. The values of $\hat{U}$ are represented by a cross sign in the figures, in which N^2, instead of ΔT_E, is the abscissa for easier comparison with Figure 7.2. Indeed, $\hat{U}$ is an implicit function of N^2. $\hat{U}_c$ is still a linear function of N^2 and is represented by the dotted line. $\hat{U}_E$ is represented by the dot-dashed line and is determined by the controling parameter ΔT_E. Likewise, the dashed line is a best fit to the calculated points, represented by $\hat{U} = 4.86 \times 10^4 N^2$ in case A (Figure 7.3) and by $\hat{U} = 4.40 \times 10^4 N^2$ in case B (Figure 7.4).

When ΔT_E (or $\hat{U}_E$) increases, both $\hat{U}$ and N^2 increase. This feature has been demonstrated in chapter 6. When ΔT_E gets smaller, the calculated N^2 approaches a limiting value of N_E^2, which is the equilibrium static stability in the diabatic forcing (N_E^2 is proportional to Γ_E). The calculated $\hat{U}$ also approaches $\hat{U}_E$. One of the noticable features is that the isentropic slope is insensitive to the change in ΔT_E.

The adjustments of $\hat{U}$ and N^2 compensate each other to maintain the isentropic slope at some statistical equilibrium state. Another feature is that the equilibrium slope is much closer to the critical value as defined in the Phillips system.

In fact, these features are robust. They appear for a large range of ΔT_E values. They are not dependent on the forcing of static stability (Γ_E) either. They are not sensitive to changes in other parameters. For instance, we have repeated the same experiments but with a surface drag half as strong. The obtained features of isentropic slope are very similar to the former experiments (figures not shown). Since the model results are calculated with sufficient horizontal resolutions, further increasing the resolution has little effect on these features.

The sharp contrast of isentropic slopes in the Phillips and the Lorenz system is partly due to the different formulations of thermodynamic equation, and partly due to the effect of the vertical eddy heat flux. The critical shear ($\hat{U}_c = 4.17 \times 10^4 N^2$) is derived from the Phillips system. Because of the difference in the formulations of thermodynamic equation in the Phillips and the Lorenz system, the critical shear is not unique. If we fix the static stability in the Lorenz system, and perform similar analysis of baroclinic instability as in the Phillips' model, then the critical shear will decrease by a factor of 2. After this modification, the calculated isentropic slope in the Lorenz system is still less supercritical than that in the Phillips system. For example, the supercriticality is $\sim$ 137% in the Phillips system (Figure 7.2), and $\sim$ 110% in the case B of the Lorenz system (Figure 7.4). This difference becomes more significant when ΔT_E increases.

The critical shear defined in the modified Lorenz system should be more reasonable, because the thermodynamic equation is better represented in the vertical

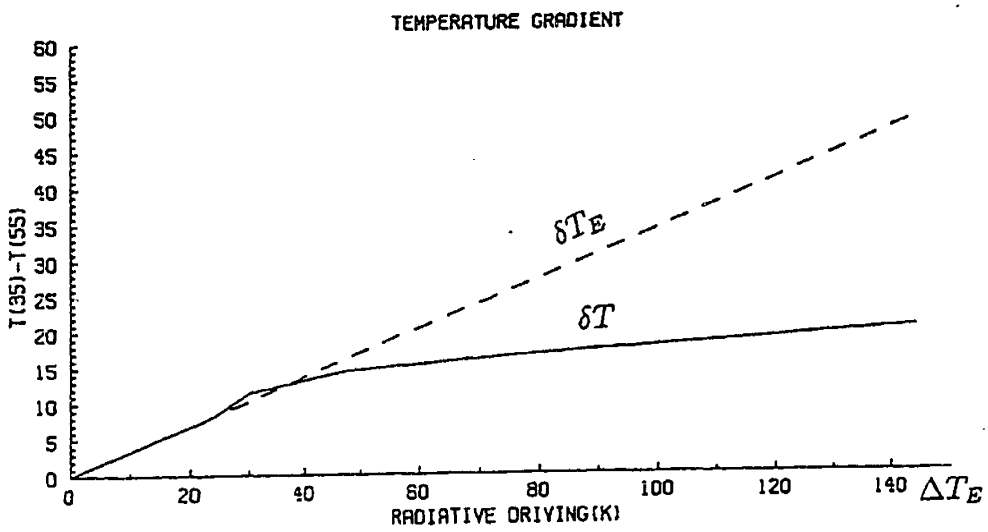

Figure 7.1: The variation of the temperature gradient at 45° with ΔT_E.

mean form. In this sense, the observed shear is indeed very supercritical. The fact that the observed shear is near the critical value defined in the Phillips' model appears to be a coincidence. Moreover, the effects of diabatic forcing, friction and meridional structure of mean flow were not taken into account in the conventional analysis of baroclinic instability. In our model, these effects are included in numerical integrations. The model results in the Lorenz system are in better agreement with observations (Stone, 1978; Stone and Carlson, 1979; Mole and James, 1990).

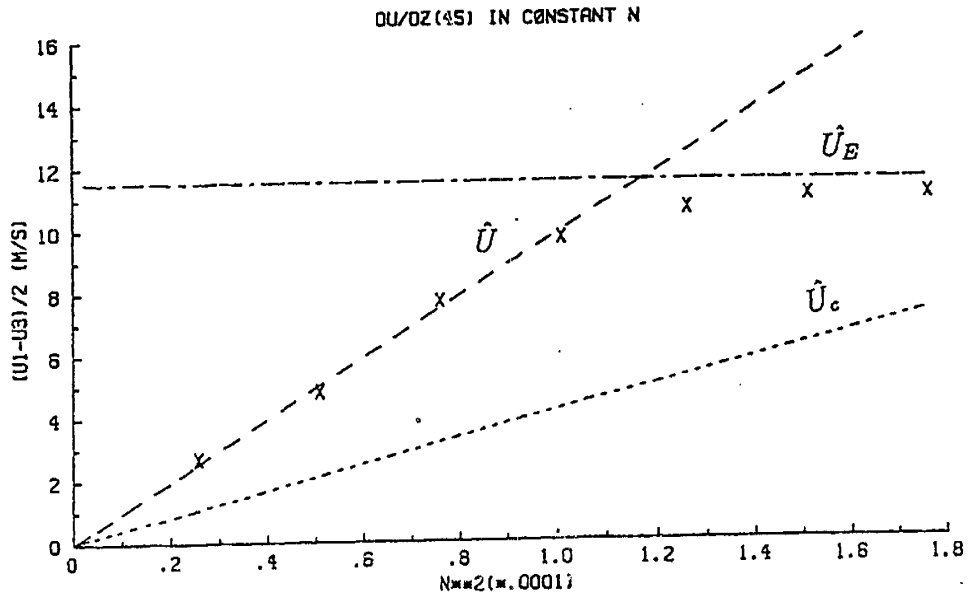

Figure 7.2: The vertical shears at 45° as a function of static stability N^2. The cross signs are model results calculated with the Phillips system; the dashed line is $\hat{U} = 9.87 \times 10^4 N^2$; the dotted line is the criterion for baroclinic instability; the dot-dashed line is the shear in radiative equilibrium state.

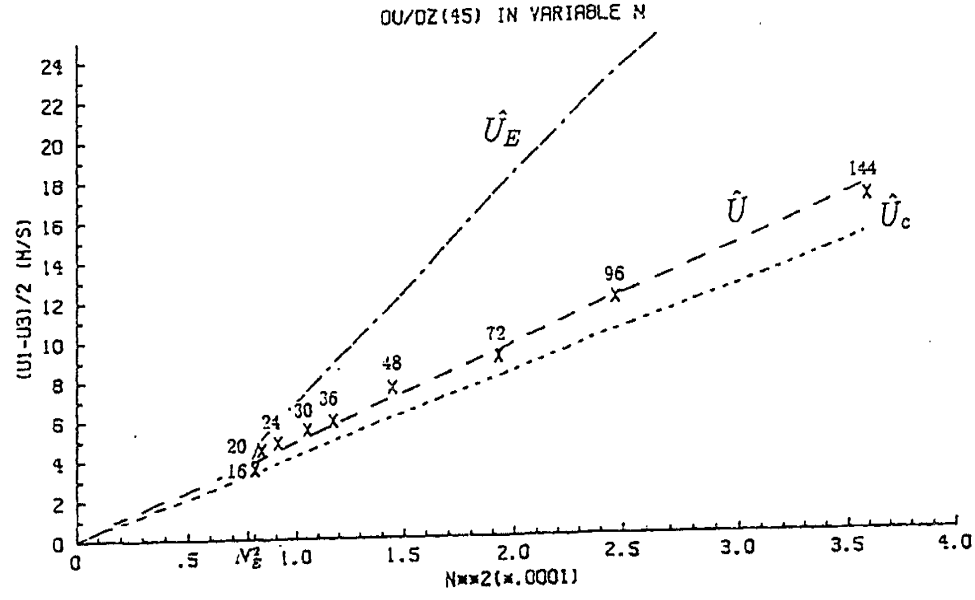

Figure 7.3: As in Figure 7.2 but the model results are calculated in the Lorenz system (Γ_E is set to curve A, i.e., radiative equilibrium). The dashed line is $\hat{U} = 4.86 \times 10^4 N^2$.

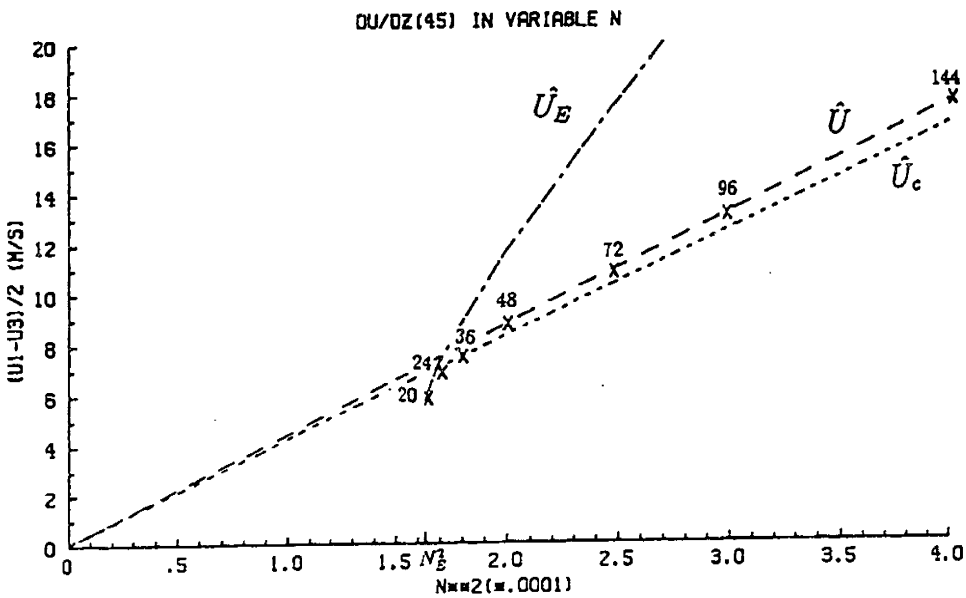

Figure 7.4: As in Figure 7.2 but the model results are calculated in the Lorenz system (Γ_E is set to curve B, i.e., radiative-convective equilibrium). The dashed line is $\hat{U} = 4.40 \times 10^4 N^2$.

7.3 Temperature gradient and eddy heat flux

Empirical power relationships between temperature gradient (δT) and the meridional eddy heat flux (T_{ed}), i.e., $T_{ed} \propto (\delta T)^n$, have been used in simple climate models to parameterize eddy heat transports. It is interesting to check if any power relationship exists in the model results. If a model describes correctly the important physics and dynamics in the atmosphere, it should simulate the basic features of observed climatology. It should also reflect some implicit information embodied in the atmosphere, such as the relationship between the eddy heat flux and the temperature gradient. We will examine how sensitive the eddy heat flux is to the change in the temperature gradient in our model. Because δT is relatively insensitive to the change in ΔT_E, whereas T_{ed} is very sensitive to the change in ΔT_E, T_{ed} should be very sensitive to δT. Moreover, we will compare the sensitivity study in the Phillips system with that in the Lorenz system to determine the effect

of interactive static stability.

Figure 7.5 shows the model results for various ΔT_E (ΔT_E = 30, 36, 48, 72, 96, 144 K). The abscissa represents the midlatitude temperature gradient, δT, and the ordinate represents the eddy heat flux, T_{ed}. Both coordinates are in logarithmic scale, so that a power relationship between δT and T_{ed} is indicated by a straight line in the figure, and the slope of the line is the exponent n. The letters "A" and "B" denote those experiments with variable static stability, identical to A(ΔT_E) and B(ΔT_E). The letter "C" denotes the experiments with constant static stability. In general, these calculated points are aligned very well, showing that the power relationship is a good approximation. However, the slopes of those lines are quite different between the Phillips system and the Lorenz system. The slope of the "C" line is much steeper than the slope of "A" or "B" line. Even within the same systems the slope varies slightly with ΔT_E.

The exponent n is explicitly shown as a function of ΔT_E in Figure 7.6. When the static stability is fixed n is appreciably large, ranging from 5 to 8. When the static stability is variable, n varies between 1 and 5. In the realistic range of radiative forcing for the earth's atmosphere ($\Delta T_E \sim 30 - 60\,K$), n is between 2 and 4, which is very close to the empirical relationships obtained from observations (Stone and Miller, 1980). Although the model is simple, it describes the eddy heat transport process very well. The magnitude of the eddy heat flux is comparable to observations (Oort, 1971) even the static stability is fixed at the realistic value. But, the relationship between T_{ed} and δT is similar to the empirical one only when the static stability is allowed to vary. In this aspect, the interaction between the vertical eddy heat flux and static stability is a key process. We also note that n

decreases with ΔT_E. When ΔT_E is very large and the static stability is variable, it seems that the diffusion law ($n = 1$) may be applicable. But, if the static stability is fixed, n is about 6 for large ΔT_E; then, neither the diffusion law nor the square relationship is applicable.

This result implies that the meridional eddy heat flux is very sensitive to the change in the temperature gradient if the effect of the vertical eddy heat flux is neglected. The meridional eddy heat flux is even more sensitive to the change in δT in the quasi-geostrophic β-plane model, e.g., Stone and Branscome (1991) found that n is about 15 in their model results. This may be related to the eddy momentum transport, which is not properly described on the β-plane. Although it does not directly affect the eddy heat flux and the temperature gradient, it has significant influence on the net heat transport through the negative feedback mechanism, as discussed in chapter 5. Therefore, both variable static stability and spherical geometry are very important to the study of climatic sensitivity. The former affects the vertical eddy heat transport, and the latter affects the meridional eddy momentum transport.

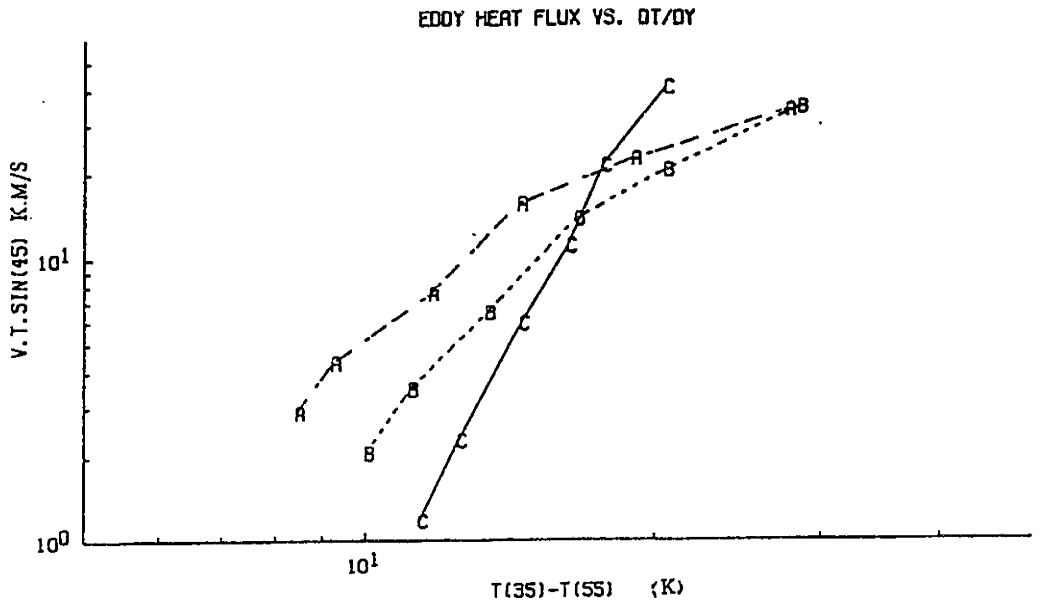

Figure 7.5: The eddy heat fluxes as a function of the temperature gradient in the mid latitudes. "A" and "B" are the model results with variable static stability (Γ_E is set to be curves A and B respectively); "C" is calculated with constant static stability.

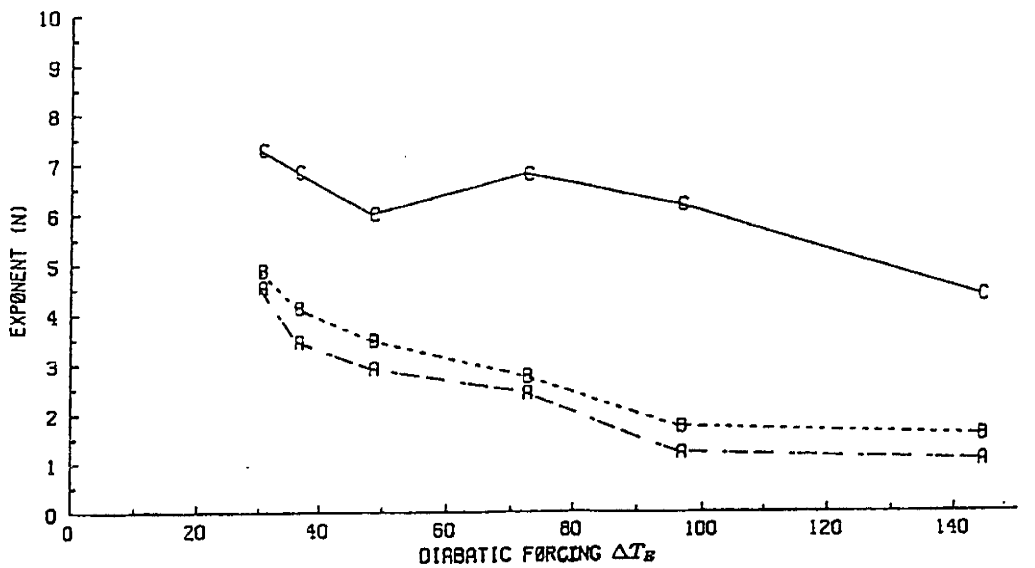

Figure 7.6: The exponents in the power relationship between the eddy heat flux and the temperature gradient, as a function of ΔT_E.

7.4 The main heat-transporting wave

The spectrum of eddy kinetic energy has shown that the longest wave in our model (wavenumber 3) becomes dominant when ΔT_E increases. If a wave possesses the largest part of the energy, it also has the largest amplitude. But we can not simply say that it transports the largest part of the heat, because the amount of heat transport is also determined by the phase correlation between v^* and T^*, in addition to the wave amplitude. In order to determine which wave transports most of the heat, we have calculated the individual eddy heat transport by each zonal wavenumbers. Figure 7.7 shows the portions of eddy heat fluxes by individual zonal wavenumbers in the experiments with constant static stability (denoted by "C") and with variable static stability (denoted by "A" and "B" according to the type of Γ_E). When ΔT_E is small, both wavenumber 3 and 6 are responsible for most of the heat transport. The maximal flux by wavenumber 3 is considerably poleward of that of the total eddy heat flux. The transport by wavenumber 9 is relatively small, and the contribution by higher wavenumbers is negligible. When ΔT_E increases, the portion of heat transported by wavenumber 3 becomes dominant, and its maximum amplitude shifts equatorward.

The peak values of the eddy heat fluxes for wavenumber 3, 6, 9 and total heat flux are shown in Figure 7.8 as a function of ΔT_E, for the experiments with fixed and variable static stability respectively. In general, the spectral features are very similar to those found in the β-plane model by Cehelsky and Tung (1991). According to Cehelsky and Tung, this is due to energy cascades to the longest wave through nonlinear wave-wave interactions. When the diabatic forcing increases to some extent, the heat transport by the most unstable wave (near wavenumber 6)

becomes saturated. Consequently, the longest wave is mainly responsible for the required heat transport.

The upscale energy cascade mechanism seems to be more effective in the model with variable static stability. For example, the portion of eddy heat flux carried by wavenumber 3 becomes more dominant in the Lorenz system than that in the Phillips system when ΔT_E increases. The portion carried by wavenumber 6 increases slightly with ΔT_E in the Phillips system. But in the Lorenz system this portion increases with ΔT_E only when $\Delta T_E \leq 72K$; it decreases when ΔT_E is larger. Moreover, the portion carried by wavenumber 9 is smaller in the Lorenz system than that in the Phillips system. This implies that when the static stability is variable there is more eddy energy cascade toward the longest wave in the model.

However, wavenumber 3 is not the longest wave in the real atmosphere or in more complete models. It is interesting to know which wavenumber is the main heat-transporting wave if wavenumber 1 and 2 are included. Since with the resolution of $5 \times 5(3)$ wavenumber 3 transports most of the heat when ΔT_E is large enough, we have chosen a strong forcing (i.e., $\Delta T_E = 96\,K$) and carried out some experiments with higher resolution. The resolutions used in these experiments are $5 \times 8(2)$ and $5 \times 15(1)$, with the fundamental wavenumber 1 and 2 respectively. The experiments were carried out in both the Phillips system and the Lorenz system (A).

The peak values of the eddy heat fluxes by individual wavenumbers are shown in Figure 7.9. In the experiments with the resolution of $5 \times 8(2)$, the second longest wave (wavenumber 4) transports the largest amount of the heat, although the transport by the longest wave (wavenumber 2) is comparable. The contribution by small-scale waves ($n > 6$) is relatively small. In the experiments with the resolution of

$5 \times 15(1)$, the most heat-transporting wave is also wavenumber 4, along with other large-scale waves ($n \leq 6$). The longest wave (wavenumber 1) does not transport the largest amount of the heat. This feature appears to be similar whether the static stability is fixed or variable. Accoding to the linear analysis of instability, the most unstable wave is wavenumber 5. Therefore, the main heat-transporting wave is close to the most unstable wave rather than the longest wave. However, the spectrum of eddy kinetic energy is different from that of the eddy heat flux. In all of the cases, the longest wave has the largest part of the energy (Figure 7.10). This feature is obviously the result of upscale cascade by wave-wave interactions.

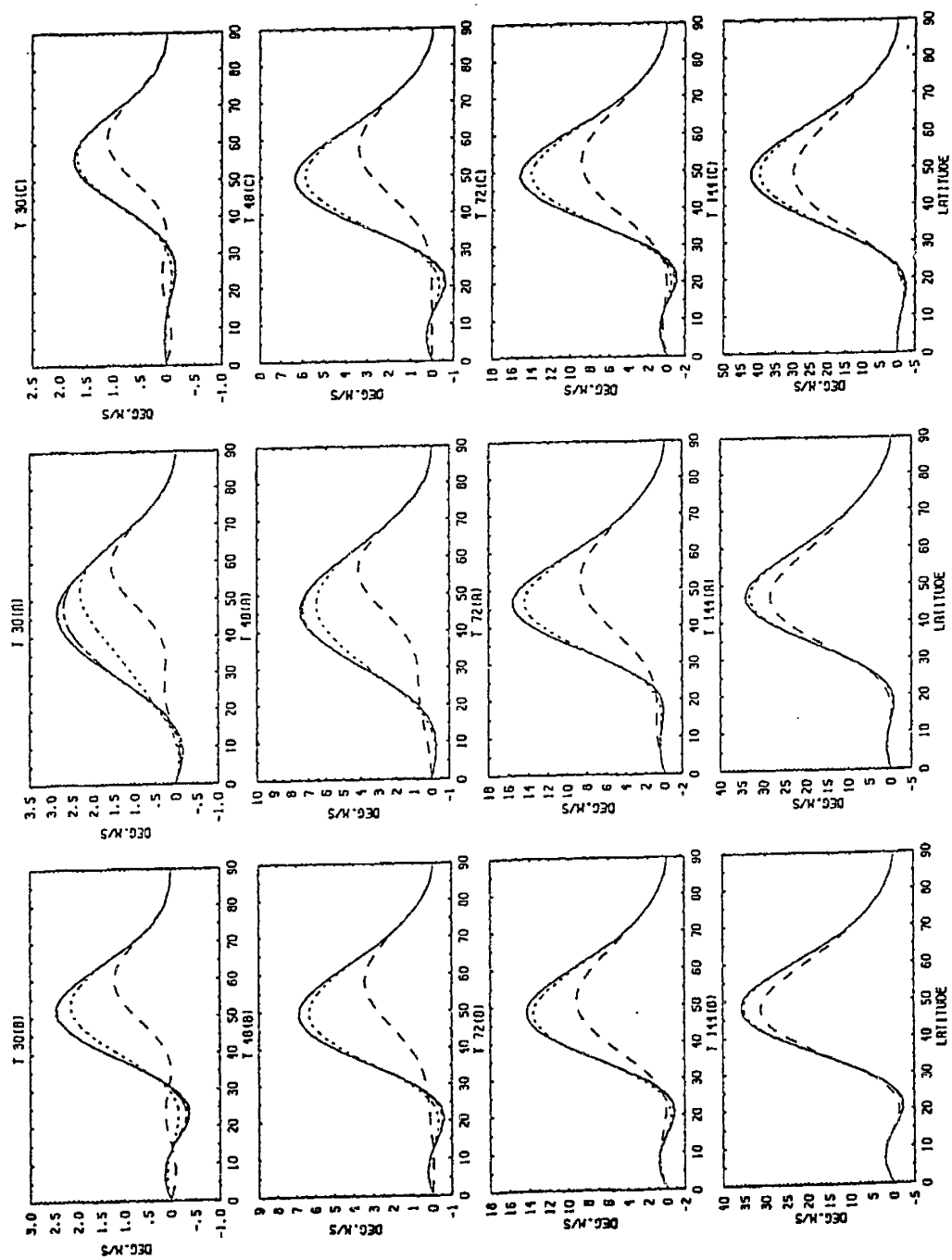

Figure 7.7: The eddy heat fluxes by individual zonal wavenumbers for ΔT_E = 30, 48, 72, 144 K. The dashed line indicates the flux by wavenumber 3, the dotted line is by wavenumbers 3 and 6, ..., the solid line is the total flux.

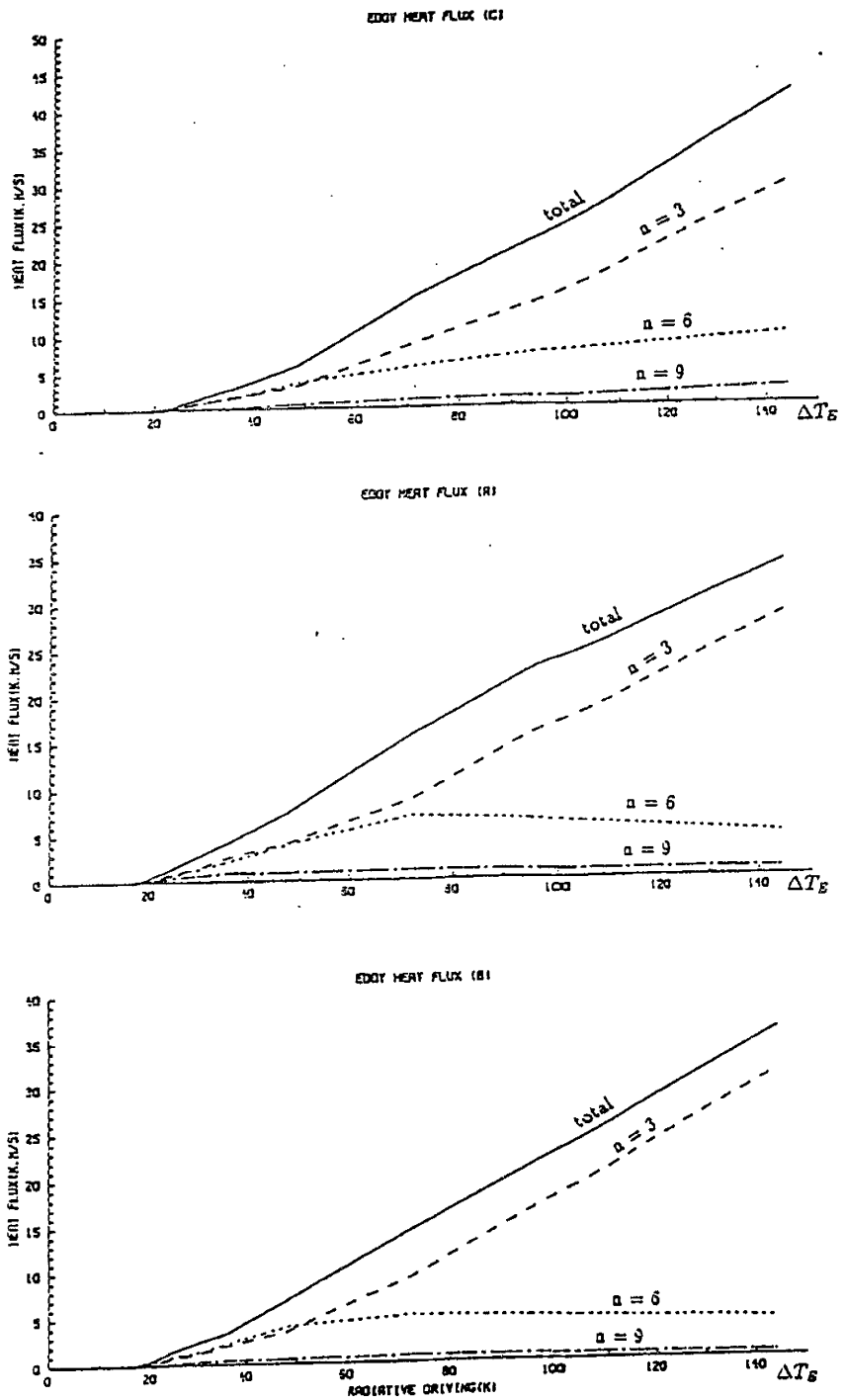

Figure 7.8: The peak values of eddy heat flux by individual wavenumbers as a function of ΔT_E. The solid line is for the total wavenumbers, the dashed, dotted and dot-dashed lines are for wavenumber 3, 6, 9 respectively.

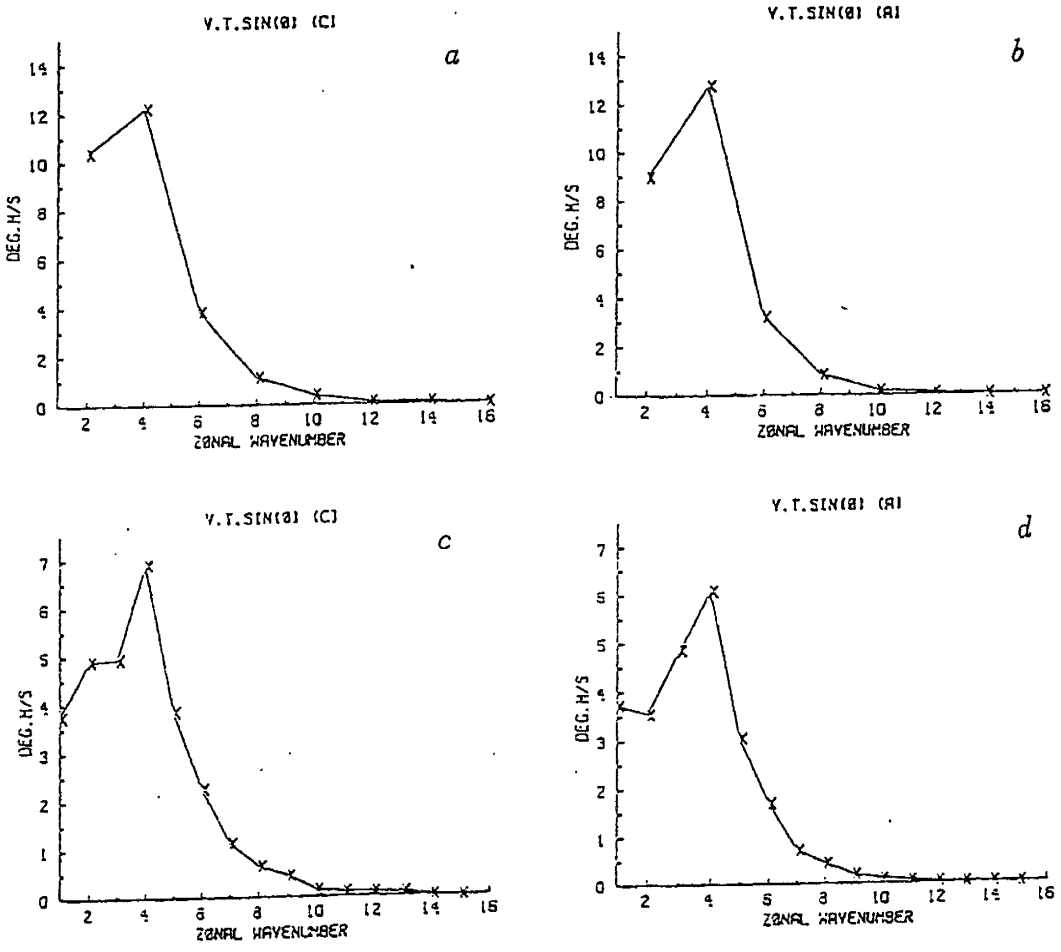

Figure 7.9: The peak values of eddy heat fluxes in the wavenumber domain. a) $5 \times 8(2)$, fixed static stability; b) $5 \times 8(2)$, variable static stability; c) $5 \times 15(1)$, fixed static stability; d) $5 \times 15(1)$, variable static stability.

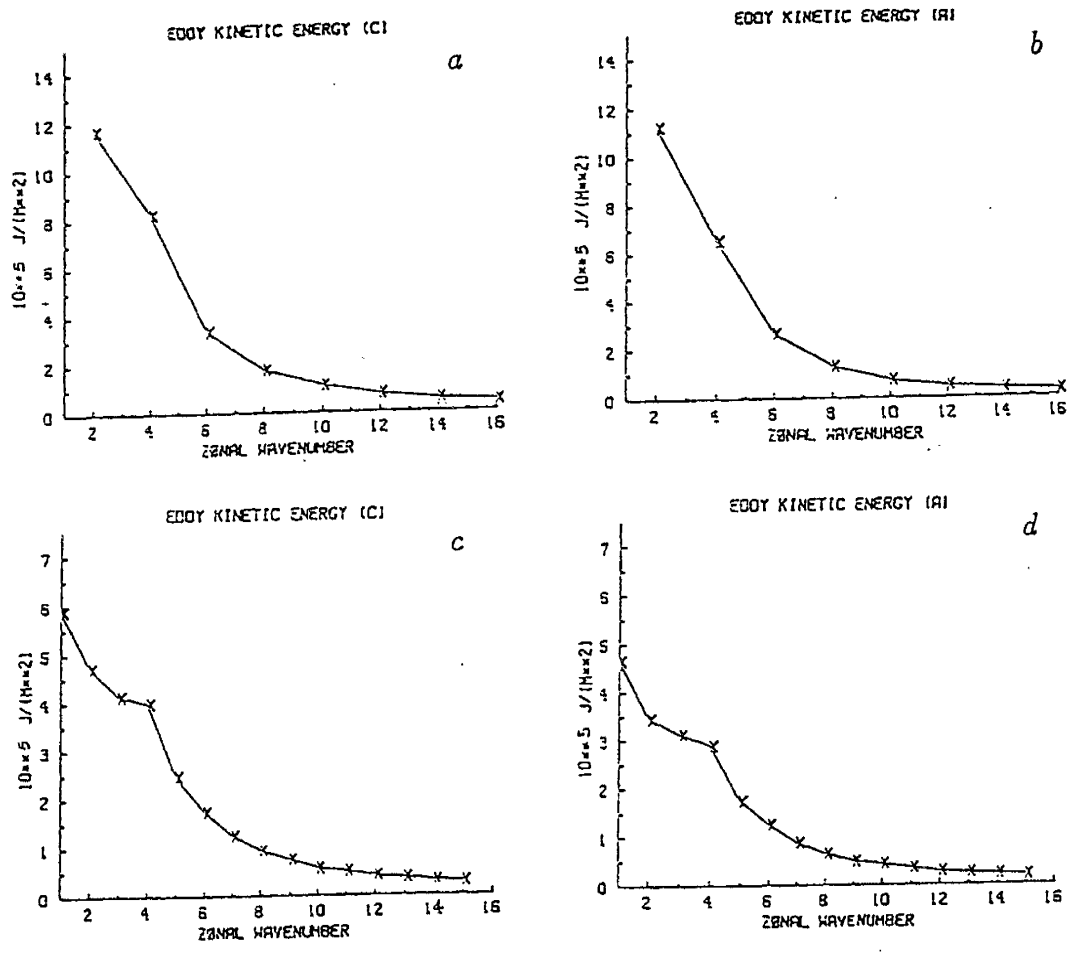

Figure 7.10: The eddy kinetic energy in the wavenumber domain. a) $5 \times 8(2)$, fixed static stability; b) $5 \times 8(2)$, variable static stability; c) $5 \times 15(1)$, fixed static stability; d) $5 \times 15(1)$, variable static stability.

Chapter 8

Summary and Conclusions

We have used a two-level spherical model with variable static stability, simple diabatic forcing and friction to study the role of large-scale eddies in climate. By progressive relaxation of the model constraints, we have carried out systematic numerical experiments in different dynamical regimes. One major conclusion we can draw from this study is that *spherical geometry and variable static stability are two very important factors in studies of climate equilibrium and sensitivity.* In other words, the quasi-geostrophic theory is largely limited in climate studies. Spherical geometry affects the eddy momentum flux which gives a negative feedback to the eddy forcing by the eddy heat flux. Variable static stability allows interactions between the vertical eddy heat flux and the temperature structure, which also affects the meridional eddy heat transport and temperature gradient.

If these two factors are missed in climate models, some important features related to climate equilibrium and sensitivity will be distorted. For instance, if spherical geometry is missed, the feedback by the Ferrel cell heat transport will be overestimated. This has been demonstrated in chapter 5 of this paper and by the comparison

of our spherical model results with the β-plane model results obtained by Stone and Branscome (1991). In our spherical model, the calculated values of the feedback factor, R, is very close to the predicted values of R_S; whereas in the β-plane model R is systematically larger, being ~ 2.5 times R_S. The sensitivity of the meridional eddy heat flux to the midlatitude temperature gradient is also overestimated in the β-plane model. In the approximate power relationship between T_{ed} and δT the power is ~ 15 in the β-plane model and ~ 6 in the spherical model with fixed static stability.

The effect of variable static stability is more significant. The variations of R with ΔT_E are of opposite directions for models with fixed and variable static stability. If the static stability is fixed, the meridional eddy heat flux is exaggerated and the isentropic slope is very supercritical to the "threshold" slope for baroclinic instability in the sense of the two-level model. On the other hand, with a variable static stability, the isentropic slope is closer to the critical value and similar to observations. The sensitivity of the eddy heat flux to the temperature gradient is also more realistic when the static stability is variable, with a power of 2 to 4, in good agreement with the empirical analysis (Stone and Miller, 1980).

In order to study the role of large-scale eddy transports, $[v^*T^*]$, $[u^*v^*]$ and $[\omega^*T^*]$, we have investigated three different dynamical regimes. The first is the Hadley regime in which all eddies are artificially suppressed. We obtained an equilibrium state which is very similar to that predicted by Held and Hou (1980)'s theory. The low latitudes are occupied by a Hadley cell which approaches a limit in a nearly inviscid atmosphere. The heat and momentum fluxes by the Hadley cell are very small. The temperature gradient is only slightly reduced from the radiative

equilibrium state in the low latitudes, and is almost unchanged in the mid-high latitudes. Through linear instability analyses we found that the Hadley regime is unstable.

Next we studied an eddy regime in which the static stability is fixed (the Phillips system). Taking the realistic values of the external parameters for the earth's atmosphere, we calculated the equilibrium states of zonal mean flow and temperature fields, the momentum and heat budgets and the energetics. We also carried out a series of experiments to examine the effects of horizontal resolution of the model. Based on a reasonable resolution, then, we studied the climatic sensitivity by varying the external parameters separately.

The third regime is also an eddy regime in which the static stability is variable (the Lorenz system). This regime allows us to study the interaction between eddy heat fluxes and midlatitude temperature structure in both meridional and vertical direction. We chose two types of equilibrium states, i.e., a radiative equilibrium and a radiative-convective equilibrium, as the forcing of static stability. With this more realistic model we carried out a series of parameter experiments, similar to those in the Phillips system. The role of vertical eddy heat flux was studied by examining the balance of the static stability equation, and by comparing the model's results with those in the Phillips system.

In our parameter experiments we confirmed that, in general, the eddy forcing is more sensitive to the diabaticity than to the dissipation, which has been pointed out by Stone and Branscome (1991) from their β-plane model results. Hence, the eddy regime can be divided into two subregimes according to the intensity of diabatic forcing: one is "strong" eddy regime, characterized by small values of R and asso-

ciated with strong diabatic heating; the other is "weak" eddy regime, characterized by large values of R ($R \sim 1$) and associated with weak diabatic forcing. The mid-latitude atmosphere belongs to the former subregime. It is forced by the strongest temperature gradient in radiative equilibrium. On the other hand, the lowlatitude atmosphere may be within the latter subregime because the forcing temperature gradient is weak.

In terms of the model results we studied the interaction between the eddy heat flux and the temperature structure in the mid latitudes. Specifically, we examined the baroclinic adjustment hypothesis and the empirical power relationship of the eddy heat flux and the temperature gradient. We emphasized the climatic sensitivity of the isentropic slope and the meridional eddy heat flux. In the mid latitudes, baroclinic adjustment seems to be the most important mechanism. Our model results support two main ideas in the baroclinic adjustment hypothesis: 1) the mid-latitude temperature gradient is not sensitive to the change in diabatic forcing; and 2) the eddy flux of sensible heat correlates very well with the temperature gradient (Stone, 1978). We have demonstrated that *the nature of baroclinic adjustment is the isentropic surface adjustment rather than the meridional temperature gradient adjustment only.* We also found that the longest wave does not necessarily transport most of the heat although it has most of the eddy kinetic energy (e.g., wavenumber 1). The main heat-transporting wave(s) is within the wavenumber subrange of the most unstable wave and the longest wave, and is close to the most unstable wave.

The emphasis of this study is on how the interaction of the vertical eddy heat flux and the temperature structure affects the climate equilibrium. In order to highlight the role of the vertical eddy heat flux, we compare the model results in the Phillips

and the Lorenz system. The similarities and differences are summarized as follows.

Similarities:

- The qualitative features of the general circulation, such as the zonal wind, the temperature field, the momentum budget, the heat budget and the energetics, are very similar.
- When τ_h increases, the eddy fluxes of heat and momentum decrease. $R \rightarrow 1$ as $\tau_h \rightarrow \infty$.
- The climate states and eddy transports are insensitive to the change in the surface drag. However, when τ_s increases R decreases.
- Baroclinic adjustment occurs in the sense that the isentropic slope is proportional to the critical value for baroclinic instability.
- T_{ed} and δT satisfy approximately a power relationship over a broad range of ΔT_E.
- Eddy kinetic energy cascades to the largest scale.

Differences:

- The static stability increases due to the vertical eddy heat flux in the Lorenz system.
- The strength of the Hadley cell in the Phillips system is much more sensitive to the change in ΔT_E than that in the Lorenz system ($3 \sim 4$ times).

- δT is more sensitive, but the isentropic slope is less sensitive, to the change in ΔT_E in the Lorenz system than in the Phillips system.

- When ΔT_E increases, R decreases in the Phillips system, but increases in the Lorenz system.

- The isentropic slope in the Lorenz system is less supercritical than that in the Phillips system. In other words, baroclinic adjustment is more effective in the Lorenz system.

- T_{ed} is less sensitive to δT, with a power of $2 \sim 4$ in the Lorenz system; the power is ~ 6 in the Phillips system.

- When ΔT_E increases, the portion of T_{ed} carried by short waves decreases more drastically in the Lorenz system, implying a more effective cascade mechanism.

- The effective static stability in the Lorenz system is half as much as that in the Phillips system; therefore, the baroclinity in the Lorenz system is in better agreement with observations.

Therefore, when the goal is just to simulate the qualitative characteristics of climate states and processes, such as the temperature field and the meridional eddy heat flux, quasi-geostrophic theory is usually adequate. This has been demonstrated by a number of numerical results obtained from β-plane models (O'Brien and Branscome, 1989; Stone and Branscome, 1991). This means that spherical geometry can be neglected and the static stability can be fixed in a first approximation. However, if the goal is to study interactions of climate processes or climatic sensitivities, quasi-geostrophic theory is no longer very good. Neither quasi-geostrophic β-plane models nor simple climate models with constant static stability are appropriate,

because the spherical geometry and the interaction of vertical eddy heat fluxes and static stability are absent in those models. Due to the fact that the important feedback mechanisms are distorted or neglected, the eddy forcing of climate states can not be correctly described by those models.

A successful model should, at least, be able to describe principal climate properties, such as the temperature structure, eddy transports of heat and momentum, the energy cycle, etc. Moreover, it should be able to describe correctly the variation of these principal climate properties with the external parameters, which is the basic requirement for climate sensitivity studies. Furthermore, it should be able to describe not only an individual climate property and its variability but also the dynamical correlations and connections among these properties. For example, the feedback factor R, the exponent n in the power relationship of T_{ed} and δT, the inverse cube law in the eddy kinetic energy spectrum, etc., all belong to these correlations and connections.

According to these "standards", our two-level spherical model is successful. It is reasonably simplified and relatively realistic. The resolution of the model is low but enough to capture the dynamics of zonal mean flow and large-scale eddies. The physics of the model are simple but represent the basic sources and sinks. The eddy fluxes are calculated explicitly and inexpensively. Therefore, this model has a strong potential in studies of climate and climatic changes. For example, an easy extension of this study can be done by incorporating topography, hydrology, zonal or annual variations of the diabatic forcing. This model can also be coupled to a simple ocean model to study the effect of air-sea interactions on climate.

One shortcoming of this model is that the tropical dynamics can not be described

satisfactorily, although including a meridionally varying interfacial friction can make some improvement. This problem is related to the balance equation approximation and insufficient meridional resolution. It may also be related to the simple formulation of diabatic forcing, e.g., convective adjustments are not included. Besides, the limitation of two levels only allows one to consider the "bulk" or vertical mean thermal properties, such as temperature, static stability, heat fluxes by eddies and by the MMC. To study their vertical structures a multi-level model is desirable.

References

Andrews, D. G., and M. E. McIntyre, 1986: Planetary waves in horizontal and vertical shear: the generalized Eliassen-Palm relation and the mean zonal acceleration. *J. Atmos. Sci.*, **33**, 2031-2048.

Arakawa, A. and S. Moorthi, 1988: Baroclinic instability in vertical discrete systems. *J. Atmos. Sci.*, **45**, 1600-1707.

Baer, F., and G. W. Platzman, 1960: A procedure for numerical integration of the spectral vorticity equation. *J. Meteor.*, **18**, 393-401.

————, and A. Y. Alyea, 1971: Effects of spectral truncation on general circulation and long-range prediction. *J. Atmos. Sci.*, 28, 457- 480.

————, and ————, 1974: Predictability and spectral truncation. *J. Atmos. Sci.*, **31**, 920-931.

Bourke, W., 1974: A multi-level spectral model. I. Formulation and hemispheric integrations. *Mon. Wea. Rev.*, **102**, 687-701.

Bryan, K., 1959: A numerical investigation of certain features of the general circulation. *Tellus*, **11**, 163-173.

Brunt, D., 1927: The period of simple vertical oscillations in the atmosphere. *Quart. J. Roy. Meteor. Soc.*, **53**, 30-32.

Budyko, M. I., 1969: The effect of solar radiation variations on the climate of the earth. *Tellus*, **21**, 611-619.

Cehelsky, P., and K. K. Tung, 1987: Theories of multiple equilibria and weather regimes – a critical reexamination. Part II: baroclinic two-layer models. *J. Atmos. Sci.*, **44**, 3282-3303.

———, and ———, 1989: Reply. *J. Atmos. Sci.*, **46**, 1865-1866.

———, and ———, 1991: Nonlinear baroclinic adjustment. Accepted by *J. Atmos. Sci.*

Charney, J. G., 1959: On the theory of the general circulation of the atmosphere. *The Rossby Memorial Volume.* B. Bolin, Ed., Rockefeller Institute Press, 178-193.

———, and M. E. Stern, 1962: On the stability of internal baroclinic jets in a rotating atmosphere. *J. Atmos. Sci.*, **19**, 159-172.

Coakley, J. A., 1979: A study of climate sensitivity using a simple energy balance model. *J. Atmos. Sci.*, **36**, 260-269.

Colton, D. E., 1973: Barotropic scale interactions in the tropical upper troposphere during the northern summer. *J. Atmos. Sci.*, **30**, 1287-1302.

Edmon, H. J., B. J. Hoskins, and M. E. McIntyre, 1980: Eliassen-Palm cross-sections for the troposphere. *J. Atmos. Sci.*, **37**, 2600-2616.

Eliasen, E., 1982: Climate modeling using an equivalent meridional circulation. *Tellus*, **34**, 228-244.

———, and B. Machenhauer, 1965: A study of the fluctuations of the atmospheric planetary flow patterns represented by spherical harmonics. *Tellus*, **17**, 220-238.

———, and L. Laursen, 1990: On the effects of horizontal resolution and diffusion in a two-layer general circulation model with a zonally symmetric forcing. *Tellus*, **42A**, 520-530.

Eliassen, A., and E. Palm, 1961: On the transfer of energy in stationary mountain waves. *Geofys. Publ.*, 22 (3), 1-23.

Galin, M. B., and S. YE. Kirichkov, 1979 (a): A limited-component model of the general circulation with a variable Coriolis parameter. *Izvestiya, Atmos. and Oceanic Phys.*, **15**, 245-252.

———, and ———, 1979 (b): Energetics of a small-component general circulation model with variable Coriolis parameter. *Izvestiya, Atmos. and Oceanic Phys.*, **15**, 397-402.

———, and ———, 1979 (c): Study of the angular momentum and heat balance on the basis of small-component model of general atmospheric circulation. *Izvestiya, Atmos. and Oceanic Phys.*, **15**, 550-554.

Gill, A. E., 1982: *Atmosphere- Ocean Dynamics.* Academic Press. New York. 662 pp.

Goody, R. M., 1964: *Atmospheric Radiation.* Oxford, Clarendon Press. 436 pp.

Gutowski, W. J., 1985 (a): A simple model for the interaction between vertical eddy heat fluxes and static stability. *J. Atmos. Sci.*, 42, 346-358.

———, 1985 (b): Baroclinic adjustment and midlatitude temperature profiles. *J. Atmos. Sci.*, **42**, 1733-1745.

Held, I. M., 1978 (a): The vertical scale of an unstable baroclinic wave and its importance for eddy heat flux parameterizations. *J. Atmos. Sci.*, **35**, 572-576.

————, 1978 (b): The tropospheric lapse rate and climatic sensitivity: Experiments with a two-level atmospheric model. *J. Atmos. Sci.*, **35**, 2083-2098.

————, and M. J. Suarez, 1978: A two-level primitive equation atmospheric model designed for climatic sensitivity experiments. *J. Atmos. Sci.*, **35**, 206-229.

————, and A. Y. Hou, 1980: Nonlinear axially symmetric circulations in a nearly inviscid atmosphere. *J. Atmos. Sci.*, **37**, 515-533.

————, and P. J. Phillipps, 1991: Sensitivity of the eddy momentum flux to meridional resolution in atmospheric GCMs. To be published.

Helfand, H. M., 1979: The effect of cumulus friction on the siulation of the January Hadley circulation by the GLAS model of the general circulation. *J. Atmos. Sci.*, **36**, 1827-1843.

Hide, R., 1969: Dynamics of the atmospheres of the major planets with an appendix on the viscous boundary layer at the rigid boundary surface of an electrically conducting rotating fluid in the presence of a megnetic field. *J. Atmos. Sci.*, **26**, 841-853.

Hollingsworth, A., 1975: Baroclinic instability of a simple flow on the sphere. *Quart. J. Roy. Meteor. Soc.*, **101**, 495-528.

Holton, J. R., 1979: *An Introduction to Dynamic Meteorology.* Academic Press. New York. 391 pp.

———, and D. E. Colton, 1972: A diagnostic study of the vorticity balance at 200 mb in the tropics in the northen summer. *J. Atmos. Sci.* , **29**, 1124-1128.

Julian *et al.*, 1970: On the spectral distribution of large-scale atmospheric kinetic energy. *J. Atmos. Sci.*, **27**, 376-387.

Kung, E. C., and H. Tanaka, 1983: Energetics analysis of the global circulation during the special observation periods of FGGE. *J. Atmos. Sci.*, **40**, 2575-2592.

Lin, S., and R. T. Pierrehumbert, 1988: Does Ekman friction suppress baroclinic instability? *J. Atmos. Sci.*, **45**, 2920-2933.

Lindzen, R. S., and B., Farrell, 1980: The role of polar regions in global climate, and a new parameterization of global heat transport. *Mon. Wea. Rev.*, **108**, 2064-2078.

Lorenz, E. N., 1960: Energy and numerical weather prediction. *Tellus*, **12**, 364-373.

———, 1963: The mechanics of vacillation. *J. Atmos. Sci.*, **20**, 130-141.

———, 1967: *The Nature and Theory of the General Circulation of the Atmosphere.* Geneva, World Meteorological Organization, 161 pp.

McIntyre, M. E., 1980: An introduction to the generalized Lagrangian-mean description of wave, mean-flow interaction. *Pure Appl. Geophys.*, **118**, 152-176.

Mole, N., and I. N. James, 1990: Baroclinic adjustment in a zonally varying flow. *Quart. J. Roy. Meteor. Soc.*, **116**, 247-268.

O'Brien, E., and L. Branscome, 1989: Minimal modeling of the extratropical general circulation. *Tellus*, **41A**, 292-307.

Oort, A. H., 1971: The observed annual cycle in the meridional transport of atmospheric energy. *J. Atmos. Sci.*, **28**, 325-339.

———, and E. R. Rasmussen, 1971: *Atmospheric Circulation Statistics*, NOAA prof. paper 5, 323 pp.

———, and J. P. Peixoto, 1974: The annual cycle of th energetics of the atmosphere on a planetary scale. *J. Geophys. Res.*, **79**, 2705-2719.

Orszag, S. A., 1970: Transform methodfor the calculation of vector- coupled sums: application to the spectral form of the vorticity equation. *J. Atmos. Sci.*, **27**, 890-895.

Palmen, E., and C. W. Newton, 1969: *Atmospheric Circulation Systems.* Academic Press, New York, 603 pp.

Peixoto, J. P., and A. H. Oort, 1974: The annual distribution of atmospheric energy on a planetary scale. *J. Geophys. Res.*, **79**, 2149-2159.

Phillips, N. A., 1951: A simple three-dimensional model for the study of large-scale extratropical flow patterns. *J. Meteor.*, **8**, 381-394.

———, 1954: Energy transformation and meridional circulations associated with simple baroclinic waves in a two-level quasi-geostrophic model. *Tellus*, **6**, 273-286.

———, 1963: Geostrophic motion. *Rev. Geophys.*, **1**, 123-176.

Platzman, G. W., 1962: The analytical dynamics of the spectral vorticity equation. *J. Atmos. Sci.*, **19**, 313-328.

Press, W. H., *et al.*, 1986: *Numerical Recipes.* Cambridge University Press. 818 pp.

Reinhold, B., 1986: Structural determinism of linear baroclinic waves and simple nonlinear equilibration. *J. Atmos. Sci.*, **43**, 1484-1504.

Rhines, P. B., 1975: Waves and turbulence on a beta-plane. *J. Fluid Mech.*, 69, 417-443.

Salmon, R., 1980: Baroclinic instability and geostrophic turbulence. *Geophys. Astrophys. Fluid Dyn.*, **15**, 167-211.

Saltzman, B., 1968: Steady state solutions for axially-symmetric climatic variables. *Pure Appl. Geophys.*, **69**, 237-259.

————, 1970: Large-scale atmospheric energetics in the wavenumber domain. *Rev. Geophys. Space Phys.*, **8**, 289-302.

Schneider, E. K., and R. S. Lindzen, 1976: A discussion of the parameterization of momentum exchange by cumulus convection. *J. Geophys. Res.*, **81**, 3158-3160.

————, and ————, 1977: Axially symmetric steady-state models of the basic state for instability and climate studies. Part I: Linearized calculations. *J. Atmos. Sci.*, **34**, 263-279.

Sellers, W. D., 1969: A global climatic model based on the energy balance of the earth-atmosphere system. *J. Appl. Meteor.*, **8**, 392-400.

Shampine, L. F., and M. K. Gordon, 1975: *Computer Solution of Ordinary Differential Equations: The Initial Value Problem.* Freeman.

Silberman, I., 1954: Planetary waves in the atmosphere. *J. Meteor.*, **11**, 27-34.

Simmons, A. J., and B. J. Hoskins, 1978: The life cycle of some baroclinic waves. *J. Atmos. Sci.*, **35**, 414-432.

————, and ————, 1980: Barotropic influences on the growth and decay of nonlinear baroclinic waves. *J. Atmos. Sci.*, **37**, 1679-1684.

Somerville, R. C. J., P. H. Stone, M. Halem, J. E. Hansen, J. S. Hogan, L. M. Druyan, G. Russell, A. A. Lacis, W. J. Quirk and J. Tenenbaum, 1974: The GISS model of the global atmosphere. *J. Atmos. Sci.*, **31**, 84-117.

Starr, V. P., 1948: An essay on the general circulation of the earth's atmosphere. *J. Meteor.*, **5**, 39-43.

Stone, P. H., 1972: A simplified radiative-dynamical model for the static stability of rotating atmospheres. *J. Atmos. Sci.*, **29**, 405-418.

————, 1973: The effect of large-scale eddies on climatic change. *J. Atmos. Sci.*, **30**, 521-529.

————, 1978: Baroclinic adjustment. *J. Atmos. Sci.*, **35**, 561-571.

————, 1990: Private communications.

————, and M. Yao, 1987: Development of a two-dimensional zonally averaged statistical-dynamical model. Part II: The role of eddy momentum fluxes in the general circulation and their parameterization. *J. Atmos. Sci.*, **44**, 3769-3786.

————, and ————, 1990: Development of a two-dimensional zonally averaged statistical-dy namical model. Part III: The parameterization of the eddy fluxes of heat and moisture. *J. Climate*, **3**, 726-740.

———, and D. A. Miller, 1980: Empirical relations between seasonal changes in meridional temperature gradients and meridional flux of heat. *J. Atmos. Sci.*, **37**, 1708-1721.

———, and J. H. Carlson, 1979: Atmospheric lapse rate regimes and their parameterization. *J. Atmos. Sci.*, **36**, 415-423.

———, and J. S. Risbey, 1990: *On the limitations of general circulation climate models.* Center for Global Change Science, MIT, Report No. 2.

———, and L. Branscome, 1991: Diabatically forced nearly inviscid eddy regimes. Accepted by *J. Atmos. Sci.*

———, W. J. Quirk, and R. C. J. Somerville, 1974: The effect of small-scale vertical mixing of horizontal momentum in a general circulation model. *Mon. Wea. Rev.*, **102**, 765-771.

Thompson, P. D., 1987: Large-scale dynamical response to differential heating: statistical equilibrium states and amplitude vacillation. *J. Atmos. Sci.*, **44**, 1237-1248.

Vallis, G. K., 1988: Numerical studies of eddy transports in eddy resolving and parameterized models. *Quart. J. Roy. Meteor. Soc.*, **114**, 183-204.

Wiin-Nielson, A., 1967: On the annual variation and spectral distribution of atmospheric energy. *Tellus*, **19**, 540-559.

———, 1970: A theoretical study of the annual variation of atmospheric energy. *Tellus*, **22**, 1-15.

Williams, G. P., 1978: Planetary circulation: 1. Barotropic representation of Jovian and terrestrial turbulence. *J. Atmos. Sci.*, **35**, 1399-1426.